UNIVERSIDAD DE GRANADA

ESCUELA INTERNACIONAL DE POSGRADO

PROGRAMA DE DOCTORADO EN INGENIERÍA CIVIL

# TESIS DOCTORAL

# GRAPHIC METHODOLOGIES, BASED IN EQUILIBRIUM HYPOTHESES, FOR THE STRUCTURAL ANALYSIS OF MASONRY DOMES. Application to a historical building

# *METODOLOGÍAS GRÁFICAS, BASADAS EN HIPÓTESIS DE EQUILIBRIO, PARA EL ANÁLISIS ESTRUCTURAL DE CÚPULAS DE FÁBRICA Y MAMPOSTERÍA. Aplicación a una construcción histórica singular*

José Antonio González Casares

Director de tesis: **Francisco Javier Suárez Medina**

Noviembre 2020

Editor: Universidad de Granada. Tesis Doctorales
Autor: José Antonio González Casares
ISBN: 978-84-1195-263-7
URI: https://hdl.handle.net/10481/90743

# GRAPHIC METHODOLOGIES, BASED IN EQUILIBRIUM HYPOTHESES, FOR THE STRUCTURAL ANALYSIS OF MASONRY DOMES. Application to a historical building

José Antonio González Casares

**Abstract**

This dissertation presents a new graphic methodology for the structural analysis of domes and other surfaces of revolution, based in the combined use of funicular and projective geometry. The new methodology is presented through its application to a hemispherical brick dome of small thickness.

The analysed model has been referenced to the inner brick dome in Basilica of San Juan de Dios in Granada (Spain). This basilica is regarded as a benchmark in the Spanish Baroque. For the first time, it is set out a detailed constructive analysis and a geometric modelling of the dome over the transept, which was built according to the "*encamonada* dome" typology, divulged by Fray Lorenzo de San Nicolás.

The structural analysis of the inner brick dome is carried out by applying different equilibrium methodologies of increasing refinement.

Firstly, an approximation is made by applying the Guastavino´s formulas. This is an experimental methodology that can be applied very quickly.

Secondly, the application of the slicing technique in the frame of limit analysis. This is a very well known, and contrasted methodology, for the stability analysis of domes, which does not take into account the influence of the parallel internal forces.

Finally, this dissertation presents a new graphic methodology, which allows to graphically determine internal forces in the dome, imposing the equilibrium in both vertical and horizontal planes. The dome is simplified into a network of longitudinal and latitudinal lines. The equilibrium in the vertical plane is assured by fitting the weight force polygon to the polar rays, so the dome geometry is a closed antifunicular polygon of the system of forces. The equilibrium in the horizontal plane is guaranteed by the formation of closed force polygons in the dual figure.

The application of the new graphic methodology considers three structural situations: complete hemisphere, hemisphere with oculus, and hemisphere with lantern. Different inclinations of the reactions at the support are considered as well as various hypotheses for the structural behaviour of the backfilling. Multiple solutions with acceptable tensional values for the brick masonry have been obtained, which makes consideration of the backfilling on the extrados unnecessary.

The results have been contrasted with the ones from the application of membrane analysis, and it indicates a strong coincidence if the number of sectors in the discretisation of the graphic methodology are high enough. Additionally, the new methodology allows its application to different structural situations, it is easy to understand, easy to program, and can be applied in domes of arbitrary geometry.

Keywords: historical structure, *encamonada* dome, structural analysis, graphic statics, funicular geometry, projective geometry.

Thesis director: Francisco Javier Suárez Medina.
Professor of University of Granada. Structural Mechanics and Hydraulic Engineering Department.

# METODOLOGÍAS GRÁFICAS, BASADAS EN HIPÓTESIS DE EQUILIBRIO, PARA EL ANÁLISIS ESTRUCTURAL DE CÚPULAS DE FÁBRICA Y MAMPOSTERÍA. Aplicación a una construcción histórica singular

José Antonio González Casares

**Resumen**

Se presenta una nueva metodología gráfica para el análisis estructural de cúpulas y otras superficies de revolución, basada en el uso combinado de geometría funicular y proyectiva. La nueva metodología se presenta mediante su aplicación a una cúpula semiesférica de poco espesor.

El modelo analizado se ha referenciado a la cúpula interior de ladrillo de la Basílica de San Juan de Dios en Granada (España). Esta basílica es considerada una de las grandes obras del barroco español. Por primera vez, se presenta un detallado análisis constructivo y una modelización geométrica de la cúpula sobre el crucero, que fue construida de acuerdo a la tipología de cúpula encamonada, difundida por Fray Lorenzo de San Nicolás.

El análisis estructural de la cúpula interior de ladrillo se ha realizado mediante la aplicación de diferentes metodologías basadas en el equilibrio y con grado de aproximación creciente.

En primer lugar, se ha realizado una aproximación aplicando las fórmulas de Guastavino. Esta es una metodología experimental de rápida aplicación.

En segundo lugar, se ha aplicado el método de los cortes en el marco del análisis límite. Esta es una metodología de análisis de estabilidad en cúpulas muy conocida y contrastada, que no considera la influencia de los esfuerzos paralelos.

Finalmente, se presenta una nueva metodología gráfica que permite determinar gráficamente los esfuerzos internos de la cúpula, asegurando el equilibrio en los planos vertical y horizontal. La cúpula es simplificada en una red de líneas longitudinales y latitudinales. El equilibrio en el plano vertical se asegura ajustando el polígono de fuerzas de los pesos a los rayos polares, por lo que la geometría de la cúpula será un polígono antifunicular cerrado del sistema de fuerzas. El equilibrio en el plano horizontal se garantiza con la formación de polígonos de fuerzas cerrados en la figura dual.

La aplicación de la nueva metodología gráfica considera tres situaciones estructurales: semiesfera completa, semiesfera con óculo, y semiesfera con linterna. Asimismo, analiza varias inclinaciones de las reacciones en el soporte y diferentes hipótesis del comportamiento estructural del relleno. Se han obtenido una multiplicidad de soluciones con valores tensionales aceptables para la fábrica de ladrillo, lo que lleva a considerar el relleno del extradós innecesario.

Los resultados se han contrastado con los obtenidos al aplicar análisis de membrana, resultando una gran coincidencia si el número de sectores de discretización, de la nueva metodología gráfica, es suficientemente alto. Además, la nueva metodología permite su aplicación a diferentes situaciones estructurales, es fácil de entender, fácil de programar y se puede aplicar a cúpulas de geometrías arbitrarias.

Palabras clave: estructuras históricas, cúpula encamonada, análisis estructural, estática gráfica, geometría funicular, geometría proyectiva.

Director de tesis: Francisco Javier Suárez Medina.
Profesor titular de la Universidad de Granada. Departamento de Mecánica de Estructuras e Ingeniería Hidráulica

# Acknowledgements

A dissertation is not possible without the encouragement and assistance of many people.

First of all, I would like to thank my thesis director, Professor Javier Suarez Medina, for his relentless support and help throughout all the process. I particularly appreciate all the effort he dedicated to this work and the passion and energy he had. No doubt, this work could have never been finished without all his help and all the opportunities he has provided me.

I would also like to thank Professor Thomas Boothby from the Penn State University (EE.UU.) for his generous contribution to the development of this work.

Special thanks to the Orden Hospitalaria de San Juan de Dios for letting us free access to the interior and exterior of the building to collect the data needed. Here I have to be grateful to Antonio Antequera for helping me with the measurement campaign.

Writing this dissertation in a foreign language was a challenge that was feasible thanks to the help of my colleagues and friends Jaynie Curtis and Michelle Symonds.

Thanks to all the members of the thesis committee for their hard work analysing and judging this work.

There have been many people along the way to tank as well: my parents and family, Félix and Fina, for the time stolen, and all the people I work with, in special to Carmen Gómez for her support and understanding.

# Index

**List of figures** ..... **5**

**Chapter 1 Introduction** ..... **10**

1.1. Outline of chapters ..... 11
1.2. Objectives ..... 12
1.3. Methodology ..... 12

**Chapter 2 Structural analysis of domes by equilibrium methods** ..... **13**

2.1. Beginning of equilibrium analysis of domes ..... 14
2.2. Slicing technique ..... 16
2.3. Graphic statics ..... 18
2.4. Membrane theory ..... 23
2.4.1. Historical outline ..... 23
2.5. Eddy´s method ..... 24
2.6. Guastavino´s experimental formulation ..... 28
2.6.1. Guastavinos´ masonry vaults and domes ..... 28
2.6.2. Guastavino´s formulation ..... 32
2.7. Graphical methods at present ..... 34
2.7.1. The slicing technique in the frame of limit analysis ..... 34
2.7.2. Trust network analysis ..... 35
2.7.3. Other current works ..... 36
2.8. New graphic methodology ..... 37

**Chapter 3 Limit analysis** ..... **38**

3.1. Thrust line ..... 38
3.2. Collapse mechanism in arches ..... 40
3.3. Fundamental theorems ..... 40
3.4. Safety in arches ..... 41
3.4.1. Geometric safety factor ..... 41

**Chapter 4 Funicular geometry** ..... **43**

4.1. Modelling forces. The parallelogram rule ..... 43
4.1.1. Moment of a couple of forces ..... 44
4.1.2. Reduction of a system of forces ..... 45
4.2. Equilibrium of a system of forces with the funicular polygon ..... 45
4.2.1. System of two forces ..... 45
4.2.2. Multiple forces with open force polygon ..... 47
4.2.3. Multiple forces with closed force polygon ..... 47
4.2.4. Equilibrating a system of forces with two forces with a pre-set direction ..... 48

4.3. Geometric properties ..... 49
4.3.1. Polar axis ..... 50
4.4. Applications of the funicular geometry ..... 51
4.4.1. Funicular polygon through two points ..... 53
4.4.2. Funicular polygon through three points ..... 53
4.4.3. Thrust line in a masonry arch. ..... 56

**Chapter 5 Projective geometry ..... 58**

**Chapter 6 New graphic methodology based on the combined use of funicular and projective geometry ..... 63**

6.1. Hemispherical brick dome ..... 63
6.2. Methodology ..... 65
6.2.1. Simplified model ..... 66
6.2.2. Nodal forces ..... 66
6.2.3. Structural reciprocity ..... 69
6.2.4. Vector increments ..... 70
6.2.5. Horizontal plane: dual figure ..... 71
6.2.6. Procedure in both directions ..... 71

**Chapter 7 Basilica of San Juan de Dios ..... 73**

7.1. Historical context. The tile vaults and domes ..... 74
7.1.1. Origins of tile domes and vaults ..... 74
7.1.2. Beginnings in the Iberian Peninsula ..... 75
7.1.3. Spanish development in the Renaissance and Baroque ..... 78
7.2. Historical background of the basilica ..... 80
7.2.1. José de Bada y Navajas ..... 80
7.3. Architectonics characteristics ..... 81
7.4. Analysis of references and data collection ..... 83
7.4.1. Fray Lorenzo´s influence ..... 84
7.4.2. Analysis of similar domes ..... 85
7.4.3. Visual inspection and measurements ..... 92
7.5. Constructive system ..... 92
7.5.1. Exterior cover ..... 98

**Chapter 8 Structural analysis with Guastavino´s formulas ..... 100**

8.1. Full hemispherical dome ..... 100
8.2. Shallow dome ..... 101

**Chapter 9 Stability applying the slicing technique ..... 102**

9.1. Modelling of the dome for the slicing technique ..... 102
9.2. Structural cases and filling hypothesis ..... 104
9.2.1. Filling hypothesis ..... 104
9.2.2. Structural cases and tests performed ..... 104
9.2.3. Results of the slicing technique ..... 115

**Chapter 10 Application of the new graphical methodology ..... 116**

10.1. Tests performed ..... 116

10.2. Results ..... 135

10.2.1. Values obtained ..... 135

10.2.2. Stresses in masonry ..... 135

**Chapter 11 The shell as a membrane ..... 139**

11.1. Shells of revolution ..... 139

11.2. Slice equilibrium ..... 140

11.3. Spherical shell ..... 141

11.4. Uniform spherical shell under self-weight ..... 141

11.5. Hemispherical dome with lantern ..... 141

11.6. Compressive stiffening ring ..... 142

**Chapter 12 Application and contrast of results ..... 144**

12.1. Orders of magnitude ..... 144

12.2. Membrane stress resultants ..... 145

12.3. Compressive stiffening ring ..... 147

12.4. Contrast of results ..... 147

**Chapter 13 Conclusions ..... 150**

**Chapter 14 Future lines of research ..... 152**

**References ..... 153**

**Research contributions derived from the development of the PhD thesis ..... 163**

# List of figures

**Figure 1** Bouguer 1734; Meridian funicular curve from (López G. , 1998). 14

**Figure 2** Drawings of domes (Frézier, 1737). 15

**Figure 3** San Peter of Rome, original drawings of the survey of the dome (1742 parere di tre matematici, biblioteca hertiziana, Rome) 16

**Figure 4** Equilibrium study, based on the catenary (Poleni, 1748) 17

**Figure 5** Study of stability of domes and vaults (Navier, 1826) 18

**Figure 6** Problem of a lever and its forces, Leonardo da Vinci Codes in (Nielsen, 1998) 18

**Figure 7** Stevin´s drawing of forces (Stevin, 1586). 19

**Figure 8** Force analysis with vectors and polygons (Varignon, 1687). 19

**Figure 9** Thrust line in arches and cracks patterns (Culmann, 1864). 20

**Figure 10** (left) Truss with three vertical forces. (right) Truss, forces and reactions with Bow´s notation. 21

**Figure 11** Thrust line analysis combined with the slicing technique (Wittmann, 1879) in (Block P. , 2009). 21

**Figure 12** Inverted photograph of Gaudi´s hanging model (Puig Boada, 1976) in (Huerta, 2006b). 22

**Figure 13** Small element of the shell acted upon by the membrane stress resultants. 23

**Figure 14** Schwedler´s graphical construction. The part of the dome that is not considered has non-admissible hoop stresses (Schwedler, 1859) in (Tempesta et al., 2015). 24

**Figure 15** Eddy´s graphical methodology to obtain membrane stresses (Eddy, 1878). 26

**Figure 16** Analysis of a masonry dome assuming a membrane compressive stress condition in the upper part (Föppl, 1881). 27

**Figure 17** Dome analysis with compression and tension sections for different hypotheses (Dunn, 1908); (a) Hemisphere; (b) hemisphere with oculus; (c) hemisphere with lantern. 27

**Figure 18** Guastavino´s drawing of Saint John the Divine. The graphic method is seen on the right part of the drawing in (Dugum, 2013). 28

**Figure 19** Construction of timbrel arches (Avery Library, Columbia University) in (Huerta, 2003). 29

**Figure 20** Stress diagram in dome of Saint Francis de Sales in Philadelphia (Avery Library, Columbia University) in (Zawisny, Fivet, & Ochsendorf, 2017). 30

**Figure 21** Patent 947,177 for a masonry dome reinforced. 31

**Figure 22** Guastavino´s analysis. (a) Forces equilibrium in the vault; (b) analogy between the hemispherical dome and a cylindrical vault loaded only in half a surface (Suárez, Boothby, & González, 2019). 32

**Figure 23** Heyman applies the same techniques from the arch to an "orange slice" to find the minimum thickness with hinges in P and Q (Heyman, 1967). e 35

**Figure 24** The primal grid $\Gamma$ and dual grid $\Gamma*$ are related by a reciprocal relationship. The equilibrium of a node in one of them is guaranteed by a closed polygon in the other and vice versa. The labelling uses Bow's notation (Block P. , 2009). 36

**Figure 25** Polygon and rope method in the plane (Scholz, 1989). ..... 36

**Figure 26** 3D models of the discretised hemisphere. (left) 160 sectors; (right) 640 sector. ..... 37

**Figure 27** (left) Conceptual drawing presented by (Moseley, 1843a); (right) analysis of Moseley´s approach in (Alexakis & Makris, 2014). ..... 39

**Figure 28** Test in a model to show the plasticity of masonry arches (Huerta, 1996) ..... 39

**Figure 29** Collapse mechanism of a semicircular arch with a load (Heyman, 1995, b). ..... 40

**Figure 30** (a) Thick semicircular arch; (b) semicircular arch of least thickness; (c) crack pattern for arch of least thickness (Heyman, 1969). ..... 42

**Figure 31** (a) Polygon of forces acting on a particle A; (b) triangle law in forces ..... 43

**Figure 32** (a) Addition of vectors; (b) couple of forces; (c) moment of a couple. ..... 44

**Figure 33** (a) Resultant of a group of forces; (b) force polygon with the sum of forces every two. ..... 45

**Figure 34** (a) Starting data and force polygon; (b) polar rays and funicular polygon; (c) resultant. ..... 46

**Figure 35** Funicular polygon for multiple forces like P1, P2, P3, P4. Scale of force polygon is ½. ..... 47

**Figure 36** (a) System of forces with a moment; (b) system of forces in equilibrium; (c) same closed polygon in both cases. 48

**Figure 37** (a) Data set and pre-set directions of reactions; (b) system in equilibrium; (c) force polygon. ..... 49

**Figure 38** Geometric properties of a system of forces. ..... 49

**Figure 39** Reciprocity between funicular polygon and force polygon. ..... 50

**Figure 40** (a) System of forces P1, P2, P3, P4 and funicular polygons; (b) force polygons with a scale 1/2. ..... 51

**Figure 41** (a) Funicular polygon of a system of forces; (b) anti-funicular of a system of forces; (c) force polygons. ..... 52

**Figure 42** (a) System of forces and first funicular polygon; (b) force polygon with arbitrary pole O, scale ½; (c) system of forces with funicular polygon through m and n; (d) force polygons, scale of ½. ..... 54

**Figure 43** (a) Initial data; (b) funicular polygon through m,n; (c) first force polygon, scale ½; (d) final funicular polygon; (e) final force polygon, scale ½. ..... 55

**Figure 44** (a) Input data; (b) first funicular polygon with arbitrary pole O; (c) second funicular polygon through a and m; (d) third funicular polygon through points n and q. ..... 57

**Figure 45** Example of reciprocal diagrams. (left) Form diagram or primal figure; (right) force diagram or dual figure, given the magnitude of force P. (Maxwell, 1870) in (Reese, Paffenroth, & Fehribach, 2016). ..... 58

**Figure 46** Example of structural reciprocity. (a) Primal figure; (b) step by step dual figure; (c) primal figure, second case; (d) dual figure, second case; (e) primal figure, third case; (f) dual figure, third case. ..... 60

**Figure 47** Example of combined use of funicular geometry and reciprocity. ..... 61

**Figure 48** Example of use reciprocity. (left) New form diagram; (right) force diagram with a new position of point 2. ..... 62

**Figure 49** Three structural situations have been considered: full hemisphere, hemisphere with oculus and hemisphere with inside brick coating of lantern. ..... 64

**Figure 50** Structural situations of the dome and filling on the extrados. ..... 65

**Figure 51** Simplified model: the dome is divided by latitude and longitude into an arbitrary number of sectors; the simplified model of the dome is obtained by considering the weight and centre of gravity of each sector, and the interaction among centroids (nodes) of adjacent sectors. ..... 67

**Figure 52** Plan and elevation of the simplified model; the different areas in the plan are named according to Bow's notation (1873). (a) Full hemisphere; (b) dome with oculus; (c) dome with lantern; shallow dome with lantern. ..... 68

**Figure 53** (left) Equilibrium at node in compression zone: the hoop forces are a radially directed forces in the plane of the line of latitude, acting outwards; (right) equilibrium at node in tension zone: the hoop forces are a radially directed forces in the plane of the line of latitude, acting inwards. ..... 69

**Figure 54** Structural reciprocity. (a) System of forces, primal figure; (b) force polygon, dual figure; (c) horizontal projection of network, primal figure; (d) force polygon, dual figure. ..... 70

**Figure 55** Dome and towers of Basilica of San Juan de Dios. ..... 73

**Figure 56** (left) Building of a double layer vault with filling in the haunches; (right) deformation of a semi-circular thin vault (Choisy, 1873). ..... 75

**Figure 57** Viollet-le-Duc´s drawings of the manner in which the Romans had constructed their concrete vaults in (Collins, 1968). ..... 75

**Figure 58** Remains of the tile vault of a stair in house number 10 in Siyasa (Almagro, 2011) ..... 76

**Figure 59** Chapter hall of the Convent of Santo Domingo in Xátiva (1329) (Zaragozá, 2011). ..... 76

**Figure 60** Trace of the tile vault and the roof in the royal chapel of the Cathedral of Barcelona (Conejo da Pena, 2012). ..... 77

**Figure 61** Planimetric survey along the axis (taken from the project of Mr Ignacio Bosch). ..... 78

**Figure 62** Interior of the extension of Cathedral of Zaragoza. View of the vaults in *quarto nuevo* (Ibáñez, 2010). ..... 79

**Figure 63** Church in Illueca (Zaragoza). View of the dome and lateral vaults (Ibáñez, 2010). ..... 79

**Figure 64** Tiled dome in the Alhambra. *Puertas de Armas* (Fortea, 2009). ..... 80

**Figure 65** Basilica plan and façade orientation. ..... 81

**Figure 66** Inside of the church under the transept. The main arches are doubled. ..... 83

**Figure 67** Constructive configuration of the *encamondada* dome in Fray Lorenzo´s treatise (1639, 1665). ..... 85

**Figure 68** Dome of Iglesia de la Magdalena in the San Pablo Convent in Seville. Repairs works in the years 1989-1991 (Pinto, 2005). ..... 86

**Figure 69** (left) Section of the dome with the constructive system and (right) axonometric view (Pinto, 2005). ..... 86

**Figure 70** Union of curved rafters or *camones* (Pinto, 2005). ..... 87

**Figure 71** Timber structure and brick dome in San Juan de la Penitencia church (Martín, 2009). ..... 88

**Figure 72** Tile inner dome, with a single layer of brick and with a reinforcement up to one third of the height (Martín, 2009) ..... 88

**Figure 73** (left) Timber structure; (right) *camones* over the rafters (Vega, 2007) ..... 88

**Figure 74** Concepción Real de Calatrava Church. Interior of the structure while restoration works (Estepa, 2015). ..... 89

**Figure 75** (left) Photograph of the metallic reinforcements in the stirrups; (right) drawing of the reinforcements in the restoration project of José Miguel Rueda (2003) in (Estepa, 2015). ..... 90

**Figure 76** 3D model according to the restoration project of José Miguel Rueda (2003) in (Estepa, 2015). ..... 90

**Figure 77** Original condition of the timber structure (Granero, 2009). ..... 91

**Figure 78** Structure and finishing after the restoration work (Granero, 2009). ..... 91

**Figure 79** On-site check-up and measurement of the different elements in the dome..... 93

**Figure 80** Constructive system, floor plan, section and elevation of the dome, with details A and B for different hypothesis of the lantern support system..... 95

**Figure 81** Floor plan, elevation and section with dimensions..... 96

**Figure 82** 3D explosive perspective of the construction system of the dome..... 97

**Figure 83** Dome, towers. The beautiful *alboaire* is seen on the cover of the dome..... 99

**Figure 84** Tiles in the exterior of San Juan de Dios dome, with the characteristics green and white tiles of the *alboaire*.. ..... 99

**Figure 85** Data from Basilica of San Juan de Dios for the Guastavino formulas. Case of full hemisphere..... 100

**Figure 86** Data from Basilica of San Juan de Dios for the Guastavino formulas. Case of shallow dome..... 101

**Figure 87** Slice and voussoirs to be used in the slice technique, with origin of coordinates at the top vertex..... 103

**Figure 88** Section of dome in the different cases: (a) hemisphere with no filling; (b) without filling and with oculus; (c) filling of loose granular material, without structural behaviour; (d) filling of firm granular material, with structural function; (e) cemented rigid filling, acting as an embedment so it is considered as a shallow dome..... 105

**Figure 89** Matrix with the tests performed with different initial and final points of the thrust line. The cases selected to be shown are highlighted..... 106

**Figure 90** Test a.2: complete brick dome without filling. Thrust line in the keystone at the bottom point of the section and the reaction in the springer at the exterior point of the section. The thrust line leaves the section. ..... 107

**Figure 91** Test c.2: dome with lantern and without filling. Thrust line in the keystone at the bottom point of the section and the reaction in the springer at the exterior point of the section. The thrust line leaves the section. ..... 108

**Figure 92** Test e.2: dome with lantern and with loose granular filling without structural behaviour. Thrust line in the keystone at the bottom point of the section and the reaction in the springer at the exterior point of the section. The thrust line leaves the section, but the thrust line is not far from the section. th structural function..... 109

**Figure 93** Test g.3: dome with lantern and with firm granular filling with structural function. Thrust line in the keystone in the middle point of the section and the reaction in the springer at 11/13 outside the impost. The thrust line is within the section with a **safety factor of 1.09.**..... 110

**Figure 94** Test g.4: dome with lantern and with firm granular filling with structural function. Thrust line at the keystone at 21/26 top point of the section and the reaction in the springer at 11/13 outside the impost. The thrust line is within the section with a **safety factor of 1.28.**..... 111

**Figure 95** Test i.2: dome with lantern and with cement rigid filling; a shallow dome. Thrust line at the keystone at 1/2 top point of the section and the reaction in the springer at 3/4 outside the impost. The thrust line is within the section with a **safety factor of 1.21.**..... 112

**Figure 96** Test i.3: dome with lantern and with cement rigid filling; a shallow dome. Thrust line at the keystone at 1/4 top point of the section and the reaction in the springer at 3/4 outside the impost. The thrust line is within the section with a **safety factor of 1.34**..... 113

**Figure 97** Test i.4: dome with lantern and with cement rigid filling; a shallow dome. Thrust line at the keystone at 3/7 top point of the section and the reaction in the springer at 5/7 outside the impost. The thrust line is within the section with a **safety factor of 1.44.**..... 114

**Figure 98** Test 1: hemispherical dome considering vertical reaction..... 119

**Figure 99** Test 2: hemispherical dome considering tilted reaction..... 120

**Figure 100** Test 3: hemispherical dome considering vertical reaction and 5% reduction in maximum tension forces absorbed by second tension forces. ..... 121

**Figure 101** Test 4: hemispherical dome considering vertical reaction and 5% reduction in maximum tension forces absorbed by the third tension forces. ..... 122

**Figure 102** Test 5: hemispherical dome considering vertical reaction and 5% reduction in maximum tension forces absorbed by the fourth tension forces. ..... 123

**Figure 103** Test 6: hemispherical dome considering vertical reaction and 15% reduction in maximum tension forces absorbed by all the other tension forces. ..... 124

**Figure 104** Test 7: hemispherical dome with oculus considering vertical reaction. ..... 125

**Figure 105** Test 8: hemispherical dome with lantern considering vertical reaction. ..... 126

**Figure 106** Test 9.1: hemispherical dome with lantern and filling on the extrados up to one third of the height. Hypothesis 1: no structural filling; considering vertical reaction. ..... 127

**Figure 107** Test 9.2a: hemispherical dome with lantern and filling on the extrados up to one third of the height. Hypothesis 2: structural filling. Stagger shape filling, considering tilted reaction (0º, 3º, 6º). ..... 128

**Figure 108** Test 9.2b: hemispherical dome with lantern and filling on the extrados up to one third of the height. Hypothesis 2: structural filling. Soft curved filling, considering tilted reaction (0º, 3º, 6º). ..... 129

**Figure 109** Test 9.3: hemispherical dome with lantern and filling on the extrados up to one third of the height. Hypothesis 3: cemented rigid filling; considering tilted reaction. ..... 130

**Figure 110** Test 10: hemispherical dome with lantern and filling on the extrados, without tension forces. ..... 131

**Figure 111** Test 11: hemispherical dome considering vertical reaction, with 640 sectors. ..... 132

**Figure 112** Test 12: hemispherical dome with oculus considering vertical reaction, with 512 sectors. ..... 133

**Figure 113** Test 13: hemispherical dome with lantern considering vertical reaction, with 512 sectors. ..... 134

**Figure 114** (left) Meridian generating curve and (right) differential element. ..... 139

**Figure 115** Slice equilibrium. ..... 140

**Figure 116** Hemispherical dome with lantern. ..... 142

**Figure 117** Line load on the edge of the dome at the oculus. ..... 143

**Figure 118** Orders of magnitude of the compressive stress necessary to support the dome. ..... 144

**Figure 119** Values of stress resultant $N\varphi$, $N\theta$ obtained by application of membrane analysis, expressed in terms of stresses ($N/mm^2$): (a) hemispherical dome; (b) hemispherical dome with oculus; (c) hemispherical dome with lantern; (d) combination of (a), (b) and (c). ..... 146

**Figure 120** Compressive stiffening ring. ..... 147

**Figure 121** Values of stress resultant $N\varphi$, $N\theta$ obtained by application of membrane analysis, expressed in terms of stresses ($N/mm^2$): (a) hemispherical dome; (b) hemispherical dome with oculus; (c) hemispherical dome with lantern; values obtained by application of the new methodology with 160 sectors are included. ..... 148

**Figure 122** Values of stress resultant $N\varphi$, $N\theta$ obtained by application of membrane analysis, expressed in terms of stresses ($N/mm^2$): (a) hemispherical dome; (b) hemispherical dome with oculus; (c) hemispherical dome with lantern; values obtained by application of the new methodology with 640 sectors are included. ..... 149

# Chapter 1

# Introduction

Masonry arches, vaults and domes have been a fundamental part of the main buildings in the western world until the end of the 19th century and beginning of the 20th. The protection of cultural heritage is crucial if a society wants to preserve its identity for future generations. This growing interest in historic structures has created the need for accurate and efficient methods for the analysis of load-bearing unreinforced masonry structures (Boothby, 2001).

A particular challenging element in its structural analysis, are the brick thin domes (timbrel domes). One case, of special significance to architectural heritage, are the thin brick domes that internally defines the constructive system known as the "*encamonada* dome". This system is described in the treatise of Fray Lorenzo de San Nicolás (1639, 1665). This typology spread quickly, thanks to being cheap, easy to build and they also were of the taste of the Counter-Reform.

In Granada (Spain), we find an outstanding example of an "*encamonada* dome" in the baroque Basilica of San Juan de Dios. Its inner brick dome is used in this dissertation to present the new graphic methodology.

In recent times, the technology and methodologies derived from the new structural materials like concrete and steel, made the traditional graphical methods to be considered approximate by engineers, strongly conditioned by the elastic theory (Huerta, 2004).

However, the accuracy of the new computer aided drawing (CAD) brings a mathematical preciseness to the graphic calculation methodologies (Allen & Zalewski, 2009). This has helped to revive the interest in this type of graphical methodologies, which are visual and easy to understand (Zalewski & Allen, 1998). In the words of the engineer Karl Culmann "Drawing is the language of the Engineers, because the geometric way of thinking is a view of the thing itself and is therefore the most natural way; while with an analytic method, as elegant as that may also be, the subject hides itself behind unfamiliar symbols" (Hines, 2012).

This dissertation develops a new graphic methodology for the structural analysis of domes and other surfaces of revolution, based in the combined use of funicular and projective geometry. It is a new tool for the analysis of historical constructions based in Thrust Network Analysis presented in section 2.7.2, and incorporating other notions from projective geometry to make a more comprehensive method for the analysis of certain classes of structures.

## 1.1. Outline of chapters

This work is divided in 14 Chapters. In **Chapter 1** there is an introduction of the subject of this thesis, along with the objectives and the methodology followed in the research process.

**Chapter 2** reviews different equilibrium methodologies used in arches, vaults and domes, in order to place the new graphic methodology into context.

**Chapter 3** outlines the foundations of limit analysis in masonry structures. This chapter includes a brief historical development of the thrust line. It also includes an introduction to the collapse mechanisms of masonry arches and the basic theorems of limit analysis.

In **Chapter 4** the funicular geometry is explained, with special attention to obtaining the thrust line of an arch.

**Chapter 5** reviews the applications of projective geometry and reciprocal figures for structure analysis, paying special attention to the works of Maxwell and Robert Bow. This chapter shows some examples to clarify the concept of reciprocity in structures and the notation system.

The new graphic methodology is laid out in **Chapter 6**. Section 6.1 specifies the characteristics of the hemispherical brick dome of small thickness that is used to present the methodology. Section 6.2 explains the methodology in detail.

**Chapter 7** addresses the historical context and background of the "*encamonada* dome" over the transept located in Basilica of San Juan de Dios in Granada (Spain). Section 7.4 analyses similar domes that have been uncovered due to refurbishments. Section 7.5 contains a detailed constructive analysis and a geometric modelling of the dome in the basilica.

In **Chapter 8** there is an application of the Guastavino´s formulas.

The dome of reference, is also analysed with the slicing technique in **Chapter 9**. Section 9.2 explains the different structural cases and backfilling hypotheses to be considered in the tests.

**Chapter 10** is devoted to the application of the new graphic methodology to the hemispherical brick dome and for different structural cases. Section 10.2 presents and discusses the results.

**Chapter 11** develops the equations of the membrane analysis for different structural cases. Those equations are applied to the dome of reference. **Chapter 12** includes the contrast of results obtained by the new methodology and those obtained in the membrane analysis.

**Chapter 13** presents the conclusions, and **Chapter 14** outlines future lines of research.

## 1.2. Objectives

The main objective of this work is to develop a new graphic methodology for the structural analysis of domes and other surfaces of revolution, based on the combined use of funicular and projective geometry. The new methodology will be presented through its application to a hemispherical brick dome of small thickness in a historical building. This type of dome is frequently the element that internally defines the constructive system known as "*encamonada* dome".

This doctoral thesis will delve into the study of the "*encamonada* dome", which is an important element of the architectural heritage in the 17th and 18th centuries, in Spain and its overseas possessions, in the frame of the treatise of Fray Lorenzo de San Nicolás.

The model to be analysed will be referenced to a real one: the hemispherical inner brick dome of the "*encamonada* dome" in Basilica de San Juan de Dios in Granada (Spain). Therefore, a detailed constructive analysis and a geometric modelling of the dome will be carried out.

## 1.3. Methodology

This work has gone through different phases that contributed to collect all the data needed to fulfil the objectives.

This dissertation started with a review of the evolution of the equilibrium methods for the structural analysis of domes. Afterwards, it began the process of developing the new graphic methodology, which consumed a significant part of the time and involved the trip of the thesis director to the USA to meet first-hand an expert in the area such as Dr Thomas Boothby, from the Penn State University, in the summer 2018.

This new graphic methodology is presented through its application to a hemispherical brick dome of small thickness. In this work, the model analysed has been referenced to a real one: the brick dome over the transept, in Basilica of San Juan de Dios in Granada (Spain).

Simultaneously, it took place a detailed constructive analysis and the geometric modelling of the dome in Basilica of San Juan de Dios. This analysis was developed from visual inspection of the different elements, and measurements made with metric tape and laser meter.

All the drawings and 3D models used in this dissertation for the tests that were made with the different methodologies, were created with Autocad®. This brings a mathematical preciseness to this graphic calculation methodology.

# Chapter 2

# Structural analysis of domes by equilibrium methods

This chapter presents a brief historical review of equilibrium methods for the structural analysis of domes, in order to place the new graphic methodology in context.

The chapter starts with a historical review of the origins of the equilibrium methodologies applied in domes. It continues with an analysis of the slicing technique, which is a method that simplifies the assessment of equilibrium in domes and it is still in use nowadays.

To understand the foundation of graphical analysis, there is a section dedicated to understand the scientific approach involved in graphic statics and its relation to structure calculation.

There is a part dedicated to the membrane analysis that deals with the calculation of equilibrium in domes in a three-dimensional way.

The graphical method developed by Eddy H. in 1878 to assess the membrane internal forces in a dome is examined. An impressive example of the application of this methodology is in the Cathedral Saint John the Divine in New York by Guastavino Jr.

Rafael Guastavino (1842–1908) was an architect of special relevance, who along with his son Rafael Jr. (1872–1950), created some of the most important spaces in the United States (Ochsendorf & Freeman, 2010). Part of the renewed interest in masonry structures, and their structural behaviour, is also due to the rediscovery of Guastavino's striking work. This is why this chapter has a section addressing both, his constructed work and his theoretical texts.

The following section deals with the graphical methods at present, with works such as that of Jacques Heyman who, in the second half of the 20$^{th}$ century, presented for the first time the slicing technique to find collapse mechanisms in masonry structures in the frame of limit analysis. Also remarkable has been the methodology Thrust Network Analysis to explore three-dimensional equilibrium by Philippe Block & John A. Ochsendorf. This section finishes with the discussion of other relevant current works in this field.

The last part of the chapter introduces the main contribution of this thesis, a new graphic methodology for the structural analysis of domes and other surfaces of revolution, based on the combined used of funicular and projective geometry.

## 2.1. Beginning of equilibrium analysis of domes

Following (Huerta, 2008), (Boothby, 2015), (Kurrer, 2008), (Baker, Beghini, Mazurek, Carrion, & Beghini, 2013) and (Galassi, Misseri, Rovero, & Tempesta, 2017), this section presents a brief historical review of the beginning of the equilibrium methods for the structural analysis of domes.

The first studies about domes started with Vitruvius, in 25-23 BC, Palladio (1570), Leon Battista Alberti (1452 (published 1485)) and Scamozzi (1615), although they only addressed geometrical design and constructions techniques (Galassi et al., 2017).

The graphic equilibrium methods to analyse a dome, started with the problem of the ideal form of an arch. There is a review of this subject in Huerta (2008), where it is stated that Robert Hooke (1676) who firstly posed the problem: What is the ideal form of the arch, and how large is the thrust of the arch against the abutments? In addition, he gave the very well-known solution "As hangs the flexible line, so but inverted will stand the rigid arch".

The history of the theory of the masonry arch is very well known, but this is not the case for the theory of spatial vaults and domes. The first building using this scientific approach was the dome of St. Paul´s Cathedral in London (1675-1710), where Hooke and Wren used the cubic parabola in the preliminary designs. However, the first contribution to the structural analysis of domes corresponds to the French mathematician Bouguer (1734) in his work *Sur les lignes courbes propres a former les voûtes en dome* [On the curved lines that are suitable for forming the arches in domes]. Bouguer solved the theoretical problem of finding the ideal form of a dome, that is, the mathematical equation of the curve, which by revolution can generate a stable dome, considering the hypothesis that there is no friction between the segments, see Figure 1. The detected shape corresponds to the rotation of a non-homogeneous catenary, assuming the dome as composed of independent arches of variable thickness (Galassi et al.,2017).

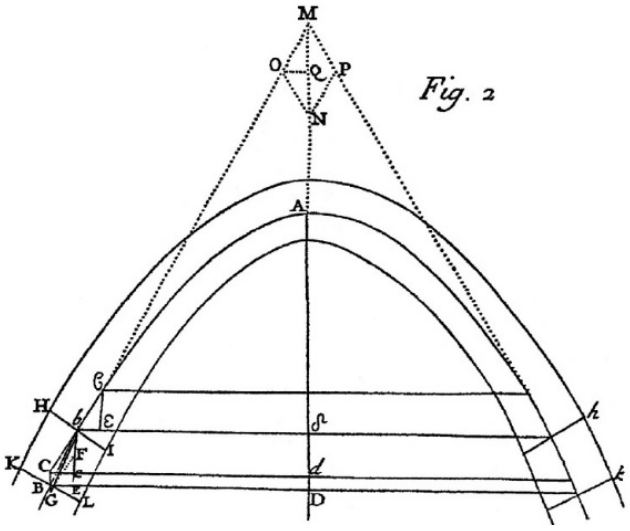


**Figure 1** Bouguer 1734; Meridian funicular curve from (López G. , 1998).

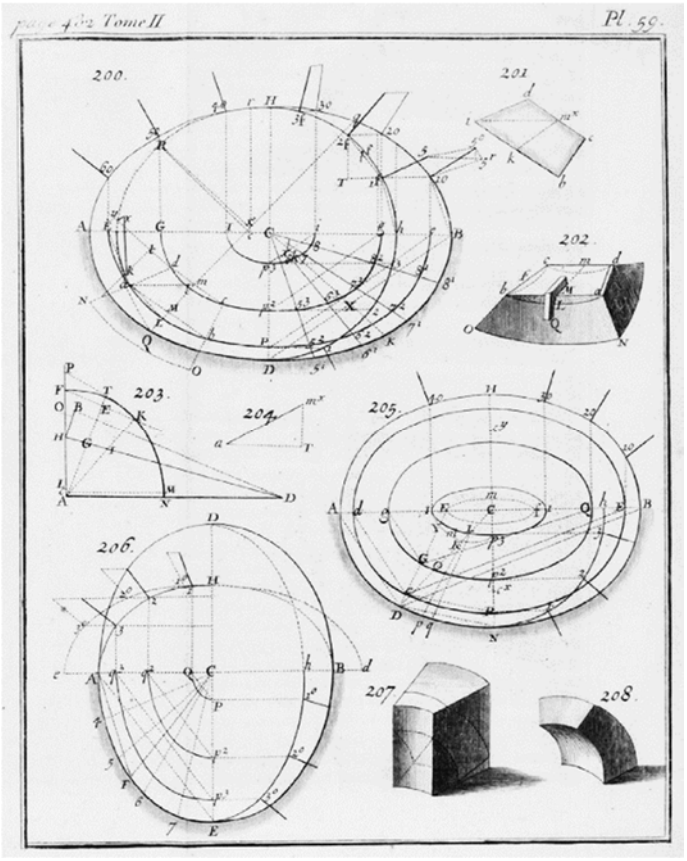


**Figure 2** Drawings of domes (Frézier, 1737).

The French engineer Frézier in his stereotomy treatise *La théorie et la pratique de la coupe des pierres et des bois pour la construction des voûtes* [The theory and practice of stone and woodcutting for the construction of vaults] (1737) dedicates a full chapter to the thrust of the vaults and divides the study in simple vaults (barrel vaults and lintel vaults) and compound vaults (spherical, ribbed vaults, cloister corner, etc.). Frézier explains how to carry out the analysis, although he did not do any (Huerta, 2004). He considers the vaults composed of elementary arches, and compares their thrust with the barrel vaults one, which he considers to be known. This is the starting point of what is called today the slicing technique, which is develop in section 2.2.

The first studies on the stability of existing domes were carried out in the 1740´s, commissioned by Pope Benedict XIV, on the occasion of the damages observed in the dome of St. Peter in Rome.

The first study was made by three mathematicians, Le Seur, Jacquier and Boscovich (1742). The authors, based on the location of the cracks and the analysis of the movement allowed by them, considered the formation of mechanisms, and established their equilibrium by applying the principle of virtual works. This surprisingly modern approach did not receive the attention it deserved and had no subsequent references.

However, it was the second expertise, written by Poleni (1748) the work that had a bigger influence in later developments of graphic calculation of masonry structures. The following section expands on this.

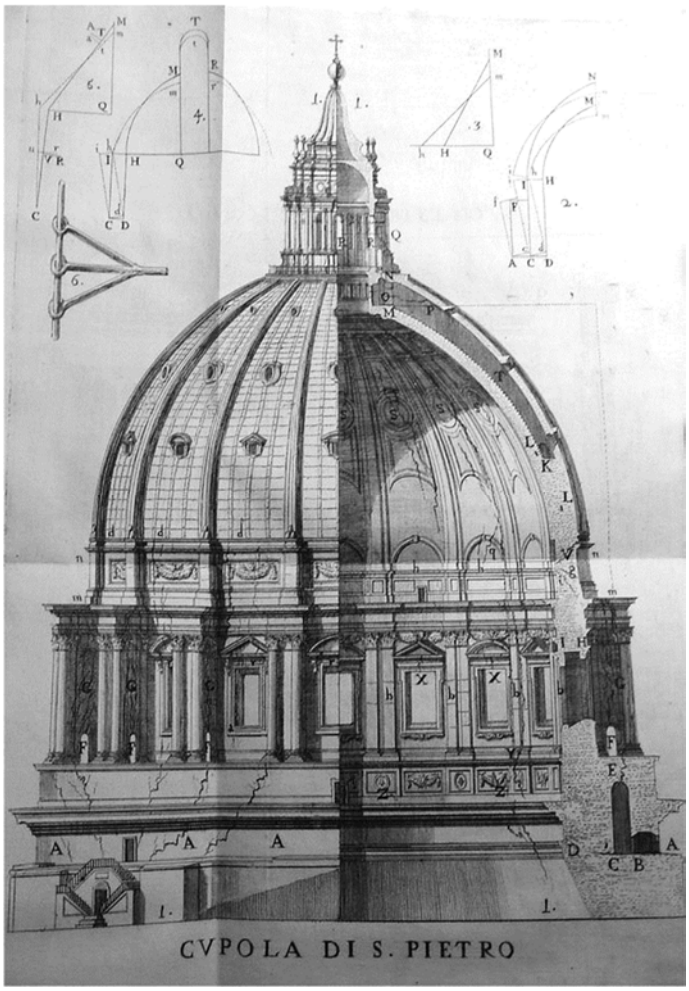


**Figure 3** San Peter of Rome, original drawings of the survey of the dome (1742 parere di tre matematici, biblioteca hertiziana, Rome).

## 2.2. Slicing technique

Poleni´s work (1748) about the stability of Saint Peter´s dome in Rome, after making a critical examination of the theories known to date on the stability of the vaults, discarded the approach of Le Seur, Jacquier, & Boscovich (1742). Instead, Poleni applied the theory of the catenary and Robert Hooke´s hanging chain idea that was already in used for arches (Hooke, 1676) to a couple of symmetric lunes as if they were forming an arc. After checking that there were meridional cracks in the structure, he decided to divide the hemisphere in 50 lunes or segments, with an angular gap of 7.2º each. To calculate the weight, he also divided radially each segment in 16 parts. By hanging proportional weights in a chain, he could verify that a thrust line could be enclosed within the dome, therefore the arch is stable (Figure 4).

Poleni boldly disregarded the discontinuity of the oculus, which implies the existence of hoop forces, at least in the oculus, to transmit the thrust from one segment to the symmetric one.

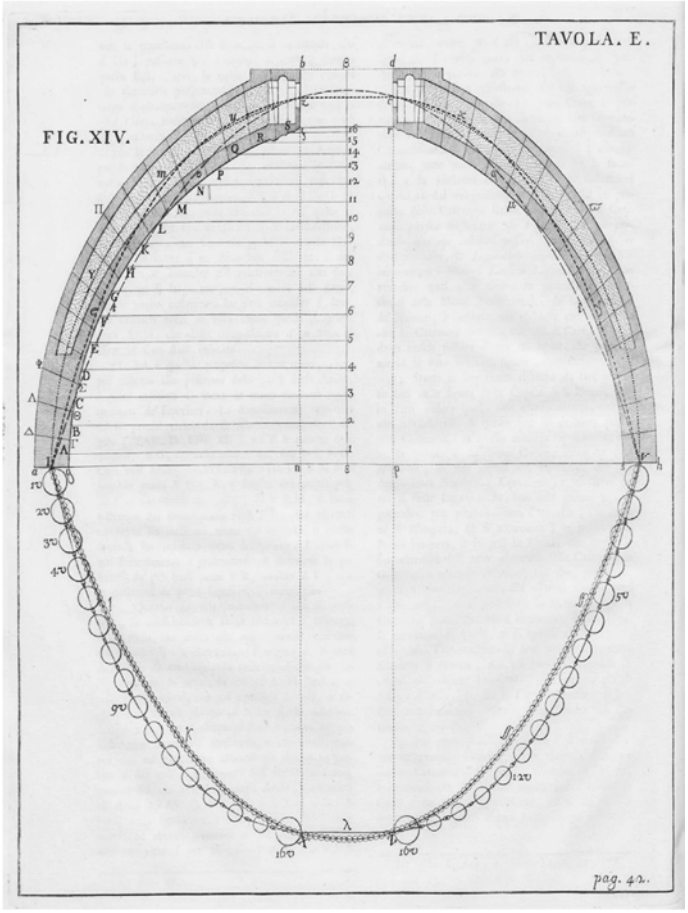


**Figure 4** Equilibrium study, based on the catenary (Poleni, 1748).

The slicing technique consists in considering the dome divided into segments, cutting by meridian planes. Every two opposite segments form an arch. If it is possible to draw a thrust line within the thickness of the arc, a possible state of equilibrium of the arch in compression is found; therefore, the arch is stable, and so is the dome.

The brilliant analysis of Poleni barely had any attention until the second half of the 19th century.

Lamé and Clapeyron (1823) also addressed, in a theoretical way, the stability of a dome by considering it divided in slices (according to the weak parts of the dome i.e. the parts between the ribs). They developed this study in relation to their work about the church of Saint Isaac in Saint Petersburg.

In the first half of the 19th century, in the context of l'École Polytechnique, l´École des Ponts et Chaussées and the development of the Elasticity Theory, the first rigorous analytical contributions appeared. Navier (1826), in his lesson book, includes theoretical assumptions for the analysis of domes, groin vaults and cloister vaults. However, the contributions are always theoretical or limited to the verification of the stability of a specific dome or vault.

In the second half of the 19th century, the usual methodology to verify the structural stability of domes was the slicing technique and the manufacture of models with catenaries.

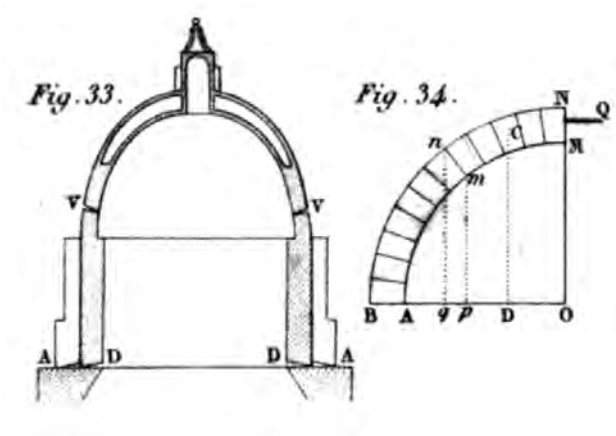


**Figure 5** Study of stability of domes and vaults (Navier, 1826).

## 2.3. Graphic statics

The history of graphic statics is addressed in (Rondeaux, 2019), (Liu, 2016), (Cavalagli & Gusella, 2015), (Allen & Zalewski, 2009), (Block, Dejong, & Ochsendorf, 2006), (Huerta, 2008), (Gerhardt, Kurrer, & Pichler, 2003) and (Nielsen, 1998) among others.

Jie Liu (2016) states that the development of graphic statics can be summarised in four stages: "1, applied as a structural calculation tool; 2, developed to graphic statics by Karl Culmann and Maxwell; 3, rarely employed as an analytical tool compared with algebraic calculation method; 4, explored by pioneers for structural innovation".

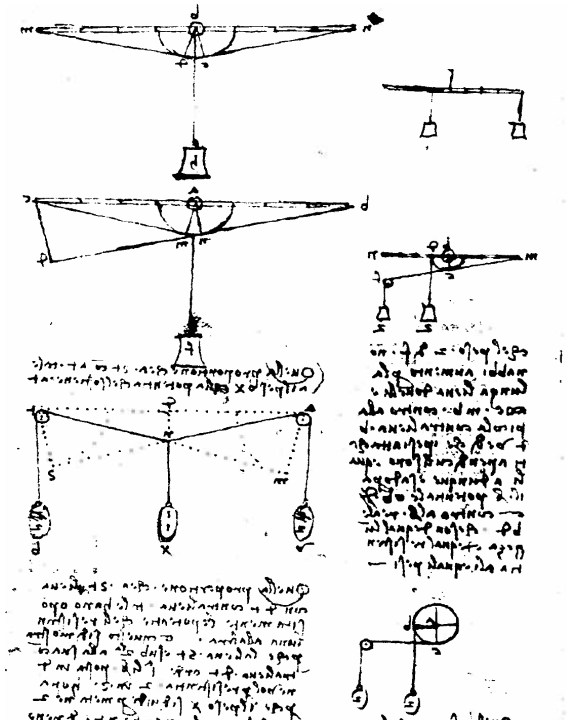

**Figure 6** Problem of a lever and its forces, Leonardo da Vinci Codes in (Nielsen, 1998).

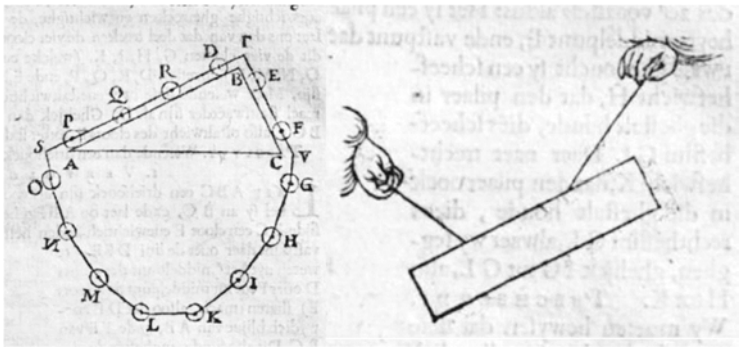

**Figure 7** Stevin´s drawing of forces (Stevin, 1586).

The origins of the graphic statics, as an analytical tool, go back to the time of the composition of forces by Italians Leonardo da Vinci and Galileo Galilei. Leonardo da Vinci around 1500 worked with forces and the way they were transmitted (Nielsen, 1998). Later, Galileo would be the first in giving a definition of *force* and stabilising the inertia law "all external impediments removed, a heavy body on a spherical surface concentric with the earth will maintain itself in that state in which it has been" (Galilei, 1638).

Dutch mathematician Simon Stevin in his work *De Beghinselen der Weeghconst* [The Principles of the Art of Weighing] (1586) presented a force as a vector probably for the first time, and he was also the first to use the parallelogram rule and the force polygon, to analyse a structure as we can see in Figure 7.

Gérard Desargues introduced the Projective Geometry in his *Brouillon Project d'une atteinte aux évènements des rencontres du Cône avec un Plan* [Rough Draft of attaining the outcome of intersecting a Cone with a Plane] (1639).

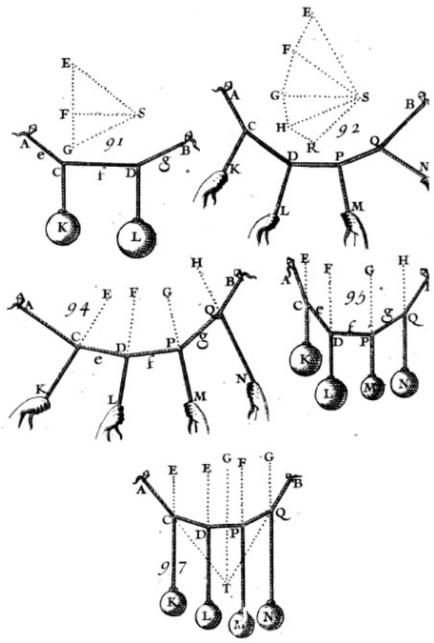

**Figure 8** Force analysis with vectors and polygons (Varignon, 1687).

Later, Pierre Varignon published *Projet d'une nouvelle mécanique* [Project of a new mechanic] (1687) (see Figure 8), where he worked out new methods of structural calculation using the force polygon and introduced the funicular polygon as the shape of a string under a set of loads. Chapter 4 addresses funicular geometry and its applications.

Jean-Victor Poncelet, director engineer of l'École Polytechnique, in his *Traite des proprietes projectives des figures* [Treatise on the projective properties of figures] (1822) developed the projective geometry from the work of Desargues.

The German engineer Karl Culmann proposed the graphical analysis of structures in a systematic way, hence he is generally acknowledged as the father of graphic statics. His seminal book *Die Graphische Statik* [The graphic statics] (1864) presented the first consistent, comprehensive body of graphical techniques. He introduced many of the fundamentals graphical methods that we use today and demonstrated how they could be used to solve a wide variety of structural problems.

Culmann's work was expanded and completed by Wilhelm Ritter. He was Culmann´s successor as a professor at the Swiss Federal Technical Institute in Zurich for graphic statics and bridge construction. In his work *Die static der tunnerlgewölbe* [The static of tunnel vaults] (Ritter, 1879) he applied and improved the work he had done together with Culmann.

As studied in (McRobie, Konstantatou, Athanasopoulos, & Hannigan, 2017), the German Otto Mohr, made supplementary contributions and enhancements in his profuse literature, of which it is worth noting *Die graphische Statik und das graphische Rechnen* [Graphic statics and graphic calculation] (Mohr, 1875) and *Beitrag zur theorie des Fachwerks* [Contribution to the theory of the truss] (Mohr, 1874).

Briton James Clerk Maxwell in his works *On reciprocal figures and diagrams of forces* (1864) and *On reciprocal figures, frames, and diagrams of forces* (1870) was the first to introduce the notion of structural reciprocity to solve structural frames (Baker et al., 2013).

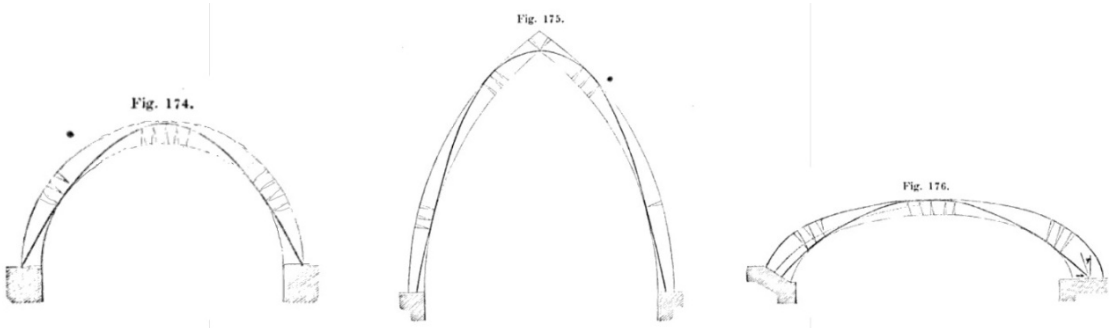


**Figure 9** Thrust line in arches and cracks patterns (Culmann, 1864).

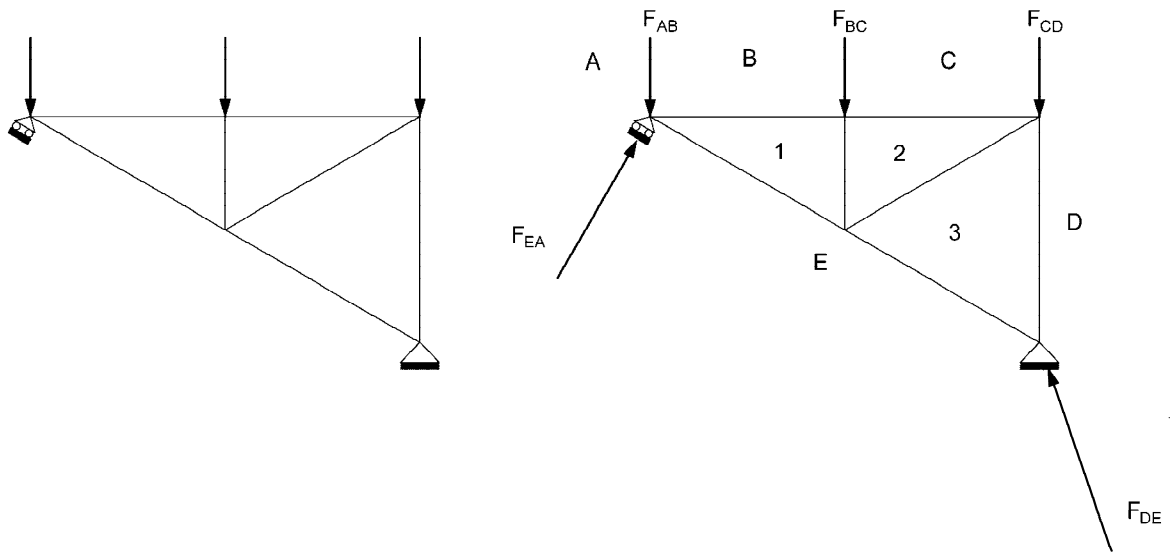


**Figure 10** (left) Truss with three vertical forces. (right) Truss, forces and reactions with Bow´s notation.

Maxwell´s method was not widely accepted until Robert H. Bow (1873) introduced the system of interval notation that is used in this thesis. However, following (Baker et al., 2013) this work is going to use a version of this where the form diagram uses capital letters between the forces clockwise A, B, C… but there are number in the interior spaces 1,2,3… see example in Figure 10.

As said in (Boothby, 2015), the relationship between projective geometry and graphic statics is noted by Karl Culmann (1875), and was discussed, among others, by A. Jay Du Bois (1877) and Eddy (1878). See section 2.5 where there is an explanation of the methodology presented by Eddy to compute dome forces.

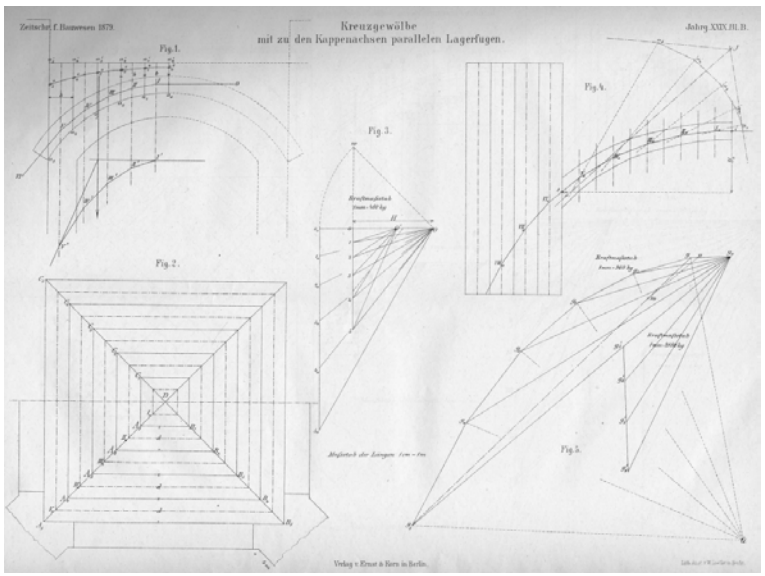


**Figure 11** Thrust line analysis combined with the slicing technique (Wittmann, 1879) in (Block P. , 2009).

In Milan, Luigi Cremona (1872) published a volume in which, independently of the British authors, he demonstrated the graphical analysis of trusses. Cremona´s diagrams were easy to understand and became very popular to calculate trusses. Detailed descriptions of Cremona´s methodology are in (Wolfe, 1921) and (Zalewski & Allen, 1998).

Incorporating graphic Statics to the slicing technique allows the analysis of any type of vault and historical construction, however complex it may be.

According to (Block P. , 2009) and (Huerta, 2008), the first known application of thrust line analysis combined with the slicing technique was by Wittmann (1879), (see Figure 11).

Körner in his work *Handbuch der Architectur* [Handbook of Architecture] (1901) showed the analysis of almost all the vaults used in historical architecture.

In the early 1900´s, graphic methods were widely used to verify previously projected forms following traditional rules of proportion.

The Spanish architect Antoni Gaudí used the graphic methods, not only to analyse already defined projects, but also to project directly with balanced catenary forms. However, for spatial complex structures with vertical loads, he also used hanging models (Huerta, 2006b) as seen in Figure 12

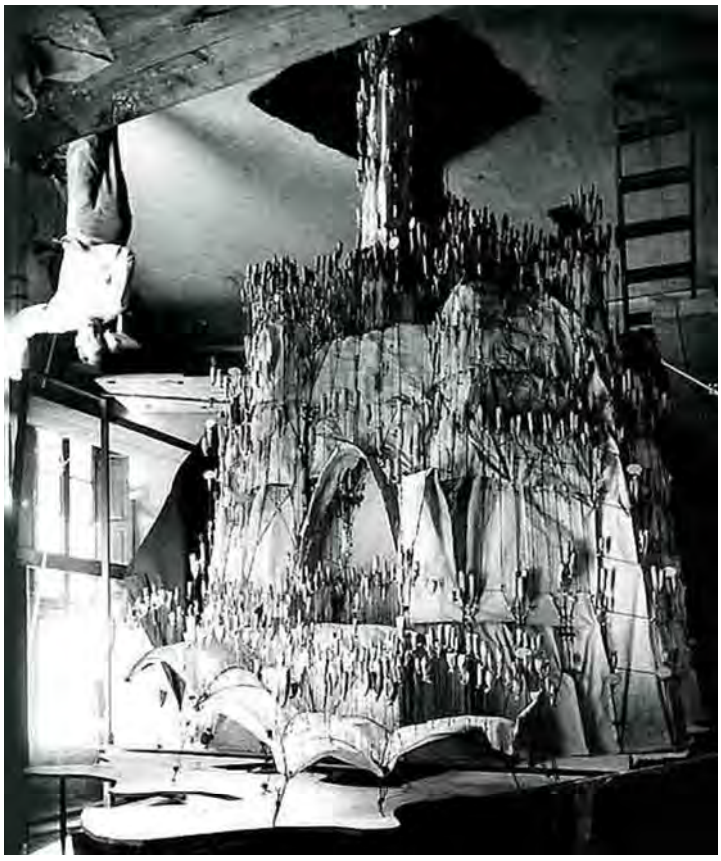

**Figure 12** Inverted photograph of Gaudi´s hanging model (Puig Boada, 1976) in (Huerta, 2006b).

## 2.4. Membrane theory

The membrane theory implies that, under appropriate loading and boundary conditions, the equilibrium is achieved with internal hoop and meridional forces, both tensile and compressive, on planes tangent to the middle surface.

According to Rankine´s and Schwedler´s hypothesis, the stresses generated by the loads are contained in planes tangent to the half-surface, see Figure 13(a). Taking into account the axial symmetry, it is concluded that no shear stresses are generated; only normal stresses either compressive of tensile will occur, see Figure 13(b). Due to the axisymmetric loading the shear stresses will be zero everywhere.

### 2.4.1. Historical outline

William J. M. Rankine was the first to work on a membrane solution for revolution domes. His works *Manual of Applied Mechanics* (Rankine W. , 1858) and *Manual of Civil Engineering* (Rankine W. , 1862) are a compilation of his main contributions on structural theory and membrane analysis. In his first work, there is an example of a spherical dome, where he calculates the angle of rupture (where the compression forces changes from compressive to tensile ones) in 51º49´ (51.8º).

Following (Tempesta, Paradiso, Stefano, & Pieroni, 2015), (Galassi et al., 2017) and (Beatini, Royer-Carfagni, & Tasora, 2018), it was in Schwedler in his work *Theorie der Stützlinie. Ein Beitrag zur Form und Stärke gewölbter Bögen* [Theory of the supporting line. A contribution to the shape and strength of curved] (1859) where it was first theorised about the bi-dimensional behaviour in the dome, and provided a detailed graphical solution to the problem, see Figure 14.

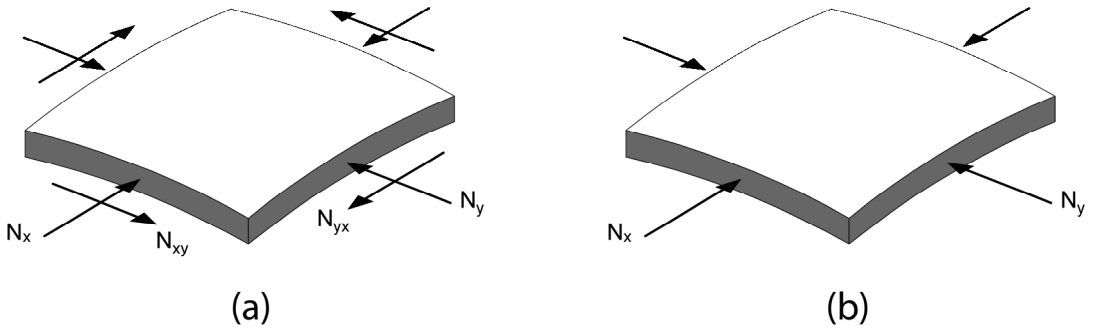


**Figure 13** Small element of the shell acted upon by the membrane stress resultants.

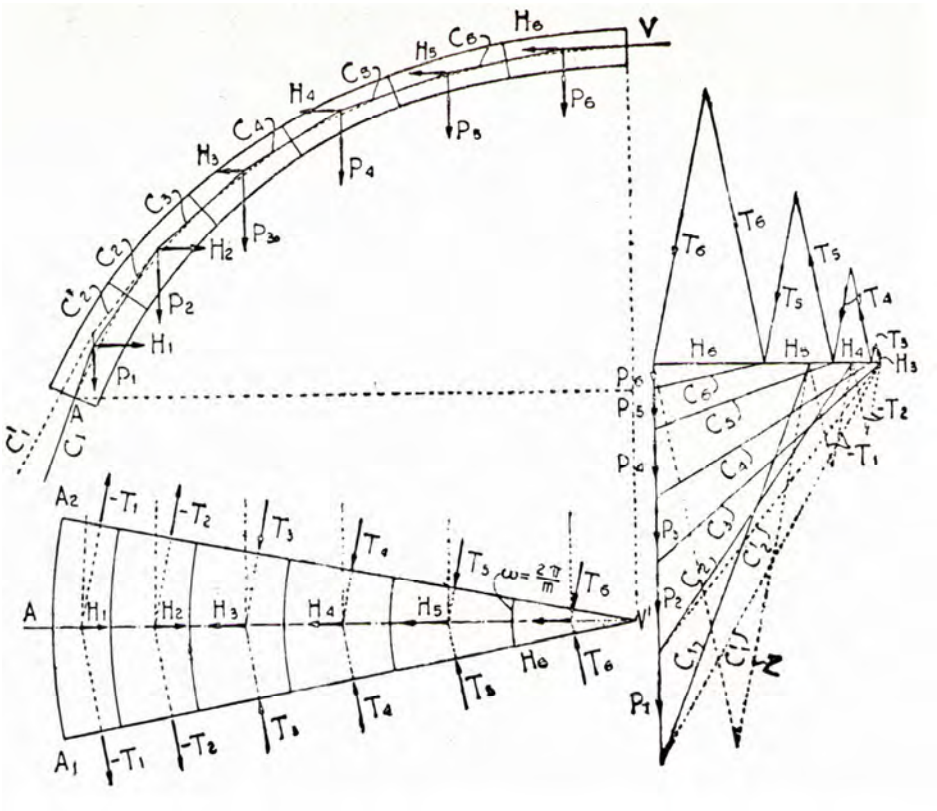


**Figure 14** Schwedler´s graphical construction. The part of the dome that is not considered has non-admissible hoop stresses (Schwedler, 1859) in (Tempesta et al., 2015).

Schwedler´s technique recognises a precise ring, which divides the superior compressed hoops and the inferior tensile hoop. This work was the membrane solution for axially symmetrically shells, both in form and load. One of the key aspects is that this technique applied the membrane stresses on the longitudinal and latitudinal lines.

In the first part of the 20th century, the theory was developed in works like (Saliger, 1932) with applications to different cases and shapes.

Later in the second half of the century, other works continued the evolution of the membrane analysis like (Flügge, 1960) and (Heyman, 1977) where all the stresses of the membrane are obtained through differential equations.

## 2.5. Eddy´s method

Henry T. Eddy (1878) developed a graphical method of analysis to obtain the membrane internal forces (both compressive and tensile hoop forces) in the hemispherical dome (Zessin et al., 2010). The method was about graphically determining the horizontal forces necessary for the arc loads to follow a

certain trajectory, see Figure 15. It is remarkable that the lune considered by Eddy did not have a defined angular opening.

As detailed in (Eddy, 1878) in its Chapter XV, the steps followed in Figure 15 for a metal dome (with negligible thickness) are:

- Height ab is divided in any number of parts $d_1$, $d_2$…, that he suggests to be the same height. The scale of the weight of the dome is such that matches the longitude ab.

- The first section a-$a_1$ is supported by a horizontal thrust in a, and a thrust in $a_1$ tangent at $a_1$.

- Drawing a line from a, parallel to the tangent to the sphere in $a_1$, it cuts a horizontal line from $d_1$ in $s_1$. a-$d_1$-$s_1$ is the triangle of forces that assures the equilibrium of voussoir a-$a_1$.

- Following similar steps, a-$u_1$-$t_1$ is the triangle of forces for the equilibrium of lune a-$g_1$.

- Considering a zone like $g_1$-$a_2$, the upper edge is subjected to a horizontal thrust of $u_1$-$t_1$, while the lower part has a horizontal thrust of $d_2$ – $s_2$. The difference of these thrusts is $s_2$-$x_2$, which generates a compression hoop in the segment proportional to $s_2$-$x_2$.

- If the lower thrust is bigger than the upper one, the hoop is in compression, otherwise the hoop is in tension. The differences of thrusts change sign at $t_3$. Being a colatitude of 51.8º.

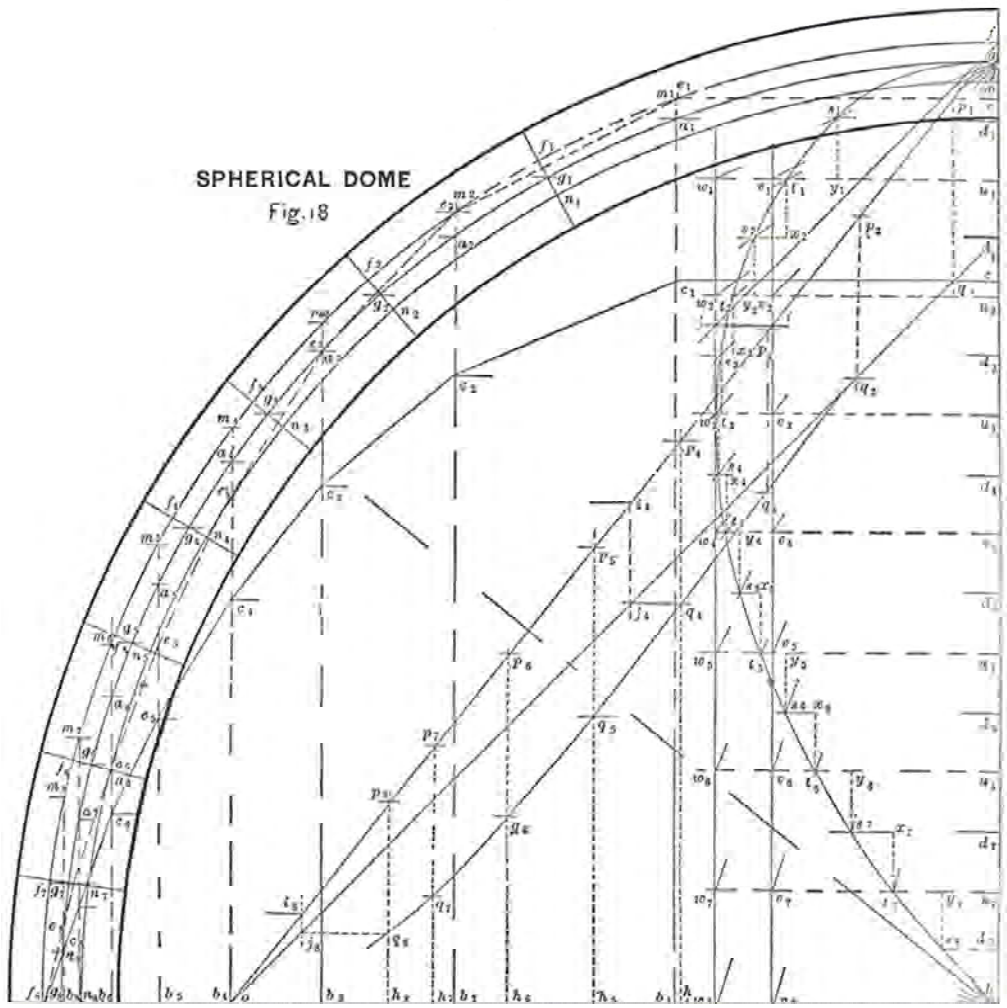


**Figure 15** Eddy´s graphical methodology to obtain membrane stresses (Eddy, 1878).

Eddy´s work in its Chapter XVI addresses the case of a masonry dome with a thickness of 1/16 of the internal diameter, and uses the same figure to analyse it. In this case the divisions of line a-b are only in points u, and points d generates horizontal planes that cuts the middle arc in points a, which are supposed to be gravity centre (if the meridian sections that generates the lune are close enough). Henceforth Eddy applies the slice technique (see section 2.2) and ensures stability by finding a funicular polygon (he names it *equilibrium curve*) within the inner third of the meridian section, and dismissing the hoop stresses. The process Eddy uses to find the *equilibrium curve* is cumbersome, but with which the curve $e_1$-$e_2$… is obtained.

Föppl (1881) adapted Eddy's method to masonry domes, considering in the upper part a state of membrane for the middle surface with compression internal forces according to the parallel rings, and from the point where tensions appear (that masonry cannot resist), he considers that the loads are transmitted according to the funicular of the vertical loads, Figure 16 (right).

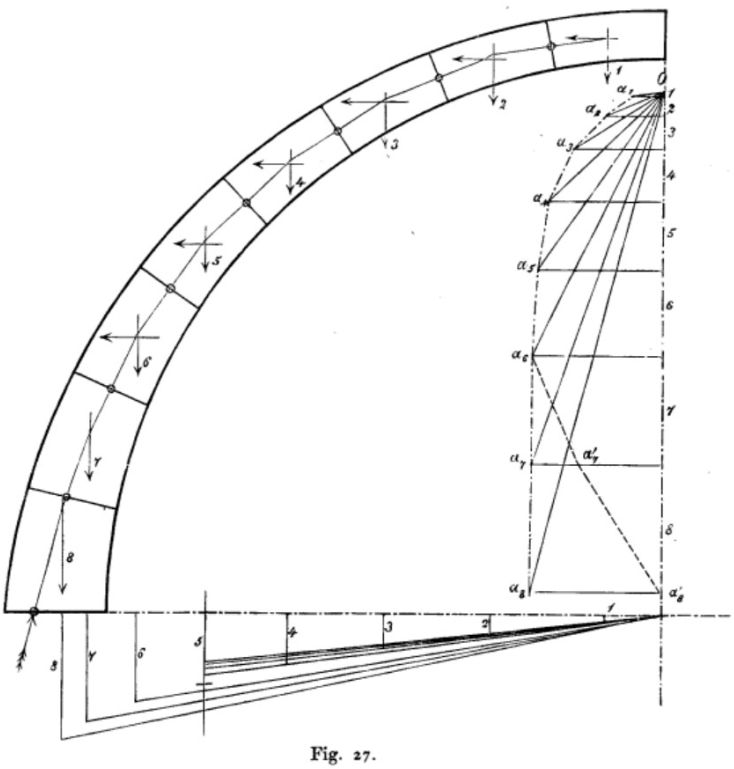


**Figure 16** Analysis of a masonry dome assuming a membrane compressive stress condition in the upper part (Föppl, 1881).

Eddy´s method was further developed by Lévy in his work *La statique graphique et ses applications aux constructions* … (Lévy, 1888) making it useful for domes of any shape or with a lantern, a detailed review of Lévy´s methodology is in (Tempesta et al., 2015) and (Galassi et al., 2017). Both Eddy and Lévy, considered that masonry domes could hold no tensile stresses, so their analysis adapted to this consideration, and design a methodology with compression hoop stresses (over certain hoop level) and no tensile stressed below it. This simultaneous structural behaviour, with compressed parallels at the top and no tensile parallels at the bottom, had already been predicted by Schwedler (1859).

Eddy's method became popular with Dunn's publications (1904) and (1908), where there are different cases of domes, see Figure 17; (a) hemisphere with angle of zero hoop stresses ring at 51°49´; (b) with oculus, angle > 51°49´; (c) with lantern, angle < 51°49´.

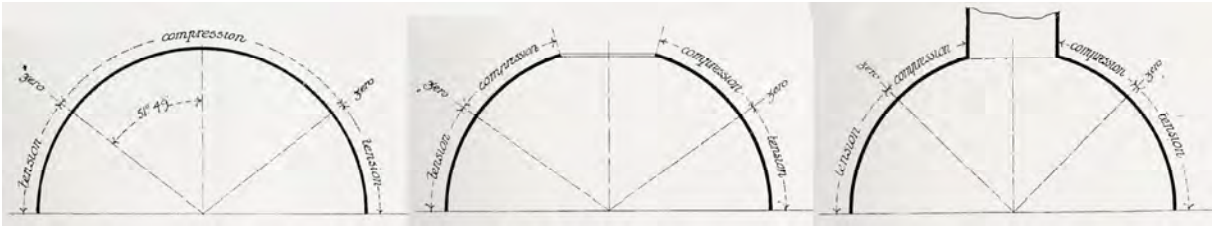


(a) (b) (c)

**Figure 17** Dome analysis with compression and tension sections for different hypotheses (Dunn, 1908); (a) Hemisphere; (b) hemisphere with oculus; (c) hemisphere with lantern.

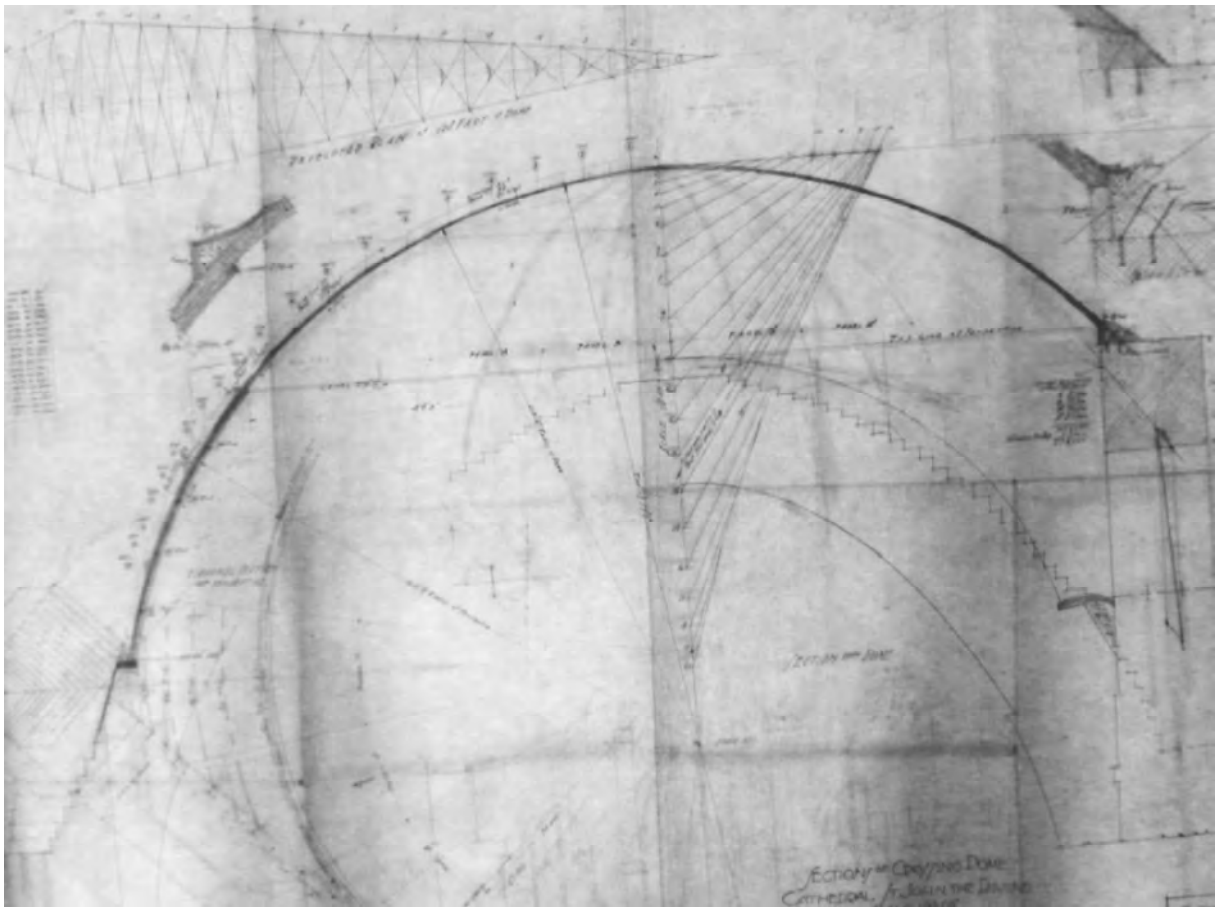

**Figure 18** Guastavino´s drawing of Saint John the Divine. The graphic method is seen on the right part of the drawing in (Dugum, 2013).

In 1909, Rafael Guastavino Jr. applied Eddy's method to calculate a large brick dome on the transept of the Cathedral of St. John the Divine, in New York, (Huerta, 2003). This dome and the graphic methodology of calculation have been analysed in (Dugum, 2013) and (Zawisny, Guastavino structural calculations. Doctoral dissertation, 2015), see Figure 18.

## 2.6. Guastavino´s experimental formulation

Rafael Guastavino (1842–1908) was an architect of special relevance, who along with his son Rafael Jr. (1872–1950), created some of the most important spaces in the United States (Ochsendorf & Freeman, 2010). Part of the renewed interest in masonry structures, and their structural behaviour, is also due to the rediscovery of Guastavino's impressive work. This is why this section addresses both his constructed work and his theoretical texts.

### 2.6.1. Guastavinos´ masonry vaults and domes

Rafael Guastavino Moreno and his son Rafael Guastavino Expósito managed to implement timbrel vaults in more than 1.000 buildings along the EEUU at the end of the 19$^{th}$ century and beginning of the 20$^{th}$.

In the last decades, there has been a growing interest in the work and theories of the Guastavinos´ constructions. This has led to an increasing number of works devoted to the analysis and study of their work and methodology of calculation and construction. The first milestone in the study of Guastavino´s work is in (Collins, 1968), where there is a complete inventory of the buildings where they worked and a compilation of the documents from the Guastavino Company. Some of the most interesting books and papers about the Guastavinos´ are (Collins, 1968), (García-Gutiérrez, 2000), (Huerta, 2003), (Loren, 2003), (Ochsendorf J. , 2005), (Huerta, 2006a), (Atamturktur & Boothby, 2007), (Ochsendorf J. , 2014), (Zawisny, Guastavino structural calculations. Doctoral dissertation, 2015), (Luengo, 2016), (Vegas, Mileto, & Cantero, 2017) and (Ochsendorf J. , 2020).

Rafael Guastavino Sr. was born in Valencia in 1842 and studied building in Barcelona (1861-1865). After finishing his studies, he did many works in Barcelona. In 1868, he started the remarkable Batlló factory, where he used the timbrel vault. From that moment, this technique would become central in his works. There is a detailed description of the works of this period in *La obra conservada de Rafael Guastavino Moreno en Cataluña. Estudio y análisis para su puesta en valor* [The preserved work of Rafael Guastavino Moreno in Catalonia. Study and analysis for its appreciation] (Luengo, 2016).

In 1871, after the Great Chicago Fire, there was an increasing demand for innovation and improving in the safety standards, which helped the success of the Guastavino fireproof tile vaulting technology.

In 1881, Guastavino Sr. went to New York with his son Rafael Guastavino Jr, and stablished his own company the Guastavino Fireproof Construction Company. In this year, he started his first big project, the Boston Public Library. This work gave him the popularity among architects that trusted in his expertise for important buildings within the Beaux Arts architectural movement. In 1885, Guastavino registered some patents that made his company a pioneer in the field of timbrel vaulting and by the early 1890´s, the company was working on major projects in Boston, New York, Chicago, Minneapolis and Providence at the same time (Kristen, 2018), see Figure 19.

**Figure 19** Construction of timbrel arches (Avery Library, Columbia University) in (Huerta, 2003).

Nevertheless, he was aware of the need to have a theoretical body that would support its practical knowledge in a demanding U.S. market. After some seminars and articles, he presented his theories in *Essay on the theory and history of cohesive construction applied especially to the timbrel vault* (Guastavino, 1893). In 1904, he published *Prolegomenos on the use of masonry in modern architectural structures, Part I and Part II* (Guastavino, 1896-1904).

In his texts, Guastavino insists in the idea of the cohesive construction and uses all kinds of examples, with greater or lesser success, to support his idea. He claims that cohesive construction (being timbrel vaults in this category) was monolithic and able to resist bending moments. He performed different tests, in real specimens, in 1880 and 1901 to back up his assumptions. He tried to obtain ultimate stress values for compression, tension, shear and bending. These values could then be used to verify the safety of his structures by comparing the working stresses with the material failure stress. The results of the tests were the following (Huerta, 2003):

- compression strength: 14.60 N/mm$^2$
- tension strength: 2 N/mm$^2$
- shear strength: 0.9 N/mm$^2$

In Guastavino´s texts, there were equilibrium equations to calculate the minimum thickness needed. See next section for an explanation of the Guastavino´s formulas.

Guastavino´s consideration of a monolithic behaviour of the timbrel vaults and domes is contradictory with the fact that they usually included metal rings to resist this thrust in his constructions (Huerta, 2003) and (Boothby, 2015).

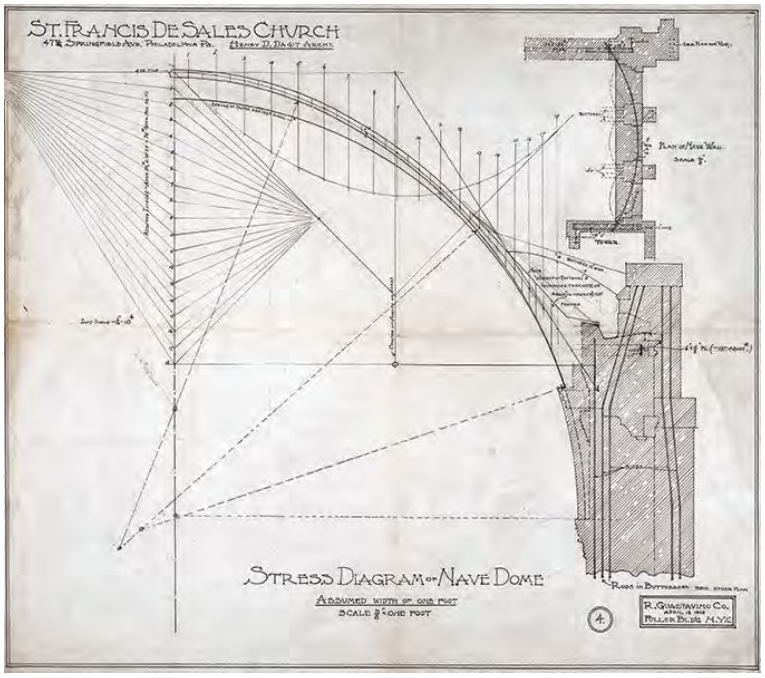


**Figure 20** Stress diagram in dome of Saint Francis de Sales in Philadelphia (Avery Library, Columbia University) in (Zawisny, Fivet, & Ochsendorf, 2017).

Guastavino Jr. did not attended a formal education, but he learned the technique since he was young, and he was always interested in developing innovations and adapting the graphic techniques to his projects.

It is clear that the Guastavino Jr used the funicular polygon to calculate the forces in his structures (thus, avoiding the monolithic behaviour and considering an equilibrium approach). In the dome section of St. Francis de Sales Church (finished in 1908), the section adapts to the thrust line in order to have a compression surface, and there are mechanisms to resist the thrust of the dome, see Figure 20.

In 1910 Guastavino Jr. was granted the patent nº 947 177 (submitted in 1908) in which he explains the process of reinforcing the domes with metal elements, see Figure 21.

An application of this system is in the dome of St. John the Divine Cathedral, with a span over 30 metres. This system is still linked to the tiled vaulting tradition, but is a predecessor of the thin shells that Torroja, Dischinger or Candela developed in the 20th century (Ochsendorf J. , 2005). A fully detailed architectural and structural analysis of this work is in (Zawisny, Guastavino structural calculations. Doctoral dissertation, 2015)

It is noteworthy that once the system was consolidated, Guastavino Jr. delved into other aspects such as the use of glazed ceramics, polychromy and acoustic conditions in his works (García-Gutiérrez, 2000).

The work of the Guastavinos is still being investigated, as new works in which the company participated continue to appear, and their bold contributions to the development of masonry structures continue to be analysed.

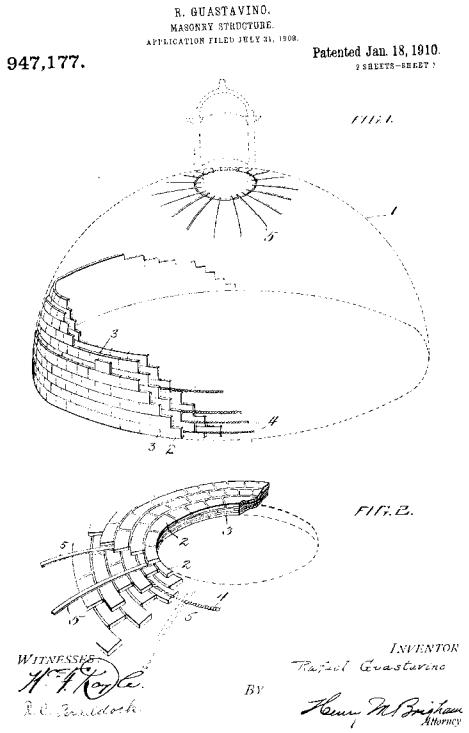


**Figure 21** Patent 947,177 for a masonry dome reinforced.

Assessing the safety of Guastavino structures remains a challenge today, but they have demonstrated to be safe enough to resist for more than a century.

"The engineering calculation of thin masonry shells presents an open challenge, and the engineer must find three-dimensional compressive solutions that lie within the thickness of the masonry" (Ochsendorf J. , 2014). This thesis, along with many other authors seeks to find new methodologies, accurate enough to explain the behaviour of thin masonry domes.

### 2.6.2. Guastavino´s formulation

In Guastavino´s book *Essay on the theory and history of cohesive construction applied especially to the timbrel vault* (Guastavino, 1893), he presented methods of calculation and design for timbrel vaults with which, as he himself indicates, he does not intend a rigorous mathematical formulation, but a practice for safe construction. Considering the equilibrium in vaults under constant distributed load, he obtains approximate formulas to apply to vaults subjected to its own weight (Guastavino, 1893) and (Huerta, 2003).

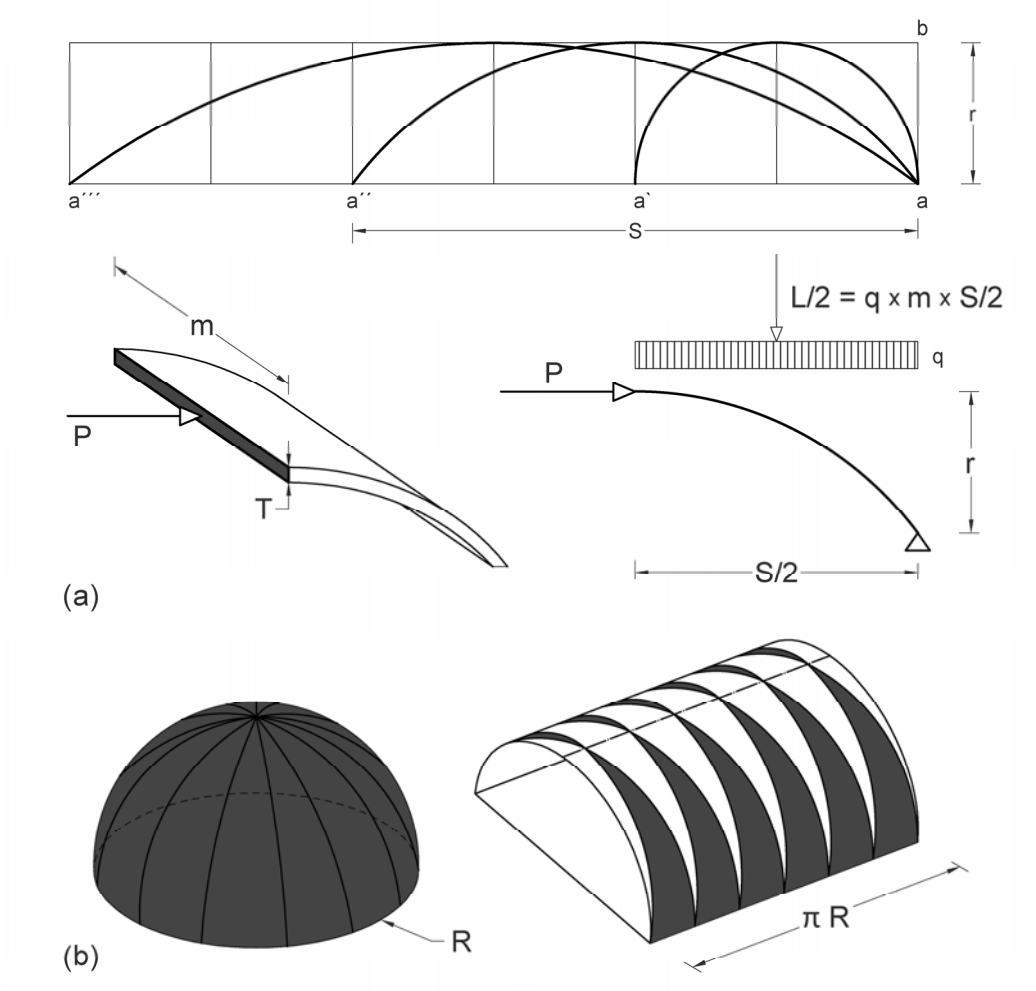


**Figure 22** Guastavino´s analysis. (a) Forces equilibrium in the vault; (b) analogy between the hemispherical dome and a cylindrical vault loaded only in half a surface (Suárez, Boothby, & González, 2020).

Being:

- ***S*** (m): span;
- ***r*** (m): rise;
- ***P*** (kN): crown thrust, Figure 22(a);
- ***L*** (kN): load;
- ***T*** (m): thickness;
- ***C*** (kN/m$^2$): coefficient for compression; material strength that Guastavino advises to divide by 10 as a safety factor.

The thickness of the vault in the keystone must be enough to allow the material to develop a value of the transverse thrust that must be in equilibrium with the moment of the vertical load. Guastavino considers an evenly distributed load, which would contrast with the different thicknesses of a usual flat top filling.

Consequently, considering moments respect to the support of the thrust and the load, and making them equal, see Figure 22(a), we have the equation:

$$\frac{L}{2} \cdot \frac{S}{4} = P \cdot r \tag{1}$$

Considering that the value *P* (crown thrust) is equal to the *C* times the transversal area:

$$P = m \cdot T \cdot C \tag{2}$$

Substituting terms and considering m=1 metre, we obtain the well-known Guastavino's formula (Guastavino, 1893).

$$T\,C = \frac{L\,S}{8\,r} \tag{3}$$

Guastavino gives an example of application of this formula with the following data (Anglo-Saxon system): ***S*** = 15 ft; ***r*** = 1.5 ft; ***L*** = 250 lbs/ft$^2$; ***C***=2120 lbs/in$^2$.

With these values, the thickness needed is 1.85 inches, which is similar to the thickness of two bricks. It is probable that the safety factor of 1/10 that Guastavino proposed, was just to obtain the desired results of a two-layer thickness. Moreover, Guastavino concedes that this safety factor is disproportionate, and admits values of 1/4.

For a hemispherical dome with radius R, Guastavino considered couples of spherical segments on a semi-cylindrical surface with radius R and height πR, as indicated in Figure 22(b), considering roughly the surface of half cylinder equal to twice the surface of the hemispherical dome.

Considering the analogy with a cylindrical vault loaded only in half of its surface, the minimum thickness of hemispherical dome will consequently be half the necessary thickness in the vault of the same radius, which is:

$$T \cdot C = \frac{L \cdot S}{16 \cdot r} \qquad (4)$$

The assumptions for the dome are just an approximation, because the gravity centre is different, so is the weight. Still these are safe assumptions (Huerta, 2001).

The application of the experimental formulas of Gaustavino is analysed in (Huerta, 2006a) and (Redondo, 2013).

## 2.7. Graphical methods at present

The outlined equilibrium methods in precedent sections were considered approximate by the engineers of the time, strongly conditioned by the elastic theory (Huerta, 2004).

Nonetheless, although it was possible to analyse an elastic arc, the elastic analysis of spatial structures was beyond the scope of manual calculation. It is noteworthy that, after World War II, the graphical equilibrium analysis methods were used again to analyse the vaults and ruined buildings before their reconstruction; this is the case, for example, of the vaults of the Cathedral of Xanten and of numerous churches and buildings rebuilt by (Pieper, 1983).

### 2.7.1. The slicing technique in the frame of limit analysis

In the second half of the 20th century, Heyman (1966), (Heyman, 1967) and (1977) presented, for the first time, the slicing technique, within the theoretical framework of limit analysis, to find collapse mechanisms of masonry structures, provided the following assumptions could be made (Heyman, 1966):

- Sliding failure does not occur. This can be thanks to the friction or interlocking of the parts.
- The material has an infinite compressive strength. This is an *unsafe* assumption. Nonetheless, this type of structures have generally a low level of stress.
- The material is incapable of carrying tension. This assumptions is clearly a *safe* assumption, and may be too conservative in some circumstances.

If these assumptions are made, we can analyse the masonry structure with the two basic theorems of limit analysis.

**Theorem 1**, lower-bound theorem or safe theorem, which implies that if it can be found a thrust line, in equilibrium with the external loads, within the masonry, the structure is safe.

**Theorem 2**, upper-bound theorem or unsafe theorem, which means that the collapse will take place if there is a hinge in unstable equilibrium.

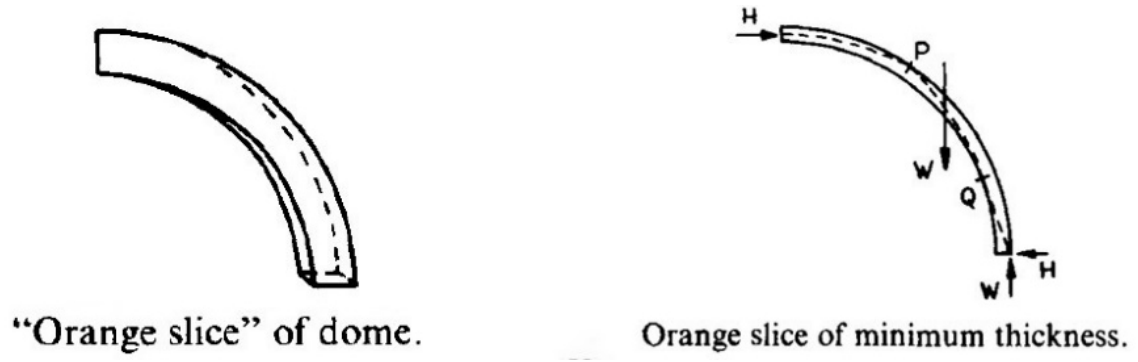


**Figure 23** Heyman applies the same techniques from the arch to an "orange slice" to find the minimum thickness with hinges in P and Q (Heyman, 1967).

The slicing technique considers the dome divided into segments, by cuts along meridian planes, and considers the stability of each two opposite parts as an arc. It does not consider the influence on the stability of parallel forces (Figure 23). Considering that it is a two-dimensional technique, is therefore most appropriate for the analysis of arches, flying buttresses or any structure, which can be reduced to a sectional analysis (Nikolinakou, Tallon, & Ochsendorf, 2011).

The slicing technique is the basis of countless modern studies of stability of structures in historical buildings.

Chapter 3 offers a deeper insight into limit analysis, and section 4.4.3 explains the procedure to find the thrust line in a masonry arch.

### 2.7.2. Trust network analysis

O´Dwyer (1999) sets out for the first time, the modelling of masonry vaults as a discrete network of forces in equilibrium with gravitational loads.

The methodology *Thrust Network Analysis* (TNA), laid out in (Block & Ochsendorf, 2007), (Block P. , 2009) and (Block, Laucher, & Rippmann, 2014), extends O´Dwyer´s Force Network Method. The methodology is based on the thrust line analysis and graphical methods, for the analysis of complex masonry vaults and generate compression-only vaulted surfaces and networks.

According to (Block P. , 2009), the TNA uses reciprocal figures to relate the geometry of the spatial networks to their internal forces. The primal figure Γ, represents the horizontal projection of the network topology. The dual figure Γ* represents the distribution of the forces in the system (Figure 24).

The spatial solution takes into account that the nodes are constrained by a lower and upper bound, as well as the supports positions.

In (Marmo & Rosati, 2017) a reformulation of the TNA is set forth, which includes horizontal forces, holes or free edges in the vault.

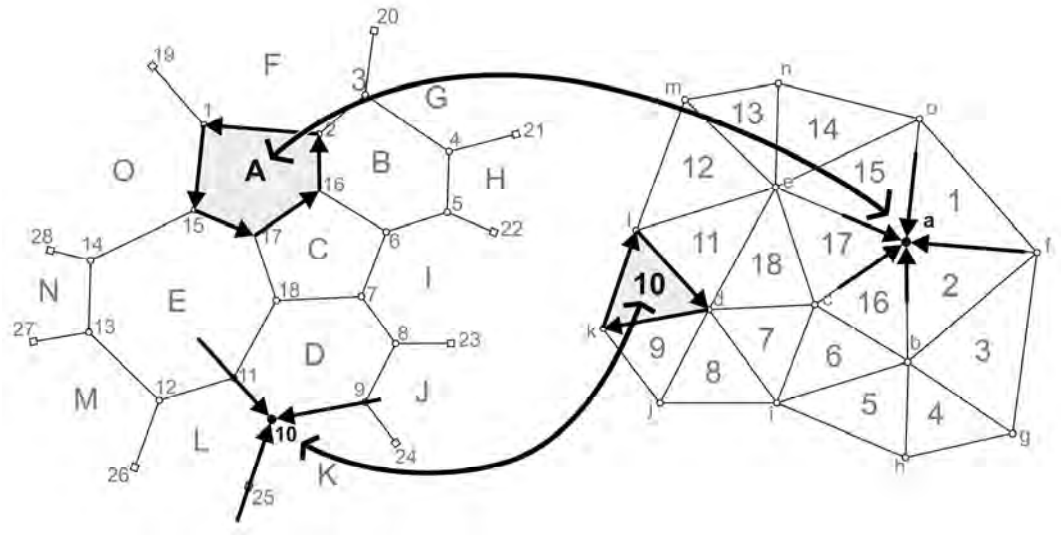


**Figure 24** The primal grid Γ and dual grid Γ∗ are related by a reciprocal relationship. The equilibrium of a node in one of them is guaranteed by a closed polygon in the other and vice versa. The labelling uses Bow's notation (Block P. , 2009).

### 2.7.3. Other current works

Erhard Scholz (1989) gives a modern account of Culmann's attempts to bring out the projective geometry character of the graphical calculations that he developed in *Die Graphische Statik* [The graphic statics] (Culmann, 1875).

Zalewski & Allen (1998) and Boothby (2015) present examples of graphical methodologies to solve structural design problems.

Block and Ochsendorf, along with other contributors, have done important developments for structural analysis of historical constructions, based on the limit analysis; in (Block, Ciblac, & Ochsendorf, 2006) is presented a real-time limit analysis of vaulted masonry buildings to predict possible collapse modes by combining kinematics and statics.

Todisco, Corres, & Mueller (2016) presented an original methodology on the basis of graphic statics, to transform a non-funicular geometry into a funicular one, through external posttensioning systems.

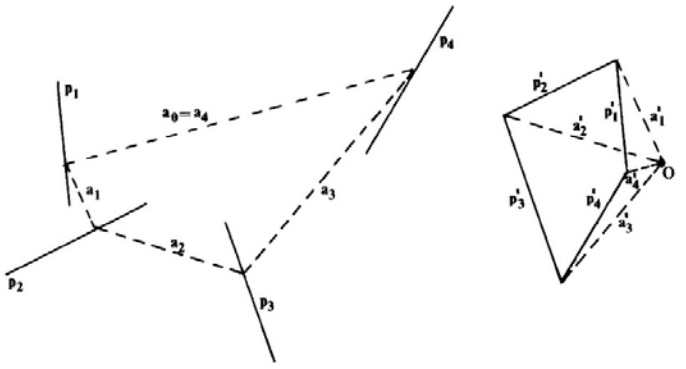

**Figure 25** Polygon and rope method in the plane (Scholz, 1989).

## 2.8. New graphic methodology

This dissertation proposes a new graphic methodology based on the combined use of funicular and projective geometry, for the quantitative determination of internal forces in revolution domes. It is a new tool for the analysis of historical constructions based in Thrust Network Analysis presented in section 2.7.2, and incorporating other notions from projective geometry to make a more comprehensive method for the analysis of certain classes of structures.

The methodology is presented through its application to a hemispherical brick dome of small thickness, considering different structural situations: complete hemisphere, hemisphere with oculus on the top, and hemisphere with lantern, and different inclinations of the reaction in the support.

The hemispherical dome is discretised into sectors by lines of latitude and longitude, considering the weight of each sector applied at its gravity centre (nodes). Thus, the dome generates a network which equilibrium is analysed in both the horizontal and vertical projection.

Firstly, the methodology is laid out by dividing the hemisphere in 160 sectors, cutting by 10 horizontal planes and 8 vertical planes, with the aim of enhancing the graphic constructions. Afterwards, a model with 640 sectors has been tested, in order to compare the results with the ones from the membrane analysis.

Multiple solutions for the internal forces, acceptable for the material, are obtained, whose equilibrium is guaranteed by this graphic methodology.

The new graphic methodology considers the hoop stresses for the equilibrium of the internal forces; therefore, it is a less conservative method than other graphic methods widely used today.

Additionally, the new methodology allows its application in the inverse way, namely, considering variations in the internal forces, and checking that they imply very little variations of the geometry of the simplified model, relative to the dome thickness.

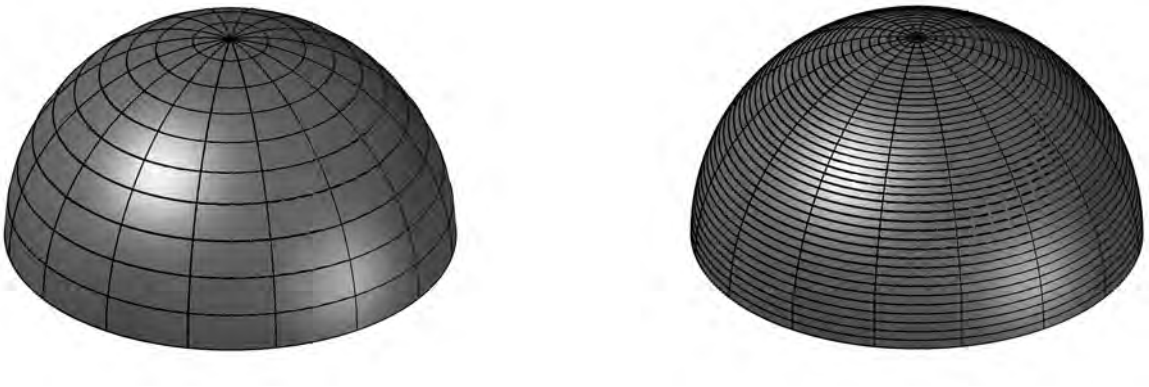

**Figure 26** 3D models of the discretised hemisphere. (left) 160 sectors; (right) 640 sector.

# Chapter 3

# Limit analysis

Following (Huerta, 2004), (Heyman, 1969) and (Heyman, 2015), this chapter outlines the foundations and historical development of limit analysis in masonry structures.

## 3.1. Thrust line

In accordance with (Heyman, 1966), (Huerta, 2004) and (Georg, 2012); it was Moseley´s works (1843a) and (1843b) where it is first raised a general principle to fix the thrust line position and to obtain a geometric safety factor. Moseley had previously proposed the principle of least resistance in (Moseley, 1833) by which the thrust line would be the one generating the least thrust at the springers. There is a detailed analysis of Moseley´s approach in (Alexakis & Makris, 2014).

Huerta (2004) and Andreu (2006) state that a similar principle to Mosely´s was developed at the same time in Germany by Gerstner (1789) and in France by Méry (1840).

Poncelet (1852) made a progress when proposing the use of the plastic properties for masonry arches instead of the rigid assumptions, in order to find the *true* thrust line.

This theory was further developed by Saavedra (1860), Castigliano (1879), but probably the most influential was Winkler in his work *Die Lage der Stützlinie im Gewölbe* [The position of the supporting line in the vault] (1879-1880).

Nevertheless, the *real* thrust line was only possible when considering an ideal state of the arch, loads and material, which all engineers at the time knew it was impossible due to imperfections, changing conditions and loads etc… (Engesser, 1880).

As laid out in (Huerta, 2004) and (Heyman, 1988), there were important attempts to demonstrate the elastic behaviour of masonry arches and other structures. In 1895, the Association of Austrian Engineers and Architects carried out numerous tests on large masonry arches to verify their elastic behaviour. The collapse followed the old equilibrium theory though. However, they could see some kind of proportionality between loads and deformation.

Sir John Fleetwood Baker conducted another series of test in 1930 in the UK. The tests were made for steel frames, and they found that there were differences between the theoretical and the real models. They concluded that minor differences, impossible to be avoided, lead to very different states of the structure. That made the structure stability problem to be approached from another perspective, being the starting point of the limit analysis.

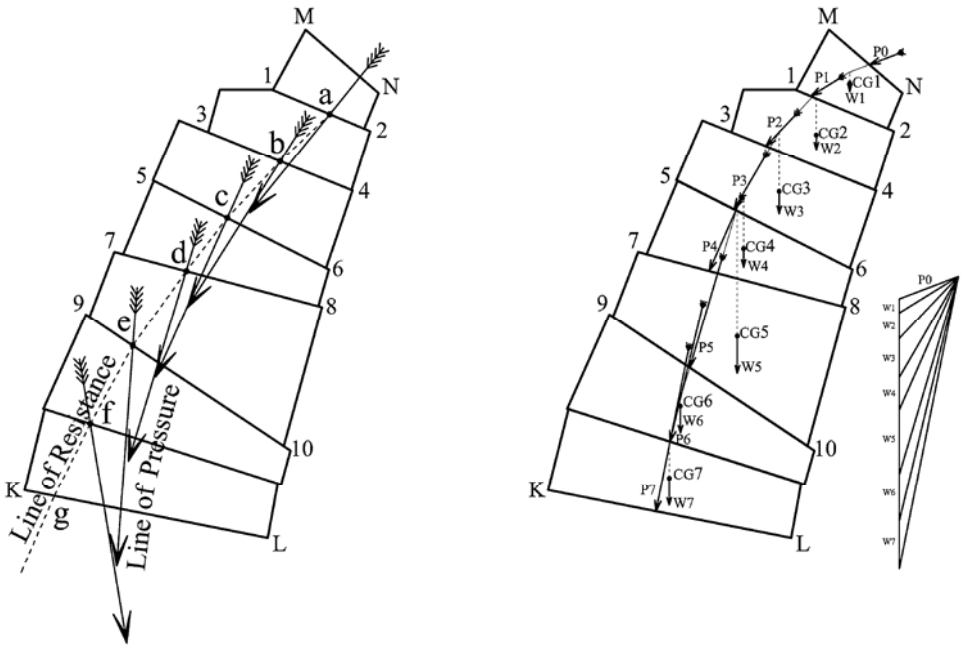


**Figure 27** (left) Conceptual drawing presented by (Moseley, 1843a); (right) analysis of Moseley´s approach in (Alexakis & Makris, 2014).

New tests revealed that despite the real state of the structure is sensitive to slight changes; nonetheless, this is not the case with the collapse load, which depends on the shape and dimensions of the structure.

As commented in section 2.7.1, Heyman (1966) states the basic assumptions to apply limit analysis in masonry structures: the material has an infinite compressive strength; the material is incapable of carrying tension; sliding failure does not occur.

With these assumptions professor Heyman has linked the positions of the line of thrusts to the yield of the supports and the cracks in the arches. To illustrate this, (Huerta, 2004) presents the cracks patterns of a model of an arc with some movements in their support, see Figure 28.

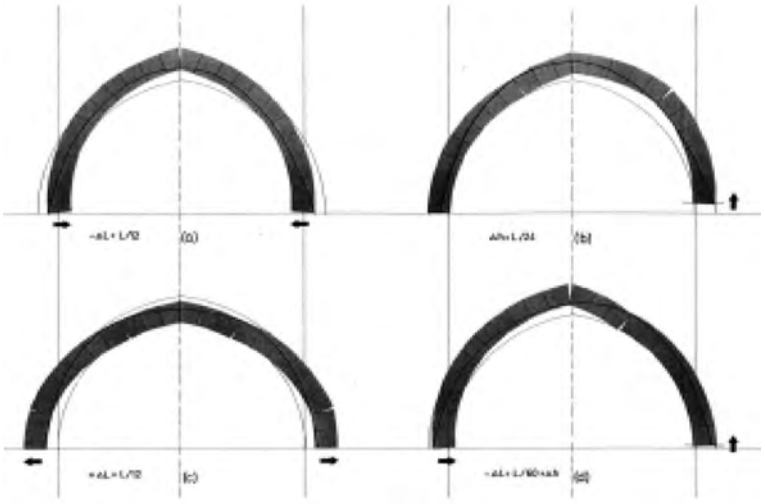

**Figure 28** Test in a model to show the plasticity of masonry arches (Huerta, 1996)

## 3.2. Collapse mechanism in arches

Hinges appear when the thrust line touches the limits of the masonry and the entire section is cracked. Cracking is not dangerous in itself, as it is the way in which the structure can adapt to changes in the conditions (Ochsendorf J. A., 2002). The structure falls when the number (and position) of collapse mechanism kinematically possible are enough.

In 1729, Pierre Couplet published *De la poussée de voûtes* [The thrust of arches] and a year after a second part of it (Couplet, 1729) and (1730). In his second work, he stablished the three assumptions needed for a correct analysis of masonry vaults and arches: masonry has no tensile strength; infinite compressive strength; sliding failure cannot occur (Heyman, 2009). He even anticipated that if the thickness of the arch were small enough (least thickness), it would develop a five-hinge mechanism with hinges at 45º. This approach was expanded by (Danyzy, 1732). In 1810, Louis Boistard performed a series of new tests in arches that were considered as a proof of the existence of the collapse mechanisms.

As the steel and concrete structures became predominant, the theoretical interest in masonry structures decrease. However, due to the increasing loads of vehicles, new tests were performed in arches to assure their stability. All the results confirmed what was known 200 years ago, that arch collapse was due to collapse mechanisms in hinges and not to the material failure.

(Heyman, 1995, b) clarifies the collapse mechanism in an arch, due to a punctual load, in a semicircular arch, using the analogy to Hooke´s hanging chain that is modified by the load. As the load increases, the chain comes closer to the edge, until it touches the edges in four points and creates a collapse mechanism kinematically possible. This last property makes that some type of arches (linteled arches), cannot create a collapse mechanism, so the only way they collapse is due to the failure of the abutments.

## 3.3. Fundamental theorems

The theoretical development of the plastic theory, initially formulated for steel structures, led to three fundamental theorems (Kooharian, 1952).

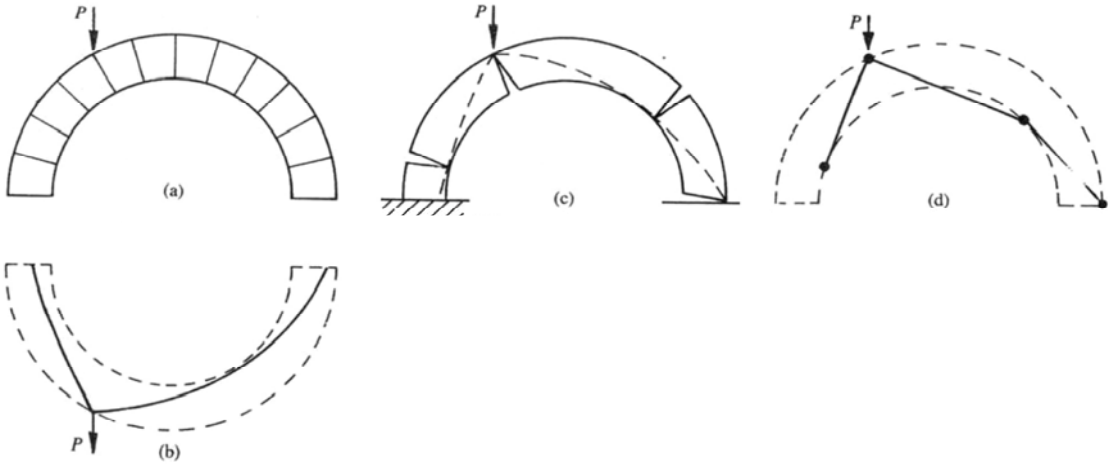


**Figure 29** Collapse mechanism of a semicircular arch with a load (Heyman, 1995, b).

- **Lower bound theorem** or safe theorem (equilibrium): If a statically admissible state of stress can be found for the loads, the structure will not collapse (static approach).
- **Upper bound theorem** or unsafe theorem (mechanism): If a kinematically admissible mechanism can be found, for which the work of external forces is greater or equal to zero, the structure is unstable (kinematic approach).
- **Uniqueness theorem**: If both conditions are satisfied by a given load factor, this represents the collapse load factor.

The conditions that the masonry has to meet to be able to apply the previous theorems, were first set out by Heyman (1966): the material has an infinite compressive strength; the material is incapable of carrying tension; sliding failure does not occur.

When applying this theory to arches, the main consequence is that if a thrust line lays within the masonry section, the masonry arch is safe. There can be infinite thrust lines for a given arch and a given set of forces, but if it possible to find one within the section, it can be said that the arch will not fall.

Section 2.7.1 explains the application of these theorems and conditions to the analysis of domes by means of the slicing technique.

## 3.4. Safety in arches

As mentioned before in this chapter, it is not possible to find the *real* thrust line. Little changes in the in the boundary conditions or the contact between voussoirs, may change the position of the line of thrust, although it does not affect the arch integrity. Nevertheless, it is crucial to define a safety factor that helps to understand the level of security of a masonry arch.

### 3.4.1. Geometric safety factor

The safe theorem states that if the thrust line is contained everywhere within the masonry, the structure is safe. When internal forces stay away from the centroid, tensile stresses may cause a crack on the opposite side (Ochsendorf J. A., 2002).

To clarify this concept, it can be considered an arch thick enough to find easily different thrust lines within, as in Figure 30(a). If the thickness decreases, it comes the moment that only one thrust line lies within, as in Figure 30(b); this is the *limit arch* with five points where the thrust line touches the edges. Figure 30(c) shows five hinges, which is enough to create a mechanism kinematically possible.

Heyman (1969) proposed a geometric safety factor, which consists in dividing the thickness of the arch with that of its limit arch. The arch in Figure 30 has double the thickness than the limit arch, so its geometric safety factor is two.

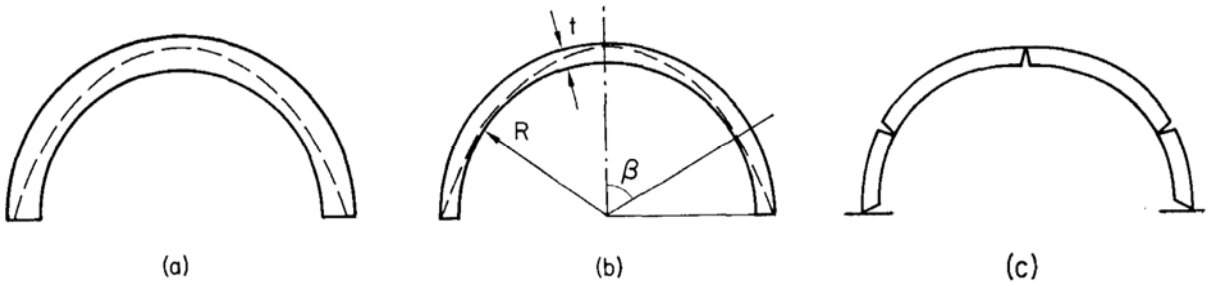


**Figure 30** (a) Thick semicircular arch; (b) semicircular arch of least thickness; (c) crack pattern for arch of least thickness (Heyman, 1969).

# Chapter 4

# Funicular geometry

Graphical methods allow the designer to generate and analyse structures in a very comprehensive way, and shed light on structural concepts that equations hide under symbols alien to engineering or architectural practice. Accordingly, this chapter analyses the basics of funicular geometry that will serve as the foundation of the new methodology.

## 4.1. Modelling forces. The parallelogram rule

The resulting force R obtained by means of the graphic construction indicated in Figure 31(a), can replace two forces P1 and P2 acting on a particle A.

From the parallelogram law, the sum of two vectors can be found graphically, placing both vectors from end to end, and joining the tail of the first with the end of the second, as indicated in Figure 31(b).

To add up the vectors of a coplanar system, the successive application of the triangle law is equivalent to the formation of the force polygon, as indicated in Figure 32(a). Inverting the direction of the resultant MN in the force polygon creates a closed polygon in which each vector in the inverted direction is equal to the sum of the others.

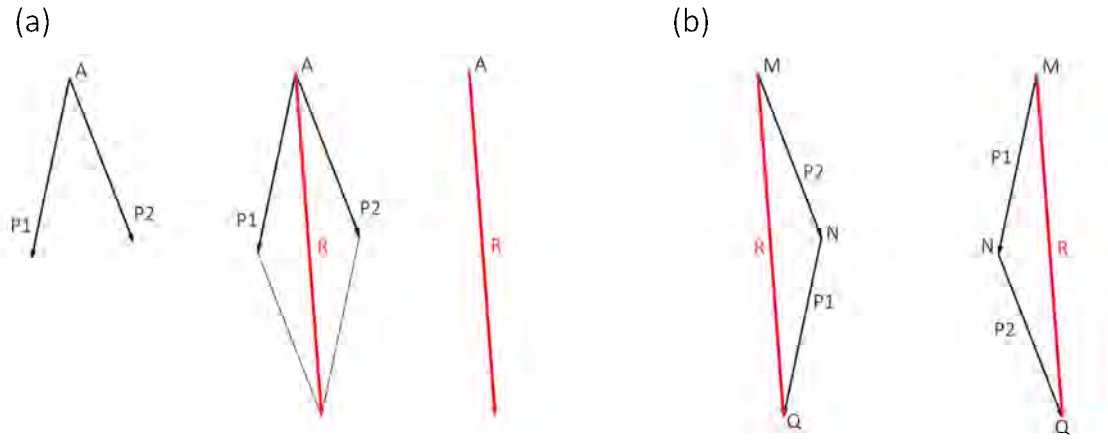


**Figure 31** (a) Polygon of forces acting on a particle A; (b) triangle law in forces.

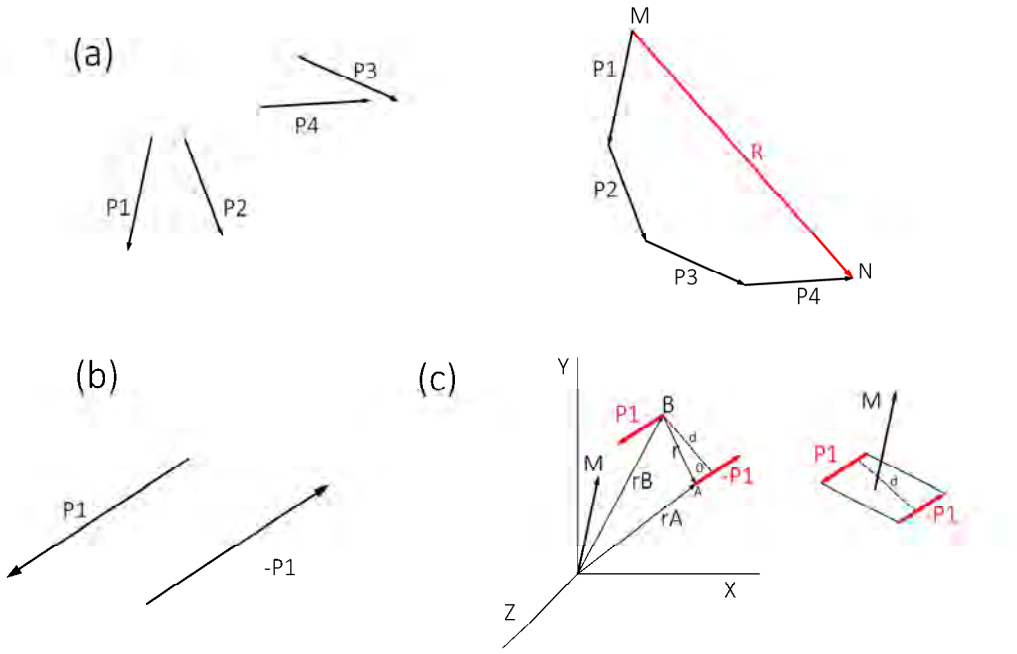


**Figure 32** (a) Addition of vectors; (b) couple of forces; (c) moment of a couple.

### 4.1.1. Moment of a couple of forces

Two forces of equal magnitude, parallel lines of action and opposite directions form a *couple*, Figure 32(b).

The resultant of the forces is equal to zero, but not the sum of the moments of the two forces respect to a point. The pair of forces does not cause translation of the body on which it acts, but it does tend to rotate it, Figure 32(c). The sum of the moments of the two forces *P1* and *–P1* with respect to point O is:

$$rA \cdot P1 + rB \cdot (-P1) = (rA - rB) \cdot P1 \quad (5)$$

If $r = rA - rB$, where r is the vector that joins the points of application of the forces, it is concluded that the sum of the moments of F and –F with respect to O, is represented by the vector $M = r \cdot P1$.

The vector M is called the *couple moment*. It is perpendicular to the plane containing the two forces and its magnitude is given by $M = r \cdot P1 \cdot sin\theta = P1 \cdot d$, where d is the perpendicular distance between the lines of action of the forces. The direction of M is defined by the right-hand rule. Vector M is a free vector, which can be applied at any point, see Figure 32(c).

Equilibrium in a system of forces happens if the following two conditions are met:

- The resultant of the forces is equal to zero.
- The resulting moment with respect to an arbitrary point is zero.

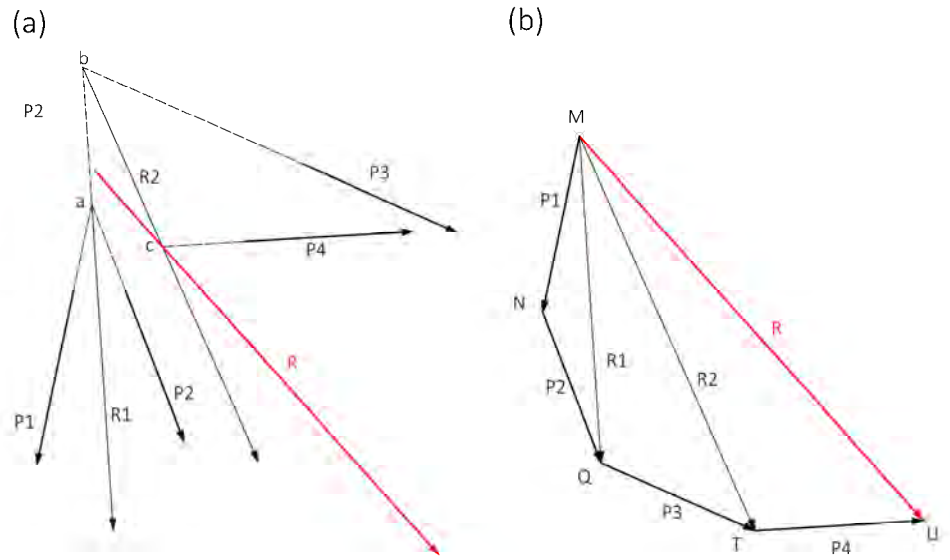


**Figure 33** (a) Resultant of a group of forces; (b) force polygon with the sum of forces every two.

### 4.1.2. Reduction of a system of forces

Any system of forces can be reduced to an equivalent force-torque system that acts at a given point O.

In Figure 32(a) the force polygon allows to obtain the direction and magnitude of the resulting force for a group of forces. In order to obtain the application point that produces an effect mechanically equivalent to the sum of the four forces P1, P2, P3 and P4 as indicated in Figure 33(a), it can be obtained by partial resultants of two in two forces. The sum of the forces has been done in the polygon of equivalent forces in Figure 33(b).

First, the forces P1 and P2 are extended to the point a, where the resultant R1, which comes from adding P1 + P2, is applied. This resultant R1 cuts the line of action of P3 in b, where the resultant R2 is applied (R2 is the sum of R1 + P3). This resultant R2 cuts the line of action of P4 in c, where the total resultant R is applied, see Figure 33(a).

## 4.2. Equilibrium of a system of forces with the funicular polygon

### 4.2.1. System of two forces

With the method presented in section 4.1 it is possible to obtain the resultant of any system of concurrent forces. However, for forces with a meeting point outside the graphic area, the force polygon determines the value of the resultant and the funicular polygon its position.

Having P1 and P2, the process to form the funicular polygon is the following (Figure 34):

- Create the force polygon with vertex M, N, Q, which offers the resultant R. (This force polygon has a scale of 1/2).
- The pole O is arbitrary.
- Lines MO, NO, QO are the *polar rays*.
- Starting from an arbitrary point a, the line parallel to the polar ray 1 is drawn, until it cuts the line of action of P1 at point b; through point b is drawn a line parallel to the polar ray 2 until cutting the line of action of P2 at point c; through c is drawn a line parallel to the polar ray 3 obtaining d.
- The abcd polygon is called the *funicular polygon*, which has its vertices on the lines of action of the forces, and the sides parallel to the polar rays.
- Considering P1 and P2 decomposed in the vectors 1, 2 and 3 (parallels to the polar rays), the system can be reduced to vectors 1 and 3 that meet in point e, which is a way point for the resultant R. See Figure 34(c).

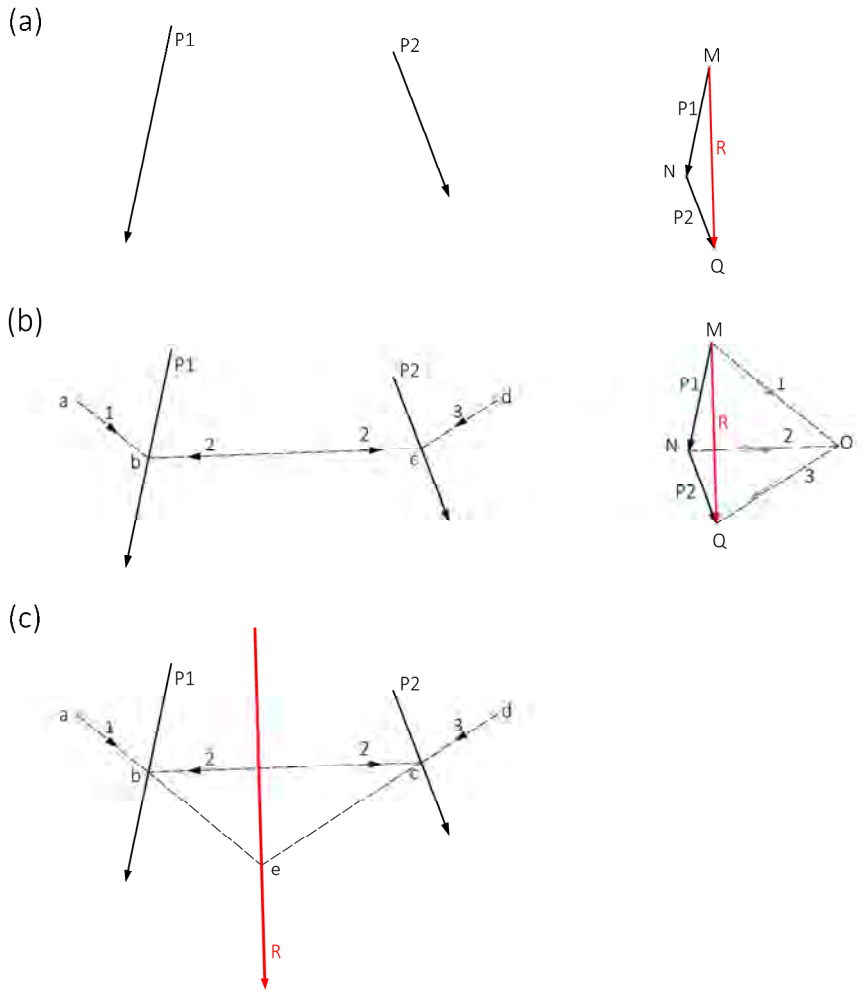


**Figure 34** (a) Starting data and force polygon; (b) polar rays and funicular polygon; (c) resultant. Scale of force polygon ½.

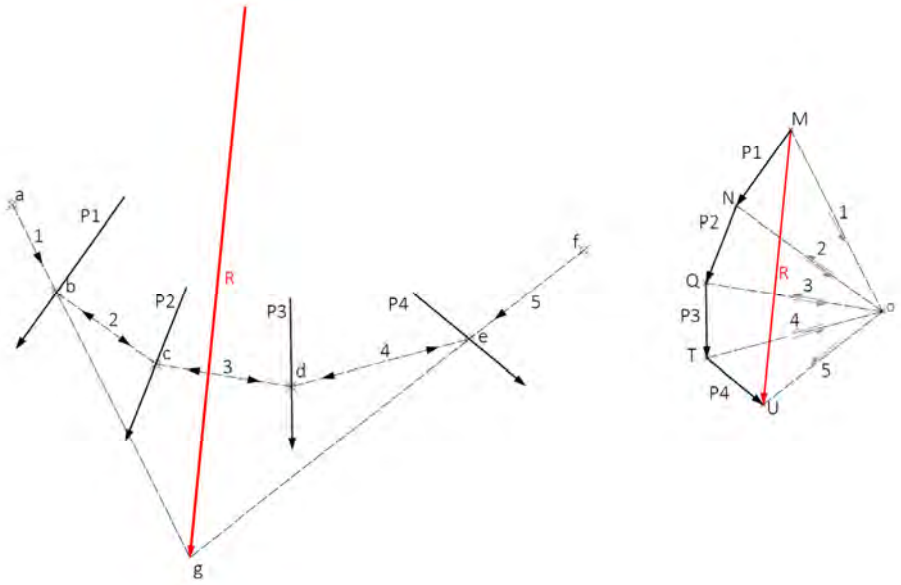


**Figure 35** Funicular polygon for multiple forces like P1, P2, P3, P4. Scale of force polygon is ½.

### 4.2.2. Multiple forces with open force polygon

A case with four forces P1, P2, P3, P4 is analysed in Figure 35. The process is similar to the previous section with two forces. In this case, the force polygon is open, that is, there is a resultant R with a point of application in point g, which is at the intersection of the first and last lines of the funicular polygon (lines 1 and 5).

### 4.2.3. Multiple forces with closed force polygon

If the force polygon is closed, as in the cases below, there will be no resultant force, so the system will be in equilibrium or with a resulting moment.

Figure 36(a), (b) show two systems of forces with the same force polygon in Figure 36(c), but in (a) the funicular polygon has forces 1 and 4 that create a moment with a lever arm h. Whereas in (b) the funicular polygon is closed and therefore creates no moment.

In summary, in the composition of forces, there are three possible cases and they can be studied using the general procedure of the funicular polygon:

- **Open polygon** of equivalent forces, from which there is a resulting force, and the system is not in equilibrium.
- **Closed force polygon and open funicular polygon**. The system is equivalent to a couple of forces, and is not in equilibrium.
- **Closed force polygon and closed funicular polygon**. The system is in equilibrium.

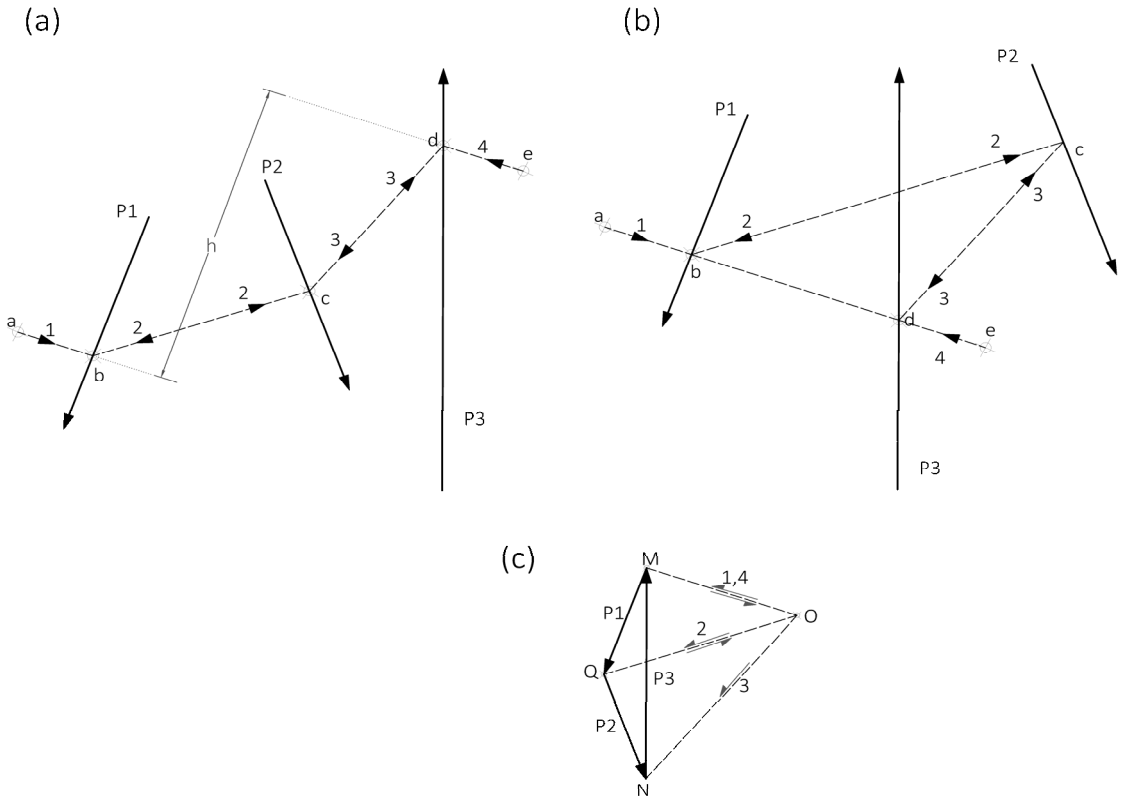


**Figure 36** (a) System of forces with a moment; (b) system of forces in equilibrium; (c) same closed polygon in both cases.

### 4.2.4. Equilibrating a system of forces with two forces with a pre-set direction

Having the system with forces P1, P2, P3. Figure 37 presents the problem of finding two reactions (Ra, Rb) with pre-set directions.

The force polygon must be closed to have a system in equilibrium, it can be achieved by drawing parallel lines to the given directions (Ra, Rb) at the end of the resultant R; these lines will meet in point C, see Figure 37(c).

The funicular polygon will be drawn as in the previous section, from an arbitrary point A, and with lines parallels to the polar rays 1,2,3,4 as seen in Figure 37(b).

The reactions Ra and Rb in the funicular polygon have to make it a closed polygon in Figure 37(b), (c), to avoid the moment in the funicular polygon. Therefore, if the funicular polygon starts in point A, the reaction Rb will be at the meeting point B, of line 4 with the parallel to OC from A.

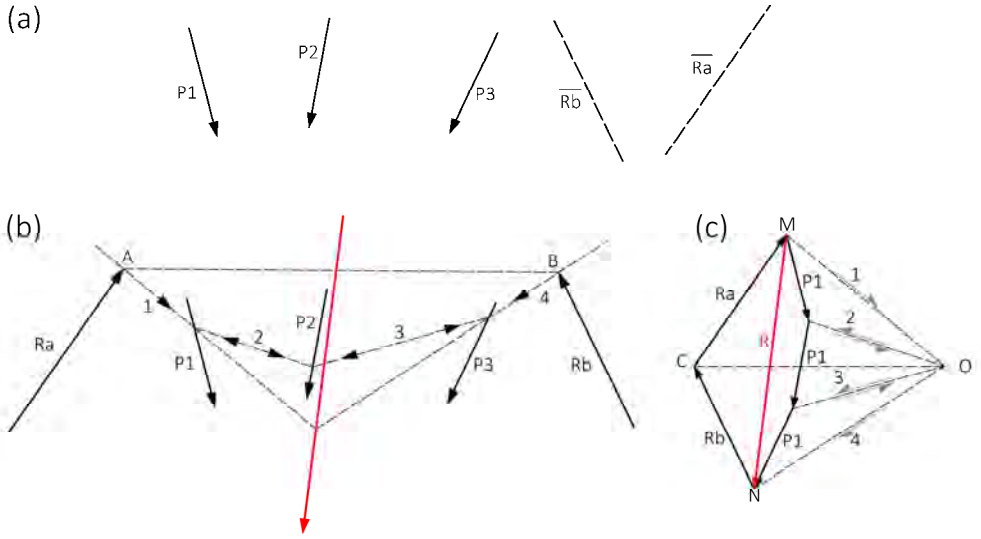


**Figure 37** (a) Data set and pre-set directions of reactions; (b) system in equilibrium; (c) force polygon.

## 4.3. Geometric properties

The resultant of a system of forces is independent of the order in which the forces are considered when drawing the force polygon. Since the order of two forces does not alter the resultant, the forces can be interchanged two by two until the desired order is adopted. Furthermore, if a system of forces is divided into groups, the resultant of the partial resultants coincides with the resultant of the given system. These properties are shown in Figure 38 for a group of forces P1, P2, P3, and P4.

Applying concepts of projective geometry (see Chapter 5 for further details), there is a reciprocity between the funicular polygon and the force polygon with its polar rays of Figure 39. This reciprocity means that changes in the position of O in the force polygon will produce changes in the funicular polygon and vice versa.

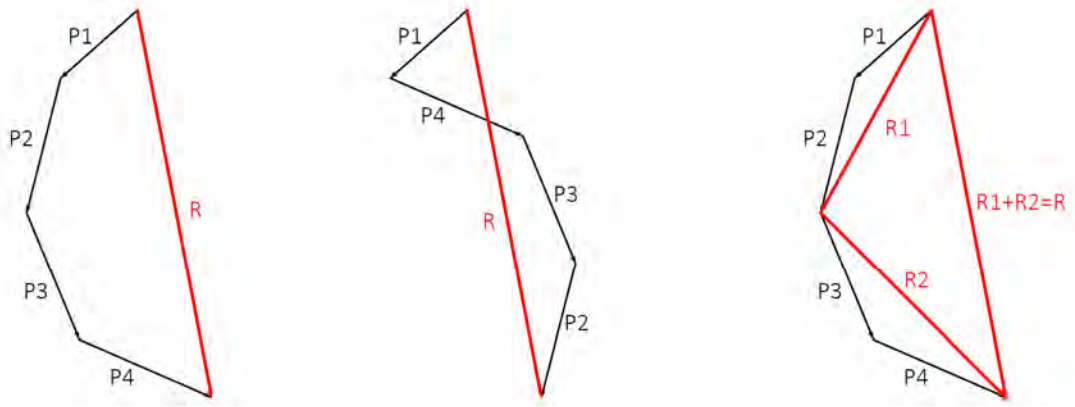


**Figure 38** Geometric properties of a system of forces.

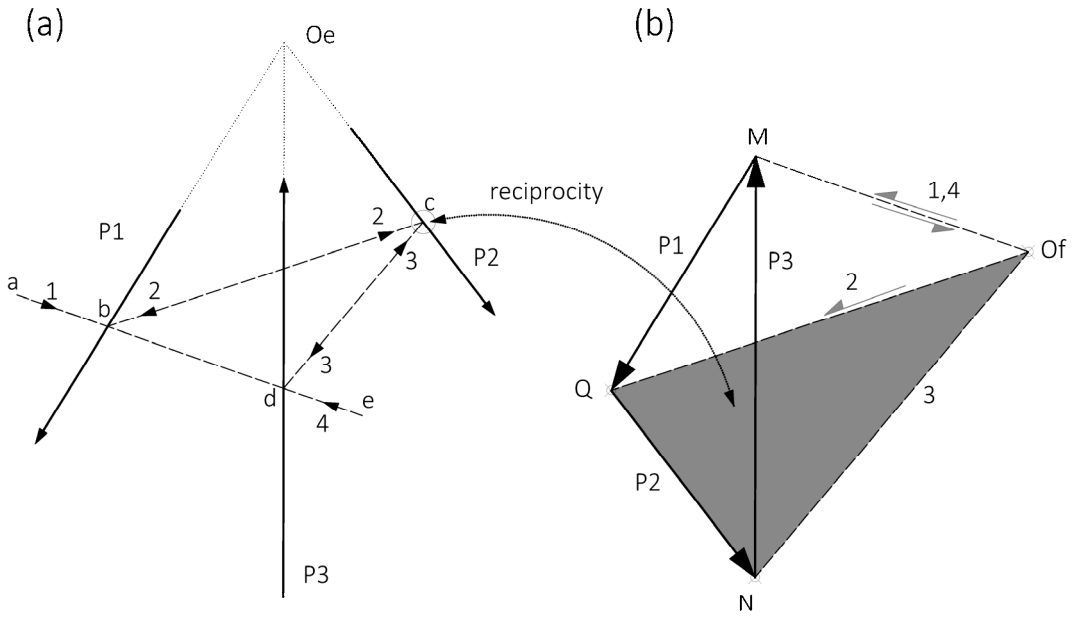


**Figure 39** Reciprocity between funicular polygon and force polygon.

### 4.3.1. Polar axis

The locus of the intersections for homologous sides of the funiculars, obtained for a system of forces, when moving the pole along a line is parallel to the line of displacement of the pole, which is called the *polar axis*.

In other words, considering a system of forces P1, P2, P2, P4 as in Figure 40(a), by constructing two equivalent polygons with poles O and O ', the homologous sides in the funicular polygons intersect at points g,h,i,j,k on a line parallel to O-O'. This line is the polar axis, as we can see in Figure 40(a), (b).

In Figure 40, if two homologous quadrilaterals like i – d – d´ -j and Q – O – O´ - R with three sides and the diagonals being parallels, then, the fourth side ij and O-O´ have to be parallel too. Therefore, it is demonstrated that the polar axis is parallel to the line O-O´.

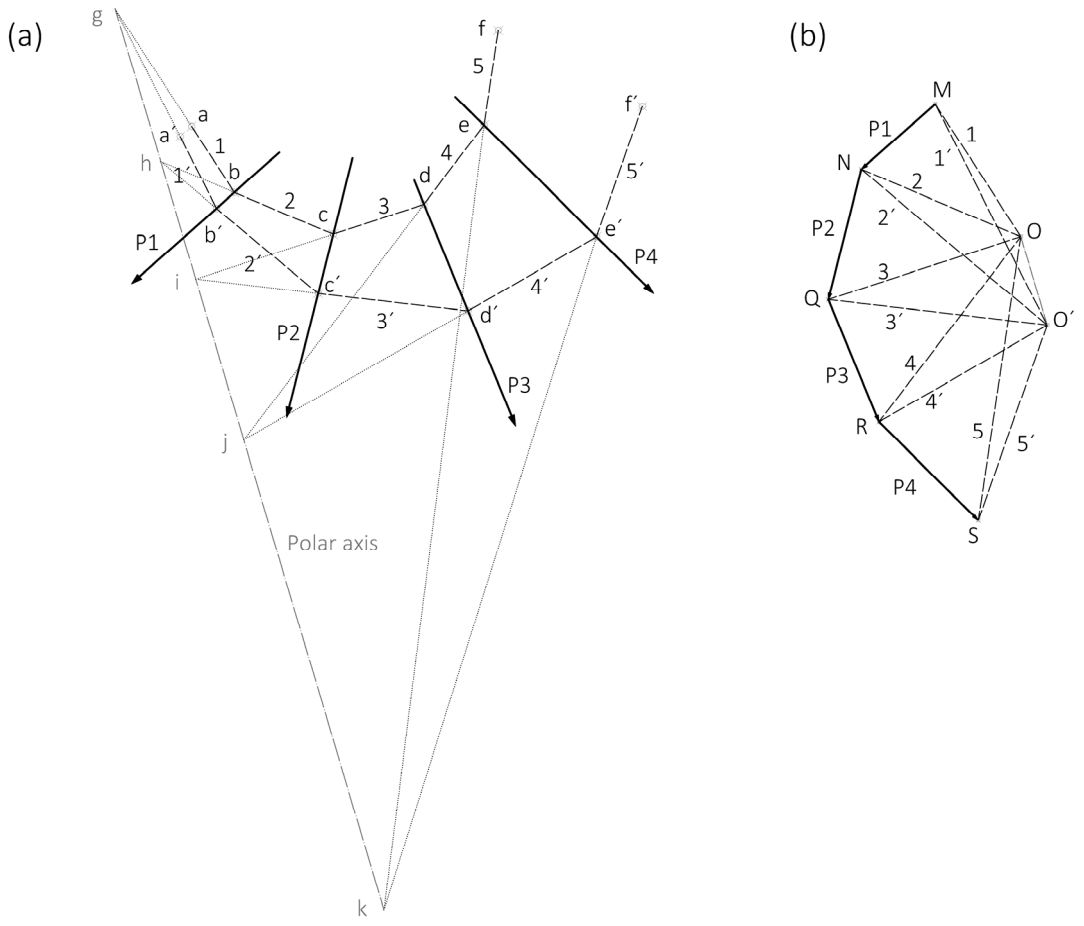


**Figure 40** (a) System of forces P1, P2, P3, P4 and funicular polygons; (b) force polygons with a scale 1/2.

## 4.4. Applications of the funicular geometry

In section 2.3 the funicular polygon was defined as the shape of a string under a set of loads. The string in this definition can only exert axial forces without any moments or shear. Expanding on this, the funicular polygon of a system of forces is one of the infinite equilibrium geometries of a weightless thread, under these forces. That is the form for the least potential energy of the system, and the most efficient form to transmit the forces with specific conditions.

An example of this physical sense of a funicular polygon is in Figure 41(a). Moreover, this approach is still applicable to the shape turned upside down and with its segments working in compression. The resulting shape is an arc with loads in equilibrium and with its bars working in pure compression as in Figure 41(b). This shape is the antifunicular polygon of the system of forces, and the force polygon would be symmetric as in Figure 41(c).

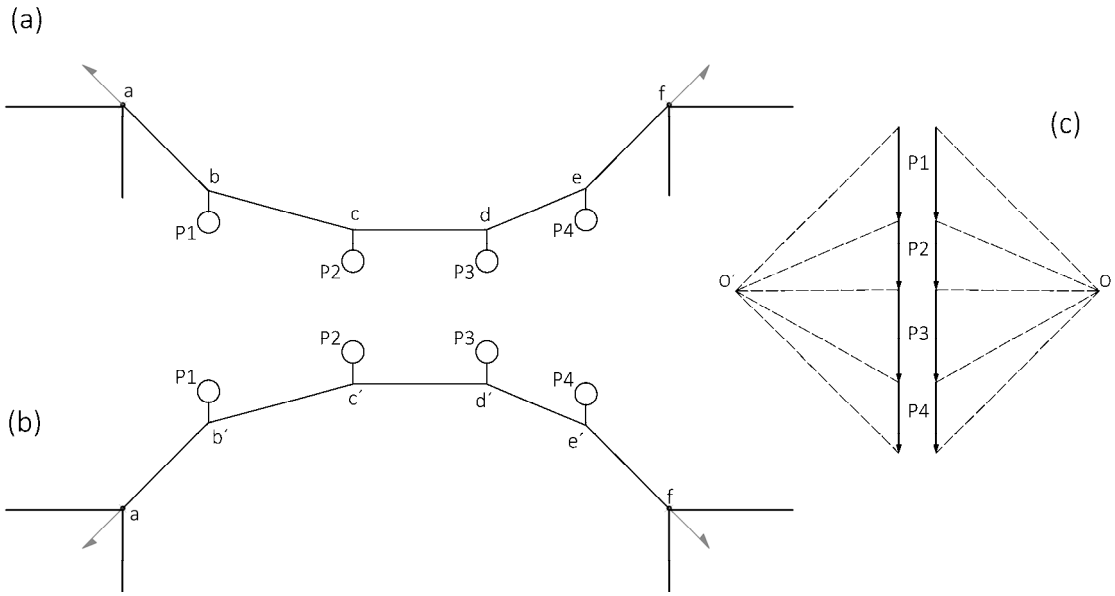


**Figure 41** (a) Funicular polygon of a system of forces; (b) anti-funicular of a system of forces; (c) force polygons.

Previous sections of this chapter laid out that all funicular polygons had infinite solutions since the position of pole O was free. However, what is the meaning of the position of O with regard to the loaded thread? A position close to the force polygon gives us small stresses, but with a long thread. With a point O far from the force polygon, there is a short funicular polygon, but large stresses. Similarly, by moving point O vertically, the direction of the thread sections change.

Nevertheless, most importantly is to understand that whatever the position of O is, the resultant of the system will be the same.

The analytical determination of the equilibrium geometry of a flexible thread without self-weight, subjected to a system of concentrated loads and two supports, determines a system of three equations (equilibrium) and four unknowns (reactions in the supports), hence, there are infinite solutions. For a unique solution, it is necessary to impose an additional condition, e.g. that the cable passes through a third point.

To apply these concepts when assessing the safety factor in section 2.7.2, requires to estimate the antifunicular that passes through two or three specific points. As said before, the funicular polygon that passes through two given points has infinite solutions, to have a unique solution there must be another condition, such as a known direction of the funicular or a third point. This can be achieved by different ways, but to simplify, next paragraphs will offer just one way for each case. For further information about funicular polygons see (Ciblac & Morel, 2014) and (Aroca Hernández-Ros, 2002)

### 4.4.1. Funicular polygon through two points

Considering a group of forces P1, P2, P3, P4 and two points m and n, Figure 42(a), the steps to draw a funicular polygon are:

Firstly, a force polygon must be drawn with a resultant R as in Figure 42(b). With this force polygon, and with an arbitrary pole O, it is easy to find a funicular polygon starting at point m. This is the funicular polygon 1-2-3-4-5 in Figure 42(a) where forces in lines 2-3-4 are cancelled. The resultant of the system R will pass through the meeting point of lines 1 and 5, point g. This funicular polygon does not pass through point n.

To find one of the infinite funiculars through m and n, it just needs to select a point along the resultant R e.g. point h and make two lines 1´and 5´ joining h with m and n, see Figure 42(c). Drawing parallels to 1´and 5´ in the force polygon as in Figure 42(d), there will be a new pole O´ in the force polygon with which a new funicular can be drawn through m and n.

Since point h could be any of the resultant, there are infinite solutions. However, knowing the direction 1´of the desired funicular, point h would be unique and so the funicular.

### 4.4.2. Funicular polygon through three points

Considering a group of five forces P1, P2, P3, P4, P5 and points m, n, p, see Figure 43(a), we can draw a funicular polygon that goes through them.

First thing is drawing the force polygon in Figure 43(c) and then the funicular polygon 1-2-3-4-5-6, starting at m with help of an arbitrary pole O as in Figure 43(b). Polar axis 1 has an arbitrary direction from point m. The extension of line 4 meets the polar axis 1 at point g (see section 4.3.1 about the polar axis). From point g and joining with point n there is the homologous line 4´ of a new funicular 1´-2´-3´-4´-5´-6´, which includes points m and n but does not include p, see Figure 43(b).

Creating a new polar axis 2, joining m and n, it is for sure that the new funicular will include these two points m and n. In Figure 43(e) is drawn a parallel to polar axis 2 from O´. The extension of line 6´ cuts the polar axis 2 in h. Joining h with p there is the first line of the final funicular polygon. A parallel in Figure 43(e) defines a new pole O´ in axis 2, with which to find the directions of the funicular polygon 1´´, 2´´, 3´´, 4´´, 5´´, 6´´ that passes through m, n, p.

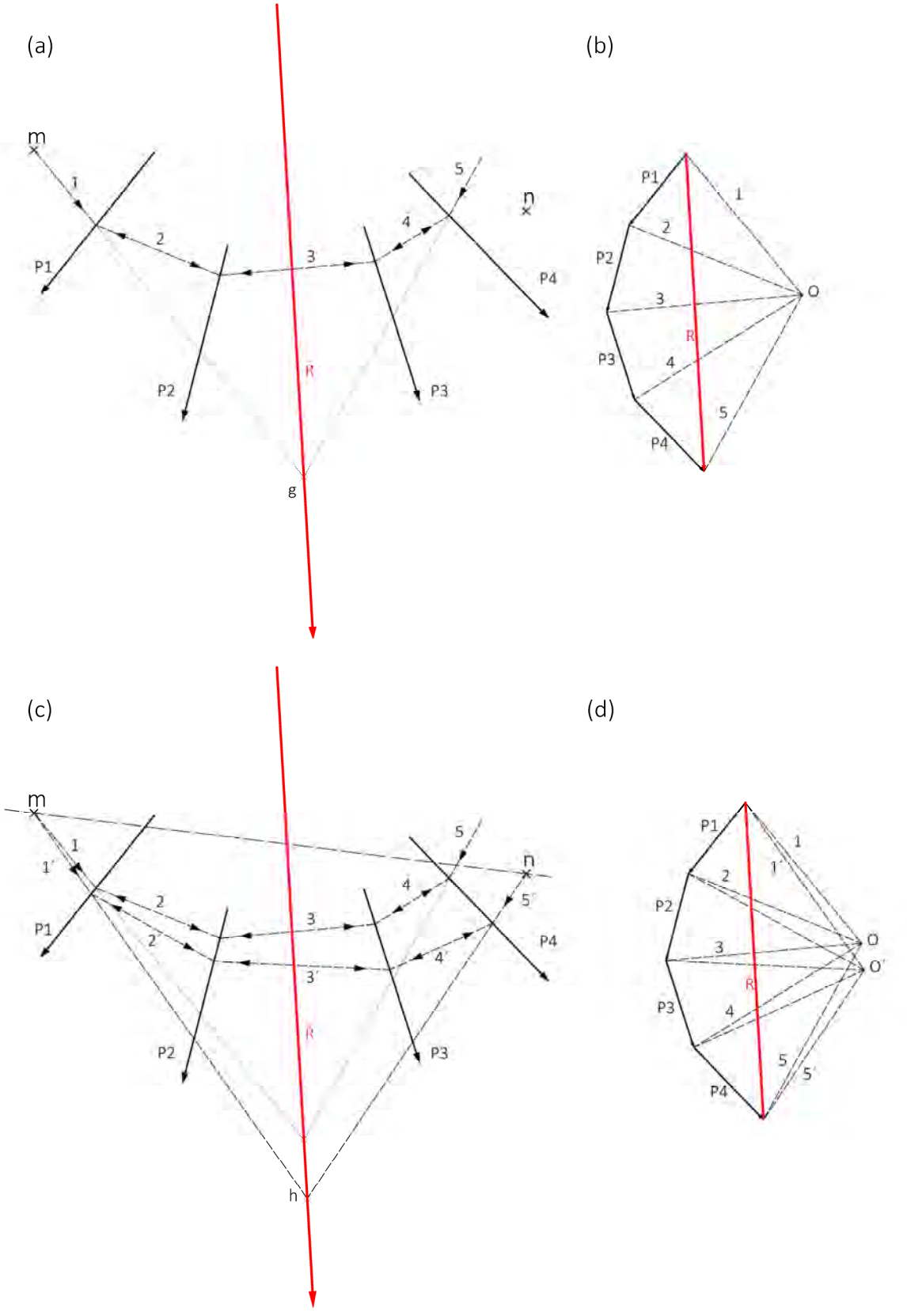


**Figure 42** (a) System of forces and first funicular polygon; (b) force polygon with arbitrary pole O, scale ½; (c) system of forces with funicular polygon through m and n; (d) force polygons, scale of ½.

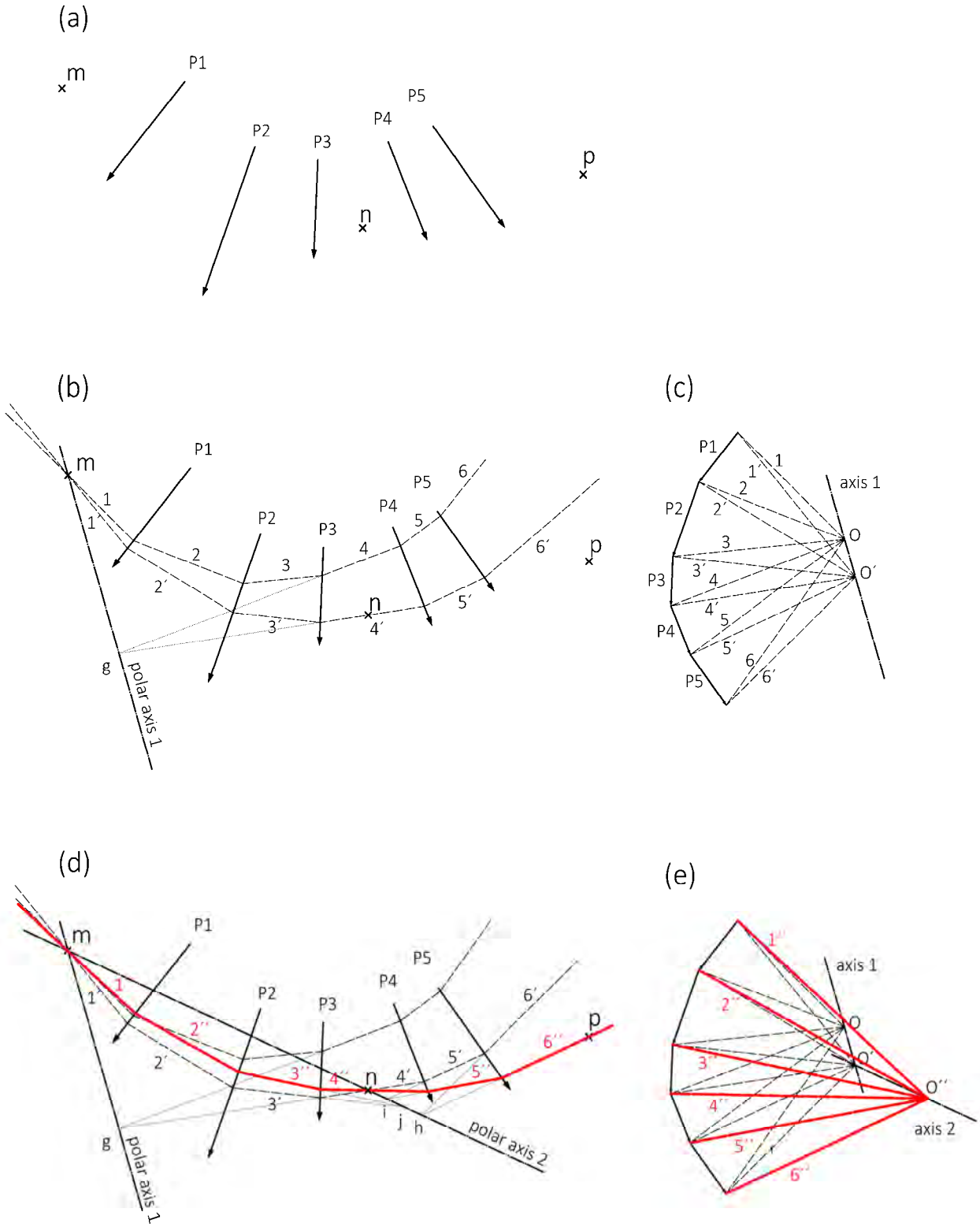


**Figure 43** (a) Initial data; (b) funicular polygon through m,n; (c) first force polygon, scale ½; (d) final funicular polygon; (e) final force polygon, scale ½.

### 4.4.3. Thrust line in a masonry arch.

This section analyses the case of finding a thrust line in a masonry arch with compression-only stresses, no sliding between voussoirs and infinite resistance to compression, as stated in (Heyman, 1977), (Huerta, 2004) among others. To expand the basis of this subject, please review section 2.2.

Considering only the weight vectors of the voussoirs in Figure 44(a), an antifunicular polygon of the system included in the masonry section, defines a possible thrust line geometry in the arc. The weight vectors are located in the gravity centre of each voussoir.

Due to the symmetry, it can be considered only half of the arch, with a horizontal force at the key. It is easy to find a resultant R of the system of forces with a funicular polygon a-b-c-d-e-f-g, by means of a force polygon with an arbitrary pole O, Figure 44(b). The resultant R is located in the meeting point h of the first and last line of the funicular polygon, a-h and g-h, respectively. Nonetheless, this funicular leaves the section; consequently, the arch is not stable.

As seen before in this chapter, it can be set the condition that the funicular must go through two points, initial point a, at the centre of the keystone, and final point m at the centre of the springer, see Figure 44(c). Since the resultant R and the first line are the same in the new funicular polygon, so is point h. Drawing a parallel of the new line m-h in the force polygon, allows to find a new pole O´ and with it a new funicular a-b-i-j-k-l-m. This new funicular is included in the masonry section, but near to touch the inner edge, which means a poor stability condition.

There are infinite possible funicular polygons, and by trying different initial and final points, it may be possible to find a solution that offers enough stability. See section 2.7.2 for definition and discussion of the safety factor. In Figure 44(d), there is a different test with initial point n at the key at 2/3 from the inner edge, and final point q at the springer at 2/3 from the inner edge. In this case, the thrust line fits completely in the section, which guarantees the stability of the arch.

As stated in Chapter 3, the lower-bound theorem stablishes that if we find a possible equilibrium situation, the structure will find it too. It means that, by obtaining different thrust lines for the same masonry arch, the stability can be assured by the one that provides the highest stability.

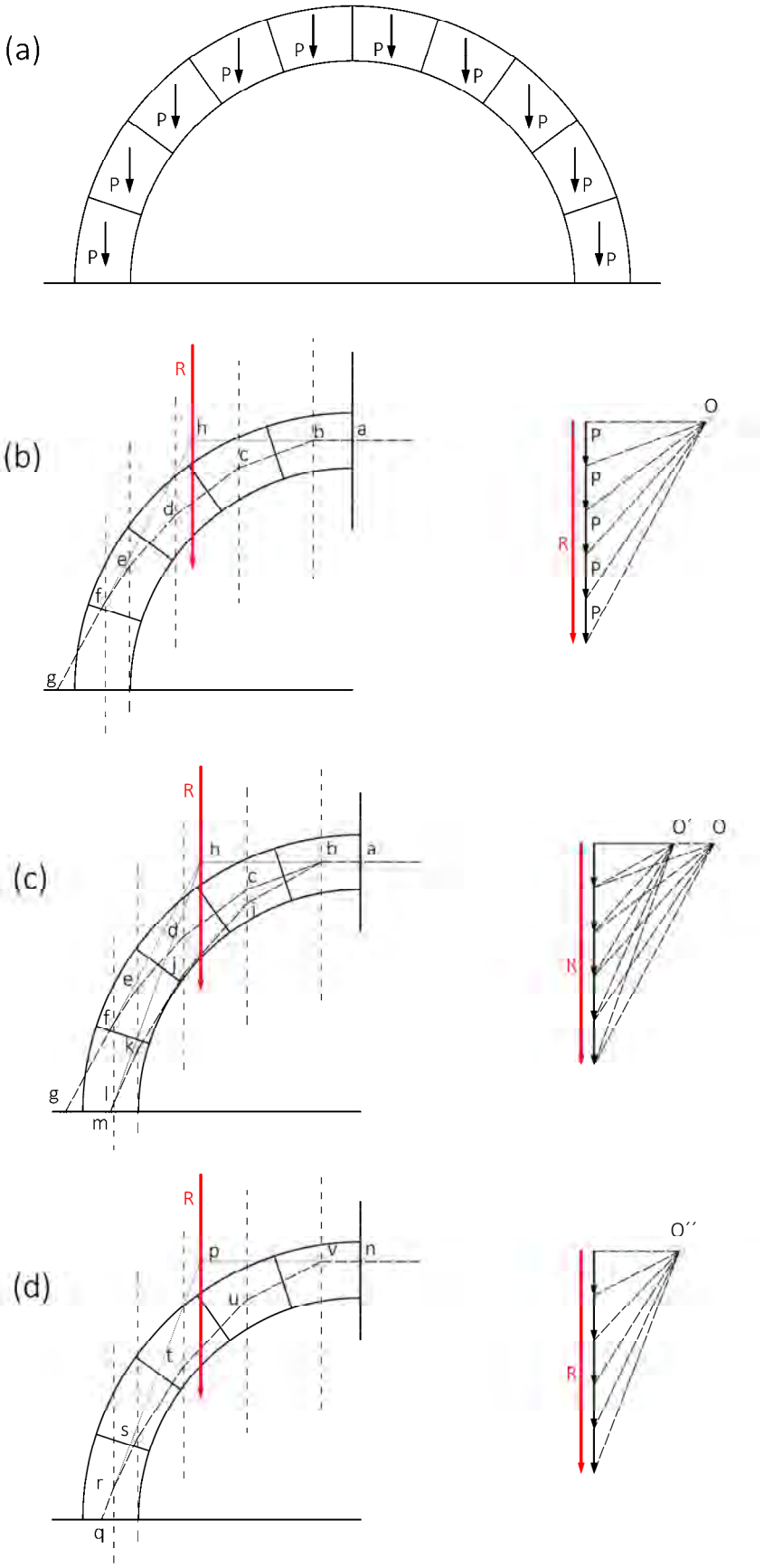


**Figure 44** (a) Input data; (b) first funicular polygon with arbitrary pole O; (c) second funicular polygon through a and m; (d) third funicular polygon through points n and q.

# Chapter 5

# Projective geometry

Notwithstanding it may be trivial for architects and engineers now, orthogonal projection was the result of a long complex process that lasted centuries and predates Descartes by more than four hundred years (Calvo-lópez, 2011).

Projective geometry "is often defined as the sum total of those properties of figures which are not altered by a projection by means of radiating lines, from line to line or from plane to plane" (Coolidge, 1940).

Briton James Clerk Maxwell (1831-1879) developed a methodology, using Projective Geometry and introducing the notion of reciprocal figures for structure analysis. In his writings, Maxwell explains how to find forces in structural frames by drawing a reciprocal diagram with lines parallel to the structural members, this way all member connected in a node create a polygon in the reciprocal diagram. As Maxwell put it, "two figures are reciprocal when the properties of the first relative to the second are the same as those of the second relative to the first". It is important to note that the lengths of the lines in the reciprocal diagram are commensurate with the loads supported by the structural member.

Maxwell used the terms *form diagram* that represents the structural members and *force diagram* for the forces carried by each member. Nonetheless, to emphasise the duality between figures, this dissertation will also name them as *primal figure* and *dual figure* respectively.

One consequence of the reciprocity is that either diagram can be considered a form diagram and the other would be the force diagram.

There is an example of a form diagram in Figure 45 (left) from (Maxwell, 1870). To draw the force polygon, there must be given a magnitude of a force like p parallel to P in the frame. Once this first magnitude is fixed, if the form diagram is in equilibrium, all the other magnitudes can be calculated by drawing the lines parallels to the ones in the form diagram. The lines of the force polygon, in Figure 45 (right), have the same letter as their parallels in the form diagram.

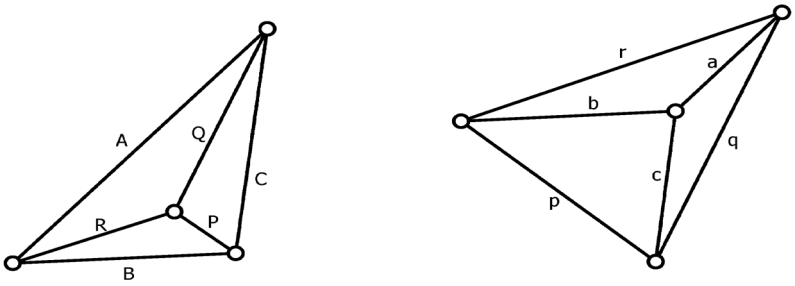


**Figure 45** Example of reciprocal diagrams. (left) Form diagram or primal figure; (right) force diagram or dual figure, given the magnitude of force P. (Maxwell, 1870) in (Reese, Paffenroth, & Fehribach, 2016).

The primal and dual figure are linked by geometric constrains, which means that any of them can be manipulated, generating changes in the other. As stated in Baker et al. (2013), the reciprocity "leads to the remarkable observation that the force diagram could also represent the geometry of another optimal truss with its own external loads."

Robert Bow, created a notation system for both primal and dual figure (Bow, 1873). For the primal figure, the capital letters, A, B, C,..., are sequentially placed clockwise in the intervals between external forces (open polygons) and numbers 1,2,3,…, are placed in the internal spaces (closed polygons). Each line in the primal figure is identified with the letters or numbers of two polygons at both sides. In the dual figure, the starting and ending points of each line (force) are named with the letter or number of these polygons at both sides of the line in the primal figure.

Figure 46 shows an example of Maxwell´s reciprocal diagrams with Bow´s notation. In Figure 46(a), there is a primal figure with three external forces, $F_{CA}$, $F_{AB}$, $F_{BC.}$ The external forces are in bold lines in both primal and dual figure to clarify the duality between them.

Each polygon in the primal figure maps to a node in the dual figure and vice versa. Each line in the primal figure maps to a parallel line in the dual figure and vice versa. In Figure 46(b.1) to (b.3), there is a systematic development of the dual figure. Figure 46(b.1) shows the first dual polygon c-a-2 with parallels to the primal members CA, A2, 2C. The magnitude of the first line is arbitrary. Moving clockwise to the next vertex in the primal figure, we find vertex AB, B1, 12, 2A, with which it can be created the next dual polygon a-b-1-2, as seen in Figure 46(b.2). Similarly, the dual figure can be finished.

The length of each member in the dual figure represents the magnitude of the stress of the member in the primal figure. Figure 46(b) has the arrows at each step, to elucidate the direction of the forces. Let´s consider the first step in Figure 46(b.1), the direction of force 2a when applied in the node of the primal figure, tends to escape from it, and so member 2A is in tension. On the contrary, the side 2c of the dual figure, when applied at the node of the primal figure, tends to go towards the node, being member 2C in compression.

Once the dual figure (force polygon) is finished, by knowing the magnitude of one of the forces and a given scale, it is easy, with a similarity relation, to find the final dual figure. See dot lines in Figure 46(b.3).

To clarify these concepts, Figure 46(c), (f) present two variations of the same figure. In Figure 46(c), (d), the dual figure shows that the structural member 1-2 now does not have any stress, because points 1-2 in the dual figure are coincident. In Figure 46(e), (f), the dual figure shows that the structural member 1-2 has changed to a compressive stress. These three examples explain how we can manipulate one of the diagrams to obtain the desired effects on its reciprocal.

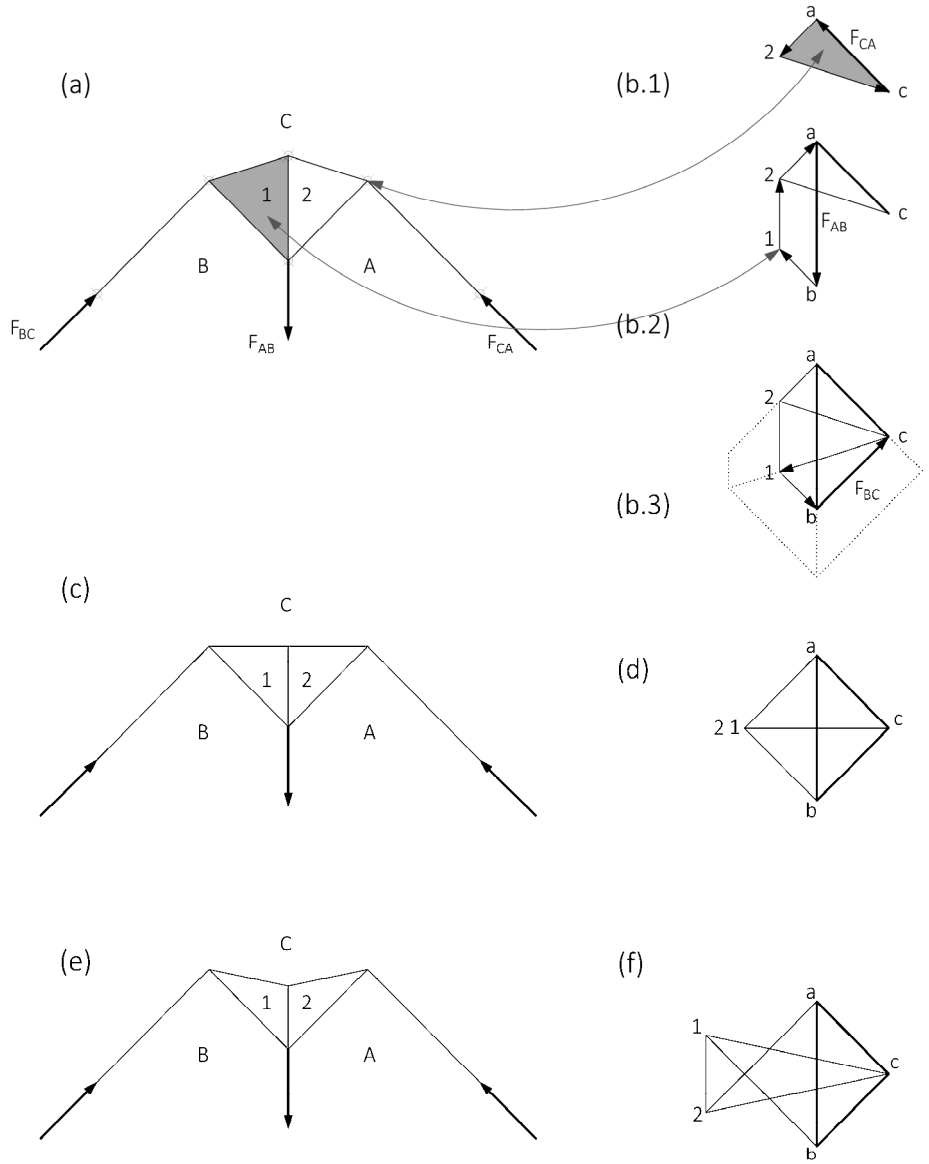


**Figure 46** Example of structural reciprocity. (a) Primal figure; (b) step by step dual figure; (c) primal figure, second case; (d) dual figure, second case; (e) primal figure, third case; (f) dual figure, third case.

Another example (Figure 47), with more external forces can shed light on the combined application of funicular geometry and reciprocity, using Bow´s notation.

Figure 47(a) show the form diagram. The direction of reaction $F_{EA}$ is known, but not in the case of reaction $F_{DE}$. Figure 47(b) is the force polygon with a random direction of $F_{DE}$*. Point O can be any. This first force polygon allows drawing an initial funicular polygon in Figure 47(c) that is open. The direction that closes the funicular polygon is 5´, so now the final reaction $F_{DE}$ can be obtained in Figure 47(b).

Analysing the different nodes in the form diagram, we can find the force diagram in Figure 47(d) (the different nodes are analysed independently in d.1, d.2., d.3, d.4, d.5).

Figure 47(e) shows which structural lines are in compression or traction.

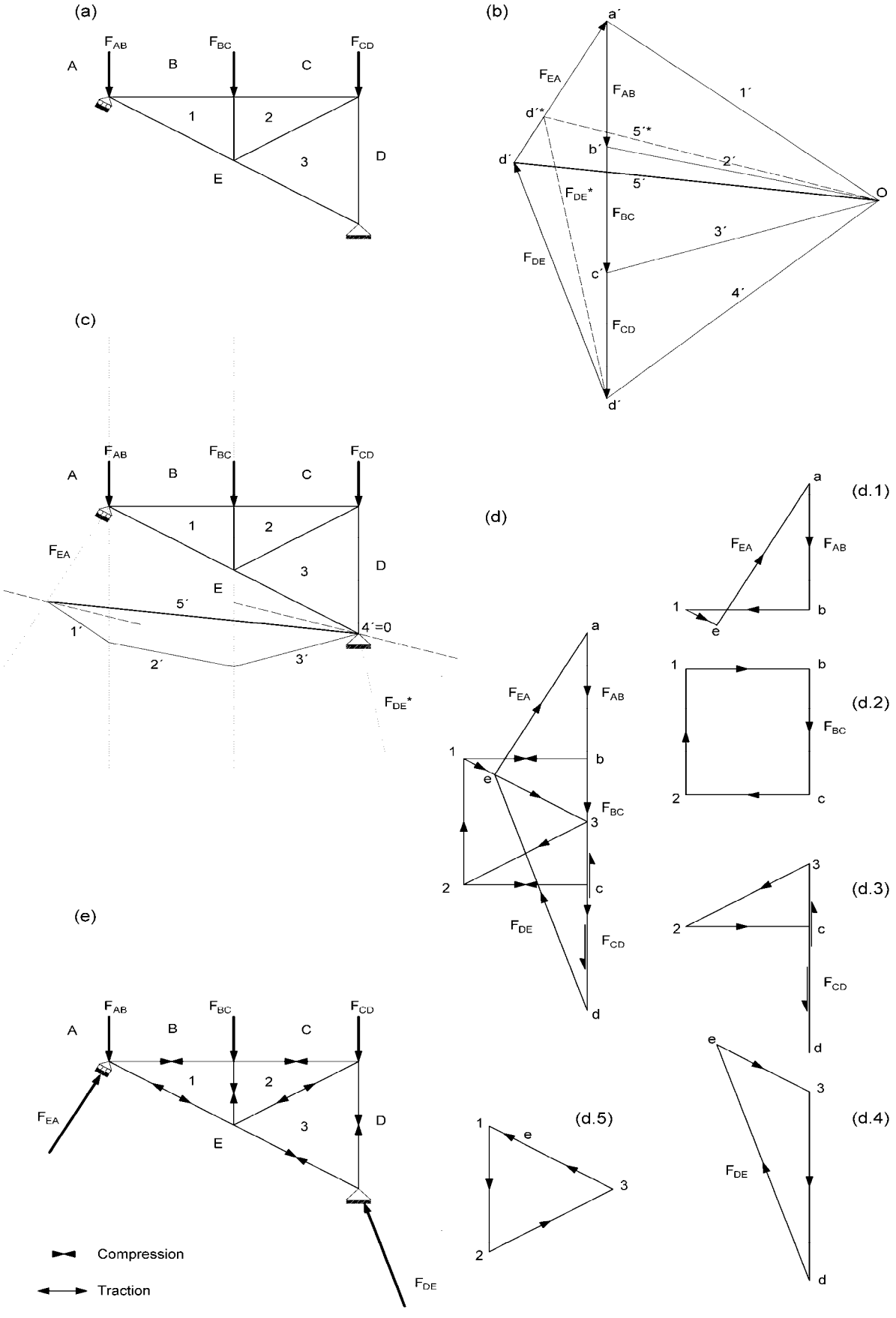


**Figure 47** Example of combined use of funicular geometry and reciprocity.

Figure 48 shows how by manipulating point 2 in the force diagram (right), it affects the form diagram by changing the direction of the structural line 2C (left).

This approach in the design and calculation of structures has allowed the development of new strategies for structural design and optimization.

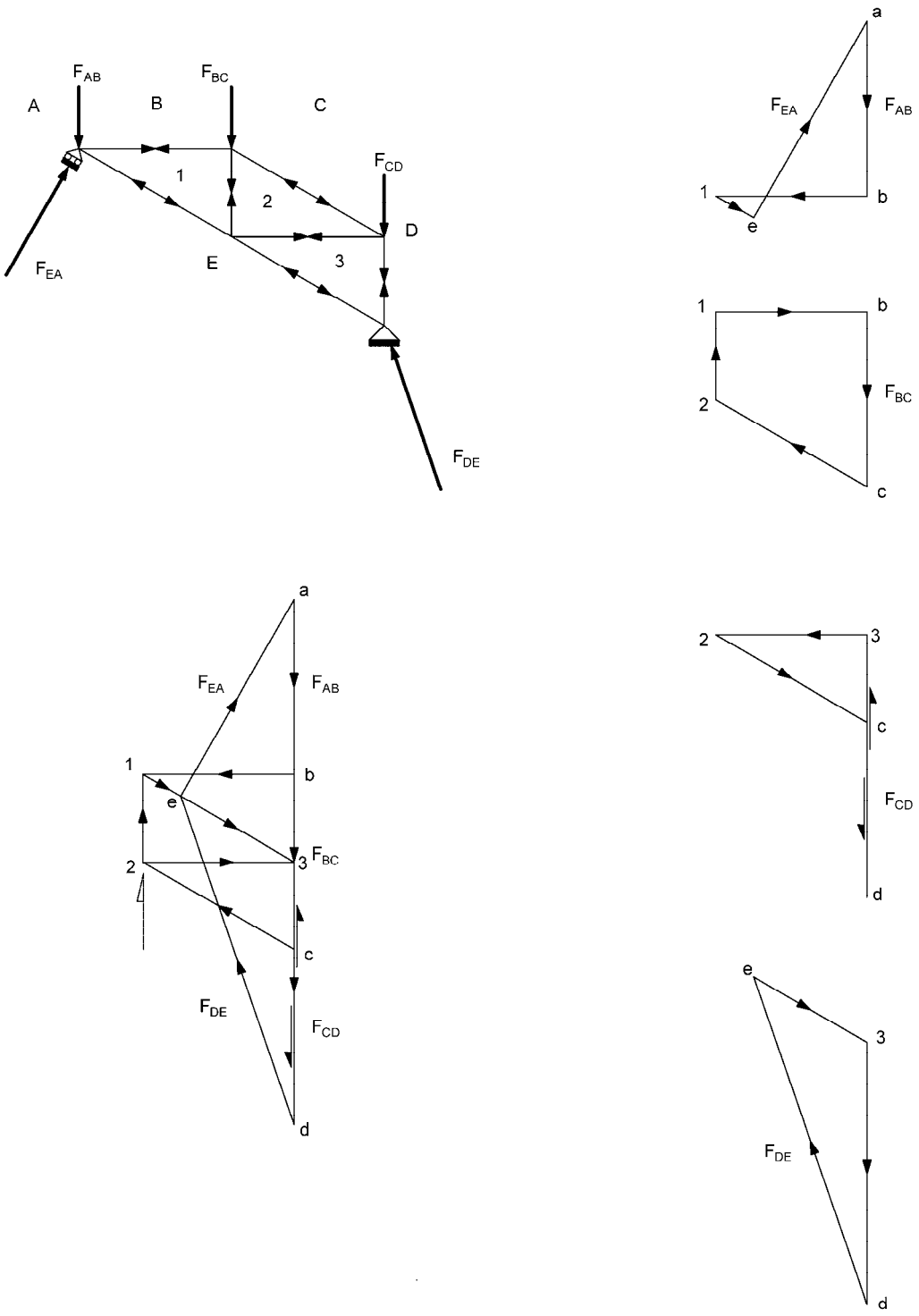


**Figure 48** Example of use reciprocity. (left) New form diagram; (right) force diagram with a new position of point 2.

# Chapter 6

# New graphic methodology based on the combined use of funicular and projective geometry

## 6.1. Hemispherical brick dome

The new methodology is presented through its application to a hemispherical brick dome of small thickness. This is frequently the constructive element that internally defines the "*encamonada* dome".

The "*encamonada* dome" is a typology of dome, that was implemented in accord with the directions of Fray Lorenzo de San Nicolás's treatise (1639, 1665), in the 17th and 18th centuries, widespread in Spain and its overseas possessions. The characteristics of the "*encamonada* dome" are presented in (Redondo, 2013) and (Huerta, 2001)

In this work, the model analysed has been referenced to a real dome: the dome over the transept, in Basilica of San Juan de Dios in Granada (Spain). The authors laid out a detailed constructive analysis of the dome in (Suárez, Bravo, & González, 2019) and (Suárez, Boothby, & González, 2020).

It is a hemispherical dome with double brick layer, of 11.71 m inside diameter and 8 cm in thickness, supporting its own weight and the weight of the inside brick coating of the lantern, of 3.89 m inside diameter and 3 cm thickness.

The unit weight of the material is $\rho = 17.65$ kN/m$^3$; the weight of the inside brick coating of the lantern has been estimated equal to 31.24 kN.

In this case, the ratio $(R/t)$ is 73.19; according to (Heyman, 1977), this can be considered a thin shell because the ratio is bigger than 20.

The three situations analysed are represented in Figure 49: full hemisphere; hemisphere with oculus and hemisphere supporting the inside brick coating lantern.

Fray Lorenzo recommended the construction of a filling on the extrados, until one third of height, to ensure the stability of the dome.

In the work (Ramos & León, 2013) the structural behaviour of the filling of the vaults is analysed, according to its morphological characterization, distinguishing between: rigid filling cemented, solid granular filling, loose granular filling, lightened filling and filling formed by construction rubble.

In this dissertation, the following three hypotheses about the structural behaviour of the backfill have been considered:

**Figure 49** Three structural situations have been considered: full hemisphere, hemisphere with oculus and hemisphere with inside brick coating of lantern.

**Hypothesis 1**: The filling is made of loose granular material; that does not contribute structural properties and it is considered a dead load on the dome. This hypothesis is modelled by incorporating the weights of the filling volumes into the system of forces, without increasing the section of the dome.

**Hypothesis 2**: The filling is of firm granular material and therefore it has a structural function. This hypothesis is modelled by increasing the thickness of the voussoirs located in the lower third of the total height. Two possibilities have been considered, staggered filling and soft curved filling.

**Hypothesis 3**: The filling is rigidly cemented, preventing the movement of the voussoirs. This hypothesis has been analysed considering the dome as a shallow dome.

Finally, this new methodology is used to design the required height and shape of the filling on the extrados to avoid any tension force on the dome.

The following structural situations for the dome and the filling are displayed in Figure 50:

- a) without filling.
- b) filling of loose granular material, without structural behaviour, until one third of the height
- c) staggered filling of firm granular material, with structural function, until one third of height
- d) soft curved filling of firm granular material, with structural function, until one third of height
- e) cemented rigid filling until one third of height, acting as an embedment. The dome is considered as a shallow dome;
- f) staggered filling on the extrados, until you get a dome without tension forces.

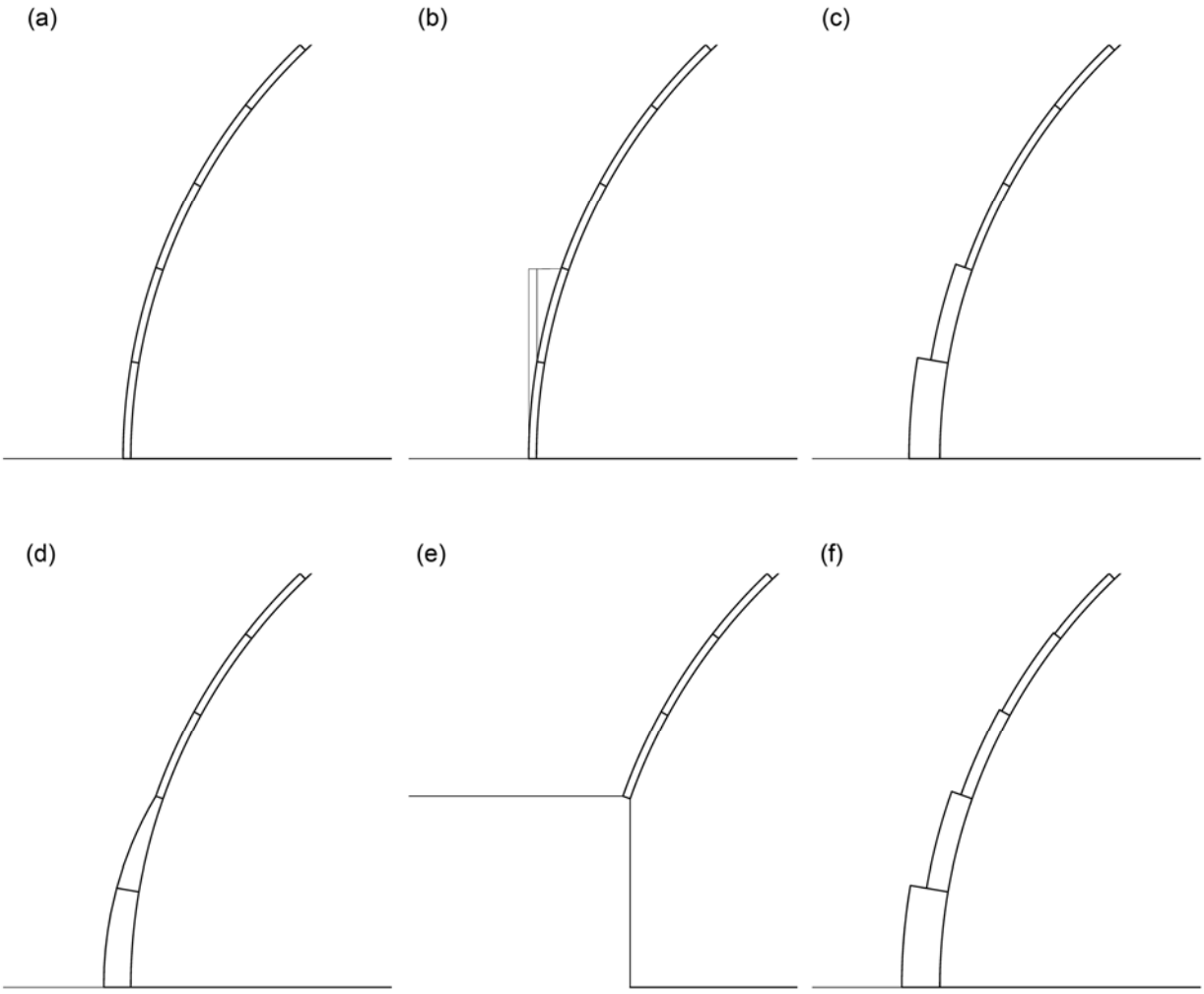


**Figure 50** Structural situations of the dome and filling on the extrados.

## 6.2. Methodology

This dissertation presents a new graphic methodology for the structural analysis of domes and other surfaces of revolution, based in Thrust-Network Analysis presented in (Block & Ochsendorf, Thrust network analysis: a new methodology for three-dimensional equilibrium., 2007), incorporating other notions from projective geometry to make a more comprehensive method for the analysis of certain classes of structure.

In (Block & Ochsendorf, 2007), the forces in a spatial network are solved by the graphical analysis of their horizontal projection, and the equilibrium of the spatial system is preserved in the projection plane. The forces are analysed within a dual system where the forces in equilibrium at each node are represented by a closed force polygon.

In this dissertation, the dome is considered as a network of lines of latitude and longitude, whose equilibrium is analysed in both horizontal and vertical projection.

The equilibrium in the vertical plane is assured by fitting the polygon of the weight forces to the polar rays, so the dome geometry is a closed antifunicular polygon of the system of forces. The equilibrium in the horizontal plane is guaranteed by considering the values of the nodal forces in the dual figure, where they form a closed polygon.

This procedure not only allows the solution of the internal forces for a given geometry of the dome, but also allows designing a geometry for a given system of internal forces that are both in equilibrium and admissible for the material.

### 6.2.1. Simplified model

The dome is divided by latitude and longitude into an arbitrary number of sectors. The simplified model of the dome is obtained by considering the centre of gravity; the weight of each sector and the interaction lines among centroids (nodes) of adjacent sectors, as it is represented in Figure 51, for the different cases: complete hemisphere; hemisphere with oculus; hemisphere with lantern.

Figure 52 shows the plan and elevation of the simplified model, where the different areas are named according to Bow's notation (1873), for the cases: full hemisphere; with oculus; with lantern; cemented rigid filling (shallow dome) with lantern.

### 6.2.2. Nodal forces

The following forces are considered at each node: the weight of the sector, two meridian forces and two parallel forces (hoop forces) equal in magnitude.

In keeping with (Eddy, 1878), (Dunn, 1904) (Dunn, 1908) and other authors, it is noted that the parallel forces can be considered for their net effect at each node; the net effect of two parallel forces, equal in magnitude, at a node is a radially directed force in the plane of the line of latitude, acting outwards (parallel compression) or inwards (parallel tension). See Figure 53 (left) for equilibrium in the compression zone and Figure 53 (right) for the tension zone.

The nodal internal forces equilibrium is considered by enforcing the equilibrium of the projected forces on both vertical and horizontal planes.

The equilibrium of the projected forces on the vertical plane is enforced by adjusting them as a system of forces whose anti-funicular polygon matches the dome geometry. In the same way, the equilibrium of the projected forces on the horizontal plane is imposed by forming closed polygons in the dual figure.

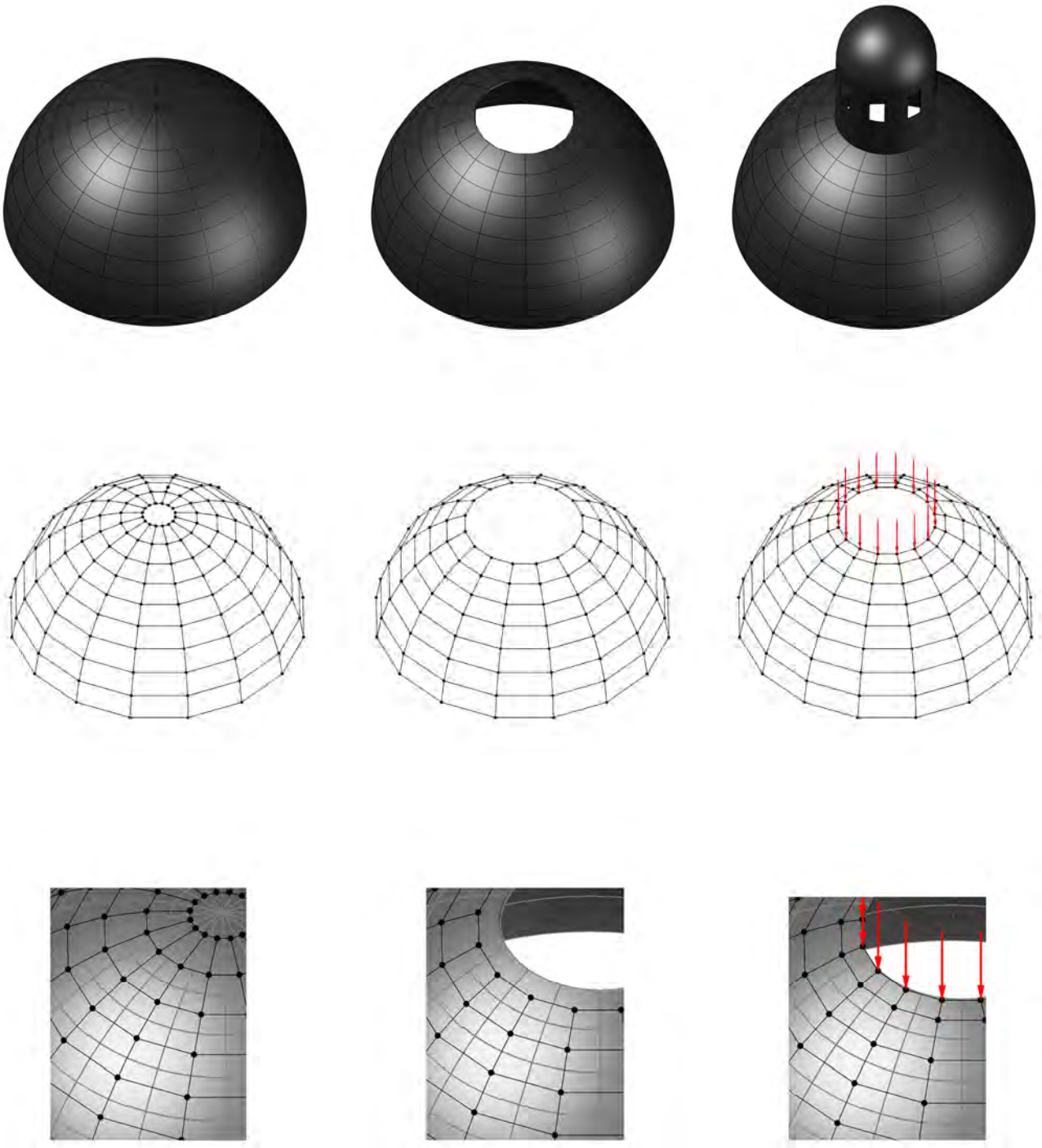

**Figure 51** Simplified model: the dome is divided by latitude and longitude into an arbitrary number of sectors; the simplified model of the dome is obtained by considering the weight and centre of gravity of each sector, and the interaction among centroids (nodes) of adjacent sectors.

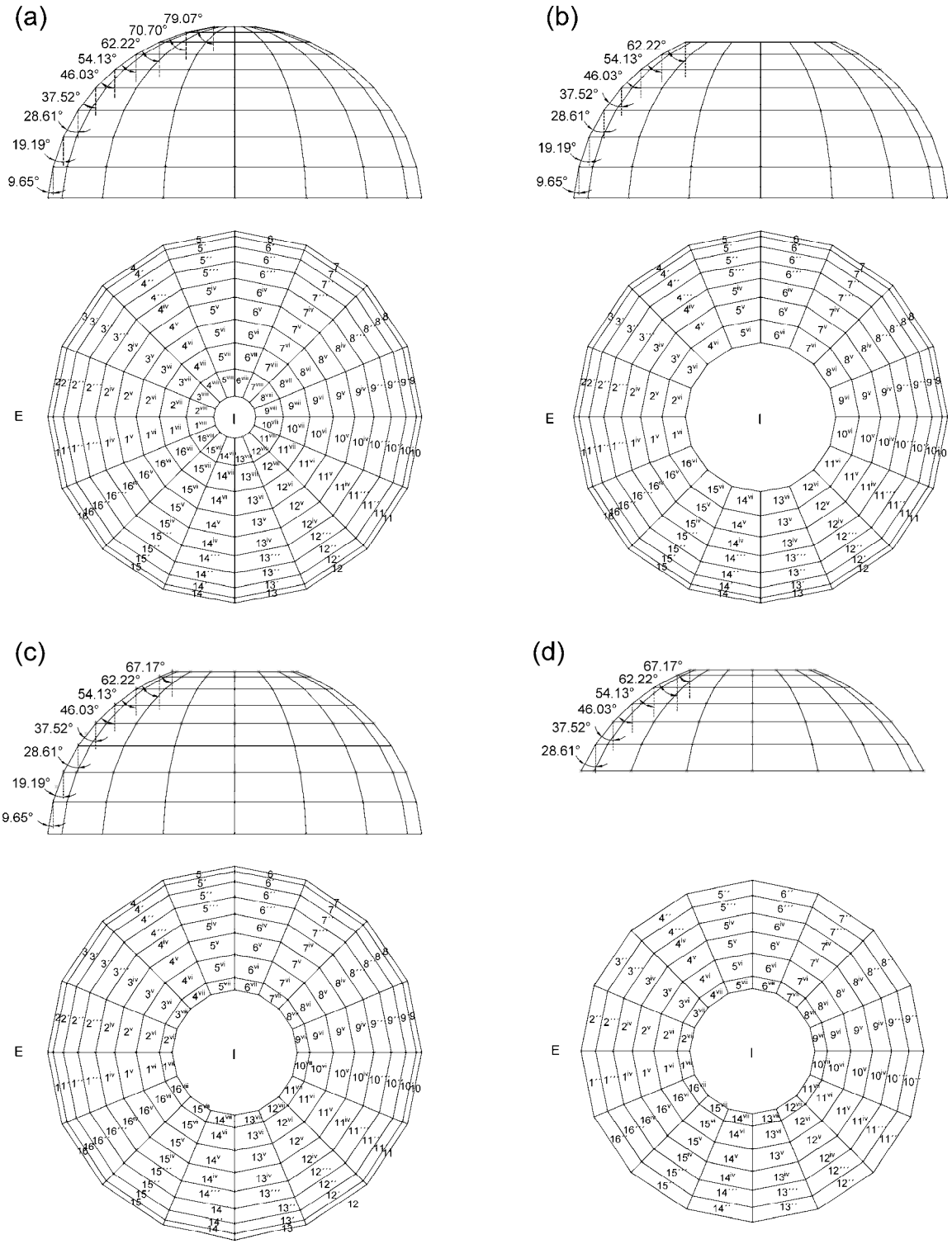


**Figure 52** Plan and elevation of the simplified model; the different areas in the plan are named according to Bow's notation (1873). (a) Full hemisphere; (b) dome with oculus; (c) dome with lantern; shallow dome with lantern.

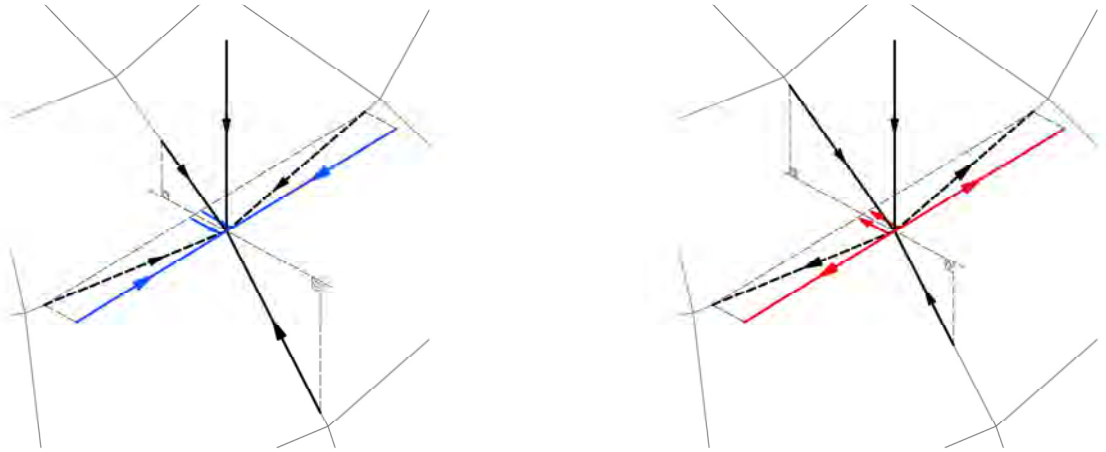

**Figure 53** (left) Equilibrium at node in compression zone: the hoop forces are a radially directed forces in the plane of the line of latitude, acting outwards; (right) equilibrium at node in tension zone: the hoop forces are a radially directed forces in the plane of the line of latitude, acting inwards.

### 6.2.3. Structural reciprocity

Chapter 5 addresses the characteristics of projective geometry and reciprocity, where it is explained how Maxwell introduced the notion of structural reciprocity to find forces in structural frames by drawing a reciprocal diagram. Chapter 5 also has some examples that help clarify the subject.

In this work, the structural reciprocity is considered doubly. In the meridional plane the structural reciprocity is considered between the antifunicular in Figure 54(a) and the force polygon in Figure 54(b).

Therefore, to each application point in (a) corresponds a closed polygon in (b) so the equilibrium in the meridional plane is assured. For clarity it is highlighted the reciprocity between the point of application of the force F8 (intersection between lines r and s) and the closed area in the force polygon among lines r,s,F8 (grey area).

In the horizontal plane, there is structural reciprocity between the projected network Figure 54(c) and its dual figure in Figure 54(d). Therefore, to each application point in (c) corresponds a closed area in (d) so the equilibrium in the horizontal plane is also guaranteed. It is highlighted the reciprocity between the point among areas $2^{vi}$, $2^{vii}$ ç, $1^{vii}$, $1^{vi}$ and the closed area in the force polygon defined by forces $F_{2vi2vii}$, $F_{2vii1vii}$, $F_{1vii1vi}$, $F_{1vi2vi}$ (grey area).

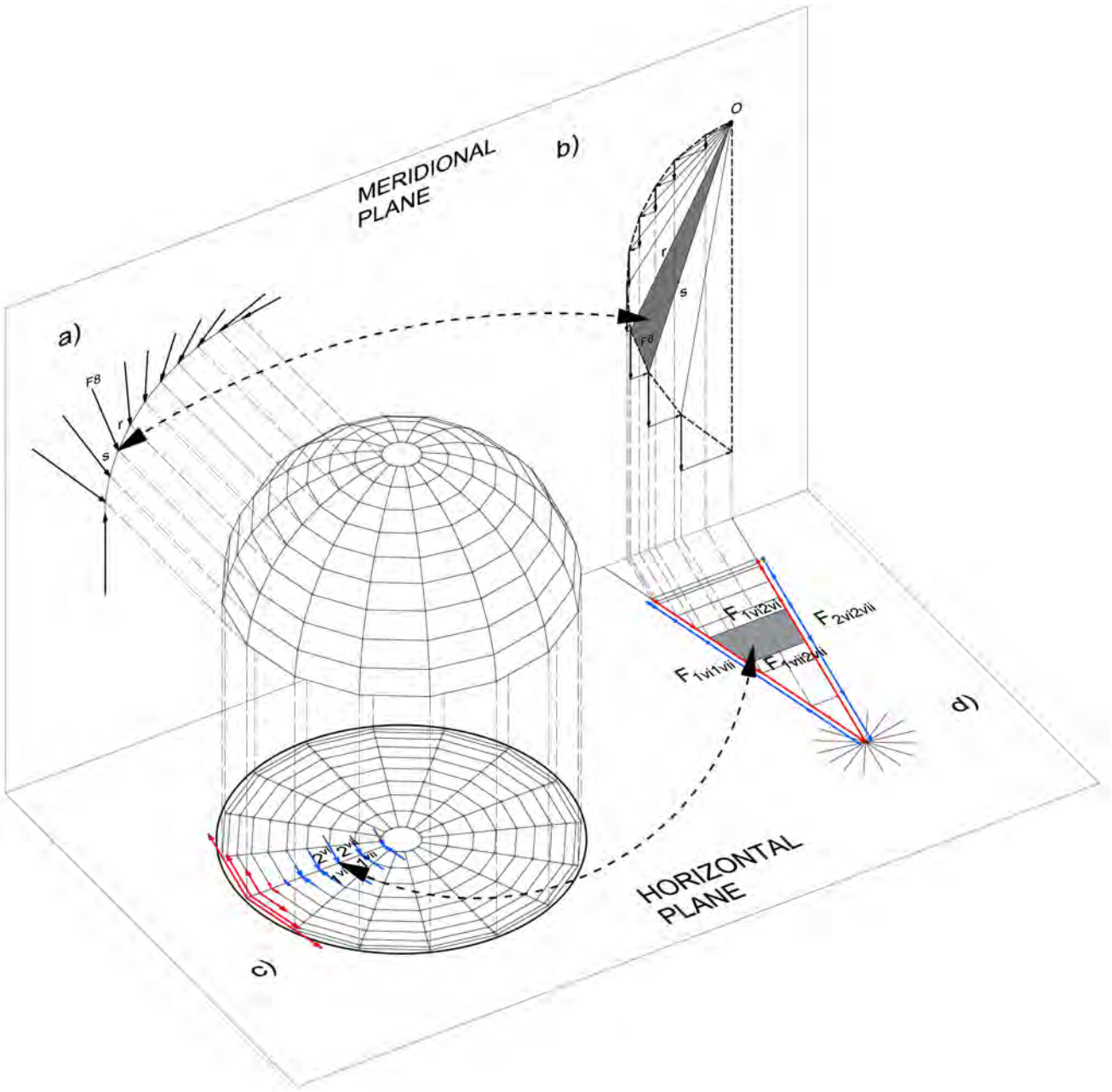


**Figure 54** Structural reciprocity. (a) System of forces, primal figure; (b) force polygon, dual figure; (c) horizontal projection of network, primal figure; (d) force polygon, dual figure.

### 6.2.4. Vector increments

Considering the weights of the different sectors, the necessary vector increment of each force is defined to fit the antifunicular polygon in the dome geometry. Therefore, the system of forces $F_1$, $F_2$, ... is formed by the weights and the vector increments.

Figure 98(b) to Figure 113(b), show the diagram of forces in the vertical plane. The dome geometry determines the angles of the polar rays ($\alpha_i$) which are parallel to the meridional lines of the simplified model. The increments ($\Delta_i$) are computed by fitting the forces in the polar rays; so the antifunicular polygon (dual figure) matches exactly the shape of the dome.

Setting the closed force polygon in the polar rays, the dome geometry matches with a closed antifunicular polygon of the system of forces. Hence the equilibrium of nodal internal forces in the vertical plane is achieved. Figure 98(a) to Figure 113(a) show the system of forces (weights plus increments) and the closed antifunicular polygon coincident with the dome geometry.

The vector increment is the difference between the horizontal projections of two consecutive meridian forces in each node. The value of the vector increment ($\Delta_i$) is the double of the radial component of the hoop forces, see Figure 53.

### 6.2.5. Horizontal plane: dual figure

As in (Block & Ochsendorf, 2007) the lines of interaction between nodes are projected in the horizontal plane, Figure 98(c) to Figure 113(c). These parallel and radial forces projected in this plane are considered in their dual form, Figure 98(d) to Figure 113(d). The reciprocity means that the dual figure (force polygon) has all of the characteristics of the primal figure but reversed: parallel lines on the primal figure are represented by radial force in the dual figure, while the radial forces in the primal figure appear as parallel lines in the dual figure. Each node in the primal system is represented by a quadrilateral of forces in the dual diagram.

Both primal and dual figure use Bow's notation (1873). For the primal figure, the capital letters, A, B, C,..., are sequentially placed clockwise in the intervals between external forces (open polygons) and numbers 1, 1', 1"… 2, 2', 2"…, are placed in the internal spaces (closed polygons) between projected network lines. Each line in the primal figure is bordered by two polygons (open or closed); thus, in the dual figure, the effort on the line is named using the corresponding letter or number of the adjacent polygons, e.g. $F_{AB}$ or $F_{12}$, $F_{11'}$…

The calculated values of vector increments ($\Delta_i$) are translated to the horizontal projection, allowing us to draw the dual figure, where the force polygons are closed, so the nodal internal forces are in equilibrium in the primal figure.

### 6.2.6. Procedure in both directions

One of the advantages of this methodology is that it can be applied in both directions, namely, determining the internal force solution for a given geometry of the dome, and inversely, choosing the geometry of the dome that is able to absorb a given internal force solution in equilibrium, and that is admissible for the material.

On the dual figure of the horizontal projection, Figure 98(d) to Figure 113(d), a statically admissible solution can be constructed with practically any position of the ring of the radial vectors $F_{AB}$, $F_{BC}$ …; the location distance of the radial vectors from the pole is arbitrary; outward or inward movement of this ring signifies increased or decreased parallel forces. The values of the forces are only limited by the strength of the material.

By an inverse procedure, it is possible to choose the angles ($\alpha_i$) of the dual figure in the vertical projection (force polygon), fitting them to the values of the radial vectors on the dual figure in the horizontal projection, that is to say, determining the dome geometry that is able to absorb the forces of a solution in equilibrium.

Figure 100 to Figure 103 show the new values of angles $\alpha_i$, for given variations in the internal forces. Figure 100(a) to Figure 103(a) (detail) illustrate that the variations in the values of the angles imply very little variations, relative to the dome thickness, of the meridional section of the simplified model.

# Chapter 7

# Basilica of San Juan de Dios

A new methodology of structural analysis of domes is presented through its application to the hemispherical dome of brick, of small thickness. Thin masonry domes are difficult to analyse with the traditional equilibrium methodologies such as the slicing technique, since it is difficult to find a thrust line within the thin section. The new methodology presented in this thesis aims to provide structural solution to the behaviour even in these type of difficult elements.

The "*encamonada* dome", typical of the Spanish Baroque, used that type of domes (thin, hemispherical and made of brick) in the inside. The Basilica de San Juan de Dios in Granada was chosen because it is a Baroque building, and it was believed to have an "*encamonada* dome". Furthermore, this is a benchmark in the Spanish Baroque, which merits study and appreciation.

Firstly, this chapter looks at the historical context of the "*encamonada* dome" typology. Thereafter, it reviews the development and architectural characteristics of the basilica, as well as a brief approach to the life and work of its architect José de Bada y Navaja.

The penultimate section analyses other similar domes (same style and time of building), which we have knowledge of their constructive system. All the data collected lead to the last section that defines the hypothesis of the constructive system of the basilica dome, with detailed 2D and 3D drawings of the different elements and the results of the measurement campaign.

**Figure 55** Dome and towers of Basilica of San Juan de Dios.

## 7.1. Historical context. The tile vaults and domes

The "*encamonada* dome" is a typology that was implemented, in accord with the directions of Fray Lorenzo de San Nicolás's treatise *Arte y uso de la arquitectura. Parte primera y segunda* [Art and use of architecture. First and second part] (1639, 1665). This typology had its peak along the 17th and 18th centuries in Spain and its overseas possessions. The "*encamonada* dome" is made up of an interior thin brick dome, with an exterior wooden structure and a slate or tile roof that defines the exterior shape. Precise details on this typology can be found at (Redondo, 2013) and (Huerta, 2003).

The concept of a tile dome or vault relates to those with one or more layers of bricks, in sailor or rowlock stretcher position. The first brick line is joined with plaster mortar. The mortar setting is fast enough to allow the construction of this type of domes without centring. The second and successive layers can be received with the same plaster, lime mortar or cement. For the new layers, the first one acts as a centring (Zaragozá, 2011).

### 7.1.1. Origins of tile domes and vaults

Traditionally there has been no consensus on the origins of this construction technique (López & Doménech, 2017), therefore this section addresses some of the main trends in this subject.

August Choisy in his work *L´art de bâtir chez les romains* [The art of building among the Romans] (1873) was one of the first to make a relation between the Roman brick layers under the concrete vaults and the tile vaults. However, he also said that these layers where to support the concrete that was the real solid and permanent structure. This Roman origin, was adopted by important authors in this field like in (Bergós, 1965).

Nonetheless, George R. Collins expressed doubts about this theory of the origin of tiled vaults in his work (Collins, 1968), and mentioned the reference of the letter of King Martin I *el Humano* of Aragon about the construction of the Royal Chapel in the Cathedral of Barcelona. Collins argued that Romans never used the bricks as in a timbrel dome.

Manuel Fortea Luna (2009) stablishes the origin of tile vaults is in those cultures that used bricks, plaster, and building without centring. He does not consider it as an "invention", but rather an evolution. Moreover, it is quite likely that areas with dry climates (and therefore it was difficult to find wood enough) had to develop systems of building without wood frames as centring.

A reference for vaults without centring are the byzantine vaults that needed no centring even with a slow setting mortar. Nevertheless, these vaults had a different arrangement of the bricks and a different structure behaviour. At present, there is a consensus about the Arabic origins of the tiled vaults and domes (Almagro, 2011); (Zaragozá, 2011); (Redondo, 2013) and (Fortea, 2009).

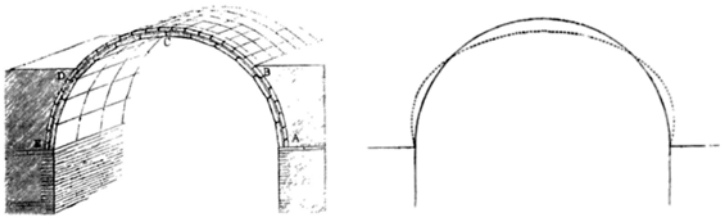

**Figure 56** (left) Building of a double layer vault with filling in the haunches; (right) deformation of a semi-circular thin vault (Choisy, 1873).

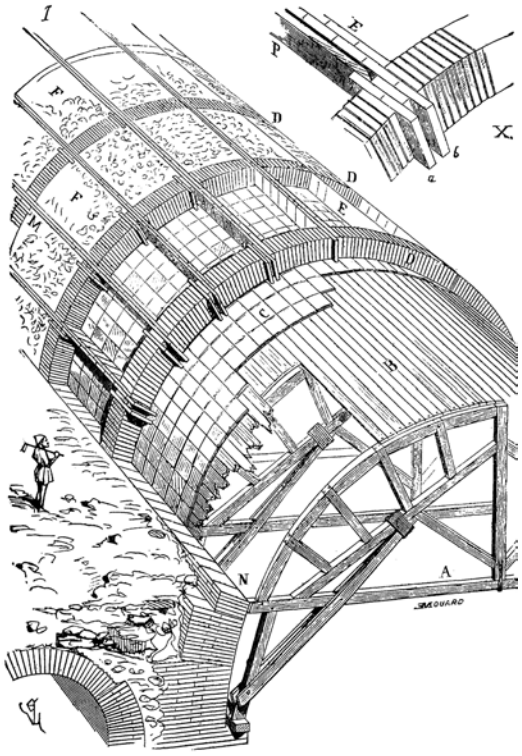

**Figure 57** Viollet-le-Duc´s drawings of the manner in which the Romans had constructed their concrete vaults in (Collins, 1968).

### 7.1.2. Beginnings in the Iberian Peninsula

This type of dome is not exclusive of Spain, and we can find examples along the Mediterranean Sea. Though it is true, that is in the Iberian peninsula where it developed more intensively, probably because of the mixture of building traditions such as the Arabic (using bricks and mortar) with the Cristian requirements (Redondo, 2013). Moreover, in the East coast of Spain along the 12th century, there was plenty of plaster and numerous manufacturing of tiles for pavement and it hardly had enough wood to supply the need for building boats.

The Arabs in the Iberian Peninsula used this technique; having one of the earliest examples in the chapel of Aznalcollar (Seville), but the exact date is not clear yet. However, it is likely that the most ancient tile vault in the Iberian Peninsula is in the ruins of Siyasa (Cieza, Murcia) (Almagro, 2011), though it is difficult to have an accurate date. It is part of the supporting structure of a stair shown in Figure 58.

**Figure 58** Remains of the tile vault of a stair in house number 10 in Siyasa (Almagro, 2011).

Zaragozá (2011) claims that one of the earliest monumental buildings with this constructive technique is in Castillo de la Atalaya de Villena (Alicante) from the end of the 12th century. Nonetheless, the same author states that this technique was fully implemented in the 14th and 15th centuries, being the first example in the convent Santo Domingo de Xátiva, see Figure 59. This building was started in 1291, and as usual in the Benedictine scheme it is organised around the cloister (1354), the chapter hall (1329) at the east, the church (1323) in the north, refectory at the south and reception at the west side. The church was not initially built with this system; it is in the Baroque period where the wooden roof of the church is substituted with tile vaulting.

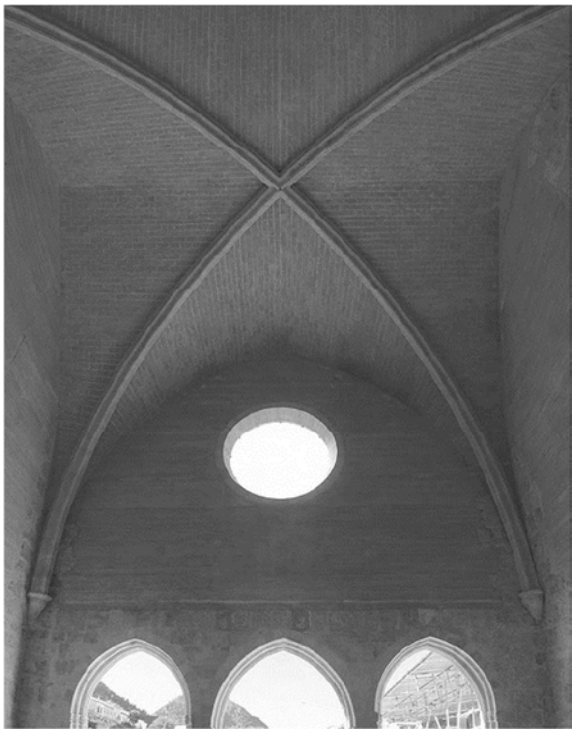

**Figure 59** Chapter hall of the Convent of Santo Domingo in Xátiva (1329) (Zaragozá, 2011).

Nonetheless, according to (Gómez, 2011), (Redondo, 2013) and (Soler-Verdú & Soler-Estrela, 2015), the first documented building with tile vaulting is the chapel of the Jofres, annex to the cloister in the Convent of Santo Domingo in Valencia. There is a building document signed in 1382, where the tiled vault construction system is detailed.

It is difficult to follow reliably the evolution of this technique along the 14th century, due to the Black Death and the war between the Crowns of Aragon and Castile, and we have to consider that before the Renaissance, all knowledge was secretly kept within the guilds.

There is a document in 1382 where the king Pedro of Aragon, showed interest in this technique for his own palace, and sent his merino[1] from Zaragoza to watch out this new technique. This lead us to think that at that time the knowledge of this type of constructions was starting to spread in the Iberian Peninsula.

Surprisingly, tiles vaults were used later in Catalonia, being one of the first examples the chapel of the Barcelona Cathedral, which is from 1407, by the Master Arnau Bargués following instructions from the king Martín *el Humano* (Bassegoda, 1978) (Collins, 1968). From this moment, this technique was fully adopted and developed in Catalonia.

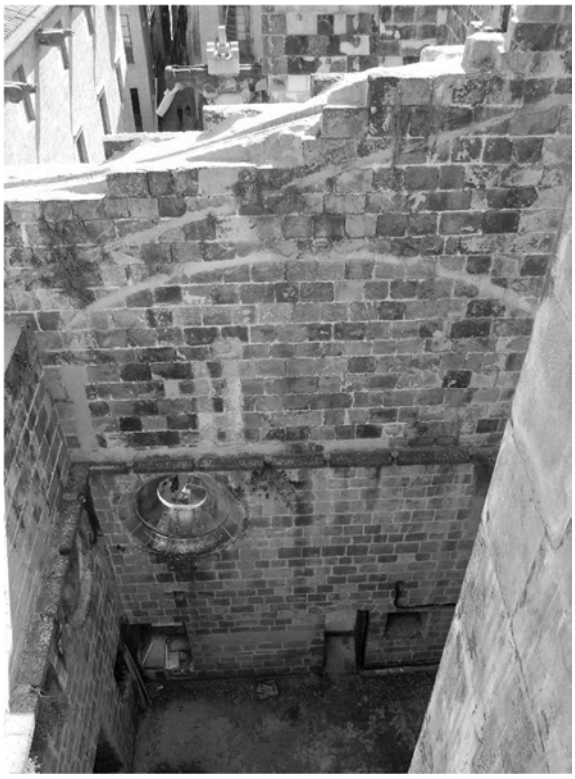

**Figure 60** Trace of the tile vault and the roof in the royal chapel of the Cathedral of Barcelona (Conejo da Pena, 2012).

[1] Merino: administrative position at that time, similar to a judge.

### 7.1.3. Spanish development in the Renaissance and Baroque

The 16th century is a period when the Gothic is still in use, but gives way to the Modern Era with the Renaissance. The ribbed vaults and pointed arches change disappeared and the new structures are semi-circular and spherical. These shapes generate an extra thrust that could be minimised by the low weight of tiled vaulting, which allows simpler structures, bigger spans and new proportions (Ibáñez, 2005).

In Valencia along the 16th century, we can find the use of tiles in webs, as in Monastery of San Miguel de los Reyes (second half of the 16th century) following the design of the Castilian master Alonso de Covarrubias. Nonetheless, it was increasingly more common to find tile vaults and domes with no ribs or key stones. Besides, a key difference was that the tiled surfaces were structural and not only a filling. This technique evolved, and it became quite popular at the end of the 17th century to add new inner vaults to gothic existing ones, in a Baroque style. A remarkable example of the end of the evolution can be found in the dome of Basilica de los Desamparados (Redondo, 2013), built in 1701, see Figure 61.

In Aragon, there was a particularity in that the ribs did not disappeared as it happened in Valencia. Initially they changed from stone to brick, and later they became purely decorative and executed with plaster. Javier Ibáñez (2005) and (2010) analysed different cases among which should be highlighted the extension of the cathedral or *quarto nuevo* between 1546 and 1550 (see Figure 62).

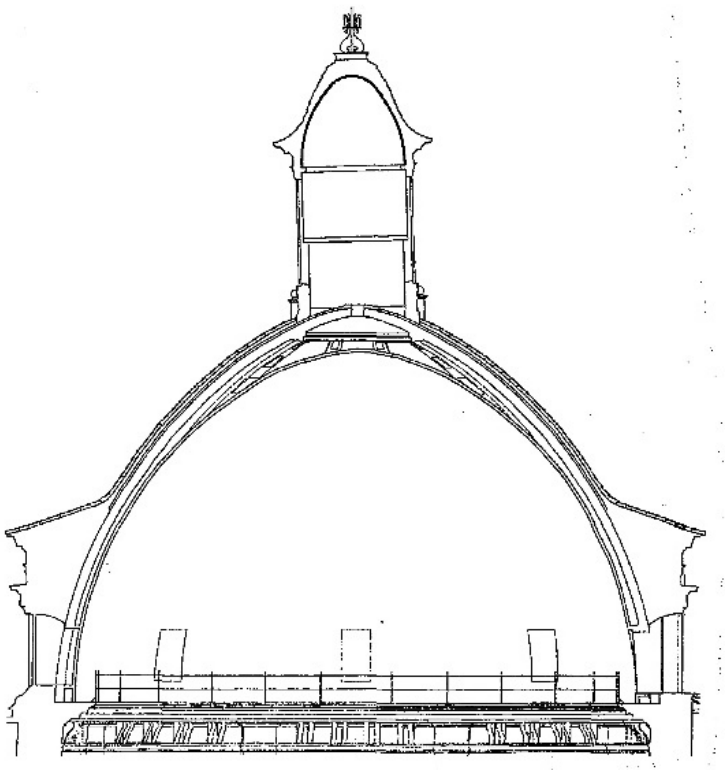

**Figure 61** Planimetric survey along the axis (taken from the project of Mr Ignacio Bosch).

**Figure 62** Interior of the extension of Cathedral of Zaragoza. View of the vaults in *quarto nuevo* (Ibáñez, 2010).

The same author states in (Ibáñez, 2010) that this system evolved into simpler, more resistant and easier to execute structures, with an increasingly Islamic influence, as it happens in the churches of Brea de Aragón or the church of Illueca, see Figure 63.

In Catalonia, there was a similar evolution as in Aragon; it means that in the 16th century there were numerous churches with ribs, key stones and tiled webs. There is an extensive study about them in (Bassegoda, 1978). The structural function of ribs and keystones progressively disappeared, but the ornamental remained.

Castile adopted this technique in the first half of the 16th century, but the main examples are Renaissance like the Hospital in Tavera (1540), being Alonso de Covarrubias the master of the construction. Esther Redondo (2013) highlights some key examples of tiled vaults like the Monastery of Santo Domingo el Antiguo in Toledo or the church of the Monastery of San Pedro Mártir in Toledo among others.

**Figure 63** Church in Illueca (Zaragoza). View of the dome and lateral vaults (Ibáñez, 2010).

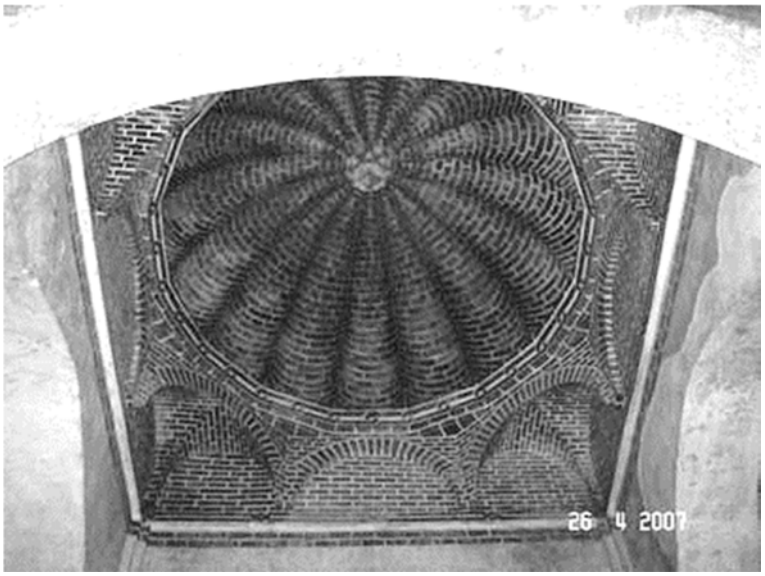


**Figure 64** Tiled dome in the Alhambra. *Puertas de Armas* (Fortea, 2009).

In Andalusia, there is the case of Aznalcollar that was mentioned in section 7.1.2. Zaragoza (2011) writes about cases of tiled vaulting in the 12th and 13th centuries like the Castle of the Atalaya de Villena. Manuel Fortea (2009) states that back in 1382, after the destruction of Algeciras, the use of tile vaulting was of common use. Furthermore, this author details some Andalusí cases but focused on some example of tiled domes in the Alhambra, which were built with flat bricks in the first half of the 14th century. The same author states that Almería was the most likely place where this technique started in the Iberian Peninsula in the 10th and 11th centuries.

## 7.2. Historical background of the basilica

The Basilica of San Juan de Dios, built by the architect José de Bada y Navajas (1691–1755), is a relevant construction in the historic heritage of Granada and constitutes a reference in the Spanish Baroque by both national (Gallego A. , 1982), (Isla, 1979), and international authors (Galloway, 1975). This dissertation presents a geometrical and constructive model of the dome over the transept, along with a structural analysis of the inner brick dome.

The Basilica was built between 1734 and 1757, and until the present day has remained largely unchanged (Galloway, 1975), with the exception of some minor renovation works that were carried out in 1913 and 1994 (and which are mentioned in this thesis).

### 7.2.1. José de Bada y Navajas

José de Bada (1691–1755) was a Baroque architect, heir of the classical tradition. He was born in Lucena (Córdoba) and shortly thereafter settled in Granada. He came from a family of stonemasons and architects and learned the profession with his uncle and father-in-law, Francisco Rodríguez Navajas, who had been Grand Master of some of the works of the first Grenadian Baroque.

In 1717, Bada succeeded him as a Grand Master of the Cathedral of Granada, and he continued the building of the Sagrario church. He was also Grand Master of the Cathedral of Málaga, carrying out the design and building of the façade and towers. Among a number of other Bada's works, of particular note are: the passageway that connects the Sagrario church with the Royal Chapel; the tower of the Compañía de Jesus church; the retrochoir of the Cathedral of Granada; the camarín of Nuestra Señora del Rosario; the altarpiece of the Basilica Virgen de las Angustias; the convent-hospital of San Juan de Dios in Lucena and the façade of the hospital of San Juan de Dios in Martos. However, Bada´s most significant work — which he completed entirely — was the Basilica de San Juan de Dios in Granada, along with the expansion and refurbishment of the adjacent hospital.

## 7.3. Architectonics characteristics

The dome was built according to the guidelines exposed in the treatise *Arte y Uso de Arquitectura* [Art and use of Architecture] from Fray Lorenzo de San Nicolás (1639, 1665). This work became a guide and a key reference in the religious architecture of the 17th century both in Spain and in the New World, since "*encamonada* domes" were more economical and structurally efficient than the previous vaulting techniques.

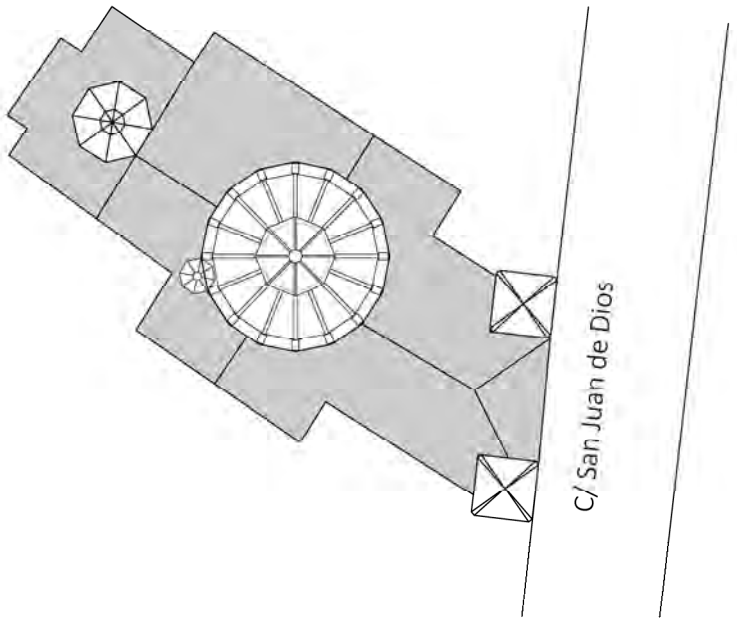


**Figure 65** Basilica plan and façade orientation.

San Juan de Dios is a basilica of a single nave with a Latin cross plan, inscribed in a rectangle, which tends to centralization (Greek cross plan) due to the similarity in the proportions of its arms, with the main nave being longer due to the choir. A space that initially seems static with a traditional cruciform plan transforms into dynamic by breaking it and penetrating it with the chapels, located on both sides of the nave, and the lateral dependencies of the main altar, which together with the choir, the arms of the transept and the grandstands create a characteristic interior space. The façade appears deviated from the axis of the main nave to adapt to the layout of the street. The axis breaks in the cancel[2], hiding this flaw, as seen in Figure 65.

A stone barrel vault covers the longitudinal nave with the choir at its feet and the main altarpiece at the head. The arms of the transept also topped by a barrel vault and finished with a straight wall. The main nave and transept intersect in the crossing that is covered by a large hemisphere on a drum where a union of space, light and colour, form to a beautifully assembled whole. Light comes from the upper part and it is sifted by the stained glass, sliding along the curved surface of the dome, resulting in a pictorial impression that contrasts with the bombastic ornamentation used by Bada.

There are certain elements that have classical forms that could be found in the Renaissance including: a plan with a centralized tendency; hemispheric dome; barrel vaults; semi-circular main arches; pendentives... But they coexist with others elements that are characteristically Baroque, such as: chamfering of the pillars; the quarter-sphere finish of the longitudinal nave; the mullions in the tribune, apparently held in the air and finished with a plaster rosette; lateral chapels that serve as a basis for two lateral curves of the choir…

Over the crossing rises a slender hemispherical dome, enhanced by the drum and lantern. The drum is supported by the toral arches[3]. In 1738, during the works of the Sagrario church, one of the crossing piers fractured, which prompted Bada to duplicate the main arches under the dome in San Juan de Dios, therefore, they present two parallel arches (Figure 66).

Four large piers support the entire scheme. The transition between the square floor delineated by the four piers, and the circular shape of the rings of the drum of the dome, is achieved through the four massive cut-stone pendentives. The perfect assembly of the pendentive with the pier, along with its adaptation to the shape of the pier and the main arches contributes to the overall stability of the building.

On the outside of the dome, a polygonal drum can be observed (Figure 83), while a rounded shape with eight openings can be found in the interior. The extrados of the dome offers a counter-curved shape, and a protective coating of green and white roof tiles. The lantern and towers are topped with spires.

[2]Cancel: architectonic element present in the Spanish churches; It is a wooden framework (screen), with three parts, located behind main entrance of church as a separator and protector element.

[3] Toral arch: Each of the four arches that support a dome. It can also be the main arches of a vault.

**Figure 66** Inside of the church under the transept. The main arches are doubled.

## 7.4. Analysis of references and data collection

In order to analyse the San Juan de Dios dome, the constructive system of reference at that time has been taken into account. As said in previous sections, this system is called the "*encamonada* dome", and it is firstly described in Fray Lorenzo´s treatise (De San Nicolás, 1639, 1665).

An analysis of similar domes has been undertaken, especially those that have been uncovered due to refurbishments:

- Magdalena Church in Seville.
- San Juan de la Penitencia in Alcalá de Henares.
- Real Concepción de Calatrava.
- Piedad chapel in Hermandad del Baratillo, Seville.

Finally, an on-site survey and a measurement campaign have been conducted, to check the materials used and to contrast the measures taken with the laser distant meter. The measures were taken from both, interior and the exterior of the dome.

### 7.4.1. Fray Lorenzo´s influence

The constructive hypothesis for the dome is that it was designed and built as a timber dome or "*encamonada* dome" in accord with the directions of Fray Lorenzo de San Nicolás. This typology refers to the arc shaped timber structure over the rafters, which gives the dome its final outer shape. The influence of Fray Lorenzo de San Nicolás is a constant in José de Bada´s work (Isla, 1977), as revealed in the manuscripts of the architect addressed to the Council of the Cathedral of Granada while he was directing, simultaneously, the works of San Juan de Dios and the works of the Sagrario church. In these manuscripts, to ensure stability, he recommended that the domes had to be built with bricks under a timber structure to support the spires.

Fray Lorenzo's treatise (1639, 1665), compiles with detail a constructive practice existing in the Crown of Aragon since the 14th and 15th centuries (Soler-Verdú & Soler-Estrela, 2015). It soon became a reference and guide for the religious architecture of the 17th century (Huerta, 2004), both in Spain and the New World.

Fray Lorenzo proposed to build hybrid domes with a timber structure on the outside and a brick dome within, as an alternative to the stone domes. He argued that his proposal had the following advantages:

- It was a faster and less costly way of building (the cost of a stone dome was four times that of a timber dome) (Hurtado, 2013).
- Lightness; better behaviour of brick dome against seismic movements.
- Lack of stone in the area; bad prevailing practices in the use of stone (the blocks must mature for two years from their extraction until their implementation, a recommendation that was never followed).
- Easier repair of brick masonry compared to stone ones.

In the treatise (De San Nicolás, 1639, 1665), Fray Lorenzo describes in full detail the way to build a timber dome and sets out rules for the proportions that "architects must follow in order to make them stable and beautiful". Fray Lorenzo describes thoroughly two structurally independent elements: The first of these was the timber structure with resistance elements arranged radially, which transmits the lantern weight, the cover material and the effects of the atmospheric elements on the drum. The second element refers to the interior hemisphere with a double brick layer that outlines the dome from the inside of the temple, see Figure 67.

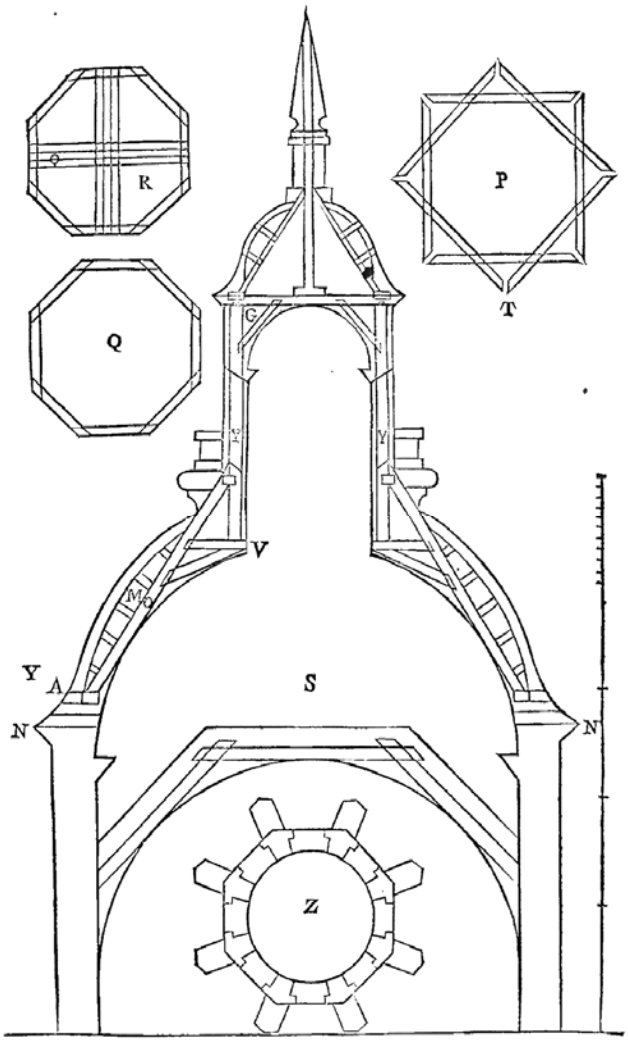


**Figure 67** Constructive configuration of the *encamondada* dome in Fray Lorenzo´s treatise (1639, 1665).

### 7.4.2. Analysis of similar domes

#### Magdalena church in Seville

The origins of the convent date back to 1248, founded by the King Fernando III. The church had undergone a previous reconstruction due to a fire in the time of Peter I of Castile and an earthquake in 1504. In 1690, a reconstruction begins, but due to the increase in the weight, in 1692 the old churched collapsed (Roda, 2016).

The dome that there is today in the Magdalena church, was built during the reconstruction works by the architect Leonardo de Figueroa in the period 1690–1709. It features a dome over a drum with an interior diameter of 9 meters, and has similar characteristics to the San Juan de Dios dome.

Between 1989 and 1991, the dome was repaired. Francisco Pinto (2005) describes the restoration works, including graphical documentation of the process. Figure 68 shows the rafters over the vertices of the octagon and the curved beams or *camones* from the cornice to the basement of the lantern.

**Figure 68** Dome of Iglesia de la Magdalena in the San Pablo Convent in Seville. Repairs works in the years 1989-1991 (Pinto, 2005).

The rafters are fastened by octagonal stirrups at the lower and upper part of the rafters. The stirrups are also secured with metal pieces in their corners, see Figure 69 (right). Over the *camones* there is a planking nailed to them, which serves as bracing.

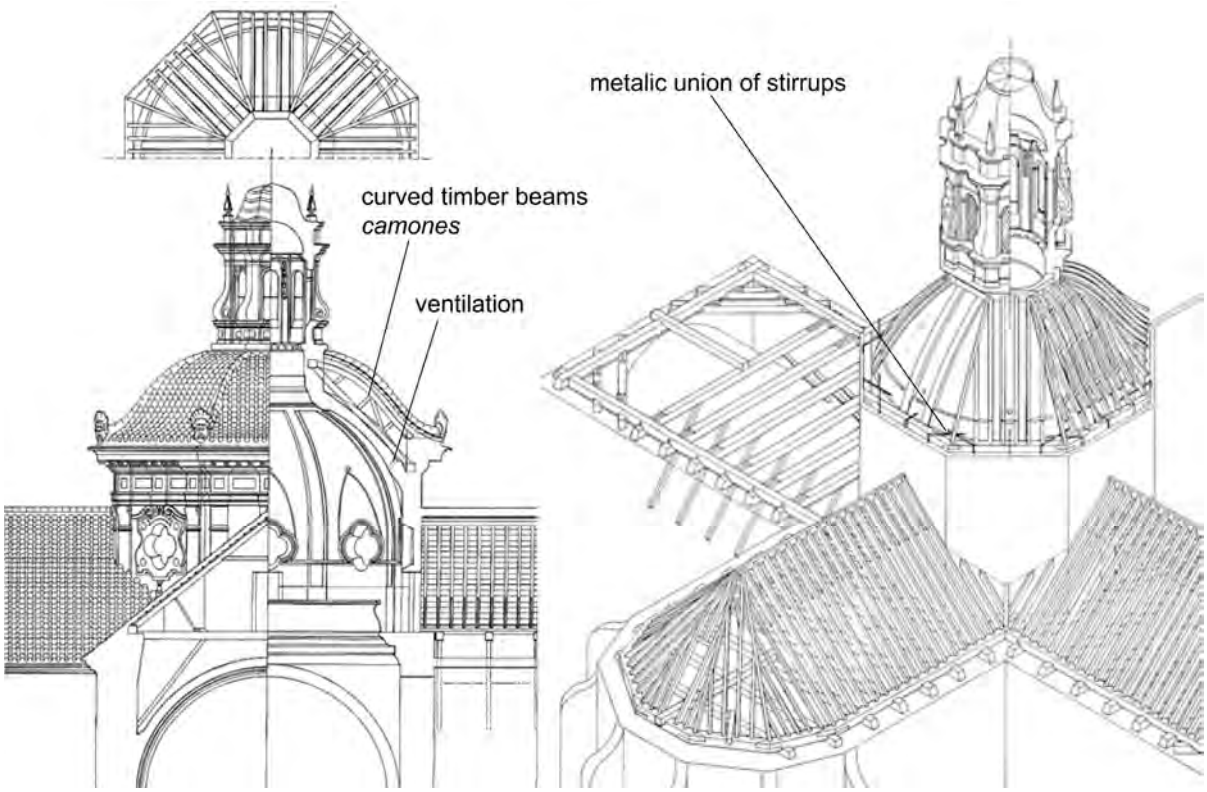


**Figure 69** (left) Section of the dome with the constructive system and (right) axonometric view (Pinto, 2005).

The exterior S-curved profile and the white and blue glazed ceramic roof tiles are typical of the baroque of the south of the peninsula (Galera, 1992). Due to the steep slope of the roofs and the big cornice, the exterior contour is slightly flattened.

Francisco Pinto specifies that this church follows Fray Lorenzo de San Nicolas´ guidelines, but with some differences, such as: The curved timber beams or *camones* do not meet the timber beams at the stirrup; the stirrups meet at their ends, so a metallic reinforcement is needed; there are ventilation openings, Figure 69.

**Figure 70** Union of curved rafters or *camones* (Pinto, 2005).

## San Juan de la Penitencia in Alcalá de Henares

The dome of the church of San Juan de la Penitencia in Alcalá de Henares (Madrid) was built in the 17th (Sánchez, 2015). The dome over the crossing is 7.30 m of inner diameter. It was rebuilt between 2004 and 2006, the renovation work is documented in (Vega, 2007) and (Martín, 2009), see Figure 71 to 73.

Although the dome completely collapsed in 1999, the architects made an in-depth survey to know the original construction system, and thus be able to reproduce it with the original techniques and crafts. This study of the original techniques is relevant to this dissertation because the authors confirm that the dome faithfully follows the guidelines of Fray Lorenzo de San Nicolas.

As discussed in (Vega, 2007), the dome collapsed in 1999, probably due to the contact between the wooden structure and the brick dome; the masonry was the first to collapsed followed by the collapse of the wooden roof. The author highlights how the backfilling of the extrados of the dome reaches exactly one third of the radius as advocated by Fray Lorenzo, underscoring the significant influence that this treatise had at the time.

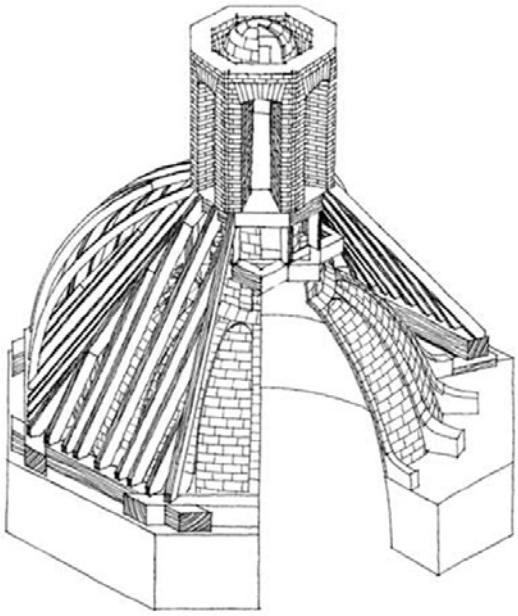

**Figure 71** Timber structure and brick dome in San Juan de la Penitencia church (Martín, 2009).

**Figure 72** Tile inner dome, with a single layer of brick and with a reinforcement up to one third of the height (Martín, 2009).

**Figure 73** (left) Timber structure; (right) *camones* over the rafters (Vega, 2007).

The study of the remains led to the conclusion that the original sleepers (crosstie) started off in a very low position instead of at the level of the third of the height of the dome; this meant an excessive closeness of the wooden structure to the brick masonry.

Since the dome has a relatively small diameter (compared to the dimensions proposed by Fray Lorenzo, see Table 1 in section 7.4.3), it was built with only one layer of brick and reinforcements up to one third of the height (though there are no archaeological traces of reinforcements in the original dome), see Figure 72. Furthermore, all the weight of the inner brick coat of the lantern rests in the inner dome.

## Real Concepción de Calatrava church in Madrid

Fray Lorenzo de San Nicolás built the Church of the Real de la Concepción de Calatrava in Madrid, between 1670 and 1678. It has an impressive dome with a diameter of about 12 metres (similar diameter to Basilica de San Juan de Dios).

In (Estepa, 2015), a photographic report is included of the interior of the structure and of the planimetry used during the renovation works in 2003. The restoration process revealed that the metallic reinforcement was more sophisticated than the one described by Fray Lorenzo (Figure 75).

The Real Concepción de Calatrava church is a magnificent example of an "*encamonada* dome", which perfectly follows what is dictated in the work of the author of the building, as it can be seen in the 3D of Figure 76.

**Figure 74** Concepción Real de Calatrava Church. Interior of the structure while restoration works (Estepa, 2015).

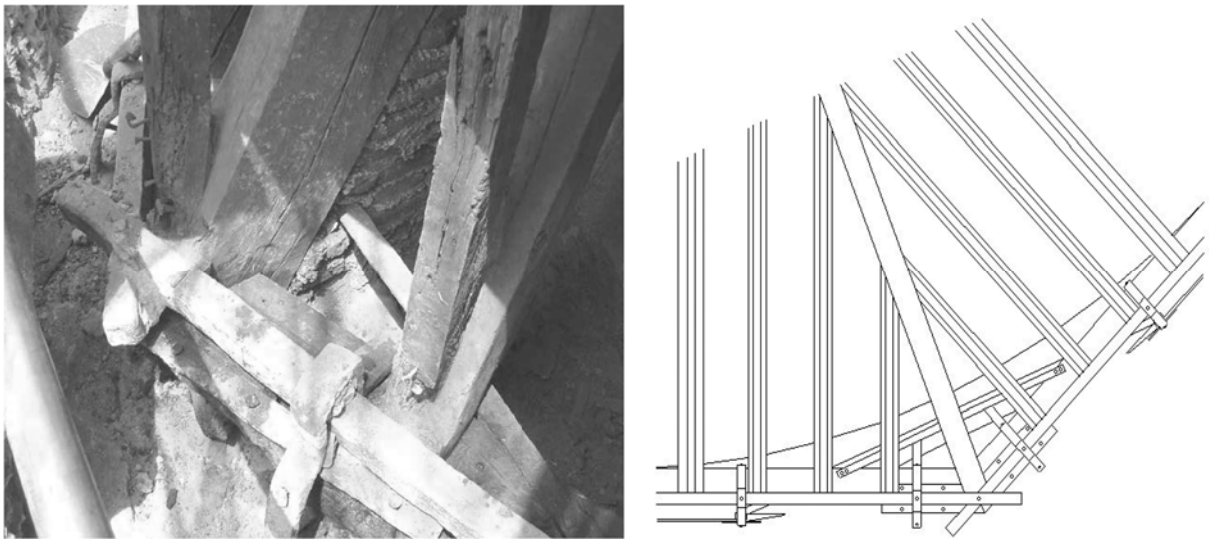

**Figure 75** (left) Photograph of the metallic reinforcements in the stirrups; (right) drawing of the reinforcements in the restoration project of José Miguel Rueda (2003) in (Estepa, 2015).

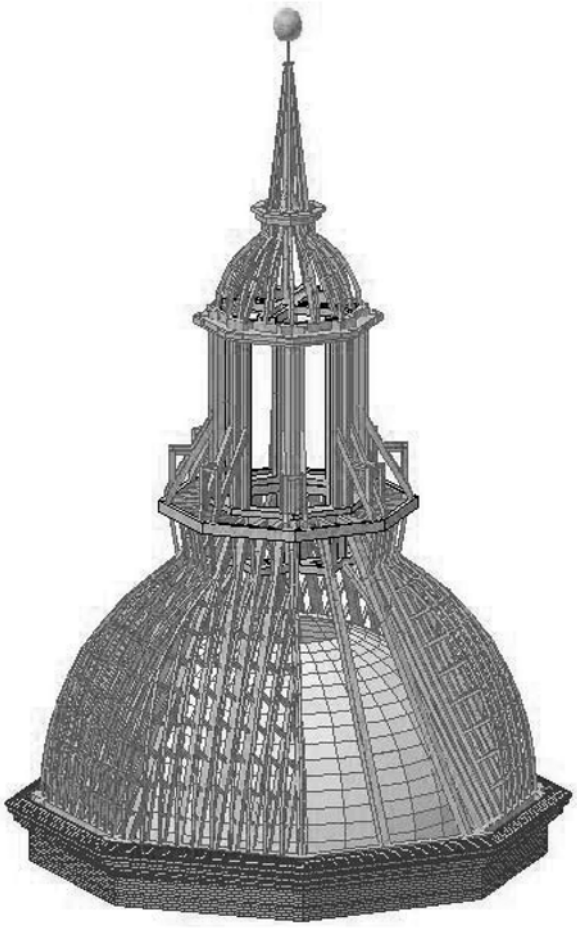

**Figure 76** 3D model according to the restoration project of José Miguel Rueda (2003) in (Estepa, 2015).

## Piedad chapel, Hermandad del Baratillo in Seville

In the Piedad chapel, Hermandad del Baratillo in Seville (Spain), which was built in 1724, the reconstruction works were carried out in 2007. All the process is documented in (Granero, 2009).

The drum is octagonal, and the dome diameter (4.60 m) is quite small compared to the dimensions proposed by Fray Lorenzo (see Table 1 in section 7.4.3). The typology is the "*encamonada* dome" as described in Fray Lorenzo de San Nicolas´ treatise, however it lacks the lantern.

The reconstruction project by Francisco Granero Martín had to renew the entire exterior, due to moisture that had rotten some of the timber, see Figure 77.

Even at a little scale, it is easy to appreciate all the elements of an "*encamonada* dome" like rafters, *camones*, planking and tile covering. The stirrups were replaced and reinforced with metallic bars. All the timber was treated against xylophages. The planking was renewed and with external waterproofing, see Figure 78.

**Figure 77** Original condition of the timber structure (Granero, 2009).

**Figure 78** Structure and finishing after the restoration work (Granero, 2009).

### 7.4.3. Visual inspection and measurements

The geometric and constructive modelling of San Juan de Dios dome has been developed from visual inspection of the different elements (see Figure 79), and measurements made with metric tape and laser meter. A first campaign of measurements is described in (Gallego F. , 2017) and (Suárez, Bravo, & González, 2019), those results were taken as a foundation to perform a new campaign of measures with a laser distance meter (Leica S910). The new measurements have allowed the generation of a 3D model with CAD software, which is shown in Figure 82.

**Table 1** General dimensions of the dome. Comparative table.

| DIMENSIONS | **Proposed by FLSN** | | | | **Obtained in San Juan de Dios** | | DIF. |
|---|---|---|---|---|---|---|---|
| | Feet | | Meters | | | Meters | |
| | Min. | Max. | Min. | Max. | | | |
| Inner diameter (d) | 30 | 40 | 8.34 | 11.12 | Inner diameter | 11.71 | 5.3% |
| Octagon-wall thickness (1/10)d | 3 | 4 | 0.83 | 1.112 | Drum wall thickness | 1.73 | 55.6% |
| Octagon-wall exterior diameter | 36 | 48 | 10.00 | 13.34 | Drum exterior diameter | 16.17 | 21.2% |
| Octagon-wall height | 20 | | 5.56 | | Drum height | 6.7 | 20.5% |
| Higher octagon-wall inner diameter (1/4)d | 7.5 | 10 | 2.08 | 2.78 | Lantern inner diameter | 3.9 | 40.3% |
| Higher octagon-wall exterior diameter (1/3)d | 12 | 13 | 3.34 | 3.61 | Lantern exterior diameter | 5.2 | 43.9% |

Table 1 compares the measurements obtained by inspection in situ, with those proposed in the treatise of Fray Lorenzo, having taken as equivalence, 1 foot = 0.278 m (Garza, 2012). While the inner diameter of the dome is similar to the maximum value proposed by Fray Lorenzo, the rest of the dimensions are between 20 and 50% larger than the maximum. Indeed, as is indicated in Table 1, for a dome of inner diameter 40 feet (11.12 m), Fray Lorenzo suggested a thickness of drum wall equal to 4 feet (1.112 m), and a thickness of the lantern drum of 0.42 m, both elements constructed of brick. In the dome of San Juan de Dios, the thickness of the drum wall is 1.73 m (55.6% larger), and the thickness of the lantern drum is 0.65 m, (55.9% larger). The greater thickness of both drum wall and lantern wall shows a conservative tendency in the design, possibly because of the collapse of the pillar under the cupola of the Sagrario Church, which could have led José de Bada to increase the thickness of the structure and to double the main arches under the dome.

## 7.5. Constructive system

Considering the data from precedent sections, Figure 80 shows the proposal for plan, elevation and section of the dome with indications for the main structural elements. In this figure, there is also two details for different hypothesis of the constructive system of the lantern. It was not allowed to do any test boring, but the structural analysis of the following chapters, will clarify which one is more likely to be, due to their structural efficiency.

**Figure 79** On-site check-up and measurement of the different elements in the dome.

**Detail hypothesis 1**: the tile dome supports the inner brick lantern.

**Detail hypothesis 2**: the timber structure supports the inner brick lantern.

Thanks to the kind help of the Orden Hospitalaria de San Juan de Dios; there could be a direct inspection of the interior and exterior of the dome. This allowed a careful inspection and precise measurement that could be contrasted with the ones obtained from the laser distant meter, as mentioned in section 7.4.3.

The results of all those inspections and measurements are reflected in the constructive model of the dome (Figure 80), where the main structural elements are:

- A: cupola of a single brick layer, of 3 cm in thickness.
- B: inside brick coating supported by the tile dome.
- B*: inside brick coating supported by the timber structure.
- C: octagonal timber ring, as base of the lantern.
- D: Inner dome with double brick layer, of 8 cm in thickness in total. The dome is built with brick of 3 cm in thickness; the bricks were laid in sailor position (with the bed visible). The speed of setting of this binder, along with the low weight of the bricks makes it possible to build them *in the air* (without falsework) (Truñó, 2004). The dome is bearing its own weight (≈ 1.2 kN/m$^2$). The density considered is 17.652 kN/m$^3$ (1800 kg/m$^3$), see (Suárez, Bravo, & González, 2019), (Suárez, Boothby, & González, 2020) and (Ministerio de la Vivienda , 1988 (revised)).

- E: timber curved centring, called *camones* that gives the S-curved exterior shape.
- F: rafters to support the *camones*, resting on the foot block. Pinewood from Sierra de Segura was used (Parra y Cote, 1759). A sixteen-sided polygonal drum supports the wooden structure, when the standard at that time was to use the octagonal polygons (De San Nicolás, 1639, 1665).
- G: planking with 3 cm thick wooden boards, nailed on the arches centring, creating a flat surface for the roof tiles, bracing the *camones* and providing a monolithic structure. There is a bonding mortar coat on the planking.
- H: white and green glazed ceramic roof tiles, on a mortar layer. In the renovation carried out in 1994, a series of galvanized steel nails of 30 cm length were placed on the roof, holding the roof tiles to the bonding mortar. In the restoration works of 1913, tiles were added that are still in the exterior of the drum (Isla, 1977).
- I: stirrups to fasten all the beams.
- J: foot block of wood, embedded in the drum.
- K: Haunch filling. Different hypotheses have been considered for the structural behaviour of this element.
- L: metallic reinforcement in corners.

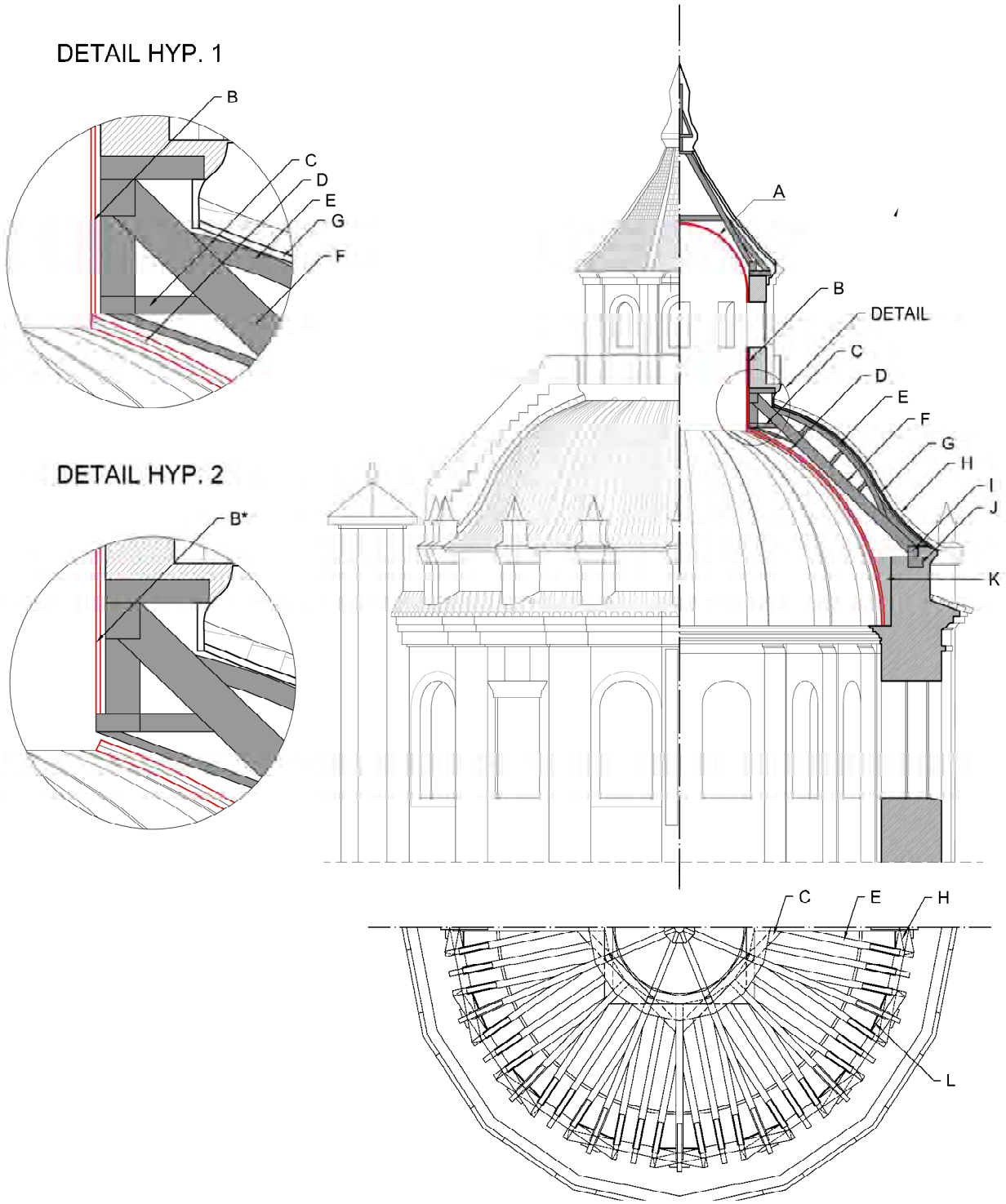


**Figure 80** Constructive system, floor plan, section and elevation of the dome, with details A and B for different hypothesis of the lantern support system.

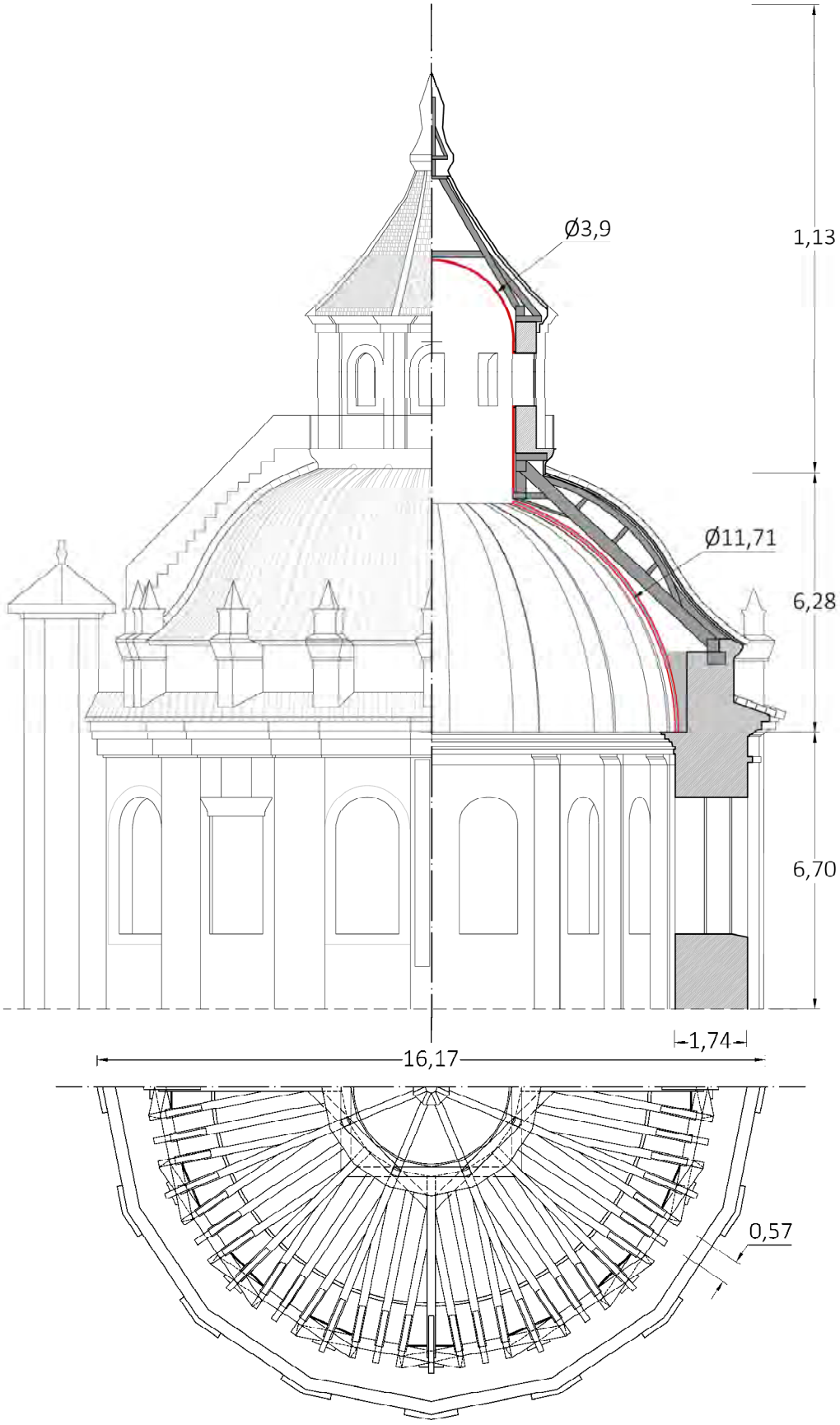


**Figure 81** Floor plan, elevation and section with dimensions.

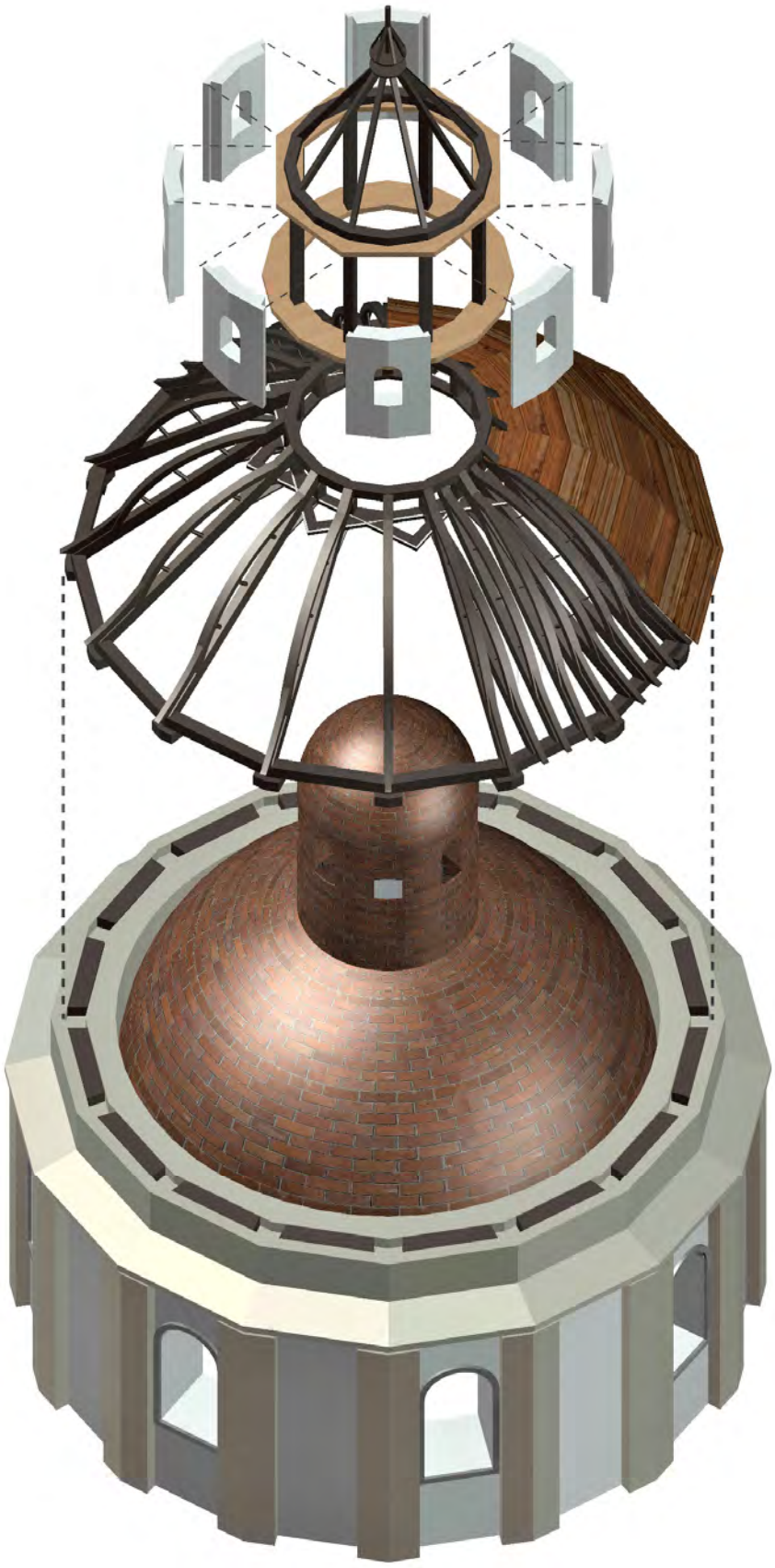

**Figure 82** 3D explosive perspective of the construction system of the dome.

### 7.5.1. Exterior cover

An element worthy of special attention is the exterior cover of white and green glazed ceramic roof tiles that defines the external appearance of the dome (Figure 84). It is a characteristic of Baroque architecture in southern Spain, unlike the Baroque of the peninsular centre where slate was used as a finishing element for the exterior covers, as indicated in Fray Lorenzo's treatise (Galera, 1992).

The use of slate appeared from the middle of the 16th century, initially in royal buildings of Felipe II (Estepa, 2015); nonetheless in Baroque works in southeastern Spain, the use of glazed tiles forming an exterior *alboaire*[4] was more frequent (Kubler, 1957) y (Gestoso, 1903).

The use of glazed ceramics dates back to ancient Egypt (Carter & Norton, 2007) and (Paz, 2008). They diffused from East to West in the 1st century BC (Torres, 1939), and it is in the Islamic Andalusian culture where it reaches its maturity as decorative element. From the 13th to the 15th centuries, the production centre was in Malaga (Benavent & Magro, 1996); later, with the decline of the kingdom of Granada, *alfares*[5] were dispersed to the east of Spain.

Probably there were different reasons why the use of slate as cover material was predominant in the central area of Spain (following the rules of Fray Lorenzo de San Nicolas regarding the exterior cover), whereas in the southeast it was the ceramic tile.

- One reason could be the presence of the *alfares* in the Southeast at that time.
- A second reason might be the climate. There is a relevant report from Alonso del Castillo de Monturque (Taylor, 1996) about a master meeting regarding the Tabernacle of the Cathedral of Granada, where Alonso explains the reasons to use glazed tiles as roof covering, *por fallezer* (the structures) *esas antizipadamente con el summon calor que se les introduze de la fuerza de el sol como la experienzia nos lo a manifestado en todas las obras de esta Ciu* [Because they died *(the structures)* early with the extreme heat of the sun´s force, as the experience has sanctioned in all the works of this city].
- A third reason, is that the use of roof tiles as cover material is related to the adaptation of the building rules from the Council of Trent (Benavent & Magro, 1996).

Figure 83 shows the beautiful drawing in the exterior of the dome, and Figure 84 displays a detail of the cover tiles from the lantern.

[4] Alboaire: Ceramic coloured tiled covering of roofs, vaults and domes, usually with geometrical designs.
[5] Alfares: Workshops to manufactures baked clay.

**Figure 83** Dome, towers. The beautiful *alboaire* is seen on the cover of the dome.

**Figure 84** Tiles in the exterior of San Juan de Dios dome, with the characteristics green and white tiles of the *alboaire*..

# Chapter 8

# Structural analysis with Guastavino´s formulas

The Guastavino´s formulation is explained in section 2.6.2. Furthermore, the application of the experimental formulas of Guastavino is analysed in (Huerta, 2001) and (Redondo, 2013). In this chapter, in order to apply the original formulas to the brick dome in the Basilica of San Juan de Dios, it is going to be considered two cases. Firstly, the case of a full hemisphere. Secondly, the case of a shallow dome (considering the first third as an embedding). For both cases the thickness will be 8 cm, and a density of 17.652 kN/m$^3$.

## 8.1. Full hemispherical dome

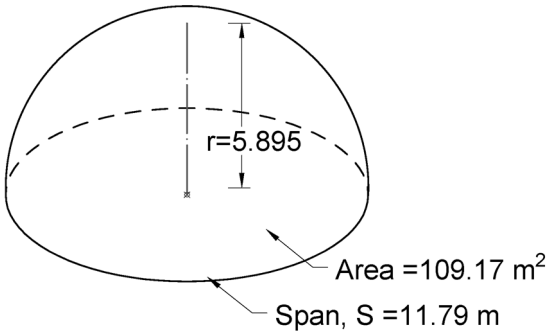


**Figure 85** Data from Basilica of San Juan de Dios for the Guastavino formulas. Case of full hemisphere.

In the full hemisphere, the values for the formula are the following:

- ***S*** (m): span: 11.79

- ***r*** (m): rise: 5.895

- ***L*** (kN) load: 26.15

- ***C*** (kN/m$^2$) coefficient for compression 14.600 from (Huerta, 2001) (reduced to 10%), giving a final coefficient of: 1.460

- ***T*** (cm) necessary thickness: unknown

Applying the data in formula (4):

$$T = \frac{L \cdot S}{C \cdot 16 \cdot r} = \frac{26.15 \cdot 11.79}{1460 \cdot 16 \cdot 5.895} = 0.0022 \quad (6)$$

The required thickness from (7) (0.0022 m – 0.22 cm) is much lower than real value (8 cm). This shows the ability of the shallow timbrel dome to resist the required stresses. However, resistance is not the determining factor in the design of a dome (Huerta, 2001)

## 8.2. Shallow dome

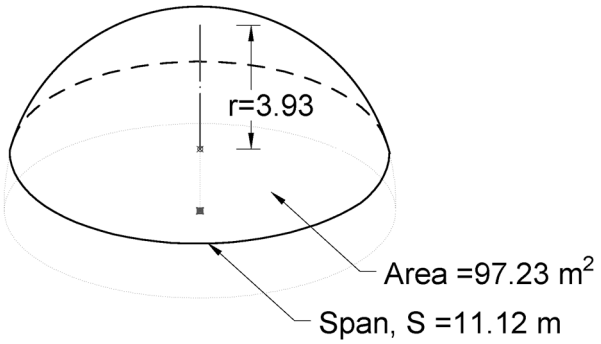


**Figure 86** Data from Basilica of San Juan de Dios for the Guastavino formulas. Case of shallow dome.

Considering the hypothesis that the filling is rigidly cemented, preventing the movement of the voussoirs. The dome is going to be considered as a shallow dome. The values for the formula are the following:

- ***S*** (m): span: 11.12

- ***r*** (m): rise: 3.93

- ***L*** (kN) load: 20.49

- ***C*** (kN/m$^2$) coefficient for compression (reduced to 10% from the breaking stress): 1460

- ***T*** (cm) necessary thickness: unknown

Applying the data in formula (4):

$$T = \frac{L \cdot S}{C \cdot 16 \cdot r} = \frac{20.49 \cdot 11.12}{1460 \cdot 16 \cdot 3.93} = 0.0025 \quad (7)$$

As commented in the previous section, the required thickness from (7) (0.0025 m – 0.25 cm) is much lower than real value (8 cm).

# Chapter 9

# Stability applying the slicing technique

In this work, the stability of the inner brick dome is also analysed by applying the slicing technique developed by Heyman (1966), (Heyman, 1995, b) and (Heyman, 2015). The suitability of this methodology to assess the stability of timbrel domes is commented in (Huerta, 2003) and (Redondo, 2013).

To apply the theory of limit analysis, the following assumptions must be assumed in the behaviour of the masonry:

- The material does not have tensile strength.
- The material can be considered with unlimited compressive strength.
- Sliding between masonry blocks cannot occur.

If this is the case, the safe theorem establishes that the masonry will be stable if it is possible to find a line of thrust, in equilibrium with the loads, which is included completely within the section of the masonry.

The geometric safety factor is defined by the ratio between the actual thickness and the minimum necessary thickness of the masonry to contain the thrust line. There is further information about the slicing technique and the safety factor in section 2.2.

## 9.1. Modelling of the dome for the slicing technique

For the present analysis, the dome is divided into fifty spherical spindles (lunes or slices); by checking the stability of each sector, the stability of the entire dome is guaranteed.

Due to symmetry, only one half of each sector is considered. Each sector is divided into 19 voussoirs; the weight of the inner brick lantern is added. Figure 87 shows the elevation and plan of the dome, with the main dimensions and colatitudes.[6]

[6] colatitude ($\varphi$): angle between the tangent to the meridian and the horizontal.

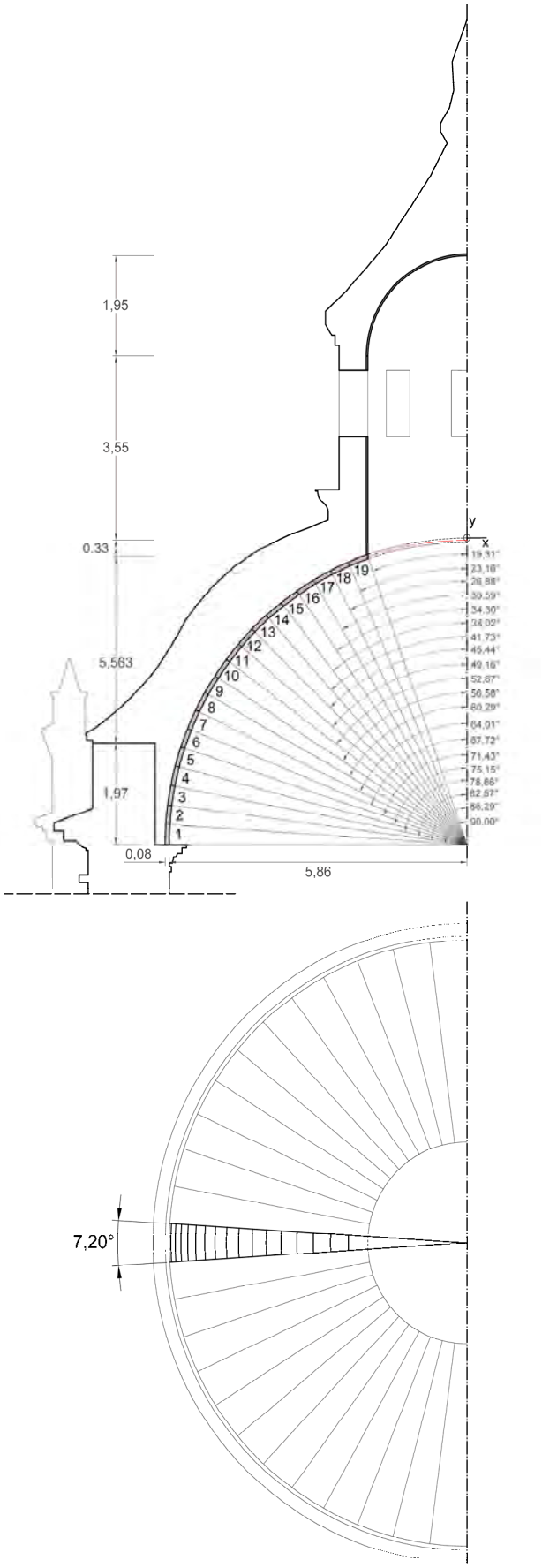


**Figure 87** Slice and voussoirs to be used in the slice technique, with origin of coordinates at the top vertex.

The stability of the dome without filling has been analysed, see 3D models in Figure 88(a) and (b), as well as, the stability of the dome with external filling up to a third of the height, as recommended Fray Lorenzo's treatise, see 3D models in Figure 88(c), (d) and (e).

Ramos and León (2013) analyse the structural behaviour of the filling of the vaults, according to its morphological characterization, distinguishing among rigid filling cemented, solid granular filling, loose granular filling, lightened filling and filling formed by construction rubble.

## 9.2. Structural cases and filling hypothesis

### 9.2.1. Filling hypothesis

This work considers the following three hypotheses to model the structural behaviour of the backfill:

**Hypothesis 1**: The filling is made of loose granular material; that does not contribute structural properties and is considered a dead load on the dome. This hypothesis is modelled by adding weights of the filling volumes into the system of forces, without increasing the section. See Figure 88(c).

**Hypothesis 2**: The filling is of firm granular material and therefore has a structural function. This hypothesis is taken by increasing thick-ness of voussoirs located in the lower third of the height. See Figure 88(d).

**Hypothesis 3**: The filling is rigidly cemented, preventing the movement of the voussoirs. This hypothesis has been analysed considering a shallow dome. See Figure 88(e).

### 9.2.2. Structural cases and tests performed

All cases, but the complete dome, consider the dome with and without the weight of the lantern. Therefore, there are nine different structural cases. There have been performed different tests for each case by considering different positions of the thrust in the keystone and the reaction in the springer. Each test has graphically determined the line of thrust.

The first test of each case a.1, b.1, c.1… is always with the thrust line in the keystone and the reaction in the springer, both at the middle point of the section. This gives us a first idea of the case. The second drawings for cases a; b; c; d; e, f and h, are extreme cases, where the start or end points are on the outer or inner edges of the section. Thus, it is easy to understand if there is any chance to find a possible solution where the thrust line is inside the masonry.

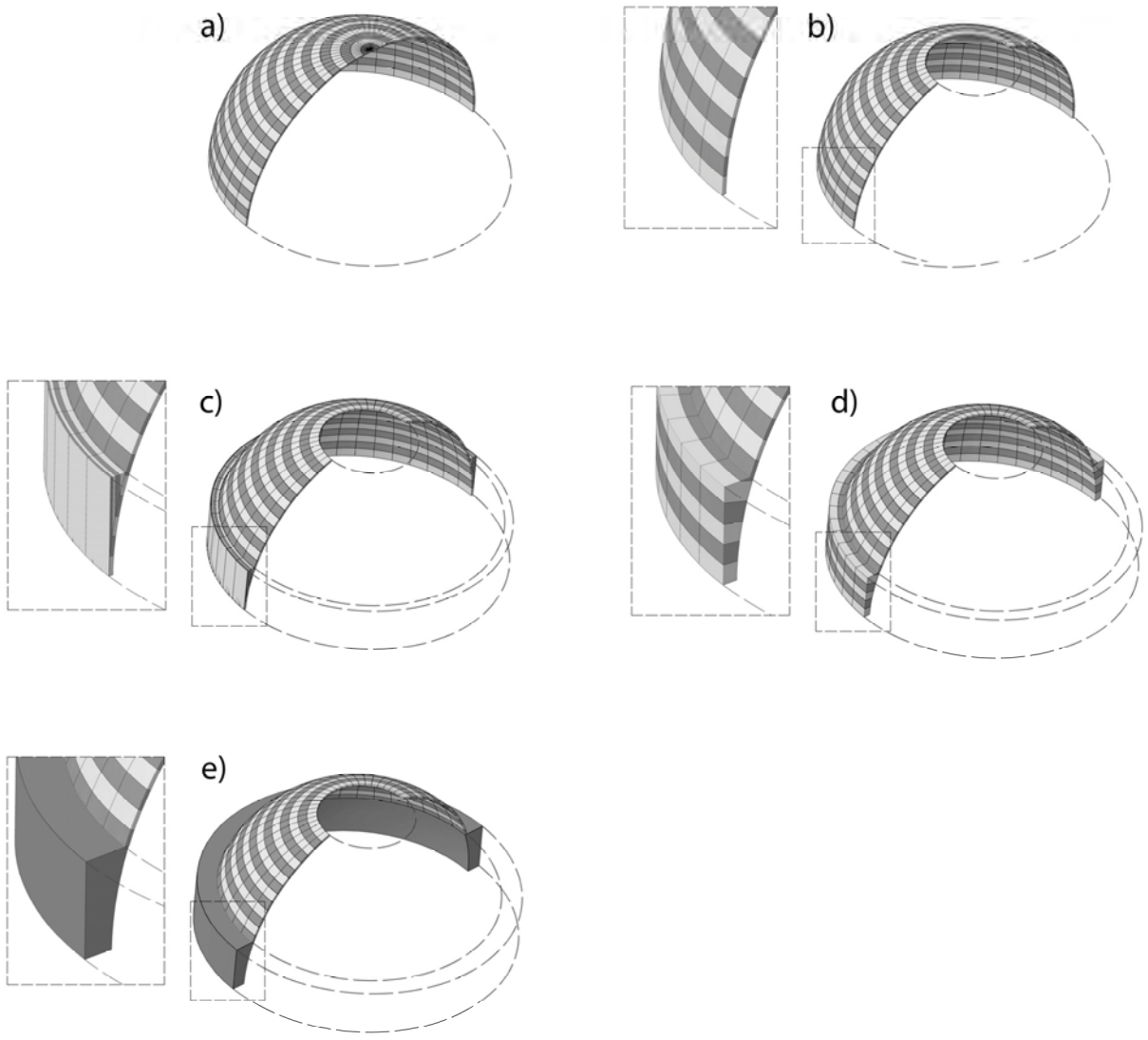


**Figure 88** Section of dome in the different cases: (a) hemisphere with no filling; (b) without filling and with oculus; (c) filling of loose granular material, without structural behaviour; (d) filling of firm granular material, with structural function; (e) cemented rigid filling, acting as an embedment so it is considered as a shallow dome.

In Figure 89, there is a matrix with thumbnails of all the tests performed.

The selected tests (within the dashed squares in the matrix) are for the cases with the thrust line within the section: dome with lantern and with firm granular filling with structural function (Tests g3, g4) Figure 93 and Figure 94; dome with lantern and with cement rigid filling (Tests i2, i3, i4) in Figure 95 to Figure 97. Additionally, other tests with lines out of the section, but close to it, are displayed: complete hemisphere (Test a2) in Figure 90 and hemisphere with lantern (Tests c2 and e2) Figure 91 and Figure 92.

For further information about the graphical process of finding the thrust line in a masonry arch, review section 4.4.


**Figure 89** Matrix with the tests performed with different initial and final points of the thrust line. The cases selected to be shown are highlighted.

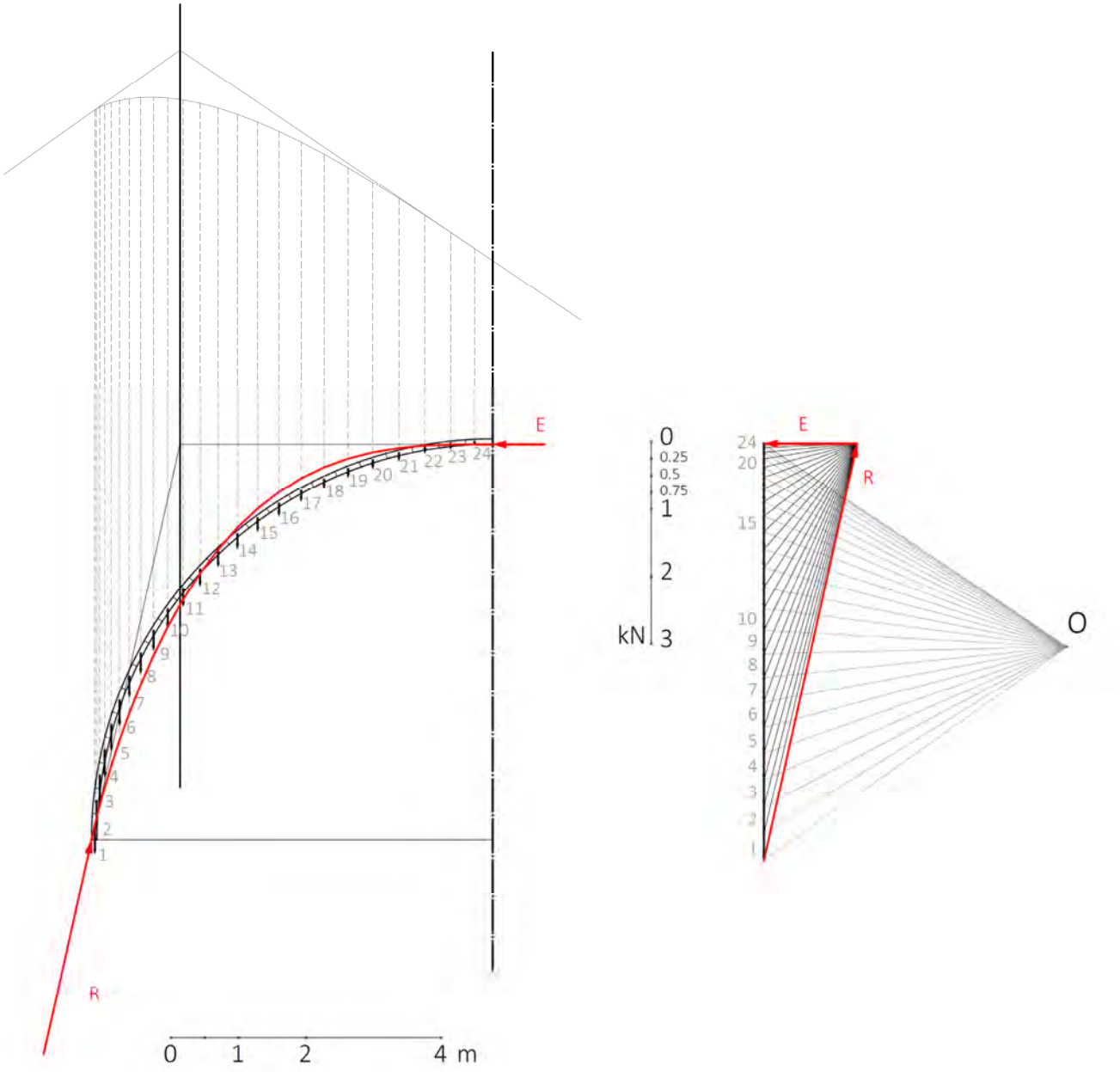


**Figure 90** Test a.2: complete brick dome without filling. Thrust line in the keystone at the bottom point of the section and the reaction in the springer at the exterior point of the section. The thrust line leaves the section.

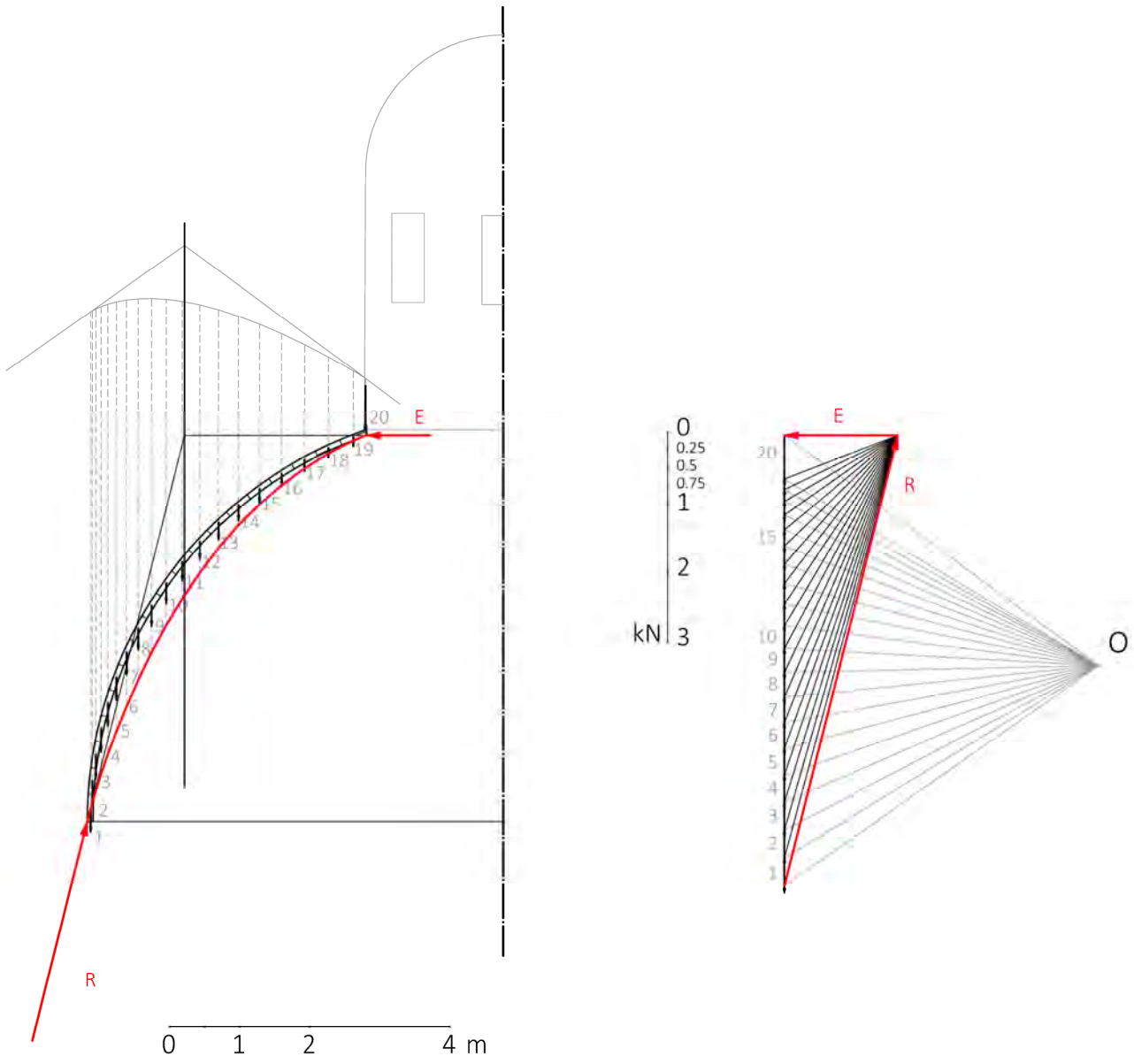


**Figure 91** Test c.2: dome with lantern and without filling. Thrust line in the keystone at the bottom point of the section and the reaction in the springer at the exterior point of the section. The thrust line leaves the section.

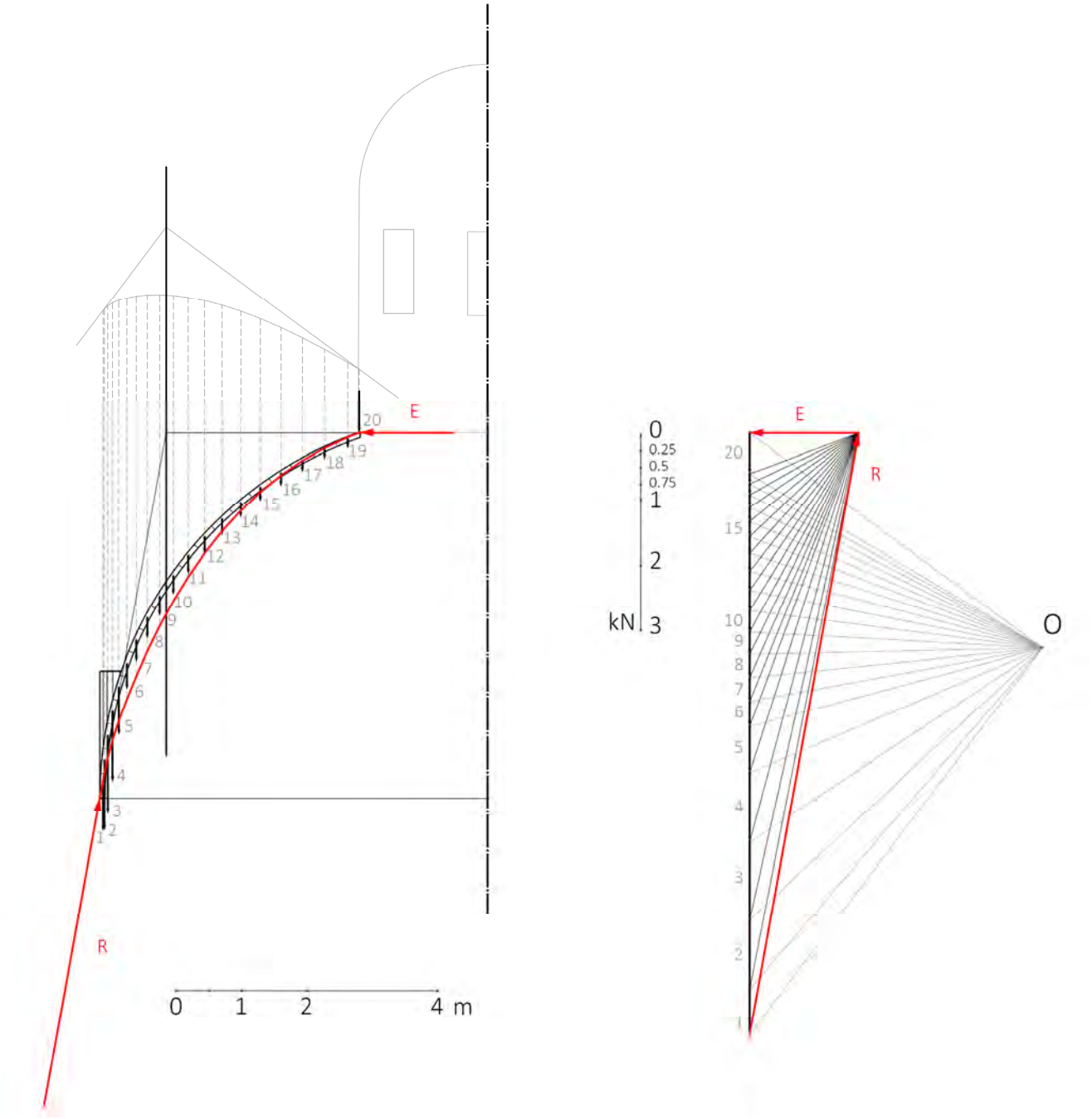


**Figure 92** Test e.2: dome with lantern and with loose granular filling without structural behaviour. Thrust line in the keystone at the top point of the section and the reaction in the springer at the exterior point of the section. The thrust line leaves the section, but the thrust line is not far from the section.

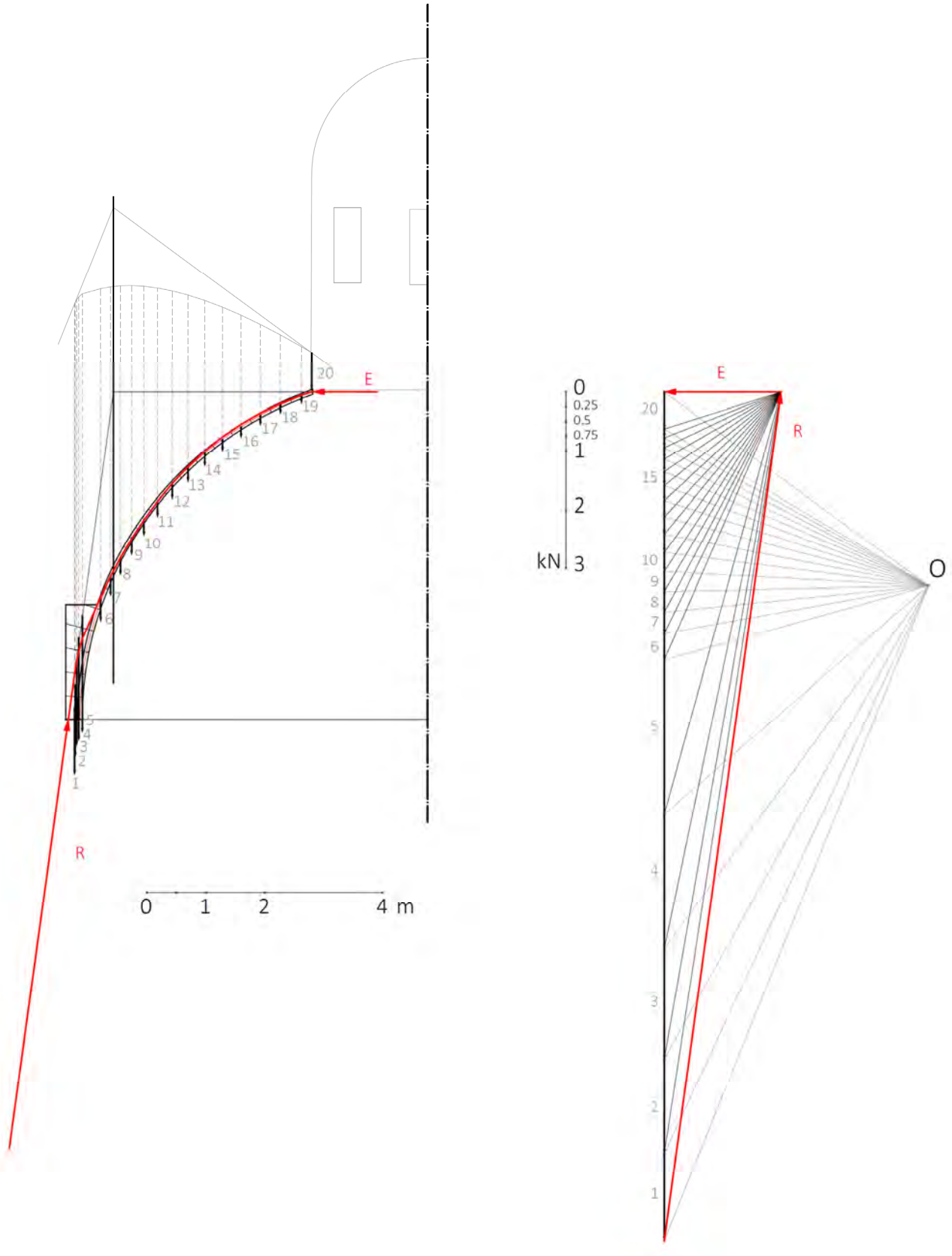


**Figure 93** Test g.3: dome with lantern and with firm granular filling with structural function. Thrust line in the keystone in the middle point of the section and the reaction in the springer at 11/13 outside the impost.
The thrust line is within the section with a **safety factor of 1.09.**

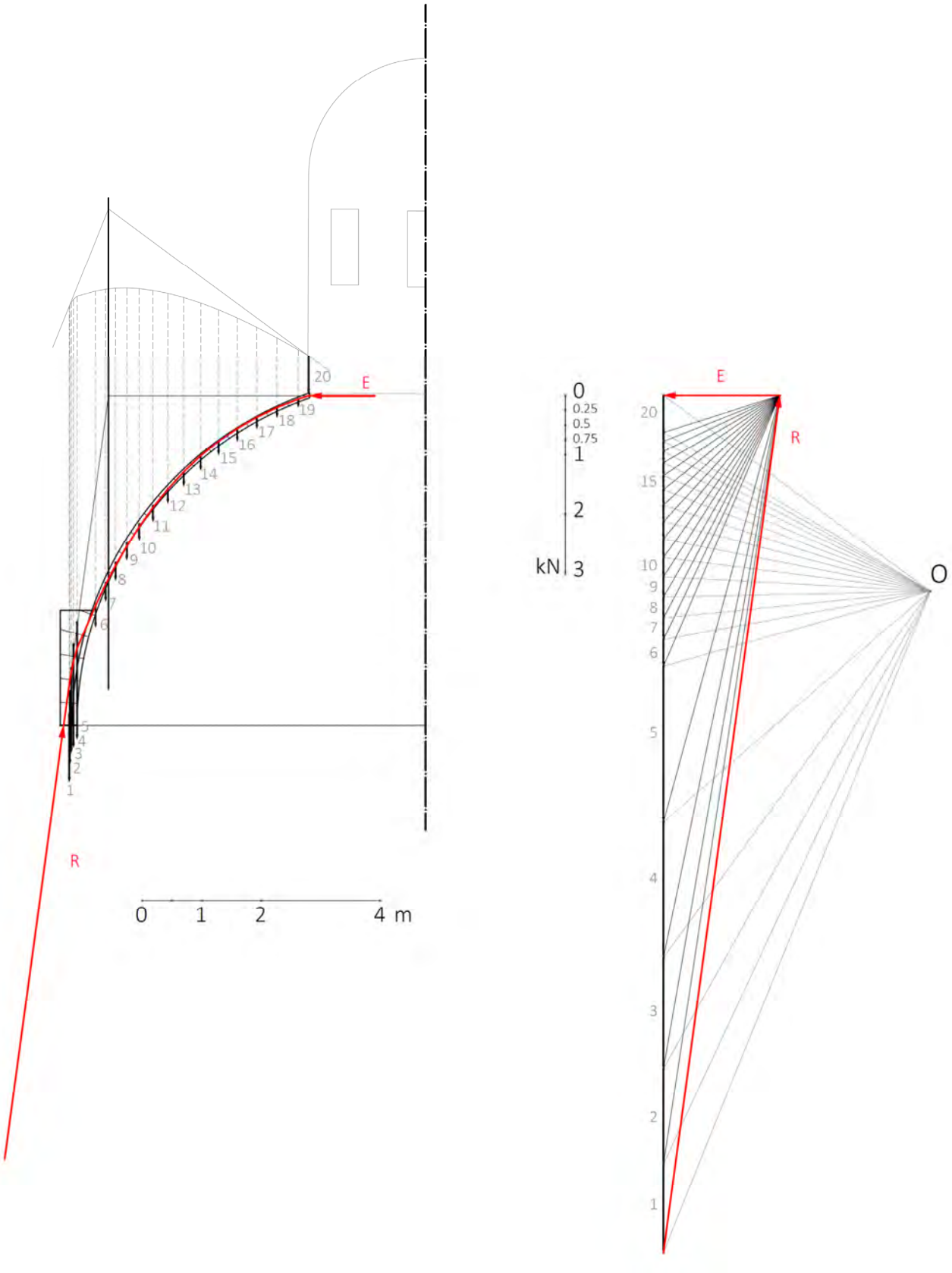


**Figure 94** Test g.4: dome with lantern and with firm granular filling with structural function. Thrust line in the keystone in the middle point of the section and the reaction in the springer at 8/10 outside the impost.
The thrust line is within the section with a **safety factor of 1.28.**

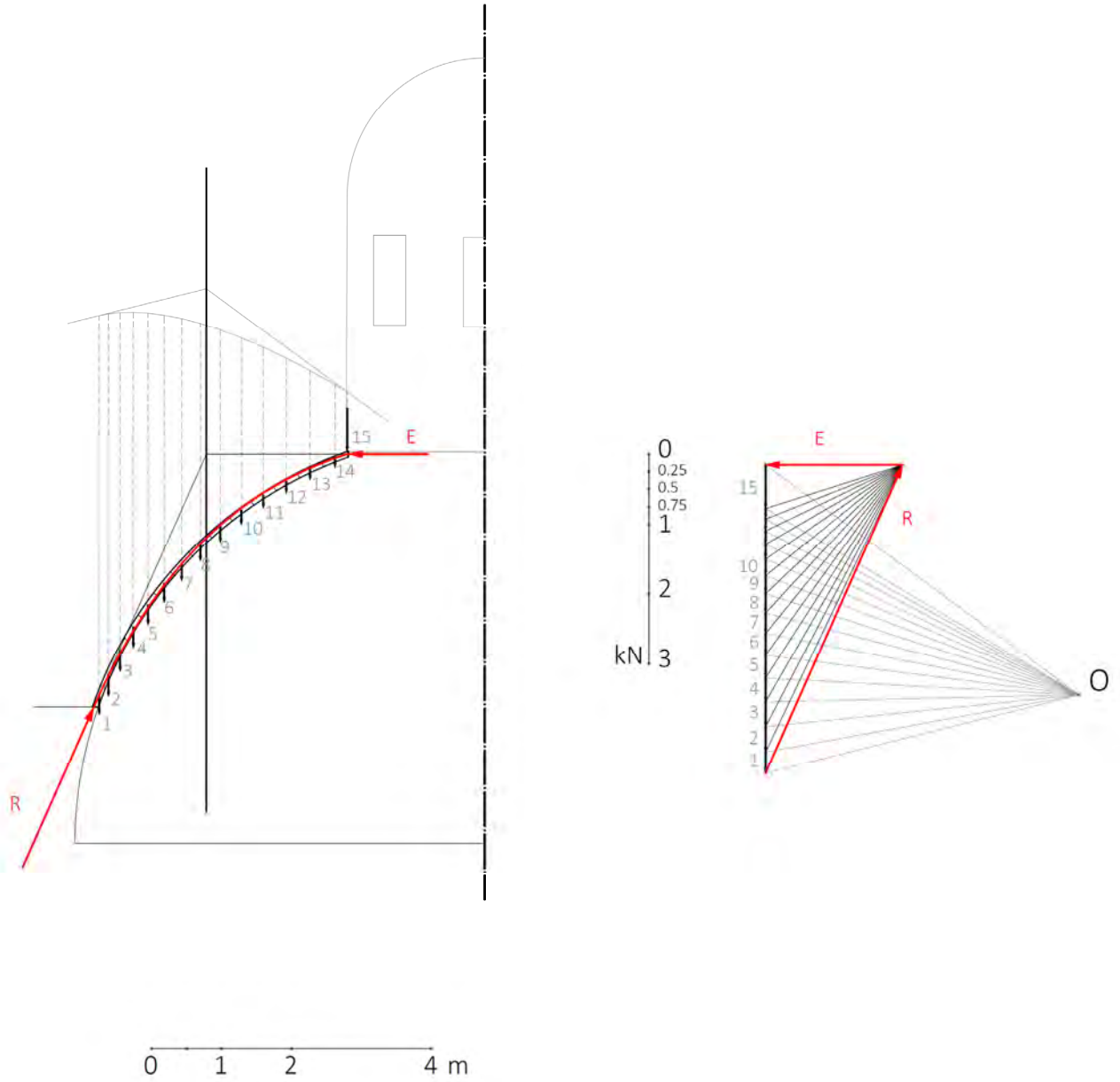


**Figure 95** Test i.2: dome with lantern and with cement rigid filling; a shallow dome. Thrust line at the keystone at the middle point of the section and the reaction in the springer at 3/4 outside the impost. The thrust line is within the section with a **safety factor of 1.21.**

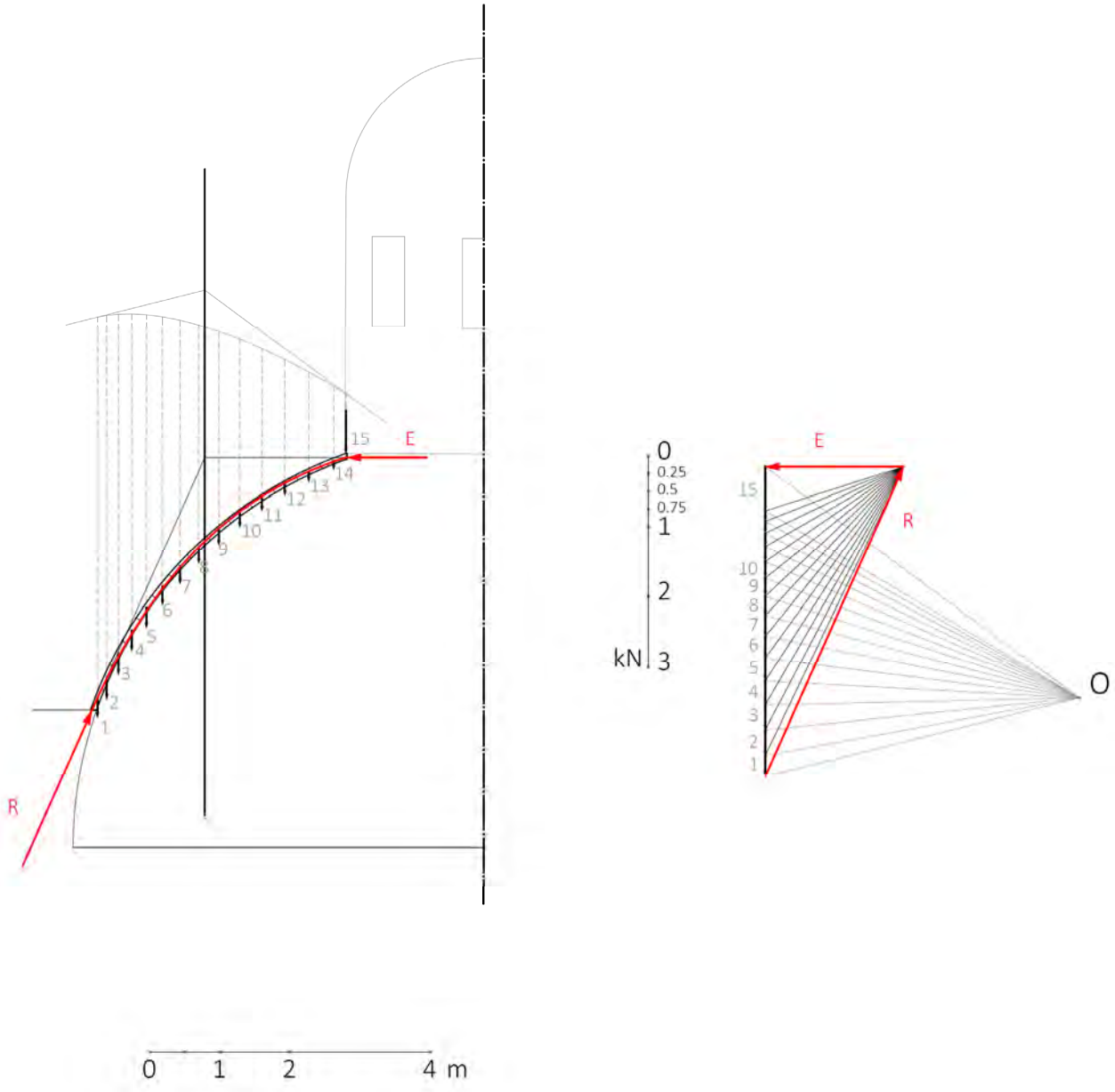


**Figure 96** Test i.3: dome with lantern and with cement rigid filling; a shallow dome. Thrust line at the keystone at 1/4 top point of the section and the reaction in the springer at 3/4 outside the impost. The thrust line is within the section with a **safety factor of 1.34**.

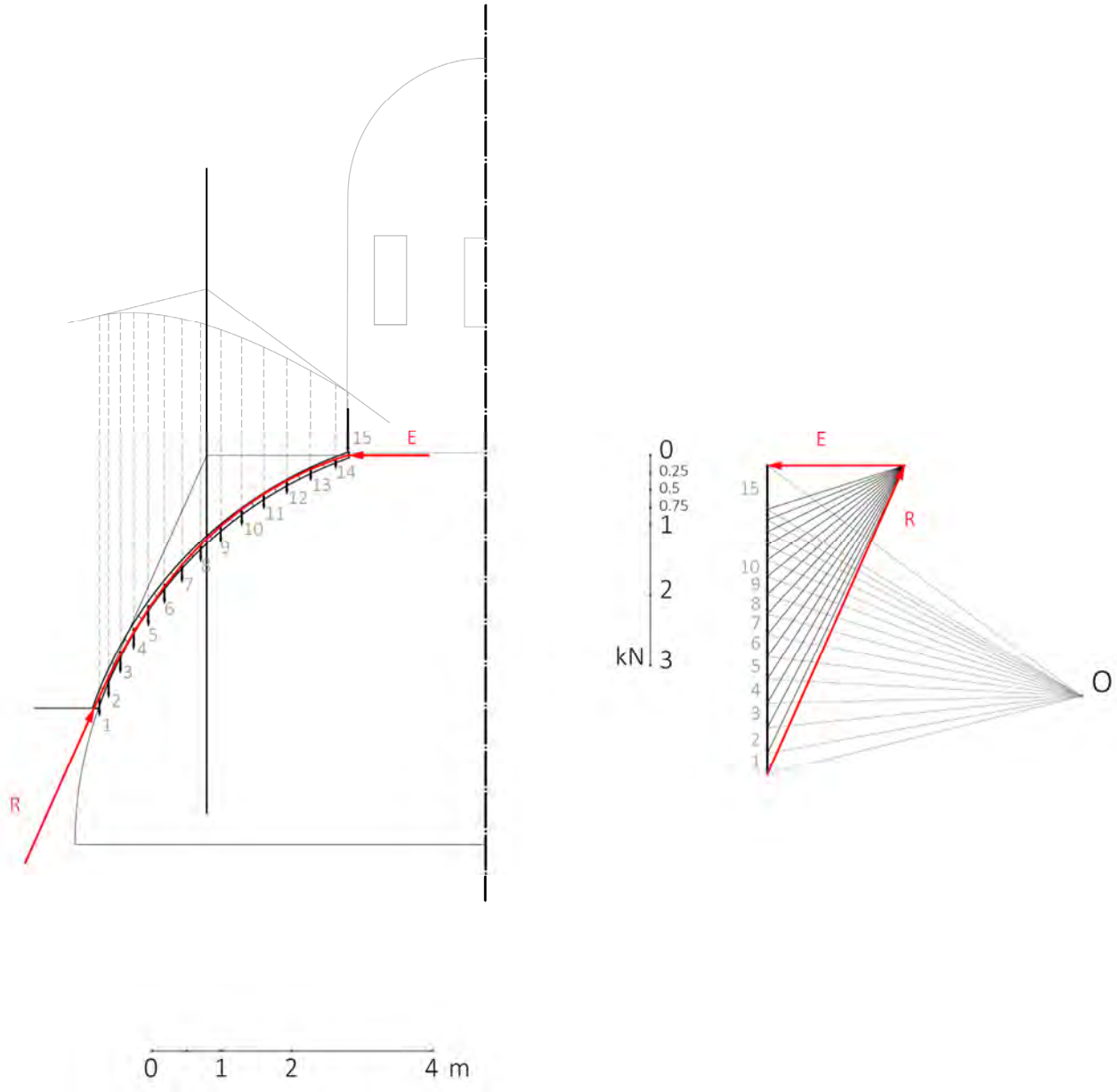


**Figure 97** Test i.4: dome with lantern and with cement rigid filling; a shallow dome. Thrust line at the keystone at 3/7 top point of the section and the reaction in the springer at 5/7 outside the impost. The thrust line is within the section with a **safety factor of 1.44.**

### 9.2.3. Results of the slicing technique

Only for some cases in hypotheses 2 and 3, and considering the weight of the inner brick coating lantern, have resulted a geometry of the thrust line in equilibrium with the loads, and which is included inside the section of the dome masonry.

The cases with the thrust line within the section of the dome masonry and their safety factor are the following:

- Test g.3: dome with lantern and with firm granular filling with structural function; Thrust line in the keystone in the middle point of the section and the reaction in the springer at 11/13 outside the impost. Safety factor of **1.09**.
- Test g.4: dome with lantern and with firm granular filling with structural function; Thrust line in the keystone in the middle point of the section and the reaction in the springer at 8/10 outside the impost. Safety factor of **1.28**.
- Test i.2: dome with lantern and with firm cement rigid filling. Thrust line at the keystone at 1/2 top point of the section and the reaction in the springer at 3/4 outside the impost. Safety factor of **1.21**.
- Test i.3: dome with lantern and with firm cement rigid filling. Thrust line at the keystone at 1/4 top point of the section and the reaction in the springer at 3/4 outside the impost. Safety factor of **1.34**.
- Test i.4: dome with lantern and with firm cement rigid filling. Thrust line at the keystone at 3/7 top point of the section and the reaction in the springer at 5/7 outside the impost. Safety factor of **1.44.**

All the safety factors are relatively low, far away from the safety factor of 2 recommended by Heyman (1995, b).

Table 2 shows a summary of the thrust and reaction forces, the angle of the reaction and the safety factor.

**Table 2** Slicing technique, data summary of results for the selected cases.

| TESTS | THRUST AND REACTION | | ANGLE OF REACTION (from vertical) | SAFETY FACTOR * |
|---|---|---|---|---|
| | E=H (kN) | R (kN) | Degrees | Dimensionless |
| g.3 | 1.98 | 14.55 | 7.83º | **1.09** |
| g.4 | 1.95 | 14.54 | 7.73º | **1.28** |
| i.2 | 1.96 | 4.82 | 23.98º | **1.21** |
| i.3 | 1.97 | 4.82 | 24.11º | **1.34** |
| i.4 | 1.96 | 4.82 | 23.98º | **1.44** |

* ratio between the actual thickness and the minimum necessary thickness of the masonry to contain the thrust line. See 2.7.2

# Chapter 10

# Application of the new graphical methodology

## 10.1. Tests performed

Tests have been carried out applying the new graphic methodology presented in Chapter 6, to determine the values of internal forces in equilibrium in the brick masonry dome that was described in section 6.1.

Firstly, the methodology is laid out by dividing the hemisphere in 160 sectors, with the aim of enhancing the graphic constructions, (Test 1 to Test 10). Afterwards, a model with 640 sectors has been tested, in order to compare the results obtained with those produced by the application of the membrane analysis, (Test 11 to Test 13).

Test 1 analyses a complete hemisphere, considering a vertical support reaction, while in Test 2 it is considered that the reaction is slightly tilted (3º). Tests 7 and 8 address the hemisphere with oculus and the hemisphere with lantern.

Test 3 to Test 6 show the application of the methodology in an inverse way. Enforcing variations in the values of the maximum tensions, new internal forces solutions in equilibrium are calculated, determining the necessary variations in the values of the angles ($\delta\alpha i$).

Tests have also been carried out considering the presence of a filling up on the extrados of the dome, until one third of the height, and considering three hypotheses about its structural behaviour (tests 9.1, 9.2a, 9.2b, 9.3): no structural function; structural filling with staggered shape; structural filling with soft curved shape; cement rigid filling (shallow dome).

Finally, Tests 11, 12 and 13, show the test on the complete hemisphere, with oculus and with lantern. They all consider vertical reaction, and the discretisation of 640 sectors.

The list of tests presented in this work is the following:

1) Hemispherical dome considering vertical reaction, with 160 sectors. (Figure 98).

2) Hemispherical dome considering tilted reaction, with 160 sectors. (Figure 99).

3) Hemispherical dome considering vertical reaction and 5% reduction in maximum tension forces ($F_{E1}$, $F_{E2}$…) absorbed by second tension forces ($F_{11'}$, $F_{22'}$…), with 160 sectors. (Figure 100).

4) Hemispherical dome considering vertical reaction and 5% reduction in maximum tension forces ($F_{E1}$, $F_{E2}$…) absorbed by third tension forces ($F_{11'}$, $F_{22'}$…), with 160 sectors. (Figure 101).

5) Hemispherical dome considering vertical reaction and 5% reduction in maximum tension forces ($F_{E1}$, $F_{E2}$…) absorbed by fourth tension forces ($F_{11'}$, $F_{22'}$…), with 160 sectors. (Figure 102).

6) Hemispherical dome considering vertical reaction and 15% reduction in maximum tension forces ($F_{E1}$, $F_{E2}$…) absorbed by all other tension forces ($F_{11'}$, $F_{22'}$… $F_{1'1''}$, $F_{2'2''}$… $F_{1''1'''}$, $F_{2''2'''}$), with 160 sectors. (Figure 103).

7) Hemispherical dome with oculus considering vertical reaction, with 128 sectors. (Figure 104).

8) Hemispherical dome with lantern considering vertical reaction, with 128 sectors. (Figure 105).

9.1) Hemispherical dome with lantern and filling on the extrados up to one third of the height, with 128 sectors. Hypothesis 1: no structural filling; considering vertical reaction. (Figure 106).

9.2a) Hemispherical dome with lantern and filling on the extrados up to one third of the height, with 128 sectors. Hypothesis 2: structural filling. Stagger shape filling, considering tilted reaction (0º, 3º, 6º). (Figure 107).

9.2b) Hemispherical dome with lantern and filling on the extrados up to one third of the height, with 128 sectors. Hypothesis 2: structural filling. Soft curved filling, considering tilted reaction (0º, 3º, 6º). (Figure 108).

9.3) Hemispherical dome with lantern and filling on the extrados up to one third of the height, with 96 sectors Hypothesis 3: cemented rigid filling; considering tilted reaction (Figure 109).

10) Hemispherical dome with lantern and filling on the extrados, without tension forces, with 128 sectors. (Figure 110)

11) Hemispherical dome considering vertical reaction, with 640 sectors. (Figure 111).

12) Hemispherical dome with oculus considering vertical reaction, with 512 sectors. (Figure 112).

13) Hemispherical dome with lantern considering vertical reaction, with 512 sectors. (Figure 113).

In all the figures (Figure 98 to Figure 110 and Figure 111 to Figure 113), the content is as follows:

Figures (a): system of forces (weights plus increments) and the closed antifunicular polygon, coincident with the dome geometry.

Figures (b): force polygon, where vector increments are determined so the simplified model fits to an antifunicular polygon of the system of forces.

Figures (c): plan of the simplified model; the hoop forces, of tension and compression, obtained in figures (d) are also represented.

Figures (d): dual figure of the plan of the simplified model; the values of the hoop forces (radial vectors) are defined from the calculated values of increments; and conversely, from any value of hoop forces, the angles $\alpha i$ are determined.

See Figure 54 for a three-dimensional analysis.

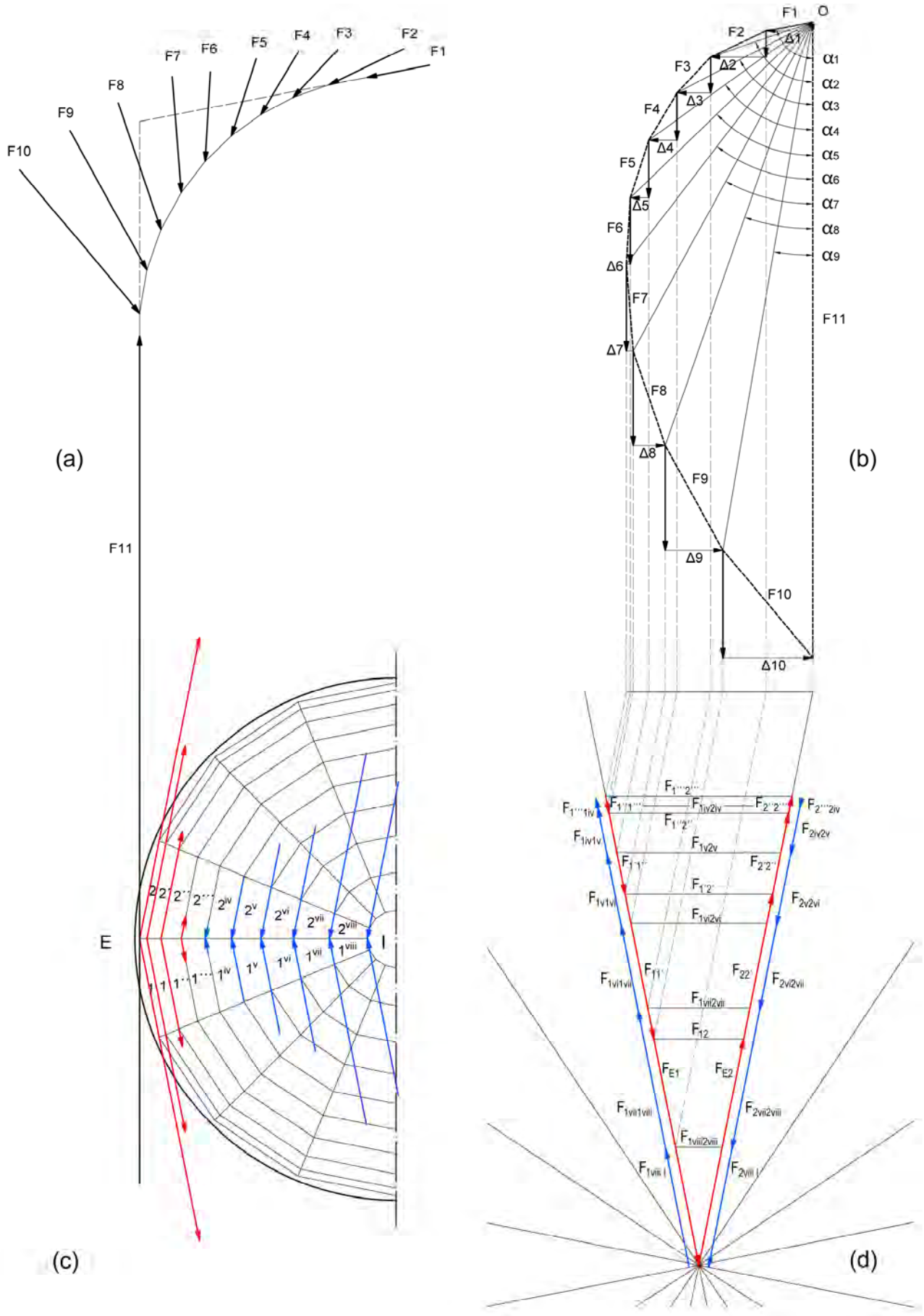


**Figure 98** Test 1: hemispherical dome considering vertical reaction.

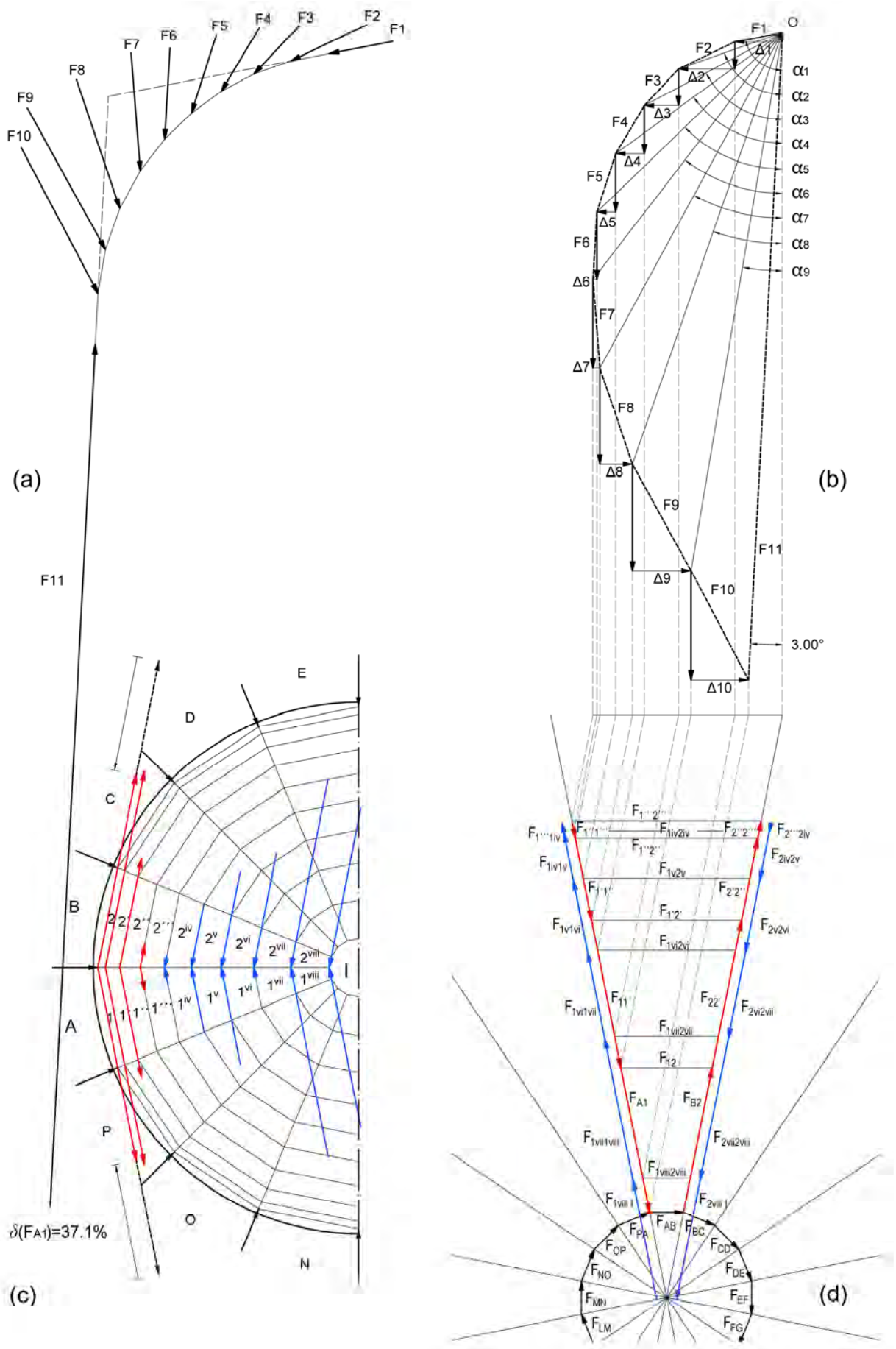


**Figure 99** Test 2: hemispherical dome considering tilted reaction.

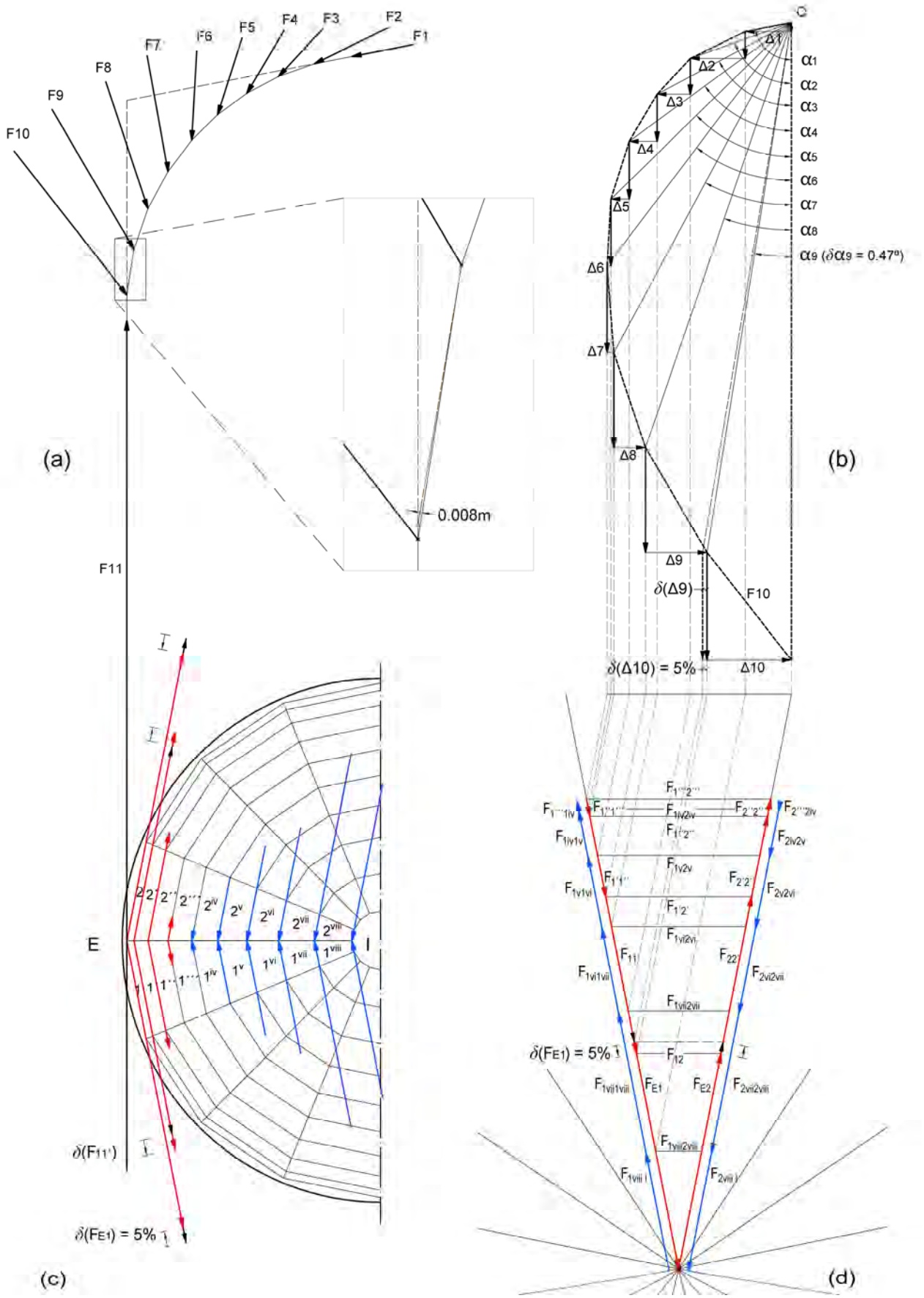


**Figure 100** Test 3: hemispherical dome considering vertical reaction and 5% reduction in maximum tension forces absorbed by the second tension forces.

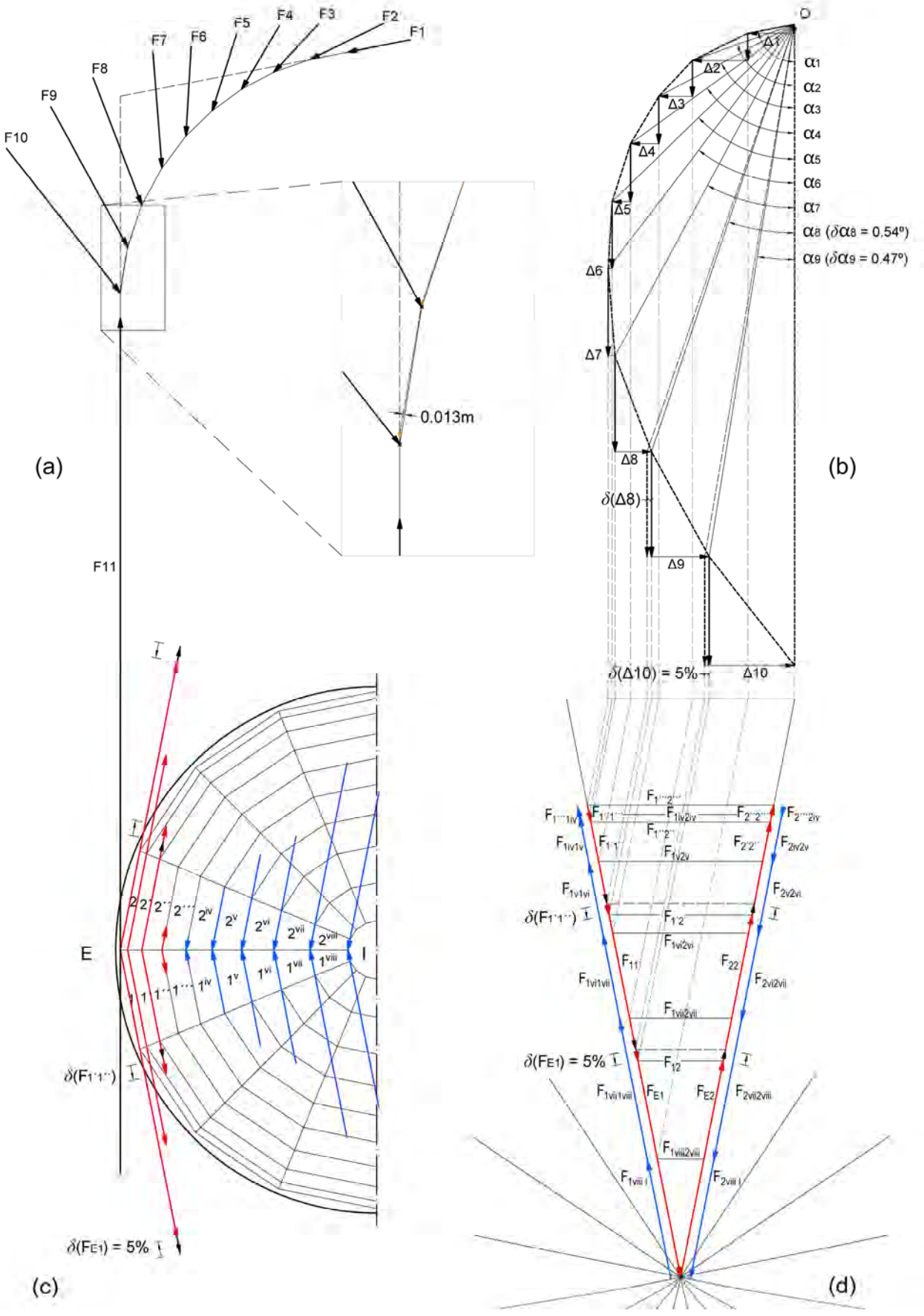


**Figure 101** Test 4: hemispherical dome considering vertical reaction and 5% reduction in maximum tension forces absorbed by the third tension forces.

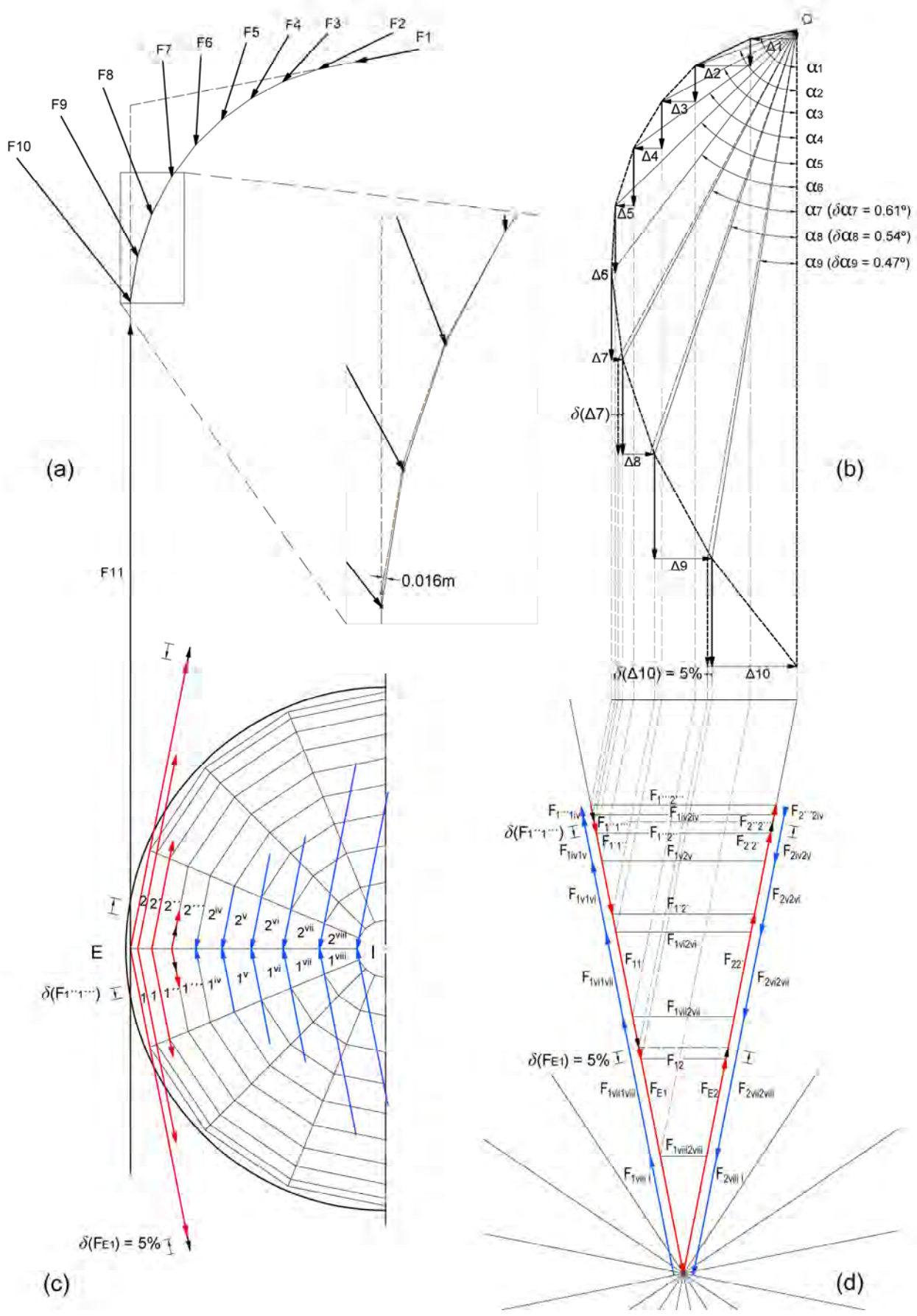


**Figure 102** Test 5: hemispherical dome considering vertical reaction and 5% reduction in maximum tension forces absorbed by the fourth tension forces.

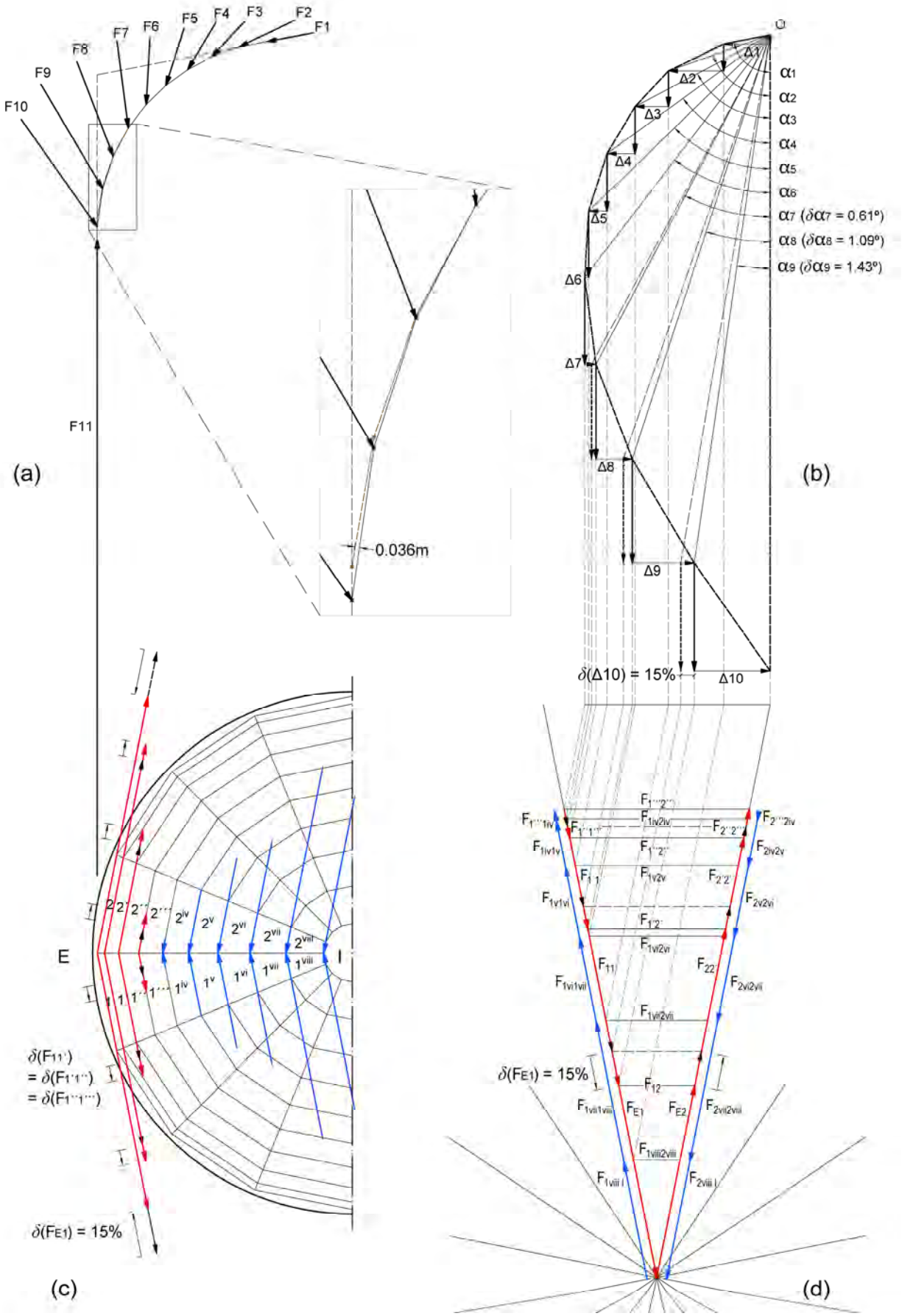


**Figure 103** Test 6: hemispherical dome considering vertical reaction and 15% reduction in maximum tension forces absorbed by all the other tension forces.

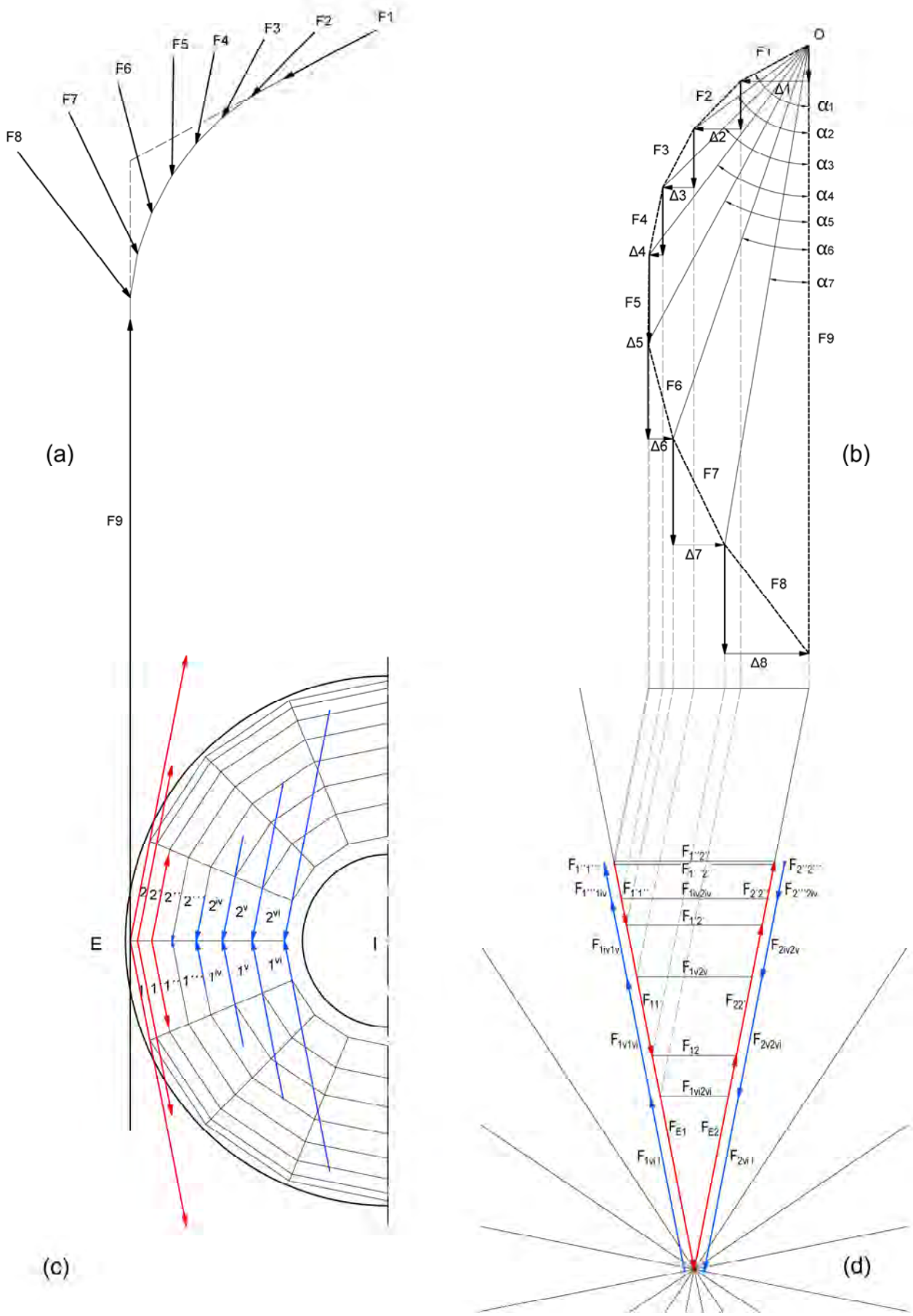


**Figure 104** Test 7: hemispherical dome with oculus considering vertical reaction.

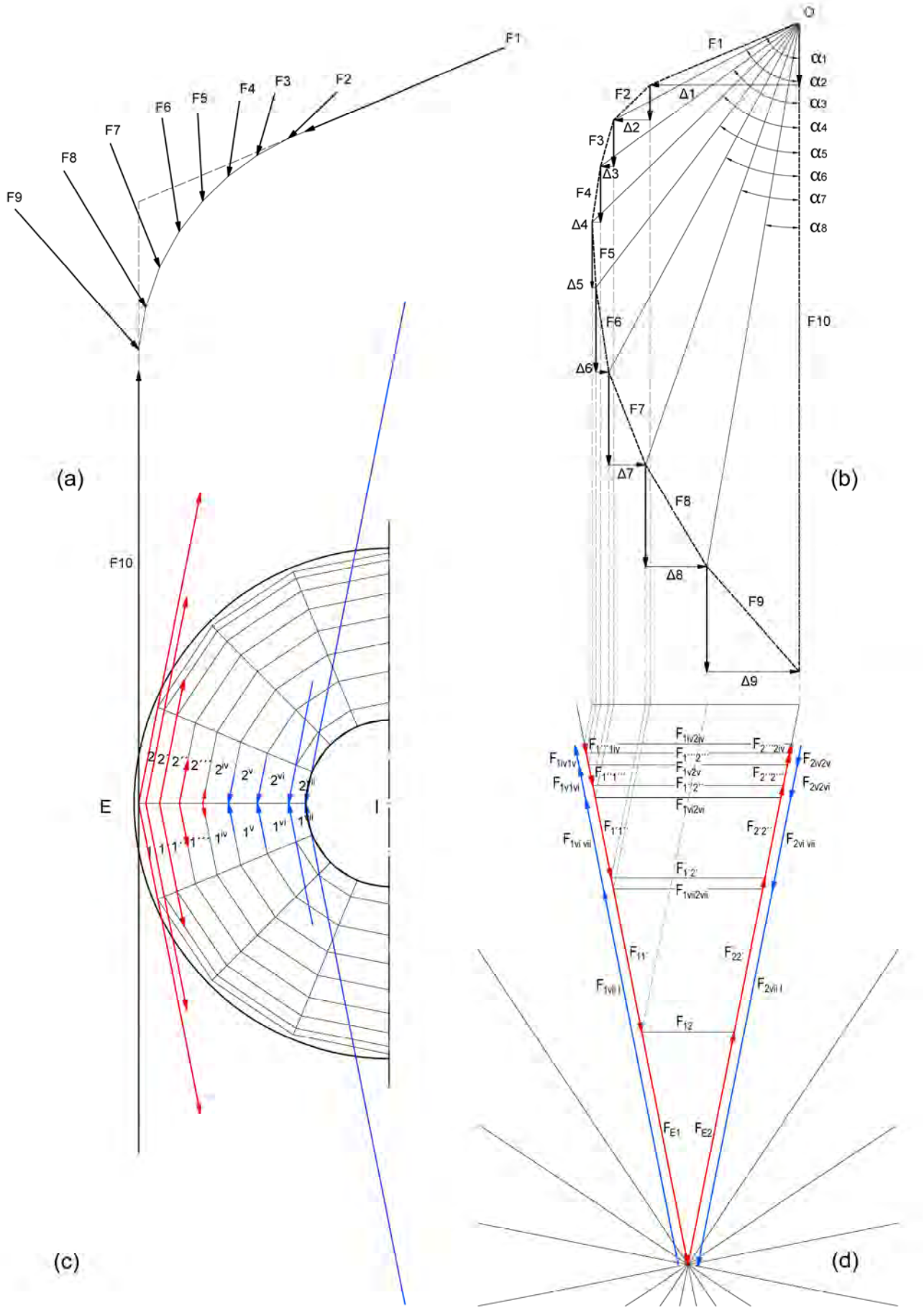


**Figure 105** Test 8: hemispherical dome with lantern considering vertical reaction.

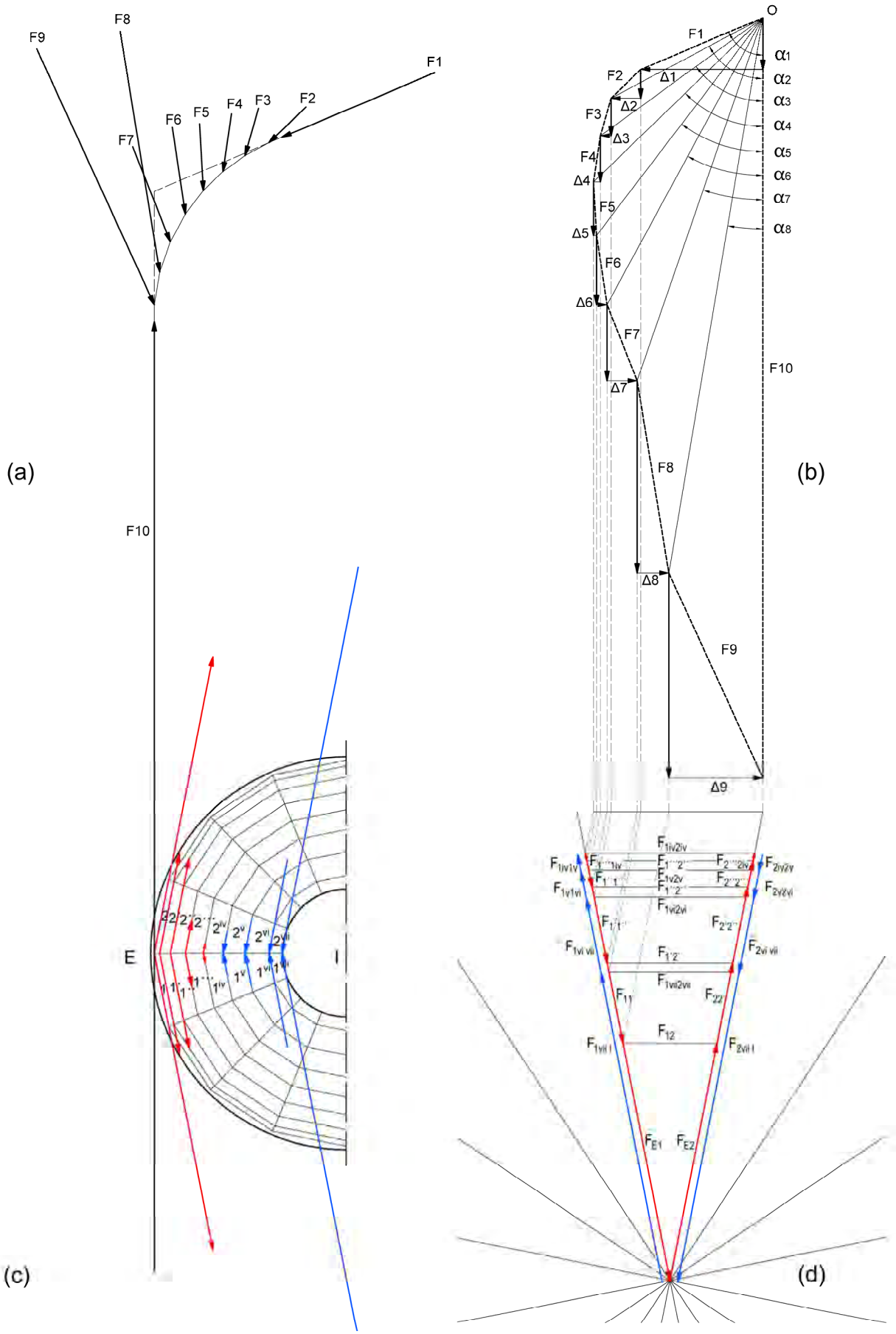


**Figure 106** Test 9.1: hemispherical dome with lantern and filling on the extrados up to one third of the height. Hypothesis 1: no structural filling; considering vertical reaction.

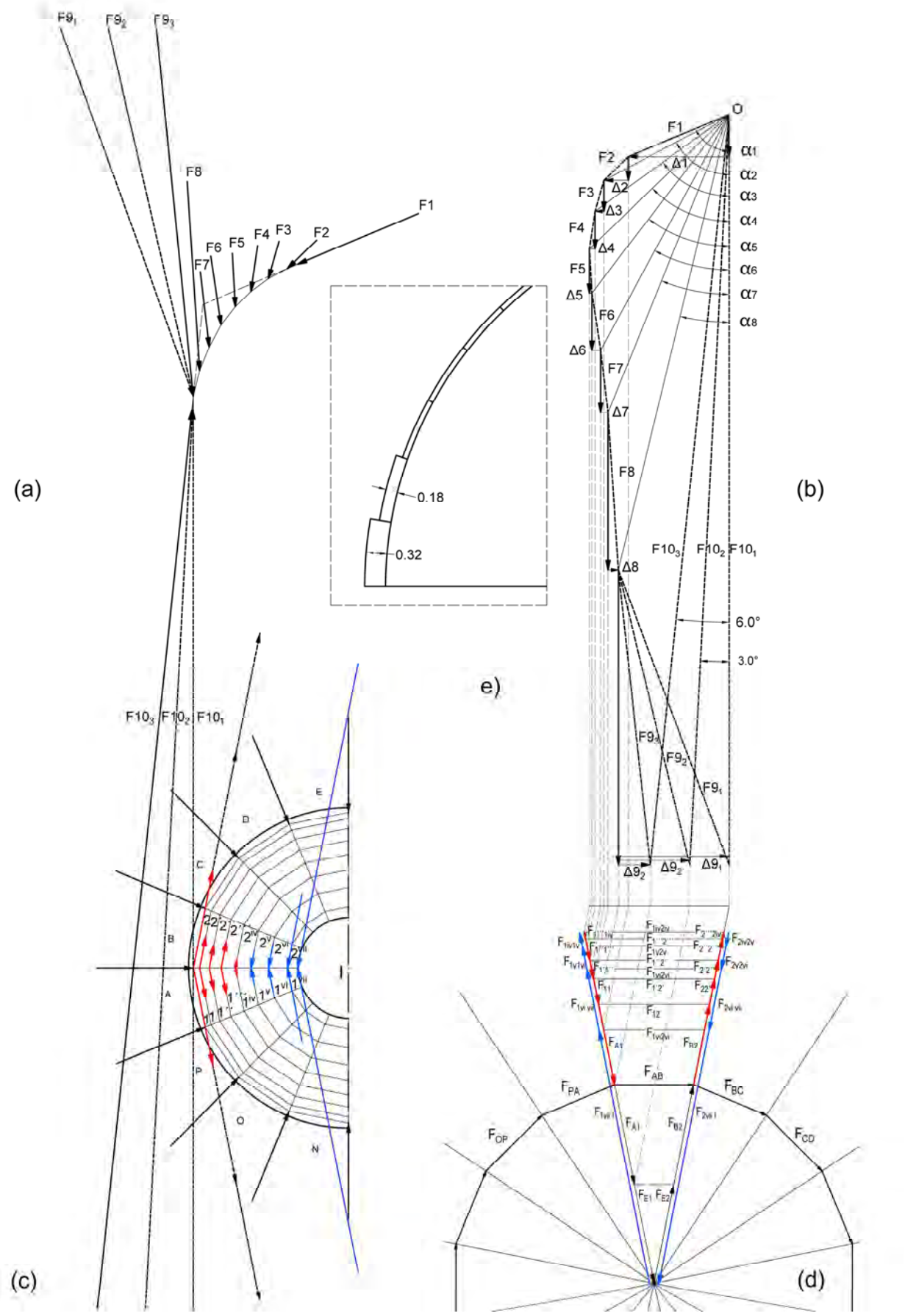


**Figure 107** Test 9.2a: hemispherical dome with lantern and filling on the extrados up to one third of the height. Hypothesis 2: structural filling. Stagger shape filling, considering tilted reaction (0º, 3º, 6º).

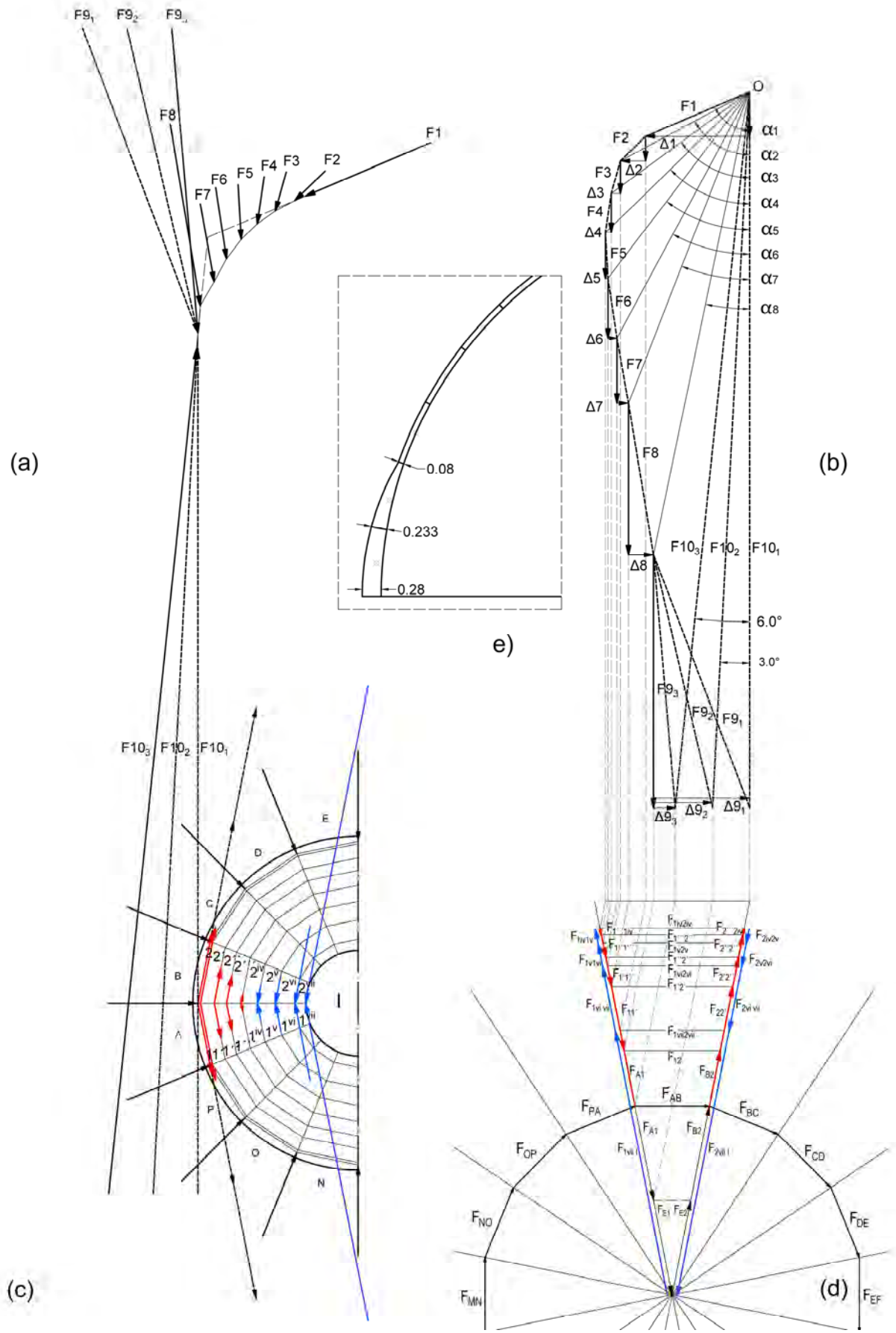


**Figure 108** Test 9.2b: hemispherical dome with lantern and filling on the extrados up to one third of the height. Hypothesis 2: structural filling. Soft curved filling, considering tilted reaction (0°, 3°, 6°).

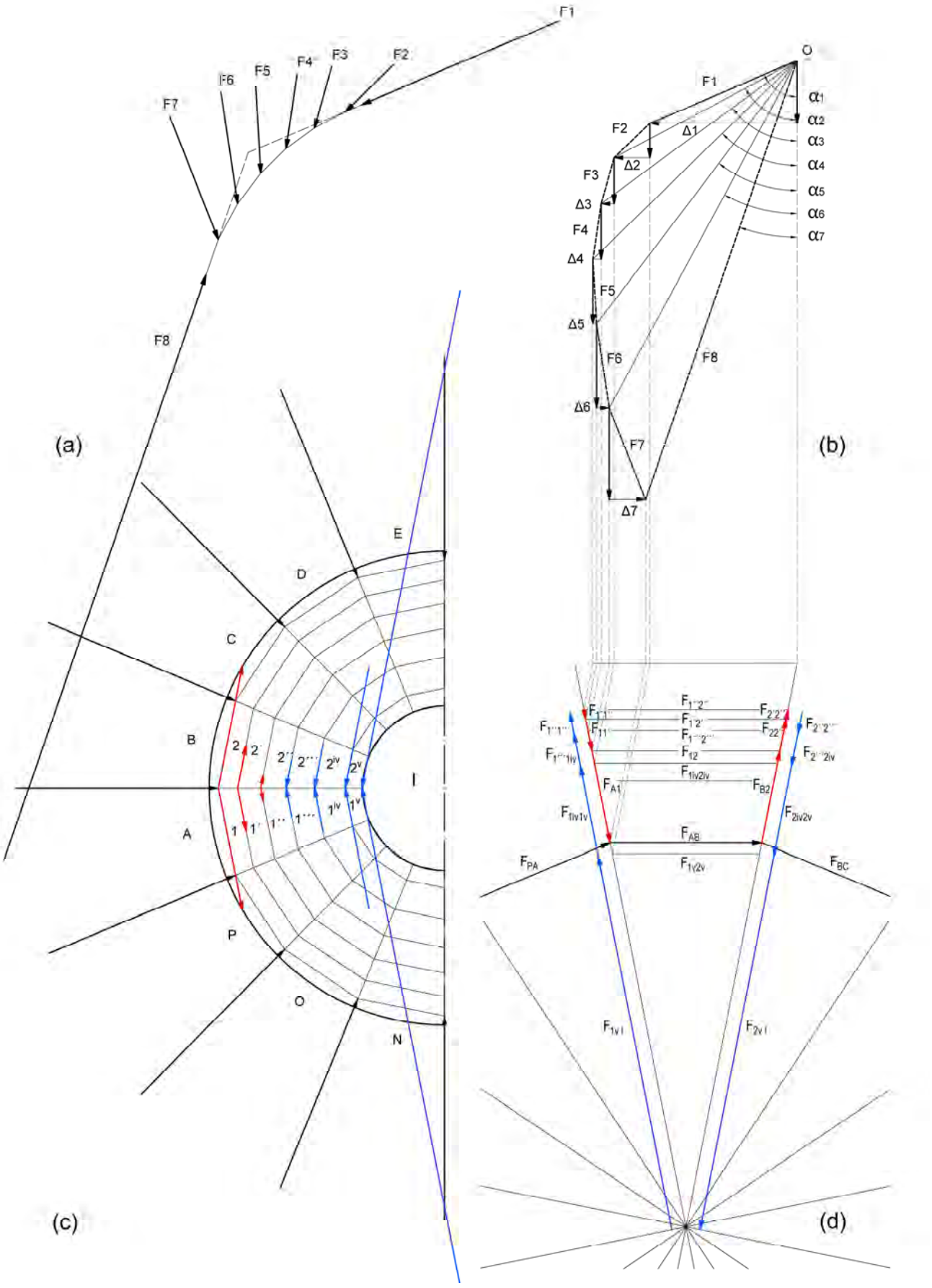


**Figure 109** Test 9.3: hemispherical dome with lantern and filling on the extrados up to one third of the height. Hypothesis 3: cemented rigid filling; considering tilted reaction.

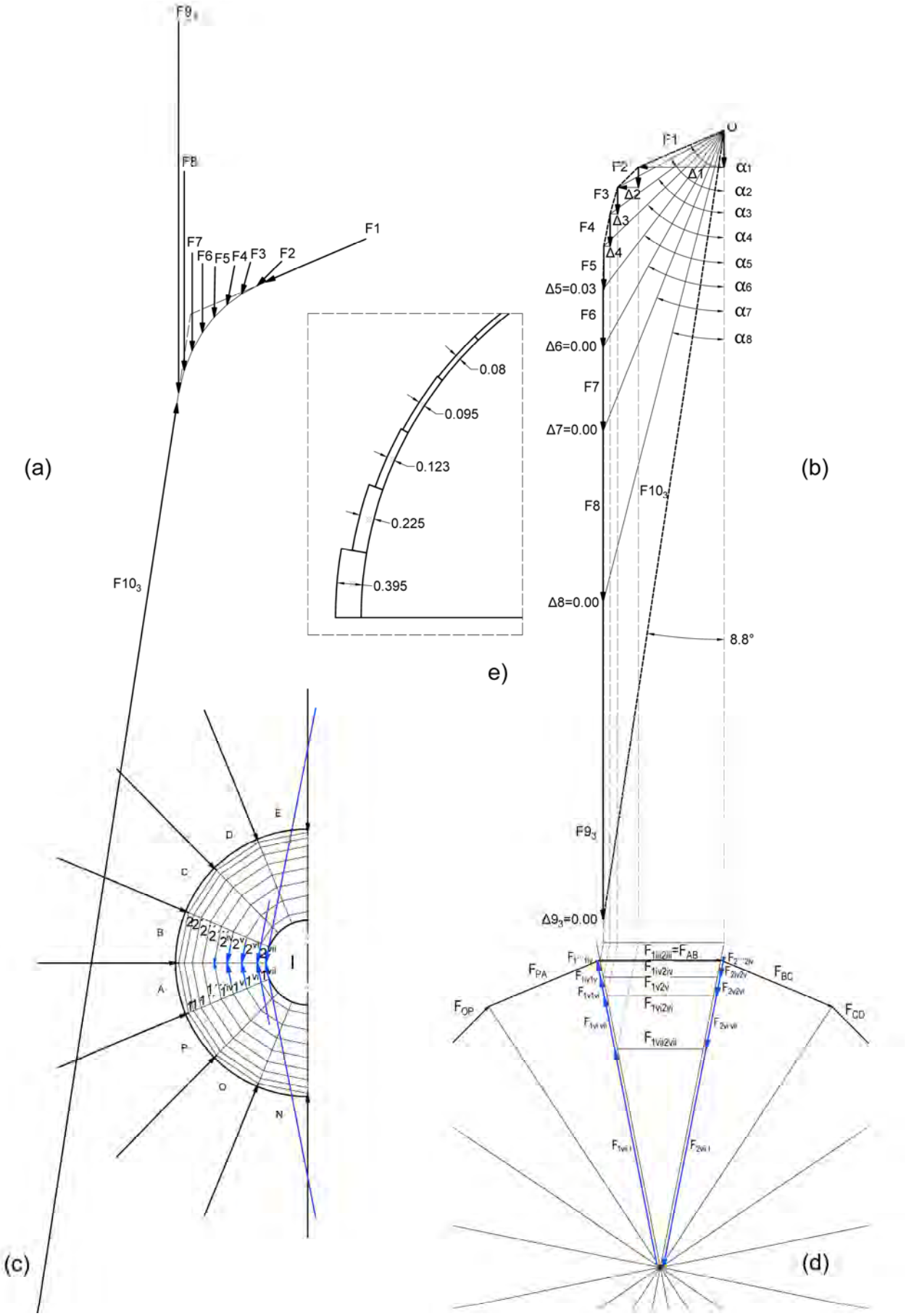


**Figure 110** Test 10: hemispherical dome with lantern and filling on the extrados, without tension forces.

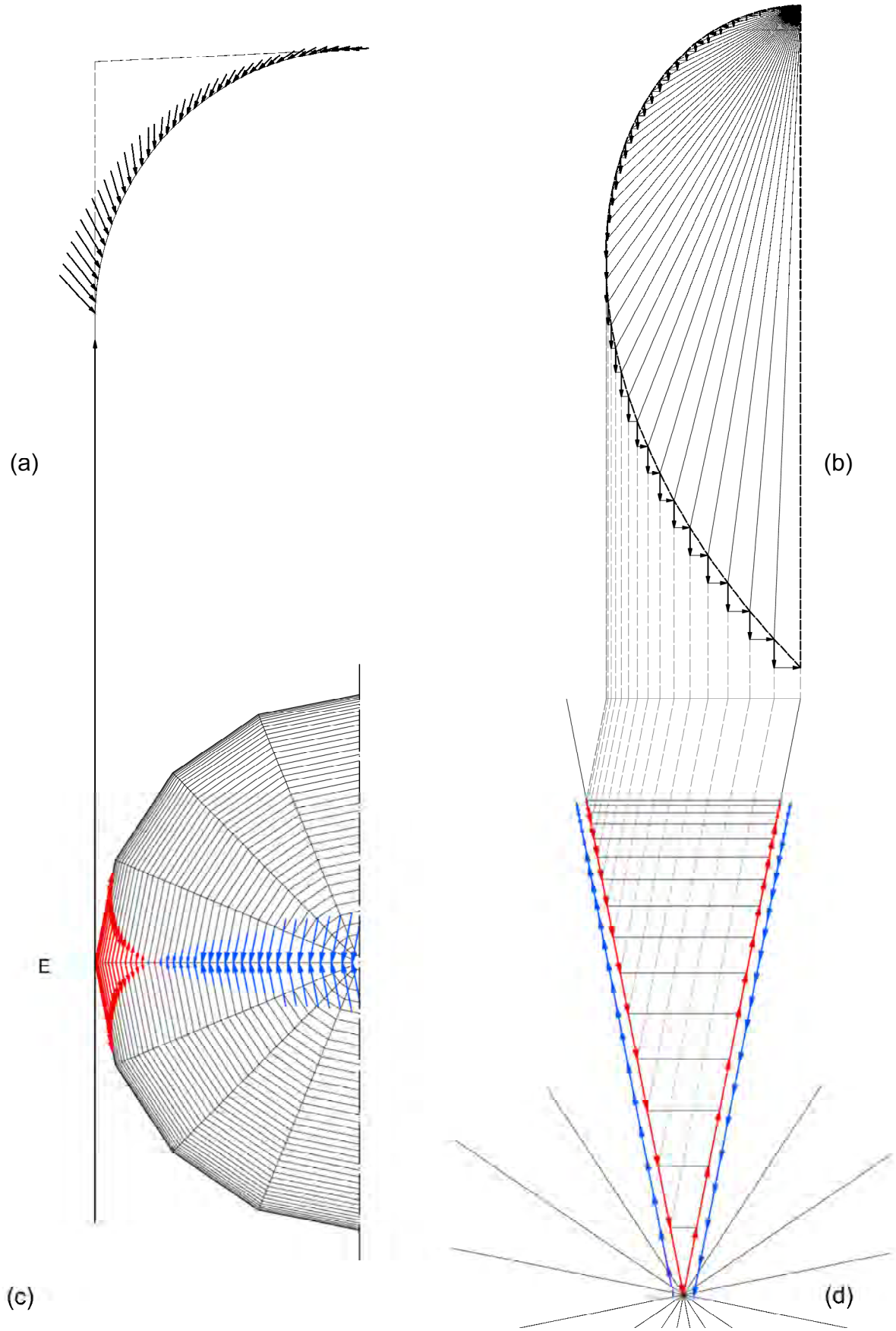


**Figure 111** Test 11: hemispherical dome considering vertical reaction, with 640 sectors.

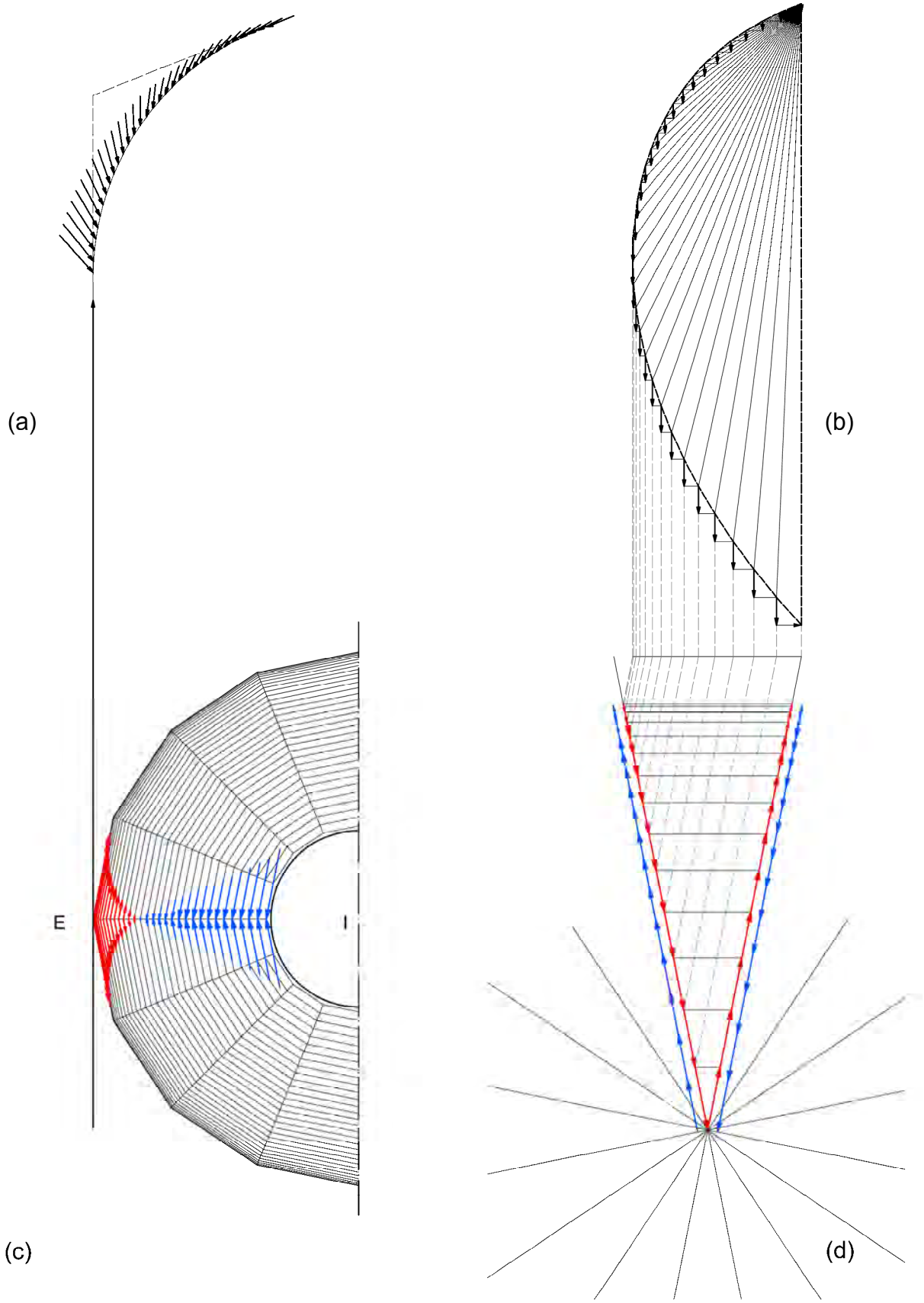


**Figure 112** Test 12: hemispherical dome with oculus considering vertical reaction, with 512 sectors.

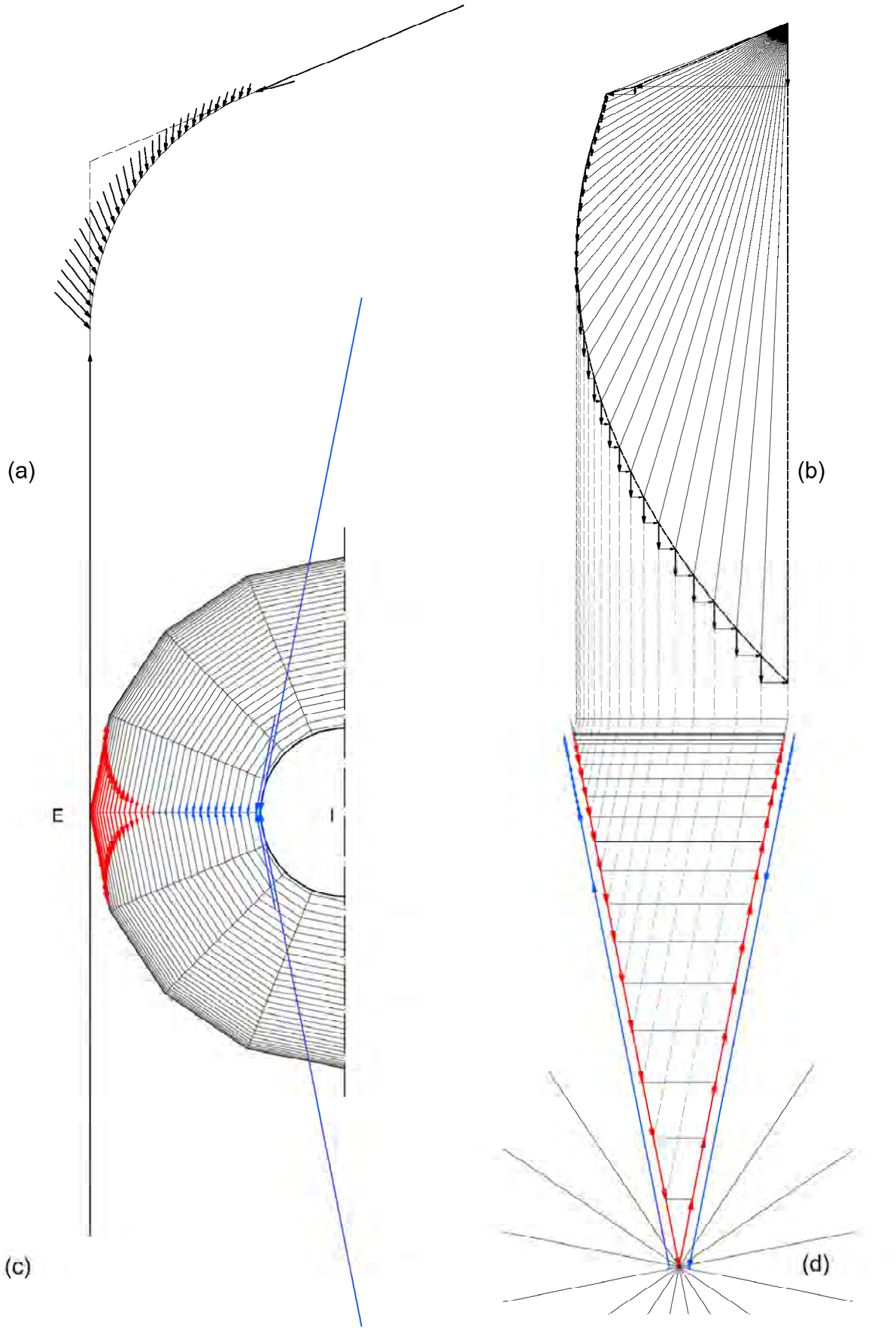


**Figure 113** Test 13: hemispherical dome with lantern considering vertical reaction, with 512 sectors.

## 10.2. Results

### 10.2.1. Values obtained

The values of internal forces and stresses, from measures in either the dual figure or the force polygon, are set out in Table 3 (for meridian forces) and Table 4 (for parallel forces). Values for 160 and 640 sectors are included and for different values of colatitude[7] of the dome.

Multiple tension solutions in the dome are presented, whose equilibrium is guaranteed by the corresponding graphic constructions.

Some of the most significant values are:

- maximum value of compression forces: **42.65 kN** (Test 10, hemisphere with lantern and structural backfilling without tension stresses, 128 sectors; φ=90º. Figure 110(b), force polygon).
- maximum value of compression stress: **1.87 N/mm²** (Test 13, hemisphere with lantern, 512 sectors; φ=19.32º. Figure 113(d), dual figure, application surface: 0.0064 m²).
- maximum value of tension forces: **13.07 kN** (Test 9.2.a, hemisphere with lantern and stagger shape filling for a reaction angle=0º; 128 sectors; φ=90º. Figure 107(d), dual figure, $F_{E1}$, $F_{E2}$, …).
- maximum value of tension stress: **0.11 N/mm²** (Test 9.1, hemisphere with lantern and filling non-structural; 128 sector; φ=90º. Figure 106(d), dual figure, $F_{E1}$, $F_{E2}$, …, application surface: 0.0801 m²).

### 10.2.2. Stresses in masonry

The values of strength of brick masonry have been examined in several authors.

As it is presented in (Huerta, 2003), Guastavino made systematic tests on timbrel specimens in 1887. He tried to obtain ultimate stress values for compression, tension, shear and bending. These values could then be used to verify the safety of his structures by comparing the working stresses with the material failure stress. The results of the tests were the following:

- compression strength: 14.60 N/mm².
- tension strength: 2 N/mm².
- shear strength: 0.9 N/mm².

Lourenço (1998) reflects that Van der Pluijm (1992) used tensile strength values of the masonry unit ranging from 1.5 to 3.5 N/mm².

[7] colatitude (φ): angle between the tangent to the meridian and the horizontal.

Therefore, considering the usual values of brick masonry strength proposed by different authors, the values obtained in this work (Table 3 and Table 4) are acceptable for the material.

As said in section 6.2.6, Test 3 to Test 6 (Figure 100 to Figure 103) show how enforcing variations in the value of the maximum tension ($\delta F_{E1}$, $\delta F_{11'}$…), generates new solutions of the internal forces. These solutions determine some variations in the angles ($\delta\alpha_i$) to be in equilibrium. Figure 100(a) to Figure 103(a) (detail), show that the necessary variations of angle values ($\delta\alpha_i$) involve very littles changes, relative to dome thickness, of the meridional section of the simplified model.

Table 3 shows the values of meridian forces and stresses for different values of colatitude on the dome, obtained from measures in the dual figure and the force polygon. It includes the values for the discretisations of 160 and 640 sectors. All the forces are compressive.

Table 4 shows the values of parallel forces and stresses for different values of colatitude on the dome, obtained from measures in the dual figure and the force polygon. It includes the values for the discretisations of 160 and 640 sectors. Positive values are for compressive forces, negative values (in red) are for tensile forces.

**Table 3** Values of meridian forces and stresses for different values of colatitude on the dome, obtained from measures in the dual figure and the force polygon.

**MERIDAN STRESSES**

| TEST | | 1 | 2 | 3 | 4 | 5 | 6 | 7 | 8 | 9.1 | 9.2a. | | | 9.2.b | | | 9.3 | 10 | 11 | 12 | 13 |
|---|---|---|---|---|---|---|---|---|---|---|---|---|---|---|---|---|---|---|---|---|---|
| | | vertical reaction | tilted reaciont | vertical reaction 5% reduction | vertical reaction 5% reduction | vertical reaction 5% reduction | vertical reaction 15% reduction | with oculus | with lantern | Filling with no structural function | Hypothesis 2: structural filling. Stagger shape filling, considering tilted reaction (0º, 3º, 6º). | | | Hypothesis 2: structural filling. Soft curved filling, considering tilted reaction (0º, 3º, 6º). | | | Hypothesis 3: cemented rigid filling | lantern and structural filling non-tension stresses | vertical reaction | with oculus | with lantern |
| | | 0º | 3º | 0º | 0º | 0º | 0º | 0º | 0º | 0º | 0º | 3º | 6º | 0º | 3º | 6º | 19.18º | 8,8º | 0º | 0º | 0º |
| φ (°) | VALUES | DISCRETISATION: 160 SECTOR | | | | | | | | | | | | | | | | | DISCRETISATION: 640 | | |
| 2,4146 | kN | | | | | | | | | | | | | | | | | | 0,3587 | | |
| | N/mm² | | | | | | | | | | | | | | | | | | 0,0460 | | |
| 4,8292 | kN | | | | | | | | | | | | | | | | | | 0,7896 | | |
| | N/mm² | | | | | | | | | | | | | | | | | | 0,0506 | | |
| 7,2437 | kN | | | | | | | | | | | | | | | | | | 1,2007 | | |
| | N/mm² | | | | | | | | | | | | | | | | | | 0,0514 | | |
| 9,6583 | kN | 1,4410 | 1,4410 | 1,4410 | 1,4410 | 1,4410 | 1,4410 | | | | | | | | | | | | 1,6096 | | |
| | N/mm² | 0,0464 | 0,0464 | 0,0464 | 0,0464 | 0,0464 | 0,0464 | | | | | | | | | | | | 0,0518 | | |
| 12,0729 | kN | | | | | | | | | | | | | | | | | | 2,0188 | | |
| | N/mm² | | | | | | | | | | | | | | | | | | 0,0521 | | |
| 14,4875 | kN | | | | | | | | | | | | | | | | | | 2,4294 | | |
| | N/mm² | | | | | | | | | | | | | | | | | | 0,0524 | | |
| 16,9021 | kN | | | | | | | | | | | | | | | | | | 2,8419 | | |
| | N/mm² | | | | | | | | | | | | | | | | | | 0,0528 | | |
| 19,3167 | kN | 3,2822 | 3,2822 | 3,2822 | 3,2822 | 3,2822 | 3,2822 | | 5,0320 | 5,0320 | 5,0320 | 5,0320 | 5,0320 | 5,0320 | 5,0320 | 5,0320 | 5,0320 | 5,0320 | 3,2785 | | 5,0739 |
| | N/mm² | 0,0536 | 0,0536 | 0,0536 | 0,0536 | 0,0536 | 0,0536 | | 0,0821 | 0,0821 | 0,0821 | 0,0821 | 0,0821 | 0,0821 | 0,0821 | 0,0821 | 0,0821 | 0,0821 | 0,0535 | | 0,0828 |
| 21,3469 | kN | | | | | | | | | | | | | | | | | | 3,6095 | 0,6477 | 5,9786 |
| | N/mm² | | | | | | | | | | | | | | | | | | 0,0535 | 0,0096 | 0,0887 |
| 23,3771 | kN | | | | | | | | | | | | | | | | | | 3,9632 | 1,2452 | 6,1372 |
| | N/mm² | | | | | | | | | | | | | | | | | | 0,0539 | 0,0169 | 0,0835 |
| 25,4073 | kN | | | | | | | | | | | | | | | | | | 4,3196 | 1,8054 | 6,3307 |
| | N/mm² | | | | | | | | | | | | | | | | | | 0,0544 | 0,0227 | 0,0797 |
| 27,4375 | kN | 4,6511 | 4,6528 | 4,6528 | 4,6528 | 4,6511 | 4,6528 | 2,3234 | 6,5130 | 6,5130 | 6,5130 | 6,5130 | 6,5130 | 6,5130 | 6,5130 | 6,5130 | 6,5130 | 6,5130 | 4,6790 | 2,3373 | 6,5521 |
| | N/mm² | 0,0545 | 0,0545 | 0,0545 | 0,0545 | 0,0545 | 0,0545 | 0,0272 | 0,0764 | 0,0763 | 0,0763 | 0,0763 | 0,0763 | 0,0763 | 0,0763 | 0,0763 | 0,0763 | 0,0763 | 0,0548 | 0,0274 | 0,0768 |
| 29,4677 | kN | | | | | | | | | | | | | | | | | | 5,0417 | 2,8478 | 6,7966 |
| | N/mm² | | | | | | | | | | | | | | | | | | 0,0553 | 0,0313 | 0,0746 |
| 31,4979 | kN | | | | | | | | | | | | | | | | | | 5,4080 | 3,3417 | 7,0607 |
| | N/mm² | | | | | | | | | | | | | | | | | | 0,0559 | 0,0345 | 0,0730 |
| 33,5281 | kN | | | | | | | | | | | | | | | | | | 5,7780 | 3,8231 | 7,3418 |
| | N/mm² | | | | | | | | | | | | | | | | | | 0,0565 | 0,0374 | 0,0718 |
| 35,5583 | kN | 6,1331 | 6,1331 | 6,1331 | 6,1331 | 6,1331 | 6,1331 | 4,2816 | 7,6141 | 7,6141 | 7,6141 | 7,6141 | 7,6141 | 7,6141 | 7,6141 | 7,6141 | 7,6141 | 7,6141 | 6,1523 | 4,2950 | 7,6379 |
| | N/mm² | 0,0569 | 0,0569 | 0,0569 | 0,0569 | 0,0569 | 0,0569 | 0,0398 | 0,0707 | 0,0707 | 0,0707 | 0,0707 | 0,0707 | 0,0707 | 0,0707 | 0,0707 | 0,0707 | 0,0707 | 0,0571 | 0,0399 | 0,0709 |
| 37,5885 | kN | | | | | | | | | | | | | | | | | | 6,5309 | 4,7598 | 7,9476 |
| | N/mm² | | | | | | | | | | | | | | | | | | 0,0578 | 0,0421 | 0,0704 |
| 39,6187 | kN | | | | | | | | | | | | | | | | | | 6,9143 | 5,2197 | 8,2698 |
| | N/mm² | | | | | | | | | | | | | | | | | | 0,0585 | 0,0442 | 0,0700 |
| 41,6490 | kN | | | | | | | | | | | | | | | | | | 7,3029 | 5,6764 | 8,6038 |
| | N/mm² | | | | | | | | | | | | | | | | | | 0,0593 | 0,0461 | 0,0699 |
| 43,6792 | kN | 7,6835 | 7,6835 | 7,6835 | 7,6835 | 7,6835 | 7,6835 | 6,1207 | 8,9335 | 8,9335 | 8,9335 | 8,9335 | 8,9335 | 8,9335 | 8,9335 | 8,9335 | 8,9335 | 8,9901 | 7,6968 | 6,1313 | 8,9490 |
| | N/mm² | 0,0601 | 0,0601 | 0,0601 | 0,0601 | 0,0601 | 0,0601 | 0,0479 | 0,0698 | 0,0698 | 0,0698 | 0,0698 | 0,0698 | 0,0698 | 0,0698 | 0,0698 | 0,0698 | 0,0703 | 0,0602 | 0,0479 | 0,0700 |
| 45,7094 | kN | | | | | | | | | | | | | | | | | | 8,0965 | 6,5858 | 9,3050 |
| | N/mm² | | | | | | | | | | | | | | | | | | 0,0611 | 0,0497 | 0,0702 |
| 47,7396 | kN | | | | | | | | | | | | | | | | | | 8,5024 | 7,0409 | 9,6715 |
| | N/mm² | | | | | | | | | | | | | | | | | | 0,0620 | 0,0514 | 0,0706 |
| 49,7698 | kN | | | | | | | | | | | | | | | | | | 8,9149 | 7,4977 | 10,0484 |
| | N/mm² | | | | | | | | | | | | | | | | | | 0,0631 | 0,0530 | 0,0711 |
| 51,8000 | kN | 9,2721 | 9,2721 | 9,2721 | 9,2721 | 9,2721 | 9,2721 | 7,9042 | 10,3662 | 10,3662 | 10,3662 | 10,3662 | 10,3662 | 10,3662 | 10,3662 | 10,3662 | 10,3662 | 10,7125 | 9,3211 | 7,9459 | 10,4210 |
| | N/mm² | 0,0637 | 0,0637 | 0,0637 | 0,0637 | 0,0637 | 0,0637 | 0,0543 | 0,0712 | 0,0712 | 0,0712 | 0,0712 | 0,0712 | 0,0712 | 0,0712 | 0,0712 | 0,0712 | 0,0654 | 0,0640 | 0,0546 | 0,0716 |
| 54,1411 | kN | | | | | | | | | | | | | | | | | | 9,8269 | 8,4914 | 10,8953 |
| | N/mm² | | | | | | | | | | | | | | | | | | 0,0655 | 0,0566 | 0,0726 |
| 56,4822 | kN | | | | | | | | | | | | | | | | | | 10,3303 | 9,0317 | 11,3691 |
| | N/mm² | | | | | | | | | | | | | | | | | | 0,0669 | 0,0585 | 0,0736 |
| 58,8233 | kN | | | | | | | | | | | | | | | | | | 10,8450 | 9,5792 | 11,8575 |
| | N/mm² | | | | | | | | | | | | | | | | | | 0,0684 | 0,0605 | 0,0748 |
| 61,1644 | kN | 11,3645 | 11,3645 | 11,3645 | 11,3645 | 11,3000 | 11,3000 | 10,1287 | 12,3530 | 12,3530 | 12,3530 | 12,3530 | 12,3530 | 12,3530 | 12,3530 | 12,3530 | 12,3530 | 13,3220 | 11,3717 | 10,1351 | 12,3608 |
| | N/mm² | 0,0700 | 0,0700 | 0,0700 | 0,0700 | 0,0697 | 0,0697 | 0,0624 | 0,0762 | 0,0761 | 0,0761 | 0,0761 | 0,0761 | 0,0761 | 0,0761 | 0,0761 | 0,0761 | 0,0691 | 0,0701 | 0,0625 | 0,0762 |
| 63,5055 | kN | | | | | | | | | | | | | | | | | | 11,9113 | 10,7007 | 12,8797 |
| | N/mm² | | | | | | | | | | | | | | | | | | 0,0719 | 0,0646 | 0,0777 |
| 65,8466 | kN | | | | | | | | | | | | | | | | | | 12,4648 | 11,2771 | 13,4148 |
| | N/mm² | | | | | | | | | | | | | | | | | | 0,0738 | 0,0667 | 0,0794 |
| 68,1877 | kN | | | | | | | | | | | | | | | | | | 13,0330 | 11,8655 | 13,9669 |
| | N/mm² | | | | | | | | | | | | | | | | | | 0,0758 | 0,0690 | 0,0812 |
| 70,5288 | kN | 13,6034 | 13,6034 | 13,6034 | 13,5592 | 13,5592 | 13,5163 | 12,4547 | 14,5220 | 14,5222 | 14,8047 | 14,8047 | 14,8047 | 14,7409 | 14,7409 | 14,7409 | 14,5220 | 17,3288 | 13,6146 | 12,4649 | 14,5342 |
| | N/mm² | 0,0779 | 0,0779 | 0,0779 | 0,0777 | 0,0777 | 0,0774 | 0,0713 | 0,0832 | 0,0832 | 0,0848 | 0,0848 | 0,0848 | 0,0844 | 0,0844 | 0,0844 | 0,0832 | 0,0643 | 0,0780 | 0,0714 | 0,0832 |
| 72,9627 | kN | | | | | | | | | | | | | | | | | | 14,2425 | 13,1085 | 15,1496 |
| | N/mm² | | | | | | | | | | | | | | | | | | 0,0804 | 0,0740 | 0,0856 |
| 75,3966 | kN | | | | | | | | | | | | | | | | | | 14,8877 | 13,7670 | 15,7841 |
| | N/mm² | | | | | | | | | | | | | | | | | | 0,0831 | 0,0768 | 0,0881 |
| 77,8302 | kN | | | | | | | | | | | | | | | | | | 15,5542 | 14,4447 | 16,4417 |
| | N/mm² | | | | | | | | | | | | | | | | | | 0,0859 | 0,0798 | 0,0908 |
| 80,2644 | kN | 16,2426 | 16,2426 | 16,2426 | 16,2204 | 16,2204 | 16,1792 | 15,1422 | 17,1229 | 21,2928 | 21,5698 | 21,5698 | 21,5698 | 20,8334 | 20,8334 | 20,8334 | | 26,0029 | 16,2437 | 15,1431 | 17,1240 |
| | N/mm² | 0,0890 | 0,0890 | 0,0890 | 0,0889 | 0,0889 | 0,0886 | 0,0830 | 0,0938 | 0,1167 | 0,0521 | 0,0521 | 0,0521 | 0,0386 | 0,0386 | 0,0386 | | 0,0500 | 0,0890 | 0,0830 | 0,0938 |
| 82,6983 | kN | | | | | | | | | | | | | | | | | | 16,9580 | 15,8644 | 17,8328 |
| | N/mm² | | | | | | | | | | | | | | | | | | 0,0923 | 0,0864 | 0,0971 |
| 85,1322 | kN | | | | | | | | | | | | | | | | | | 17,6993 | 16,6105 | 18,5702 |
| | N/mm² | | | | | | | | | | | | | | | | | | 0,0959 | 0,0900 | 0,1006 |
| 87,5661 | kN | | | | | | | | | | | | | | | | | | 18,4697 | 17,3838 | 19,3382 |
| | N/mm² | | | | | | | | | | | | | | | | | | 0,0998 | 0,0940 | 0,1045 |
| 90,0000 | kN | 19,2717 | 19,2981 | 19,2717 | 19,2717 | 19,2717 | 19,2717 | 18,1868 | 20,1394 | 28,7280 | 34,5329 | 34,5803 | 34,7231 | 31,5615 | 31,6048 | 31,7354 | | 42,6538 | 19,2716 | 18,1867 | 20,1394 |
| | N/mm² | 0,1041 | 0,1042 | 0,1041 | 0,1041 | 0,1041 | 0,1041 | 0,0982 | 0,1087 | 0,1551 | 0,0457 | 0,0457 | 0,0459 | 0,0479 | 0,0479 | 0,0481 | | 0,0454 | 0,1041 | 0,0982 | 0,1087 |
| Rh | kN | | 1,0100 | | | | | | | | | 1,8098 | 3,6296 | | 1,6541 | 3,3172 | 4,7725 | 6,5314 | | | |
| | N/mm² | | 0,0055 | | | | | | | | | 0,0024 | 0,0048 | | 0,0025 | 0,0050 | 0,0273 | 0,0070 | | | |
| Rv | kN | 19,2717 | 19,2716 | 19,2717 | 19,2717 | 19,2717 | 19,2717 | 18,1868 | 20,1394 | 28,7280 | 34,5329 | 34,5329 | 34,5329 | 31,5615 | 31,5615 | 31,5615 | 13,7156 | 42,1507 | 19,2716 | 18,1867 | 20,1394 |
| | N/mm² | 0,1041 | 0,1041 | 0,1041 | 0,1041 | 0,1041 | 0,1041 | 0,0982 | 0,1087 | 0,1551 | 0,0457 | 0,0457 | 0,0457 | 0,0479 | 0,0479 | 0,0479 | 0,0786 | 0,0449 | 0,1041 | 0,0982 | 0,1087 |

**Table 4** Values of parallel forces and stresses for different values of colatitude on the dome, obtained from measures in the dual figure and the force polygon.

**PARALLEL STRESSES**

| TEST | | 1 | 2 | 3 | 4 | 5 | 6 | 7 | 8 | 9.1 | 9.2a. | | | 9.2.b | | | 9.3 | 10 | 11 | 12 | 13 |
|---|---|---|---|---|---|---|---|---|---|---|---|---|---|---|---|---|---|---|---|---|---|
| | | vertical reaction | tilted reaciont | vertical reaction 5% reduction | vertical reaction 5% reduction | vertical reaction 5% reduction | vertical reaction 15% reduction | with oculus | with lantern | Filling with no structural function | Hypothesis 2: structural filling. Stagger shape filling. considering tilted reaction (0°, 3°, 0°). | | | Hypothesis 2: structural filling. Soft curved filling. considering tilted reaction (0°, 3°, 0°). | | | Hypothesis 3: cemented rigid filling | lantern and structural filling non-tension stresses | vertical reaction | with oculus | with lantern |
| | | 0° | 3° | 0° | 0° | 0° | 0° | 0° | 0° | 0° | 0° | 3° | 6° | 0° | 3° | 6° | 19.18° | 8,8° | 0° | 0° | 0° |
| φ (°) | VALUES | DISCRETISATION: 160 SECTOR | | | | | | | | | | | | | | | | | DISCRETISATION: 640 | | |
| 2,4146 | kN | | | | | | | | | | | | | | | | | | 0,9184 | | |
| | N/mm² | | | | | | | | | | | | | | | | | | 0,0462 | | |
| 4,8292 | kN | | | | | | | | | | | | | | | | | | 1,0977 | | |
| | N/mm² | | | | | | | | | | | | | | | | | | 0,0552 | | |
| 7,2437 | kN | | | | | | | | | | | | | | | | | | 1,0360 | | |
| | N/mm² | | | | | | | | | | | | | | | | | | 0,0521 | | |
| 9,6583 | kN | 3,6262 | 3,6262 | 3,6262 | 3,6262 | 3,6262 | 3,6262 | | | | | | | | | | | | 1,0134 | | |
| | N/mm² | 0,0456 | 0,0456 | 0,0456 | 0,0456 | 0,0456 | 0,0456 | | | | | | | | | | | | 0,0510 | | |
| 12,0729 | kN | | | | | | | | | | | | | | | | | | 0,9919 | | |
| | N/mm² | | | | | | | | | | | | | | | | | | 0,0499 | | |
| 14,4875 | kN | | | | | | | | | | | | | | | | | | 0,9675 | | |
| | N/mm² | | | | | | | | | | | | | | | | | | 0,0487 | | |
| 16,9021 | kN | | | | | | | | | | | | | | | | | | 0,9392 | | |
| | N/mm² | | | | | | | | | | | | | | | | | | 0,0473 | | |
| 19,3167 | kN | 4,3129 | 4,3129 | 4,3129 | 4,3129 | 4,3129 | 4,3129 | | 11,8861 | 11,8861 | 11,8861 | 11,8861 | 11,8861 | 11,8861 | 11,8861 | 11,8861 | 11,8861 | 11,8861 | 0,9649 | | 12,0024 |
| | N/mm² | 0,0543 | 0,0543 | 0,0543 | 0,0543 | 0,0543 | 0,0543 | | 1,8572 | 1,8572 | 1,8572 | 1,8572 | 1,8572 | 1,8572 | 1,8572 | 1,8572 | 1,8572 | 1,8572 | 0,0486 | | 1,8754 |
| 21,3469 | kN | | | | | | | | | | | | | | | | | | 0,6788 | 1,5446 | 2,2551 |
| | N/mm² | | | | | | | | | | | | | | | | | | 0,0406 | 0,0924 | 0,1349 |
| 23,3771 | kN | | | | | | | | | | | | | | | | | | 0,7052 | 1,3815 | 0,1643 |
| | N/mm² | | | | | | | | | | | | | | | | | | 0,0422 | 0,0827 | 0,0098 |
| 25,4073 | kN | | | | | | | | | | | | | | | | | | 0,6740 | 1,2480 | 0,2149 |
| | N/mm² | | | | | | | | | | | | | | | | | | 0,0403 | 0,0747 | 0,0129 |
| 27,4375 | kN | 2,6074 | 2,6074 | 2,6074 | 2,6074 | 2,6074 | 2,6074 | 5,2684 | 2,8823 | 2,8823 | 2,8823 | 2,8823 | 2,8823 | 2,8823 | 2,8823 | 2,8823 | 2,8823 | 2,8823 | 0,6402 | 1,1346 | 0,2448 |
| | N/mm² | 0,0390 | 0,0390 | 0,0390 | 0,0390 | 0,0390 | 0,0390 | 0,0789 | 0,0431 | 0,0431 | 0,0431 | 0,0431 | 0,0431 | 0,0431 | 0,0431 | 0,0431 | 0,0431 | 0,0431 | 0,0383 | 0,0679 | 0,0146 |
| 29,4677 | kN | | | | | | | | | | | | | | | | | | 0,6038 | 1,0351 | 0,2588 |
| | N/mm² | | | | | | | | | | | | | | | | | | 0,0361 | 0,0619 | 0,0155 |
| 31,4979 | kN | | | | | | | | | | | | | | | | | | 0,5648 | 0,9452 | 0,2605 |
| | N/mm² | | | | | | | | | | | | | | | | | | 0,0338 | 0,0566 | 0,0156 |
| 33,5281 | kN | | | | | | | | | | | | | | | | | | 0,5232 | 0,8620 | 0,2521 |
| | N/mm² | | | | | | | | | | | | | | | | | | 0,0313 | 0,0516 | 0,0151 |
| 35,5583 | kN | 2,1911 | 2,1911 | 2,1911 | 2,1911 | 2,1911 | 2,1911 | 3,6239 | 1,0450 | 1,0450 | 1,0450 | 1,0450 | 1,0450 | 1,0450 | 1,0450 | 1,0450 | 1,0450 | 1,0450 | 0,4790 | 0,7835 | 0,2355 |
| | N/mm² | 0,0328 | 0,0328 | 0,0328 | 0,0328 | 0,0328 | 0,0328 | 0,0543 | 0,0156 | 0,0156 | 0,0156 | 0,0156 | 0,0156 | 0,0156 | 0,0156 | 0,0156 | 0,0156 | 0,0156 | 0,0287 | 0,0469 | 0,0141 |
| 37,5885 | kN | | | | | | | | | | | | | | | | | | 0,4322 | 0,7080 | 0,2117 |
| | N/mm² | | | | | | | | | | | | | | | | | | 0,0259 | 0,0424 | 0,0127 |
| 39,6187 | kN | | | | | | | | | | | | | | | | | | 0,3029 | 0,5344 | 0,1818 |
| | N/mm² | | | | | | | | | | | | | | | | | | 0,0229 | 0,0380 | 0,0109 |
| 41,6490 | kN | | | | | | | | | | | | | | | | | | 0,3311 | 0,5619 | 0,1465 |
| | N/mm² | | | | | | | | | | | | | | | | | | 0,0198 | 0,0336 | 0,0088 |
| 43,6792 | kN | 1,4360 | 1,4360 | 1,4360 | 1,4360 | 1,4360 | 1,4360 | 2,3986 | 0,6661 | 0,6661 | 0,6661 | 0,6661 | 0,6661 | 0,6661 | 0,6661 | 0,6661 | 0,6661 | 0,8670 | 0,2767 | 0,4899 | 0,1062 |
| | N/mm² | 0,0215 | 0,0215 | 0,0215 | 0,0215 | 0,0215 | 0,0215 | 0,0359 | 0,0100 | 0,0100 | 0,0100 | 0,0100 | 0,0100 | 0,0100 | 0,0100 | 0,0100 | 0,0100 | 0,0130 | 0,0166 | 0,0293 | 0,0064 |
| 45,7094 | kN | | | | | | | | | | | | | | | | | | 0,2198 | 0,4177 | 0,0615 |
| | N/mm² | | | | | | | | | | | | | | | | | | 0,0132 | 0,0250 | 0,0037 |
| 47,7396 | kN | | | | | | | | | | | | | | | | | | 0,1604 | 0,3451 | 0,0127 |
| | N/mm² | | | | | | | | | | | | | | | | | | 0,0096 | 0,0206 | 0,0008 |
| 49,7698 | kN | | | | | | | | | | | | | | | | | | 0,0682 | 0,1715 | -0,0800 |
| | N/mm² | | | | | | | | | | | | | | | | | | 0,0059 | 0,0163 | -0,0014 |
| 51,8000 | kN | 0,2999 | 0,2999 | 0,2999 | 0,2999 | 0,2999 | 0,2999 | 1,0474 | -0,2981 | -0,2981 | -0,2981 | -0,2981 | -0,2981 | -0,2981 | -0,2981 | -0,2981 | -0,2981 | 0,0591 | -0,0213 | 0,1502 | -0,1580 |
| | N/mm² | 0,0045 | 0,0045 | 0,0045 | 0,0045 | 0,0045 | 0,0045 | 0,0157 | -0,0045 | -0,0045 | -0,0045 | -0,0045 | -0,0045 | -0,0045 | -0,0045 | -0,0045 | -0,0045 | 0,0009 | -0,0013 | 0,0090 | -0,0095 |
| 54,1411 | kN | | | | | | | | | | | | | | | | | | 0,0104 | 0,1795 | -0,1748 |
| | N/mm² | | | | | | | | | | | | | | | | | | 0,0005 | 0,0093 | -0,0065 |
| 56,4822 | kN | | | | | | | | | | | | | | | | | | -0,1367 | 0,0301 | -0,3703 |
| | N/mm² | | | | | | | | | | | | | | | | | | -0,0071 | 0,0016 | -0,0140 |
| 58,8233 | kN | | | | | | | | | | | | | | | | | | -0,2334 | -0,0752 | -0,3527 |
| | N/mm² | | | | | | | | | | | | | | | | | | -0,0121 | -0,0039 | -0,0187 |
| 61,1644 | kN | -0,5268 | -0,5268 | -0,5268 | -0,5268 | -0,8757 | -0,8757 | 0,0919 | -1,0217 | -1,0217 | -1,0217 | -1,0217 | -1,0217 | -1,0217 | -1,0217 | -1,0217 | -1,0217 | 0,0000 | -0,3359 | -0,1834 | -0,4543 |
| | N/mm² | -0,0068 | -0,0068 | -0,0068 | -0,0068 | -0,0114 | -0,0114 | 0,0012 | -0,0133 | -0,0133 | -0,0133 | -0,0133 | -0,0133 | -0,0133 | -0,0133 | -0,0133 | -0,0133 | 0,0000 | -0,0173 | -0,0095 | -0,0236 |
| 63,5055 | kN | | | | | | | | | | | | | | | | | | -0,4384 | -0,1944 | -0,5535 |
| | N/mm² | | | | | | | | | | | | | | | | | | -0,0227 | -0,0101 | -0,0287 |
| 65,8466 | kN | | | | | | | | | | | | | | | | | | -0,5467 | -0,2086 | -0,6573 |
| | N/mm² | | | | | | | | | | | | | | | | | | -0,0284 | -0,0108 | -0,0341 |
| 68,1877 | kN | | | | | | | | | | | | | | | | | | -0,6591 | -0,2249 | -0,7657 |
| | N/mm² | | | | | | | | | | | | | | | | | | -0,0342 | -0,0117 | -0,0397 |
| 70,5288 | kN | -2,4889 | -2,4889 | -2,4889 | -2,8379 | -2,4889 | -2,8379 | -1,9399 | -2,9281 | -2,9281 | -0,8758 | -0,8758 | -0,8758 | -1,9161 | -1,9161 | -1,9161 | -2,9281 | 0,0000 | -0,7956 | -0,6650 | -0,9001 |
| | N/mm² | -0,0323 | -0,0323 | -0,0323 | -0,0368 | -0,0323 | -0,0368 | -0,0252 | -0,0380 | -0,0380 | -0,0114 | -0,0114 | -0,0114 | -0,0171 | -0,0171 | -0,0171 | -0,0380 | 0,0000 | -0,0414 | -0,0345 | -0,0466 |
| 72,9627 | kN | | | | | | | | | | | | | | | | | | -0,9147 | -0,7852 | -1,0174 |
| | N/mm² | | | | | | | | | | | | | | | | | | -0,0457 | -0,0392 | -0,0508 |
| 75,3966 | kN | | | | | | | | | | | | | | | | | | -1,0808 | -0,9430 | -1,1712 |
| | N/mm² | | | | | | | | | | | | | | | | | | -0,0534 | -0,0471 | -0,0585 |
| 77,8302 | kN | | | | | | | | | | | | | | | | | | -1,2101 | -1,0841 | -1,3031 |
| | N/mm² | | | | | | | | | | | | | | | | | | -0,0604 | -0,0541 | -0,0651 |
| 80,2644 | kN | -4,4791 | -4,4791 | -4,8281 | -4,4791 | -4,4791 | -4,7353 | -3,9644 | -4,8748 | -3,0835 | -1,2145 | -1,2145 | -1,2145 | -2,8587 | -2,8587 | -2,8587 | | 0,0000 | -1,3557 | -1,2359 | -1,4531 |
| | N/mm² | -0,0559 | -0,0559 | -0,0603 | -0,0559 | -0,0559 | -0,0591 | -0,0497 | -0,0609 | -0,0385 | -0,0067 | -0,0067 | -0,0067 | -0,0171 | -0,0171 | -0,0171 | | 0,0000 | -0,0677 | -0,0617 | -0,0725 |
| 82,6983 | kN | | | | | | | | | | | | | | | | | | -1,5789 | -1,4869 | -1,6029 |
| | N/mm² | | | | | | | | | | | | | | | | | | -0,0753 | -0,0693 | -0,0800 |
| 85,1322 | kN | | | | | | | | | | | | | | | | | | -1,8039 | -1,7452 | -1,7588 |
| | N/mm² | | | | | | | | | | | | | | | | | | -0,0841 | -0,0771 | -0,0878 |
| 87,5661 | kN | | | | | | | | | | | | | | | | | | -1,8271 | -1,7093 | -1,9214 |
| | N/mm² | | | | | | | | | | | | | | | | | | -0,0912 | -0,0854 | -0,0959 |
| 90,0000 | kN | -6,9788 | -4,3501 | -6,6296 | -6,6296 | -6,6296 | -5,9318 | -6,5058 | -7,3568 | -9,1481 | -11,0694 | -8,4311 | -3,7672 | -10,9349 | -6,7456 | -2,4831 | | 0,0000 | -1,9970 | -1,8796 | -2,0856 |
| | N/mm² | -0,0871 | -0,0548 | -0,0828 | -0,0828 | -0,0828 | -0,0741 | -0,0812 | -0,0918 | -0,1142 | -0,0400 | -0,0258 | -0,0115 | -0,0406 | -0,0249 | -0,0092 | | 0,0000 | -0,0997 | -0,0938 | -0,1044 |

# Chapter 11

# The shell as a membrane

Following (Heyman, 1977), (Flügge, 1960) and (Saliger, 1932), this section provides a summary of the membrane analysis formulation.

A shell is a structure which can be idealized mathematically as a curved surface. Thus, the thickness of the shell is small compared with the leading dimensions of the shell.

Such a curved surface, when acted upon by external loads (or by its own weight), might be imagined as resisting the action of those loads both by bending of the surface and by thrust (or tensions) acting on the surface; this section is concerned entirely with membrane forces, acting in the surface. It is assumed that effects due to bending are negligible.

Thus, imagining an infinitesimal cut through the thickness of the shell, the faces of the cut will be subjected to a normal stress resultant (force per unit length) and a shearing stress resultant, the values of which can be related in the usual way.

## 11.1. Shells of revolution

The dome is a surface of revolution with a vertical axis, consequently, the vertical sections will be meridians and the horizontals will be circular hoops; the stress generated by the loads are contained in planes tangent to the half-surface at the point of application; due to the axisymmetric loading the shear stress will be zero everywhere, (Figure 114).

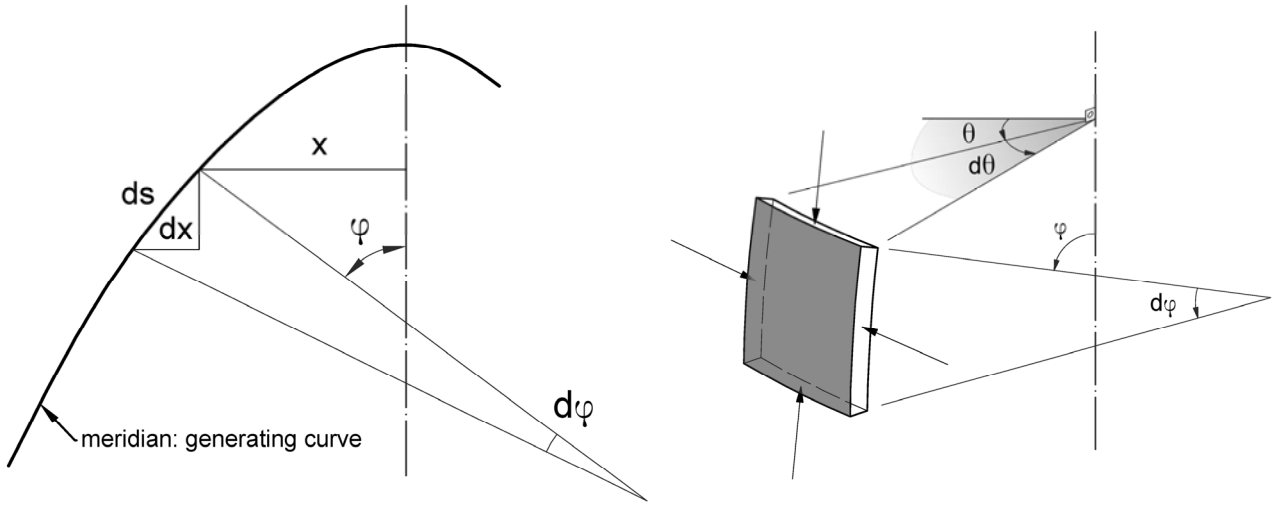


**Figure 114** (left) Meridian generating curve and (right) differential element.

## 11.2. Slice equilibrium

Figure 115 shows the equilibrium forces in a slice of a generic revolution dome, being,

- *W*: weight of portion of dome upper to parallel x.
- *φ*: colatitude (angle between the tangent to the meridian and the horizontal).
- *θ*: angle in the horizontal plane.
- *x*: distance to the axial axis.
- *y*: distance to the top of the dome.
- *s*: meridian longitude from top.
- *Nφ*: meridian compression force per parallel unit length (tangent to the meridian).
- *Nθ*: parallel compression force per meridian unit length (tangent to the parallel).
- *R1*: radial force per parallel unit length.

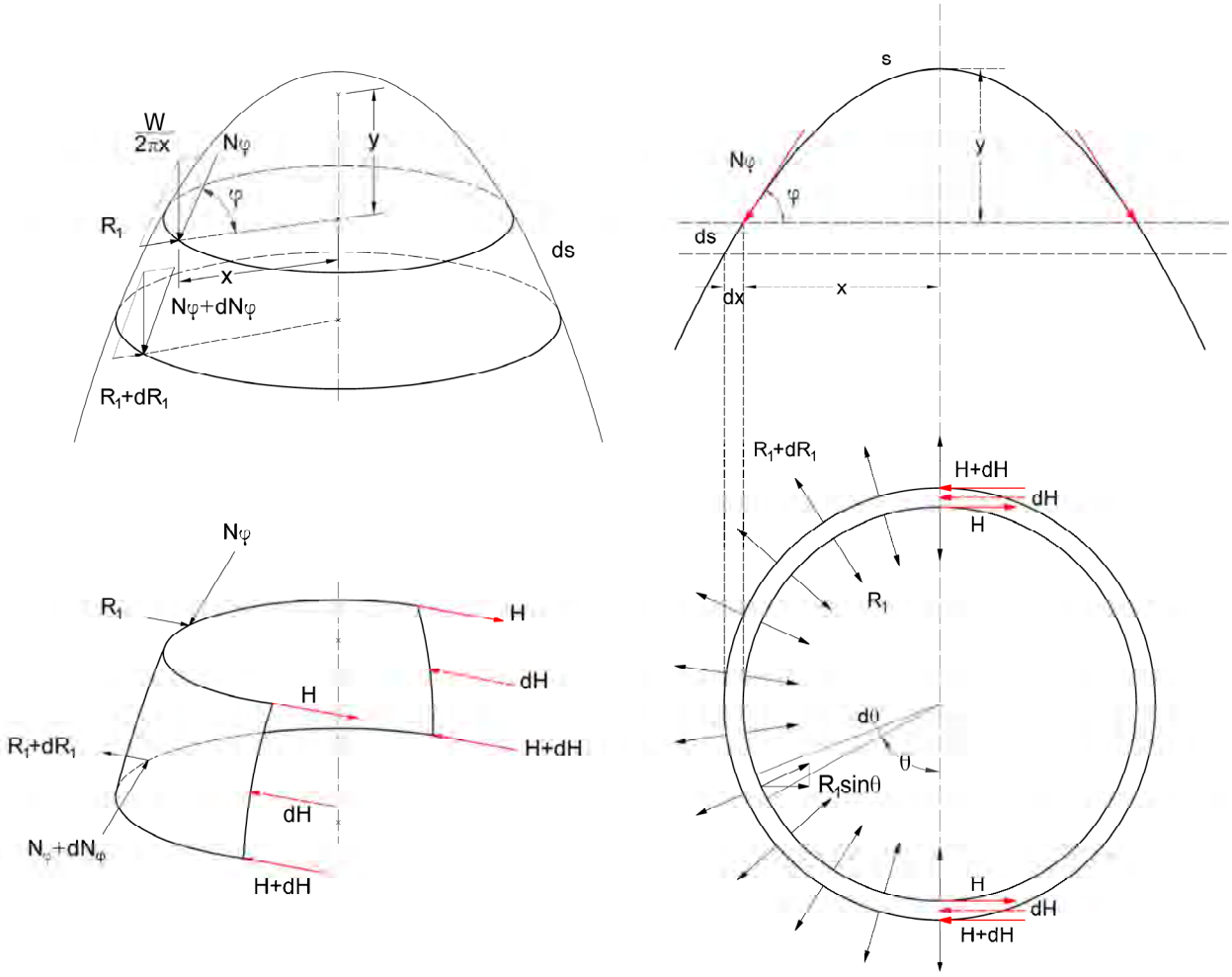


**Figure 115** Slice equilibrium.

The weight distributed along the perimeter decomposes in two directions, one is radial and the other is tangent to the meridian; the values of H can be obtained by integrating the component of $R_1$ along the length of the hoop, Figure 115 (right).

$$N_\varphi = \frac{W}{2\pi x sen\varphi} \qquad R_1 = \frac{W cot\varphi}{2\pi x} \qquad N_\theta = \frac{dH}{ds} = \frac{1}{2\pi}\frac{d}{ds}(W\,cot\,\varphi) \qquad (8)$$

The expression obtained for the meridian compression thrust ($N_\varphi$) indicates that its value is always positive (it is always compression thrust), while the expression for the parallel thrust ($N_\theta$) indicates that it can change of sign, so it can be compression or traction thrust.

## 11.3. Spherical shell

Taking into account the geometric relationships of sphericity (12), the expressions of the stress resultant become:

$$N_\varphi = \frac{W}{2\pi R sen^2\varphi} \qquad N_\theta = \frac{1}{2\pi R}\left(cot\,\varphi\frac{dW}{d\varphi} - \frac{W}{sen^2\varphi}\right) \qquad (9)$$

## 11.4. Uniform spherical shell under self-weight

The following expressions are obtained for the stress resultant, being $w$ the weight per unit area:

$$N_\varphi = \frac{wR}{1+cos\varphi} = \frac{R^2 w}{2R-y} \qquad (10)$$

$$N_\theta = Rw\frac{(cos^2\varphi + cos\varphi - 1)}{1+cos\varphi} = w\frac{y^2 - 3Ry + R^2}{2R-y} \qquad (11)$$

By application of expressions (10), the value of $N_\varphi$ increases with $\varphi$ from a compressive value of $\frac{wR}{2}$ at the crown to $wR$ at 90º; however, by application of expressions (11) the value of $N_\theta$ changes sign at $\varphi = 51{,}82°$.

## 11.5. Hemispherical dome with lantern

The spherical dome is considered starting from $\varphi = \varphi_K$ (Figure 116). The previous mathematical development incorporates the weight of the lantern into the W function.

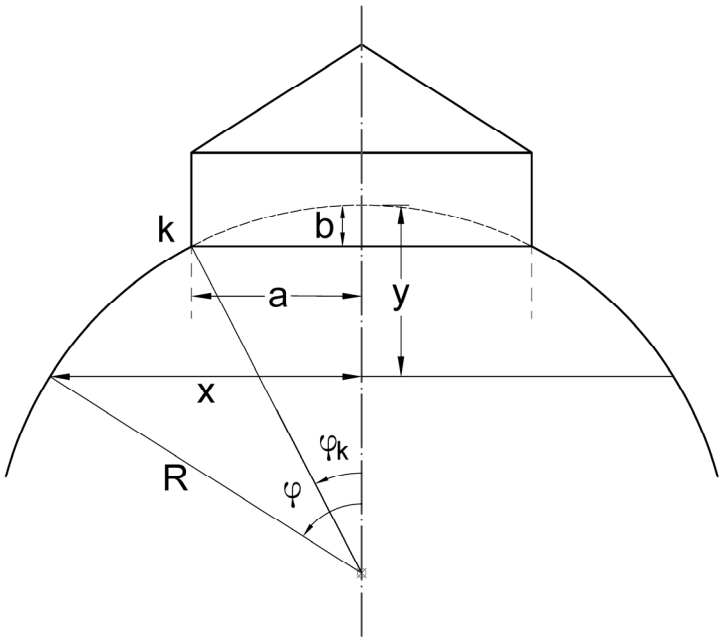


**Figure 116** Hemispherical dome with lantern.

Geometric relationships of sphericity: $x = Rsen\varphi \quad y = R(1 - cos\varphi)$ (12)

Lantern weight: $L$

Added weight: $W_1 = L - 2\pi Rbw = cte.$

Total weight: $W = 2\pi Ryw + W_1 = 2\pi R^2 w(1 - cos\varphi) + W_1$

Substituting in expressions (9):

$$N_\varphi = \frac{wR}{1 + cos\varphi} + \frac{RW_1}{2\pi x^2} = \frac{R^2 w}{2R - y} + \frac{RW_1}{2\pi x^2} \tag{13}$$

$$N_\theta = Rw\frac{(cos^2\varphi + cos\varphi - 1)}{1 + cos\varphi} - \frac{W_1 R}{2\pi x^2} = w\frac{y^2 - 3Ry + R^2}{2R - y} - \frac{W_1 R}{2\pi x^2} \tag{14}$$

## 11.6. Compressive stiffening ring

As explained in (Heyman, 1977) and (Flügge, 1960), a ring beam is necessary at the lantern base that could be contained within the shell itself. The edge of the dome must be stiffened at this point with a ring (which will be in compression) since the shell can only resist tangentially applied external forces.

There is a lack of fit between the ring and the shell proper. The compressive force in the ring will give rise to a hoop stress in the ring, which will not in general have the same value as the hoop stress in the adjacent portion of the shell, since from (14) the hoop stress in the shell at the lantern base is virtually zero.

The weight of the lantern is considered as a distributed load of value *l* per unit length, acting vertically along the edge of the dome at the oculus. According to Figure 117 the stress in the crown (lantern base) is:

$$N_{\varphi c} = -\frac{l}{sen\varphi_K} = -\frac{lR}{a}; \qquad N_{\theta C} = \int_0^{\pi/2} R_{1C} sen\theta d\theta = aR_{1C} = alcot\varphi_K = l(R-b) \qquad (15)$$

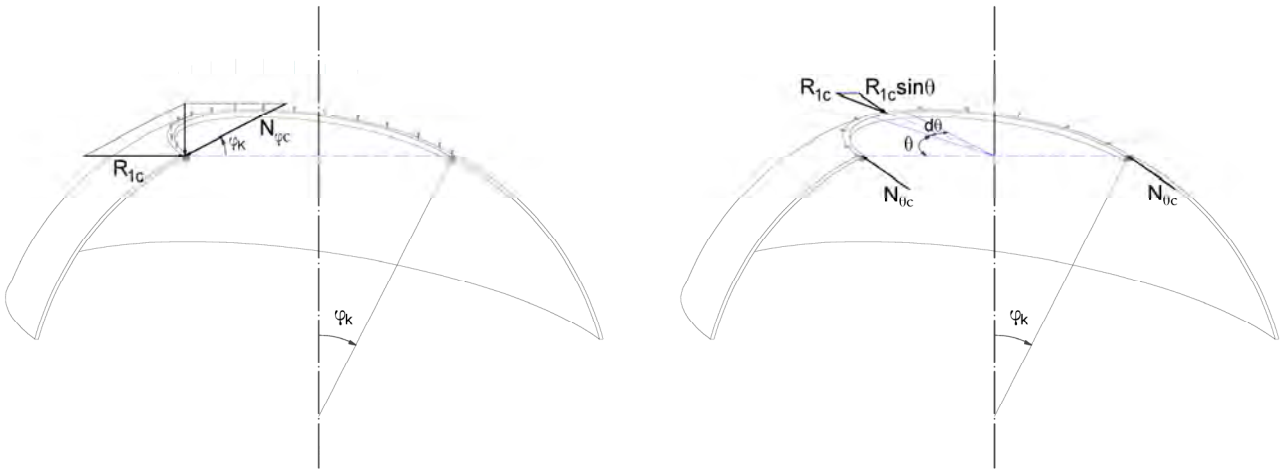


**Figure 117** Line load on the edge of the dome at the oculus.

# Chapter 12

# Application and contrast of results

The expressions (13) and (14) are applied to the hemispherical dome of brick, of small thickness described in 6.1.

## 12.1. Orders of magnitude

It is a uniform thin-walled hemisphere, and it is subjected only to its own weight. It is supported around its horizontal diametrical plane by forces, which produce a uniform compressive stresses $\sigma$. Figure 118 shows the calculations of the orders of magnitude for the compressive stress needed to support the dome.

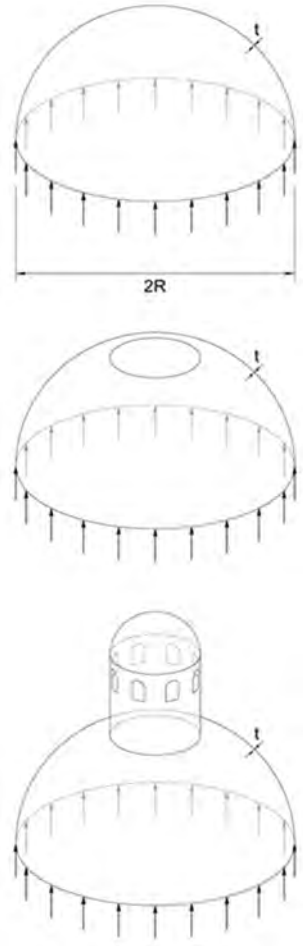


$$\sigma 2\pi Rt = \rho 2\pi R^2 t \rightarrow \sigma = \rho R = 0.1041\ N/mm^2 \quad (16)$$

$$\sigma 2\pi Rt = \rho 2\pi R^2 t - \rho 2\pi R\left(R - \sqrt{R^2 - \left(\frac{\emptyset_C}{2}\right)^2}\right)t \rightarrow$$

$$\sigma = \rho\sqrt{R^2 - \left(\frac{\emptyset_C}{2}\right)^2} = 0.0982\ N/mm^2 \quad (17)$$

$$\sigma 2\pi Rt = \rho 2\pi R^2 t - \rho 2\pi R\left(R - \sqrt{R^2 - \left(\frac{\emptyset_C}{2}\right)^2}\right)t + L \rightarrow$$

$$\sigma = \rho\sqrt{R^2 - \left(\frac{\emptyset_C}{2}\right)^2} + \frac{L}{2\pi Rt} = 0.1087\ N/mm^2 \quad (18)$$

**Figure 118** Orders of magnitude of the compressive stress necessary to support the dome.

## 12.2. Membrane stress resultants

It is conventional in membrane shell analysis to work in term of stress resultants $N_\varphi$, $N_\theta$. The membrane stress resultants have dimensions of force per unit length.

In this work is convenient to work in terms of stresses $\sigma$ ($\frac{N}{mm^2}$), to be able to compare the results of the different methodologies.

Figure 119(a), (b), (c), show the values of $N_\varphi$ and $N_\theta$ calculated by expressions (13) and (14), expressed in terms of stresses (N/mm$^2$).

Figure 119(a), displays the values of meridian and parallel stresses for the hemispherical dome ($W_1 = 0$). For $\varphi = 0°$ the values of $N_\varphi$ and $N_\theta$ are $\frac{1}{2}wR = 4.16\frac{kN}{m}$ $\left(\sigma = 0.05\frac{N}{mm^2}\right)$. The value of $N_\varphi$ increases with $\varphi$, from a compressive value of $\frac{1}{2}wR$ at the crown, to $wR = 8.32\frac{kN}{m}\left(\sigma = 0.1\frac{N}{mm^2}\right)$ at $\varphi = 90°$; this last value is in accord with the result of equation (16). The value of $N_\theta$, however, changes sign at $\varphi = 51{,}82°$, reaching a tension value equal to $wR = 8.32\frac{kN}{m}\left(\sigma = 0.1\frac{N}{mm^2}\right)$ at $\varphi = 90°$.

Figure 119(b) presents the values of meridian and parallel stresses for a hemispherical dome with oculus, calculated by expressions (13) and (14), for $W_1 = -2\pi Rbw$, and expressed in terms of stresses (N/mm$^2$). For $\varphi = \varphi_K = 19.315°$, the values are, $N_\varphi = 0$ and $N_\theta = 7.86\frac{kN}{m}$ $\left(\sigma = 0.098\ \frac{N}{mm^2}\right)$. The value of $N_\varphi$ increases with $\varphi$ to $N_\varphi = 7.86\frac{kN}{m}$ $\left(\sigma = 0.098\ \frac{N}{mm^2}\right)$, according with equation (17). The value of $N_\theta$ change of sign at $\varphi = 56°$, and decreases until $N_\theta = -7.86\frac{kN}{m}$ $\left(\sigma = -0.098\ \frac{N}{mm^2}\right)$.

Figure 119(c) shows the values of $N_\varphi$ and $N_\theta$, for a hemispherical dome with lantern, calculated by expressions (13) and (14) and expressed in terms of stresses (N/mm$^2$). The meridian stress resultant at the base of the lantern is $N_\varphi = 7.71\frac{kN}{m}$ $\left(\sigma = 0.096\ \frac{N}{mm^2}\right)$. After a decrease, from $\varphi = 44°$ it starts to grow. The meridian stress at the base is $N_\varphi = 8.7\frac{kN}{m}$ $\left(\sigma = 0.1087\ \frac{N}{mm^2}\right)$, in agreement with equation (18). The parallel stress resultant at the base of the lantern is $N_\theta = 0.15\frac{kN}{m}$ $\left(\sigma = 0.0018\ \frac{N}{mm^2}\right)$, up to $\varphi = 47.2°$ are compression forces. As de value of $\varphi$ increases, the value of $N_\varphi$ and $N_\theta$, in traction and compression respectively, tend to match.

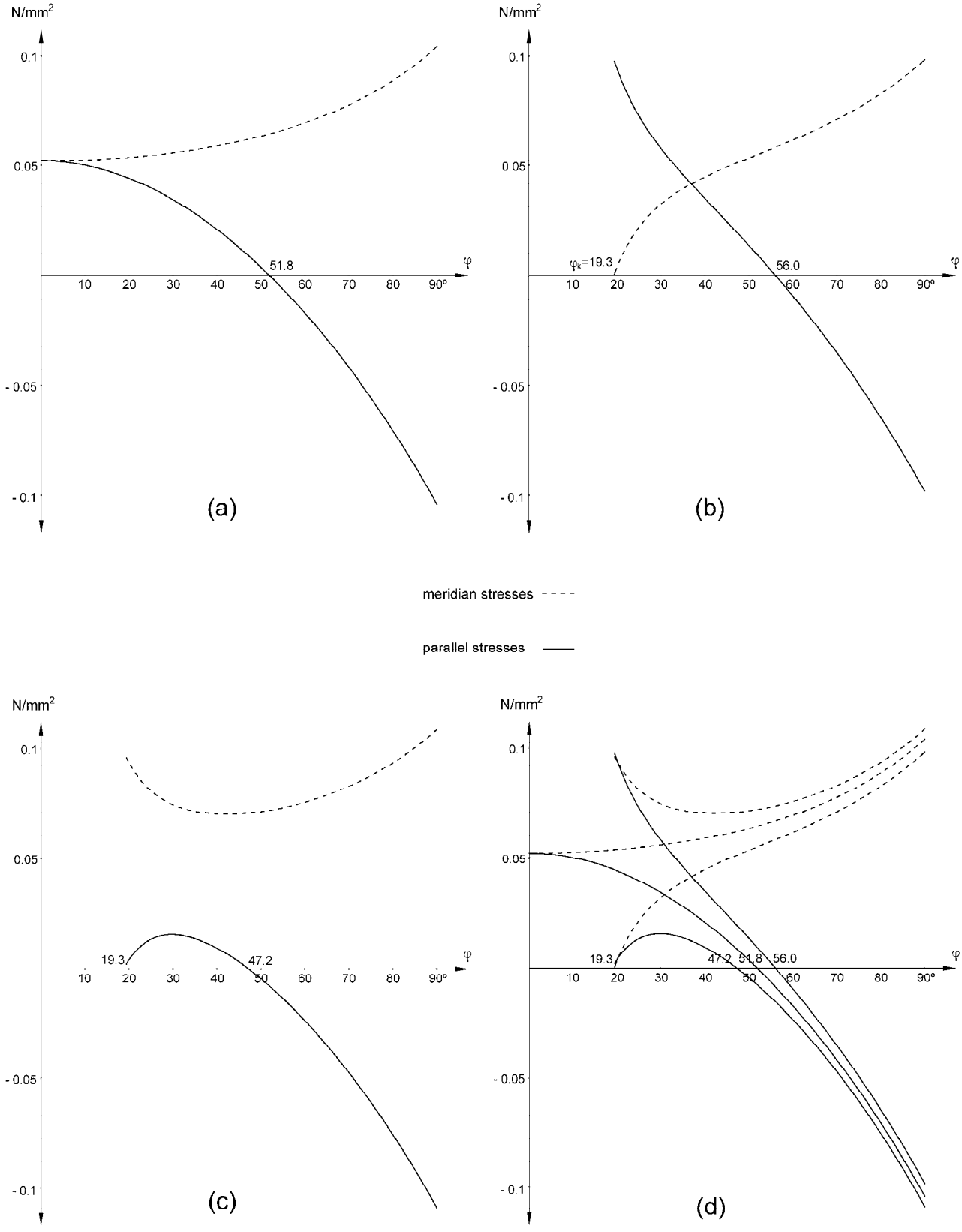


**Figure 119** Values of stress resultant Nφ, Nθ obtained by application of membrane analysis, expressed in terms of stresses (N/mm²): (a) hemispherical dome; (b) hemispherical dome with oculus; (c) hemispherical dome with lantern; (d) combination of (a), (b) and (c).

## 12.3. Compressive stiffening ring

Considering that the edge of the dome has been stiffened at the last 8 cm, as indicated in Figure 120, and by applying expression (15) the following values for the stiffening ring are obtained.

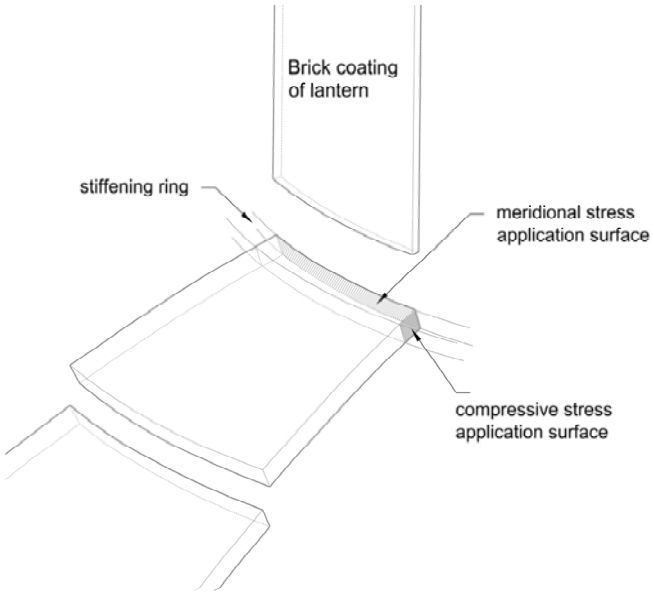


Stiffening ring:

$$N_{\varphi c}\ (kN/m) = 7.71$$

$$N_{\varphi c}\ (N/mm^2) = 0.096$$

Compressive stiffening ring:

$$N_{\theta C}\ (kN) = 14.18$$

$$N_{\theta C}\ (N/mm2) = 2.21 \qquad (19)$$

**Figure 120** Compressive stiffening ring.

## 12.4. Contrast of results

Figure 121(a), (b), (c) show the values obtained with the new methodology for 160 sectors (included in Table 3 and Table 4), along with the curves mentioned in a previous section.

The values obtained with the new graphic methodology for 640 sectors are displayed in Figure 122(a), (b), (c).

Figure 122(a), (b), (c) reflect a high degree of agreement between the results obtained by the new methodology and those obtained in the membrane analysis.

There is a singular disagreement in Figure 122(c). The values of parallel stresses obtained at the base of the lantern ($\varphi = 19.3°$) with the new graphic methodology are close to those obtained by applying expression (15).

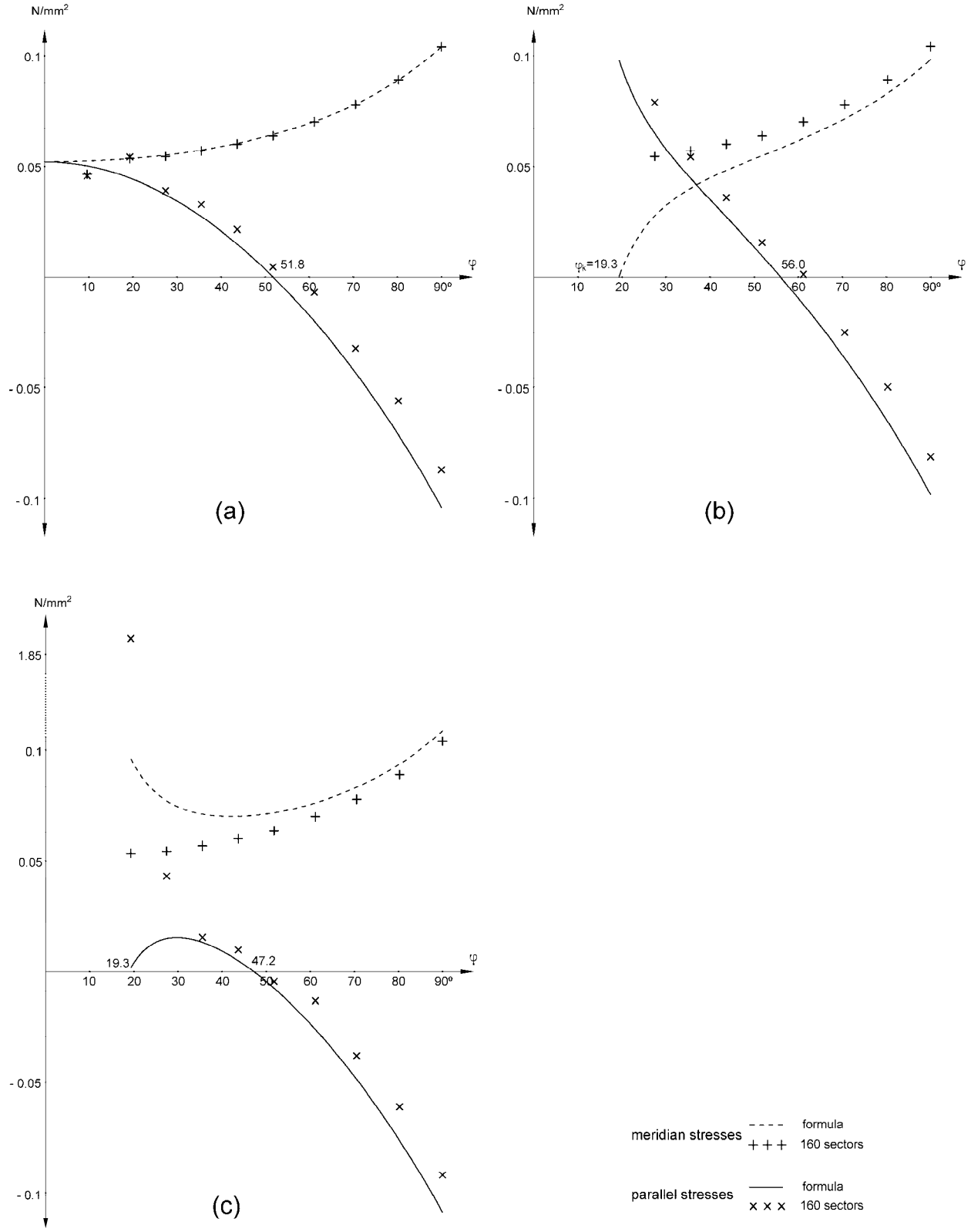


**Figure 121** Values of stress resultant Nφ, Nθ obtained by application of membrane analysis, expressed in terms of stresses (N/mm²): (a) hemispherical dome; (b) hemispherical dome with oculus; (c) hemispherical dome with lantern; values obtained by application of the new methodology with 160 sectors are included.

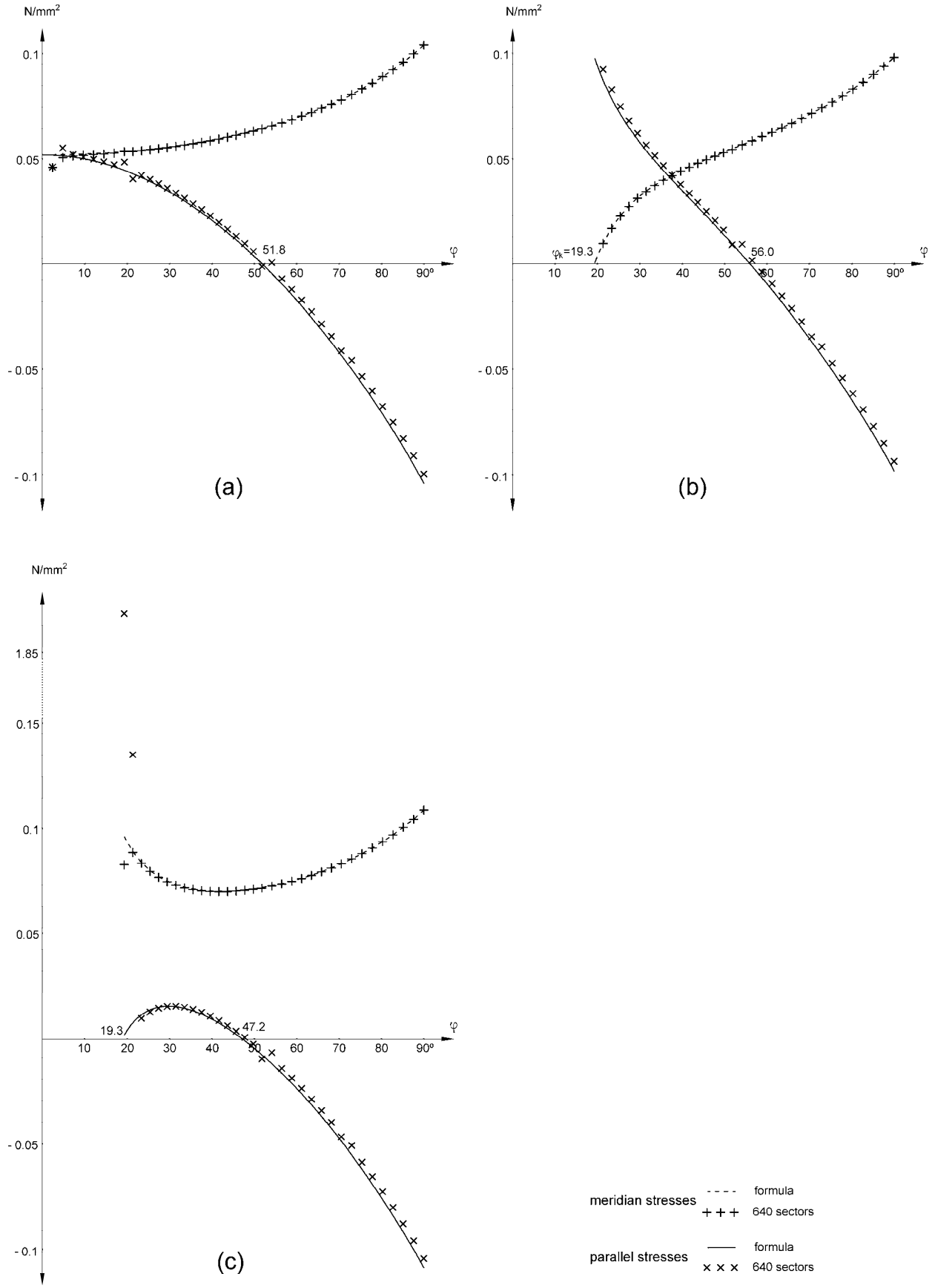


**Figure 122** Values of stress resultant Nφ, Nθ obtained by application of membrane analysis, expressed in terms of stresses (N/mm²): (a) hemispherical dome; (b) hemispherical dome with oculus; (c) hemispherical dome with lantern; values obtained by application of the new methodology with 640 sectors are included.

# Chapter 13

# Conclusions

This dissertation lays out a new graphic methodology for the structural analysis of domes and other surfaces of revolution, based in the combined use of funicular and projective geometry. The new methodology is presented through its application to a hemispherical brick dome of small thickness. This is frequently the element that internally defines the constructive system known as "*encamonada* dome". This doctoral thesis has been an opportunity to delve into the study of this typology of domes, which are an important element of the architectural heritage in the 17th and 18th centuries, in Spain and its overseas possessions, in the frame of the treatise of Fray Lorenzo de San Nicolás.

The analysed model has been referenced to a real dome: the hemispherical inner brick dome of the "*encamonada* dome" in Basilica de San Juan de Dios in Granada (Spain). The Basilica is regarded as a benchmark in the Baroque Spanish Architecture. Until now, this Basilica had only been studied from the artistic and architectural point of view. For the first time, the detailed constructive analysis and the geometric modelling of the dome over the transept is presented.

The structural analysis of the inner brick dome (or timbrel dome) has been presented by applying different equilibrium methodologies of increasing refinement, and it puts forward the gradual application of them.

Firstly, an approximation by applying the Guastavino´s formulas. This is an experimental methodology that can be used very quickly.

Secondly, the application of the slicing technique in the frame of the limit analysis theorems. It is a very well known, and contrasted methodology, for the stability analysis of domes, which does not take into account the tangential forces. Following Fray Lorenzo´s recommendations on the inclusion of a backfilling in the bottom third, this work analyses different structural behaviours of the backfilling, according to its morphological characterisation: non-structural filling (adding weight); structural filling (increases the section); rigidly cemented filling (considering a shallow dome). The results of these analysis highlight the importance for the stability of the timbrel dome of the filling up to one third of the height, as recommended by Fray Lorenzo de San Nicolás.

Finally, this dissertation presents a new graphic methodology for the structural analysis of domes, based in the combined use of funicular and projective geometry. The results obtained by the application of the new methodology have been contrasted with the solutions achieved by the application of the membrane analysis.

The new graphic methodology takes into account the hoop forces to find in the dome a solution for internal forces in equilibrium, therefore, it is a less conservative method than other graphic methods widely used, such as Eddy's method or the slicing technique.

This new methodology allows to graphically determine internal forces in the dome, by enforcing the equilibrium in both vertical and horizontal planes.

The equilibrium in the vertical plane is assured by fitting in the polar rays the system of weight forces, which is closed, hence the antifunicular polygon, closed too, fits within the dome geometry. The equilibrium in the horizontal plane is guaranteed by the formation of closed force polygons in the dual figure.

The methodology is presented through its application to a hemispherical brick dome of small thickness, considering different situations: complete hemisphere, hemisphere with oculus on the top, and hemisphere with lantern; different inclinations of the reaction in the support are considered too. A multiplicity of solutions with acceptable tensional values for the brick masonry has been obtained. The results have been contrasted with those from the application of membrane analysis.

The evaluation of the methodology with the membrane analysis indicates that there is a strong coincidence of results if the number of sectors in the discretisation of the graphic methodology is high enough.

The value of the parallel force obtained at the base of the lantern, by applying the graphic methodology, approaches the value of the force calculated for the necessary compression ring, thus improving the lack of fit between the ring and the shell proper when applying membrane analysis.

The new methodology allows its application, and so it has been applied in this work, in the inverse way, namely, reducing the value of the maximum tension, and determining the necessary variations in the values of the polar rays angles ($\alpha_i$); checking that they imply very little variations, relative to the dome thickness, of the meridional section of the simplified model.

The proposed graphic methodology accurately reproduces the results of the membrane analysis equations. Furthermore, it allows its application to different structural situations. It is easy to understand, easy to program, and can be applied in domes of arbitrary geometry.

# Chapter 14

# Future lines of research

- Apply the new graphic methodology to non-thin shells, where the application of limit analysis, will allow a wider range of geometric variations of the simplified model.

- Apply the new graphic methodology to other non-spherical surfaces of revolution.

- Develop a graphic software to automate the methodology following Philippe Block's work.

- Contrast the results of the new graphic methodology with the results obtained through the application of numerical methods.

# References


Alexakis, H., & Makris, N. (2014). Limit equilibrium analysis of masonry arches. *Archive of Applied Mechanics, 85*(9), 1363-1381. doi:10.1007/s00419-014-0963-6

Allen, E., & Zalewski, W. (2009). *Form and forces. Designing efficient, expressive structures.* Hoboken, New Jersey: John Wiley & Sons.

Almagro, A. (2011). Bóvedas tabicadas en la Cartuja de Granada: el final de un proceso evolutivo. *Actas del Simpio Internacional sobre Bóvedas Tabicadas* (pp. 3-14). Valencia: Universidad Politécnica de Valencia.

Andreu, A. (2006). *Análisis resistente de estructuras de obra de fábrica mediante redes funiculares simuladas computacionalmente. Doctoral dissertation.* Barcelona: Universidad Politécnica de Cataluña.

Aroca Hernández-Ros, R. (2002). *Funiculares.* Madrid: Universidad Politécnica.

Atamturktur, S., & Boothby, T. E. (2007). The development of finite-element models and the horizontal thrust of Guastavino domes. *APT bulletin, 39*(4), 21-29.

Baker, W. F., Beghini, L. L., Mazurek, A., Carrion, J., & Beghini, A. (2013). Maxwell's reciprocal diagrams and discrete Michell frames. *Structural and Multidisciplinar Optimization, 48*, 267-277. doi:10.1007/s00158-013-0910-0

Bassegoda, J. (1978). *La cerámica popular de la arquitectura gótica* (Vol. 8). Barcelona: Nuevo Arte Thor.

Battista Alberti, L. (1452 (published 1485)). *De re aedificatoria.* Florence: Nicolai Laurentii Alamani.

Beatini, V., Royer-Carfagni, G., & Tasora, A. (2018). The role of frictional contact of constituent blocks on the stability of masonry domes. *Proceedings of the Royal Society A, 474*(2209), 1-21. doi:0.1098/rspa.2017.0740

Benavent, F., & Magro, J. V. (1996). Evolución de los sistemas de cubierta sobre la construcción abovedada en la arquitectura religiosa de la Comunidad valenciana, entre los siglos XIV y XVIII. *Actas del Primer Congreso Nacional de Historia de la Construcción* (pp. 85-90). Madrid: Instituto Juan de Herrera.

Bergós, J. (1965). *Tabicados huecos.* Barcelona: Colegio Oficial de Arquitectos de Cataluña y Baleares.

Block, P. (2009). *Thrust network analysis: exploring three-dimensional equilibrium. Doctoral dissertation.* Massachusetts: Massachusetts Institute of Technology.

Block, P., & Ochsendorf, J. (2007). Thrust network analysis: a new methodology for three-dimensional equilibrium. *Journal of the International Association for shell and spatial structures, 48*(3), 167-173.

Block, P., Ciblac, T., & Ochsendorf, J. (2006). Real-time limit analysis of vaulted masonry buildings. *Computers & Structures, 84*(29-30), 1841-1852. doi:10.1016/j.compstruc.2006.08.002

Block, P., Dejong, M., & Ochsendorf, J. (2006). As Hangs the Flexible Line: Equilibrium of Masonry Arches. *Nexus Network Journal, 8*(2), 9-19. doi:10.1007/s00004-006-0015-9

Block, P., Laucher, L., & Rippmann, M. (2014). Thurst network analysis. In *Shell structures for Arquitecture* (pp. 71-87). Abingdon - New York: Routledge. doi:10.4324/9781315849270

Boothby, T. (2001). Analysis of masonry arches and vaults. *Progress in Structural Engineering and Materials, 3*, 246-256. doi:10.1002/pse.84

Boothby, T. (2015). *Engineering Iron and Stone: Understanding Structural Analysis and Design Methods of the Late 19th Century.* American Society of Civil Engineers.

Bouguer, P. (1734). Sur les lignes courbes propres a former les voûtes en dôme. *Mémoires de l'Académie Royale de Sciences de Paris*, 149-166.

Bow, R. H. (1873). *Economics of construction in relation to frame structures.* London: ICE Publishing.

Calvo-lópez, J. (2011). From mediaeval stonecutting to projective geometry. *Nexus newtwork journal, 13*(3), 503-533. doi:10.1007/s00004-011-0081-5

Carter, C. B., & Norton, M. G. (2007). *Ceramic materials: science and engineering.* New York: Springer. doi:10.1007/978-1-4614-3523-5

Castigliano, A. (1879). *Théorie de l'equilibre des systémes élastiques et ses applications.* Turin: Augusto Federico Negro.

Cavalagli, N., & Gusella, V. (2015). On the graphic statics for the analysis of masonry domes. *Proceedin in Applied Mathematics and Mechanics, 15*(1), 701-702. doi:doi.org/10.1002/pamm.201510340

Choisy, A. (1873). L´art de bâtir chez les romains. Forni.

Ciblac, T., & Morel, J.-C. (2014). *Sustainable Masonry: Stability and Behavior of Structures.* London: ISTE Ltd. doi:10.1002/9781119003564

Collins, G. R. (1968). The transfer of thin masonry vaulting from Spain to America. *Journal of the Society of Architectural Historians, 27*(3), 176-201. doi:10.2307/988501

Conejo da Pena, A. (2012). Volta de rajola, volta de maó pla o volta catalana: reflexiones en torno a las bóvedas tabicadas en Cataluña durante los siglos del gótico. *Actas del Simposio Internacional sobre Bóvedas Tabicadas* (pp. 101-117). Valencia: Universidad Politénica de Valencia.

Coolidge, J. L. (1940). *A history of geometrical methods.* Oxford: Claredon Press.

Couplet, P. (1729). De la poussée des voûtes. *Mémoires de l'Académie Royale des Sciences*, 79-117, figures 4-7.

Couplet, P. (1730). Seconde partie de l'examen de la poussée des voûtes. *Mémoires de l'Académie de Paris*, 117-141, figures 6-7.

Cremona, L. (1872). *Le figure reciproche nella statica grafica.* Milan: Tipografia di G. Bernardoni.

Culmann, K. (1864). *Die Graphische Statik.* Zürich: Meyer und Zeller.

Culmann, K. (1875). *Die Graphische Statik.* Zürich: Meyer und Zeller.

Danyzy, A. H. (1732). Méthode générale pour déterminer la résistance qu'il faut opposer à la poussée des voûtes. *Histoire de la Société Royale des Sciences établie à Montpellier, 2*(1718-1745), 40-56.

De San Nicolás, F. L. (1639, 1665). *Arte y uso de la arquitectura. Parte primera y segunda.* Madrid.

Desargues, G. (1639). *Brouillon Project d'une atteinte aux évènements des rencontres du Cône avec un Plan.*

Du Bois, A. J. (1877). *The Elements of Graphical Statics and Their Application to Framed Structures.* New York: Wiley and son.

Dugum, H. (2013). *Structural assessment of the Guastavino masonry dome of the Cathedral of Saint John the Divine. Master dissertation.* Oxford, Massachusetts: Massachusetts institute of technology.

Dunn, W. (1904). Notes on the stresses in framed spires and domes. *Journal of the Royal Institute of British Architects, 11*, 401-412.

Dunn, W. (1908). The Principles of Dome Construction. (G. N. Street, Ed.) *Architectural review, 23*, 63-73; 108-112.

Eddy, H. T. (1878). *Researches in graphical statics.* New York: Van Nostrand.

Engesser, F. (1880). Ueber die Lage der Stützlinie in Gewölben. *Deutsche Bauzeitung, 14*, 184-186, 210, 243.

Estepa, R. (2015). *Chapiteles del siglo XVIII en Madrid y su entorno. Sus armaduras de madera. Doctoral dissertation.* Madrid: Universidad Politécnica de Madrid.

Flügge, W. (1960). *Stresses in shells.* Berlin: Springer-Verlag. doi:10.1007/978-3-662-01028-0

Föppl, A. (1881). *Ausgewählte Capitel der mathematischen Theorie der Bauconstructionen.* Leipzig: Felix.

Fortea, M. (2009). Origen de la bóveda tabicada. *Actas del sexto congreso nacional de historia de la construcción.* (pp. 491-500). Valencia: Instituto Juan de Herrera.

Frézier, A. -F. (1737). *La théorie et la pratique de la coupe des pierres et des bois, pour la construction des voûtes...ou Traité de steréotomie à l'usage de l'architecture* (Vol. 1). París: Charles Antoine Jombert.

Galassi, S., Misseri, G., Rovero, L., & Tempesta, G. (2017). Equilibrium analysis of masonry domes. On the analytical interpretation of the Eddy-Lévy graphical method. *International Journal of Architectural Heritage, 11*(8), 1195-1211. doi:10.1080/15583058.2017.1372823

Galera, P. A. (1992). La cúpula de perfil contracurvo en el Barroco murciano y andaluz. *Imafronte*(8-9), 167-188.

Galilei, G. (1638). *Discorsi, e dimostrationi matematiche, intorno a due nuoue scienze, attenenti alla meccanica, & i mouimenti locali.*

Gallego, A. (1982). *Granada, guía artística e histórica de la ciudad.* Granada: Don Quijote.

Gallego, F. (2017). Análisis constructivo y estructural de la cúpula de San Juande Dios en Granada (España). Final Degree Project. *School of Architecture, University of Granada.* Granada.

Galloway, H. A. (1975). *Aspects of Baroque Arts in Granada, Spain: The Basilica of San Juan de Dios. Doctoral dissertation.* Ohio: Ohio University.

García-Gutiérrez, J. (2000). Las bóvedas tabicadas de Guastavino: forma y construcción. *Tercer Congreso Nacional de Historia de la Construcción* (pp. 365-374). Sevilla: Instituto Juan de Herrera.

Garza, V. (2012). Medidas y caminos en la época colonial: expediciones, visitas y viajes al norte de la Nueva Españaa (siglos XVI-XVIII). *Fronteras de la historia, 17*(2), 191-219.

Georg, R. (2012). *Historical analysis of arches and modern shells. Master dissertation.* Platteville: University of Wisconsin.

Gerhardt, R., Kurrer, K.-E., & Pichler, G. (2003). The methods of graphical statics and their relation to the structural form. *International Congress on Construction History* (pp. 997-1006). Madrid: I. Juan Herrerra.

Gerstner, F. (1789). *Einleitung in die statische Baukunst.* Prague: Normalschul-Buchdruckerey.

Gestoso, J. (1903). *Historia de los barros vidriados sevillanos. Desde sus orígenes hasta nuestros días.* Sevilla: Tipografía La Andalucía Moderna.

Gómez, M. (2011). Las bóvedas tabicadas en la arquitectura valenciana. *Simposio internacional sobre bóvedas tabicadas* (pp. 60-80). Valencia: Universidad Politécnica de Valencia.

Granero, F. (2009). Capilla de la Piedad, Hermandad del Baratillo (Sevilla). *Research Association of Wood Indus-tries, Boletín de información técnica*(258), 44-49.

Guastavino, R. (1893). *Essay on the theory and history of cohesive construction applied especially to the timbrel vault.* Boston: Ticknor and Company.

Guastavino, R. (1896-1904). *Prolegomenos on the use of masonry in modern architectural structures. Part I - Part II.* New York: Record & Guide press.

Heyman, J. (1966). The stone skeleton. *International Journal of Solids and Structures, 2*(2), 249-279. doi:10.1016/0020-7683(66)90018-7

Heyman, J. (1967). On shell solutions of masonry domes. *International Journal of Solids and Structures, 3*(2), 227-241. doi:10.1016/0020-7683(67)90072-8

Heyman, J. (1969). The safety of masonry arches. *International Journal of Mechanical Sciences, 11*(4), 363-385. doi:10.1016/0020-7403(69)90070-8

Heyman, J. (1977). *Equilibrium of shell structures.* Oxford: Oxford University Press. doi:10.1017/S0003581500056237

Heyman, J. (1988). Poleni´s problem. *Proceedings of the Institution of Civil Engineers, 84*(4), 737-759. doi:https://doi.org/10.1680/iicep.1988.139

Heyman, J. (1995, b). *The stone sketeton. Structural engineering of masonry architecture.* Cambridge: Cambridge University Press. doi:10.1017/CBO9781107050310

Heyman, J. (2009). La coupe des pierres. *Proceedings of the 3rd International Congress on Construction History. 2*, pp. 807-812. Brandenburg: Brandenburg University of Technology.

Heyman, J. (2015). *Teoría, historia y restauración de estructuras de fábrica.* Madrid: Instituto Juan de Herrera.

Hines, E. (2012). Principles for Engineering Education. *Structure magazine*, 38-39.

Hooke, R. (1676). *A description of helioscopes, and some other instruments.* London: J. Martyn.

Huerta, S. (1996). La teoría del arco de fábrica: desarrollo histórico. *Obra pública*(38), 18-29.

Huerta, S. (2001). La mecánica de las bóvedas tabicadas en su contexto histórico: la aportación de los Guastavino. En *Las bóvedas de Guastavino en América.* Madrid: Instituto Juan de Herrera.

Huerta, S. (2003). The mechanics of timbrel vaults: a historical outline. In *Essays on the History of Mechanics* (pp. 89-134). Basel: Birkhäuser. doi:doi.org/10.1007/978-3-0348-8091-6_5

Huerta, S. (2004). *Arcos, bóvedas y cúpulas. Geometría y equilibrio en el cálculo tradicional de estructuras de fábrica.* Madrid: Instituto Juan de Herrera.

Huerta, S. (2006a). La construcción tabicada y la teoría cohesiva de Rafael Guastavino. In *Escritos sobre la construcción cohesiva y su función en la arquitectura* (pp. 15-62). Madrid: Instituto Juan de Herrera.

Huerta, S. (2006b). Structural design in the work of Gaudí. *Architectural Science Review, 49*(4), 324-339. doi:10.3763/asre.2006.4943

Huerta, S. (2008). The analysis of masonry architecture: a historical approach. *Architectural Science Review, 54*(4), 297-328. doi:10.3763/asre.2008.5136

Hurtado, P. (2013). Bovedas de madera: características constructivas y consideraciones estructurales de las bóvedas encamonadas edificadas en Castill. *Informes de la Construcción, 65*(530), 155-162. doi:10.3989/ic.12.029

Ibáñez, J. (2005). *Arquitectura Aragonesa del siglo XVI. Propuesta de renovación en tiempos de Hernando de Aragón.* Zaragoza: Instituto de estudios turolenses.

Ibáñez, J. (2010). Técnica y ornato: aproximación al estudio de la bóveda tabicada en Aragón y su decoración a lo largo de los siglos XVI y XVII. *Artigrama*(25), 363-405.

Isla, E. (1977). *José de Bada y Navajas, arquitecto andaluz (1691-1755).* Granada: Province council.

Isla, E. (1979). *Isla. Hospital y basílica de San Juan de Dios en Granada.* León: Everest.

Kooharian, A. (1952). Limit analysis of voussoir (segmental) and concrete archs. *Journal Proceedings, 49*(12), 317-328.

Körner, C. (1901). Handbuch der Architectur, Third part. Darmstadt : Verlag von Arnold Bergsträsser.

Kristen, F. (2018, December 18). *Architect of the Capitol.* Retrieved 06 15, 2020, from https://www.aoc.gov/explore-capitol-campus/blog/revealing-tiled-treasure

Kubler, G. (1957). *Arquitectura de los siglos XVII y XVIII* (Vol. XIV). Madrid: Plus-Ultra.

Kurrer, K.-E. (2008). *The history of the theory of structures. From arch analysis to computational mechanics.* Berlin: Wiley, Ernst & Sohn.

Lamé, G., & Clapeyron, E. (1823). Mémorie sur la stabilité des voûtes. *Annales des Mines, 8*, 789-836.

Le Seur, T., Jacquier, F., & Boscovich, G. R. (1742). *Parere di Tre Matematici Sopra i danni, che si sono trovati nella cupola di San Pietro.*

Lévy, M. (1888). *La statique graphique et ses applications aux constructions. IV Partie.* Paris: Gauthier-Villars Imprimeur-Libraire.

Liu, J. (2016). *Digital exploration on Graphic Statics: Its attribute matrix, interactive application and basic algorithm. Doctoral dissertation.* Hong Kong: The chinese university of Hong Kong.

López, D., & Doménech, D. (2017). *Tile vaults: structural analysis and experimentation. 2015 Guastavino Biennial.* Barcelona: Consell d´Edicions i Pulicacions del l´Ajuntament de Barcelona.

López, G. (1998). *Estabilidad y construcción de cúpulas de fábrica: el nacimiento de la teoría y su relación con la práctica. Doctoral dissertation.* Madrid: Universidad Politécnica de Madrid.

Loren, M. M. (2003). *La construcción de la identidad arquitectónica norteamericana de cambio de siglo 1880-1940.* Sevilla: Universidad de Sevilla.

Lourenço, P. B. (1998). Experimental and numerical issues in the modelling of the mechanical behaviour of masonry. In P. Roca, J. González, E. Oñate, & P. Lourenço (Ed.), *Structural Analysis of Historical Constructions II* (pp. 57-91). Barcelona: CIMNE.

Luengo, N. (2016). *La obra conservada de Rafael Guastavino Moreno en Cataluña. Estudio y análisis para su puesta en valor. Master dissertation.* Valencia: Universidad Politécnica de Valencia.

Marmo, F., & Rosati, L. (2017). Reformulation and extension of the thrust network analysis. *Computer & Structures, 182*(1), 104-118. doi:10.1016/j.compstruc.2016.11.016

Martín, C. (2009). La cúpula tabicada de San Juan de la Penitencia. *Proceedings of the Sixth National Congress on the History of Construction* (pp. 825-832). Madrid: Instituto Juan de Herrera.

Maxwell, J. (1864). On reciprocal figures and diagrams of forces. *The London, Edinburgh, and Dublin Philosophical Magazine and Journal of Science, 27*(182), 250-261. doi:10.1080/14786446408643663

Maxwell, J. (1870). On reciprocal figures, frames, and diagrams of forces. *Edinb Roy Soc Proc, 7*, 160–208. doi:10.1017/S0080456800026351

McRobie, A., Konstantatou, M., Athanasopoulos, G., & Hannigan, L. (2017). Graphic kinematics, visual virtual work and elastographics. *Royal society open science, 4*(5), 170202. doi:10.1098/rsos.170202

Méry, E. (1840). Sur l'équilibre des voûtes en berceau. *Annales des ponts et chaussées*, 50-70.

Ministerio de la Vivienda . (1988 (revised)). *Normas tecnológicas de la edificación NTE-ECG/1976. Estructuras cargas: gravitatorias.* Madrid: Ministerio de Fomento.

Mohr, O. (1874). Beitrag zur theorie des Fachwerks. *ZAIVHann*(20), 509-526.

Mohr, O. (1875). Die graphische Statik und das graphische Rechnen. *Civilingenieur*(21), 229-238.

Moseley, H. (1833). On a new principle in statics, called the principle of least pressure. *Philosophical Magazine, 3*, 285-288. doi:10.1080/14786443308648178

Moseley, H. (1843a). *The Mechanical Principles of Engineering and Architecture.* London: Longman, Brown, Green and Longmans.

Moseley, H. (1843b). On the theory of the arch. In *The theory, practice and architecture of bridges* (pp. 1-72). London: J. Weale.

Navier, C. L. (1826). *Résumé des leçons données à l'école royale des ponts et chaussées sur l'application de la mécanique à l'établissement des constructions et des machines* (Vol. 1). Paris: Didot.

Nielsen, J. (1998). Leonardo da Vinci and the parallelogram of forces. *Journal of the International Association for Shell and Spatial Structures, 39*(1), 47-53.

Nikolinakou, M.-K., Tallon, A. J., & Ochsendorf, J. A. (2011). Structure and form of early Gothic flying buttresses. *Revue Européenne de Génie Civil*, 1191-1217. doi:10.1080/17747120.2005.9692807

O´Dwyer, D. (1999). Funicular analysis of masonry vaults. *Computer and structures, 73*(1-5), 187-197. doi:10.1016/S0045-7949(98)00279-X

Ochsendorf, J. (2005). Los Guastavinos y la bóveda tabicada en Norteamérica. *Informes de la Construcción, 56*(496), 57-65. doi:10.3989/ic.2005.v57.i496.494

Ochsendorf, J. (2014). Guastavino masonry shells. *Structure, 26*.

Ochsendorf, J. (2020). Tile vaulting innovation by Rafael Guastavino Jr. and Eduardo Torroja. *International Association for Shell and Spatial Structures (IASS), 61*(203), 59-66. doi:10.20898/j.iass.2020.203.021

Ochsendorf, J. A. (2002). *Collapse of Masonry Structures. Doctoral dissertation.* Cambridge: Cambridge University.

Ochsendorf, J., & Freeman, M. (2010). *Guastavino vaulting: The art of structural tile.* New York: Princeton Architectural Press.

Palladio, A. (1570). *I quattro libri dellárchitettura.* Venice: Franceschi.

Parra y Cote, A. (1759). *Desempeño el más honroso de la obligación más fina...* Madrid: Imprenta de Francisco Xavier García.

Paz, J. Á. (2008). La producción cerámica vidriada. *Cerámicas hispanorromanas:un estado de la cuestión*, 489-496.

Pieper, K. (1983). *Sicherung historischer Bauten.* Berlin: Verlag von Wilhelm Ernst & Sohn Berlin.

Pinto, F. (2005). El cimborrio de madera del antiguo convento de San Pablo enSevilla. *Proceedings of the Fourth National Congress of Construction History* (pp. 863-873). Cadiz: Instituto Juan de Herrera.

Poleni, G. (1748). *Memorie istoriche della Gran Cupola del Tempio Vaticano e de danni di essa e de' ristoramenti loro, divisi in libri cinque.* Padova: Nella Stamperia del Seminario.

Poncelet, J. V. (1822). *Traite des proprietes projectives des figures* (Vol. 2). Paris: Bachelier.

Poncelet, J. V. (1852). Examen critique et historique des principales théories ou solutions concernant l'équilibre des voûtes. *Comptes-rendus de l'Académie des Sciences, 35*(1), 494-502,531-540,557-587.

Puig Boada, I. (1976). *L'Església de la Colónia Güell.* Barcelon: Lumen.

Ramos, A., & León, F. J. (2013). Clasificación morfológica de los rellenos en el trasdós de bóvedas de fábrica. *Informes de la Construcción, 65*(532), 471-480. doi:10.3989/ic.12.062

Rankine, W. (1858). *Manual of applied mechanics.* London: C. Griffin and Co.

Rankine, W. (1862). *Manual of civil engineering.* London: C. Griffin and Co.

Redondo, E. (2013). *La bóveda tabicada en España en el siglo XIX: la transformación de un sistema constructivo. Doctoral dissertation.* Madrid: Universidad Politécnica de Madrid.

Reese, T., Paffenroth, R., & Fehribach, J. (2016). Duality in geometric graphs: vector graphs, Kirchhoff graphs and Maxwell reciprocal figures. *Symmetry, 8*(9), 1-28. doi:10.3390/sym8030009

Ritter, W. (1879). *Statik der tunnelgewolbe.* Berlin: Julius Springer.

Roda, J. (2016). Nuevas noticias sobre la ruina y reconstrucción de la iglesia del Real Convento de San Pablo de Sevilla, según un manuscrito inédito de 1692-1708. *Revista de humanidades*(27), 193-232. doi:10.5944/rdh.27.2016.16490

Rondeaux, J.-F. (2019). *Graphical limit state analysis. Application to statically indeterminate trusses, beams and masonry arches. Doctoral dissertation.* Louvain-la-neuve: Université Catholique de Louvain.

Saavedra, E. (1860). Nota sobre la determinación del problema del equilibrio de las bóvedas. *Revista de Obras Públicas, 8*, 101-104.

Saliger, R. (1932). *Estática aplicada.* Barcelona: Labor.

Sánchez, V. (2015). *Alcalá patrimonio mundial.* Alcalá de Henares: Concejalía de turismo del Ayuntamiento de Alcalá de Henares.

Scamozzi, V. (1615). *L´idea della Architettura universale.* Venice: Girolamo Albrizzi.

Scholz, E. (1989). *Symmetrie Gruppe Dualität: Zur Beziehung zwischen theoretischer Mathematik und Anwendungen in Kristallographie und Baustatik des 19. Jahrhunderts* . Basel: Birkhäuser Verlag.

Schwedler, J. (1859). Theorie der Stützlinie. Ein Beitrag zur Form und Stärke gewölbter Bögen. *Zeitschrift für Bauwesen, 9*, 109-126.

Soler-Verdú, R., & Soler-Estrela, A. (2015). Tipología de cúpulas tabicadas. Geometría y construcción en la Valencia del siglo XVIII. *Informes de la Construcción, 67*(538), e078. doi:10.3989/ic.13.180.

Stevin, S. (1586). *De beghinselen der weeghconst.* Brugghe: Inde druckerye van Christoffel Plantijn, by Françoys van Raphelinghen.

Suárez, F. J., Boothby, T. E., & González, J. A. (2020). Constructive and structural analysis of a Baroque dome in Spain. The encamonada dome. *Journal of Cultural Heritage, 44*, 229-238. doi:10.1016/j.culher.2019.12.005

Suárez, F. J., Bravo, R., & González, J. A. (2019). Structural and constructive analysis of a faux vault, the dome of San Juan de Dios church in Granada. *International Journal of Architectural Heritage*, 1-12. doi:10.1080/15583058.2019.1645242

Taylor, R. (1996). El Sagrario de la Catedral de Granada y la junta de maestros de 1738. *Anuario del Departamento de Historia y Teoría del Arte, VII-VIII*. Granada: Universidad Autónoma de Madrid.

Tempesta, G., Paradiso, M., Stefano, G., & Pieroni, E. (2015). Maurice Lévy's original contribution to the analysis of masonry domes. *Domes and cupolas, 2*(2), 85-91.

Todisco, L., Corres, H., & Mueller, C. (2016). Funicularity through external posttensioning: Desing-Philosophy and Computational tool. *Journal of Structural Engineering, 142*(2), 04015141 (1-9). doi:10.1061/(ASCE)ST.1943-541X.0001416

Torres, L. (1939). De cerámica hispano-musulmana. *Al-andalus, 4*, 409-432.

Truñó, Á. (2004). *Construcción de bóvedas tabicadas.* Madrid: Instituto Juan de Herrera.

Van der Pluijm, R. (1992). Material properties of masonry and its components under tension and shear. *Proceedings 6th Canadian Masonry Symposium* (pp. 675-686). Saskatoon: University of Saskatchewan.

Varignon, P. (1687). *Projet d'une nouvelle mécanique.* Paris: Chez C. Jombert.

Vega, J. M. (2007). Restauración de la Iglesia del Convento de San Juan de laPenitencia. *Cercha: Magazine of Quantity Surveyors and Technical Architects*(88), 70-76.

Vegas, F., Mileto, C., & Cantero, V. M. (2017). El arquitecto Rafael Guastavino (1842-1908): obra en cuatro actos. *RS LONGA-Cuadernos de Arte, 26*, 209-230. doi:10.7203/arslonga.26.10964

Winkler, E. (1879-1880). Die Lage der Stützlinie im Gewölbe. *Deutsche Bauzeitung, 13-14*, 13: 117-119, 127-128,130 14: 58-60.

Wittmann, W. (1879). Zur theorie der gewölbe. *Zeitschrift für Bauwesen, 29*, 61-74.

Wolfe, W. S. (1921). *Graphical analysis: a text book on graphic.* New York: MacGraw-Hill.

Zalewski, W., & Allen, E. (1998). *Shaping structures: statics.* New York: Wiley.

Zaragozá, A. (2011). Hacia una historia de las bóvedas tabicadas. *Actas del Simposio Internacional sobre Bóvedas Tabicadas* (pp. 11-47). Valencia: Univerisdad Politécnica de Valencia.

Zawisny, N. (2015). *Guastavino structural calculations. Doctoral dissertation.* Cambridge: Massachusetts Institute of Technology.

Zawisny, N., Fivet, C., & Ochsendorf, J. (2017). Guastavino design of the 1909 thin brick dome of the Cathedral of St John the Divine. *Construction History, 32*(2), 39-66. doi:10.19274/CH.2017.02.03

# Research contributions derived from the development of the PhD thesis

The following is a list of the most relevant scientific contributions made during the period of elaboration of the Doctoral Thesis.

The subject matter of all the contributions included is directly related to the subject matter of the Doctoral Thesis.

The doctoral student and the thesis director, together with other collaborators, are co-authors of all the related contributions.

## 1 Publication of articles in scientific journals (chronological order)

---

*Authors*: Javier Suárez, Thomas E. Boothby, José A. González.

*Title*: Graphical methodology for structural analysis of historical constructions by combined use of funicular and projective geometry

*Date*: Article sent in 2020, currently in revision process.

*Journal*: ASCE Journal of Engineering Mechanics.

*Publisher*: ASCE LIBRARY. *ISSN*: 0733-9399.

*Journal Metrics:*

- JCR. Journal Citation Reports 2019: Impact Factor. 2,003. 5-Year Impact Factor. 2,33. Categories: Engineering, Mechanical. Rank 61/130. Quartile Q2.

---

*Authors*: Javier Suárez, Thomas E. Boothby, José A. González

*Title*: Constructive and structural analysis of a Baroque dome in Spain. The *encamonada* dome.

*Date*: 2019. Received at Editorial Office: 23 Jun 2019; article revised: 9 Dec 2019; article accepted for publication: 13 December 2019.

*Doi*: https://doi.org/10.1016/j.culher.2019.12.005

*Journal*: Journal of Cultural Heritage.

*Publisher*: Elsevier. *ISSN*: 1296-2074. *eISSN*: 1778-3674.

*Journal Metrics:*

- JCR. Journal Citation Reports 2019: Impact Factor. 2,553. 5-Year Impact Factor. 2,434. Categories: material science, multidisciplinary. Rank 157/314. Quartile Q2.
- SJR. SCImago Journal Rank 2018: 0,610. Categories: Conservation. Rank 1/65. Quartile Q1.
- Google Scholar Metrics: index h5: 30; median h5: 42.
- Source Normalized Impact per Paper. SNIP 2018: 1.654
- CiteScore 2018: 2.34

*Indexing*: Scopus; Arts and Humanities Citation Index; Science Citation

---

---

*Authors*: Javier Suarez, Rafael Bravo and José A. González.

Title: Structural and constructive analysis of the timber dome of San Juan de Dios basilica, in Granada (Spain)

*Date*: Accepted in June 2019; ref: IJMRI-237329; paper in press.

*Journal*: International Journal of Masonry Research and Innovation (IJMRI). Special issue on: 10IMC Masonry Research in the Third Millennium. From Theory to Practical Applications.

*Publisher*: Inderscience Publishers. *ISSN online*: 2056-9467 *ISSN print:* 2056-9459

*Doi*: 10.1504/IJMRI.2020.10029899

*Indexing:*

- IJMRI is indexed in: Scopus (Elsevier); Emerging Sources Citation Index (Clarivate Analytics); Asian Digital Library; cnpLINKer (CNPIEC); Google Scholar; J-Gate.
- IJMRI is listed in: Cabell's Directory of Publishing Opportunities; Norwegian Register for Scientific Journals, Series and Publishers.

---

*Authors*: Javier Suárez, Rafael Bravo and José A. González.

*Title*: Structural and Constructive Analysis of a Faux Vault, the Dome of San Juan de Dios Church, in Granada (Spain)

*Date*: 2019. Received 30 Nov 2018, accepted 15 Jul 2019, published online: 30 Jul 2019.

*Doi*: https://doi.org/10.1080/15583058.2019.1645242

*Journal*: International Journal of Architectural Heritage.

*Publisher*: Taylor & Francis Inc. *ISSN*: Print ISSN: 1558-3058 Online ISSN: 1558-3066.

*Journal Metrics:*

- JCR. Journal Citation Reports 2019: Impact Factor: 1,853. 5-Year Impact Factor: 1,807. Category: Engineering, Civil: Rank 64/134; Quartile Q2.
- SJR. SCImago Journal Rank 2018: 0,600. Categories: Architecture. Rank 9/140. Quartile Q1.
- Google Scholar Metrics: index h5: 22; median h5: 33.
- Source Normalized Impact per Paper. SNIP 2018: 0.943
- CiteScore 2018: 1.78

*Indexing:* Arts and Humanities Citation Index; CSA Technology Research Data base; Current Contents/Arts & Humanities; EBSCOhost Online Research Databases; Science Citation Index; and Scopus.

---

## 2 Publication of chapters in scientific and technical books

*Authors:* Javier Suárez, Rafael Bravo, José A. González.

*Book Title:* ICGG 2018 - Proceedings of the 18th International Conference on Geometry and Graphics.

*Book Subtitle:* 40th Anniversary - Milan, Italy, August 3-7, 2018. Part of the Advances in Intelligent Systems and Computing book series. AISC, volume 809.

*Chapter title:* Graphical Analysis of the Structural Behavior, According Hypothesis of Rankine-Schwedler, of a Large Stone Dome in Granada (Spain). pp: 1062-1074

*eBook ISBN*: 978-3-319-95588-9 Softcover *ISBN:* 978-3-319-95587-2 *ISSN:* 2194-5357 *ISSN:* 2194-5365 (electronic)

*Doi*: 10.1007/978-3-319-95588-9

*Publisher*: SPRINGER International Publishing. *Copyright*: © 2019 Copyright Holder: Springer International Publishing AG, part of Springer Nature. *Editors*: Cocchiarella, Luigi (Ed.)

*Journal Metrics:*

- SJR. SCImago Journal Rank 2018: 0,174. Categories: Computer Science (miscellaneous). Rank 227/449. Quartile Q3.
- Source Normalized Impact per Paper. SNIP 2018: 0.434
- CiteScore 2018: 0.54

*The book is included in the following databases:* ISI Proceedings, EI-Compendex, DBLP, SCOPUS, Google Scholar and Springerlink.

## 3 Presentation and publication of papers at internationally recognised conferences, with a scientific committee and a selective procedure for the admission of originals. (Chronological order)

*Authors*: Javier Suárez, Thomas E. Boothby, José A. González.

*Title*: Graphic methodology based on funicular and projective geometry, in structural analysis of historical constructions.

*Type of collaboration:* Abstract accepted.

*Congress*: ©2020 ISGG. 19th International Conference on Geometry and Graphics

*Location*: SÃO PAULO, BRAZIL *Date*: 9-13 AUGUST, 2020. Postponed a 2021 due to COVID2

*Authors*: Javier Suárez, Thomas E. Boothby, José A. González.

*Title*: Structural analysis of historical constructions by graphic methodology based on funicular and projective geometry.

*Type of collaboration*: Paper accepted.

*Congress*: SAHC 2020. 12th International Conference on Structural Analysis of Historical Constructions

*Location*: Barcelona. *Date*: 16-18 September 2020. Postponed a 2021 due to COVID2

*Authors*: Javier Suárez, Thomas E. Boothby, José A. González.
*Title*: Structural analysis of historical constructions by graphic methodology based on funicular and projective geometry.
*Type of collaboration*: Paper accepted.
*Congress*: IB2MAC 17th. 17th International Brick and Block Masonry Conference from Historical to Sustainable Masonry.
*Location*: Krakow (Poland) *Date*: 5 al 8 de July de 2020. Paper not presented due to COVID2.

---

*Authors*: Javier Suárez, Rafael Bravo, José A. González.
*Title*: Graphical analysis of the structural behavior, according hypothesis of Rankine-Schwedler, of a large stone dome in Granada (Spain)
*Congress*: 18TH International Conference on Geometry and Graphics. ©2018 ISGG. Organised by International Society for Geometry and Graphics & Dipartimento Architettura e Studi Urbani. Dipartimento di Architettura e Studi Urbani. Politecnico di Milano.
*Location*: Politecnico di Milano (Technical University of Milan). Milan (Italy)
*Date*: 3–7 August 2018.
*Type of collaboration*: Paper presentation.
*Publication*:

- Book Title: ICGG 2018 - Proceedings of the 18th International Conference on Geometry and Graphics. *eBook ISBN:* 978-3-319-95588-9 *Doi*: 10.1007/978-3-319-95588-9.
- *Publisher:* Springer International Publishing Copyright Holder: Springer International Publishing AG, part of Springer Nature

*Publication*:

- *Book of Abstracts:* The 18th International Conference on Geometry and Graphics. *Copyright:* © Poliscript 2018 Politecnico di Milano. Piazza Leonardo da Vinci, 32. 20133 Milano. *ISBN*: 97888-6493-044-2 *Editors:* Cocchiarella, Luigi (Ed.)

---

*Authors*: Javier Suárez, Rafael Bravo, José A. González.
*Title*: Structural and Constructive Analysis of a Faux Vault, the Dome of San Juan de Dios Church, in Granada (Spain)
*Congress*: 10th International Masonry Conference 2018, Milan (Italy). 10thIMC. Organised by International Masonry Society (IMS) y Politecnico di Milano (Technical University of Milan).
*Location*: Politecnico di Milano. MILÁN (Italia)
*Date*: 8-11 July 2018.
*Type of collaboration*: Paper presentation and participation in student competition (dry joint shear wall geometry).
*Publication:*

- Proceedings of the 10th International Masonry Conference. Held in Milan, Italy 9-11 July 2018. Edited by: Gabriele Milani (Politecnico di Milano, Italy), Alberto Taliercio (Politecnico di Milano, Italy) Stephen Garrity (University of Leeds, UK). A publication of IMS International Masonry Society. © 2018 The International Masonry Society (IMS). ISSN: 2523-532X Abstract Book. G. Milani, A. Taliercio and S. Garrity (eds.)

---

Authors: Javier Suárez, Rafael Bravo, José A. González.
*Title*: "Saints Justo y Pastor" church's dome. Constructive and structural analysis of a renaissance dome in Granada (Spain).
*Congress*: 6th International Conference on Heritage and Sustainable Conference. HERITAGE 2018
*Location*: ETS Edificación. Universidad de Granada. Granada (Spain)
*Date*: 12-15 June 2018.
*Type of collaboration*: Paper presentation.
Publication:

- Proceeding e-ISBN 978-84-338-6265-5. Book of Abstracts: ISBN: 978-84-338-6265-5. Dep. Legal Gr./ 768-2018. Editorial Universidad de Granada.

Authors: Javier Suárez, Rafael Bravo, José A. González.
*Title*: Encarnación Church's dome in Montefrío. Constructive and structural analysis of a neoclassical dome in Granada (Spain).
*Congress*: 6th International Conference on Heritage and Sustainable Conference. HERITAGE 2018
*Location*: ETS Edificación. Universidad de Granada. Granada (Spain)
*Date*: 12-15 June 2018.
*Type of collaboration:* Paper presentation.
*Publication*:

- Proceeding e-ISBN 978-84-338-6265-5. Book of Abstracts: ISBN: 978-84-338-6265-5. Dep. Legal Gr./ 768-2018. Editorial Universidad de Granada.

*Authors*: Javier Suárez, Rafael Bravo, José A. González.
Title: San Juan de Dios Church's dome. Constructive and structural analysis of a baroque vault in Granada (Spain).
*Congress:* 6th International Conference on Heritage and Sustainable Conference. HERITAGE 2018
*Location*: ETS Edificación. Universidad de Granada. Granada (Spain)
*Date*: 12-15 June 2018.
*Type of collaboration:* Paper presentation.
*Publication*:

- Proceeding e-ISBN 978-84-338-6265-5. Book of Abstracts: *ISBN:* 978-84-338-6265-5. Dep. Legal Gr./ 768-2018. Editorial Universidad de Granada.